The Dissertation Committee for Jason Michael Weaver certifies that this is the approved version of the following dissertation:

Innovative Energy Harvesting Technology for Wireless Bridge Monitoring Systems

Committee:

Kristin L. Wood, Supervisor

Richard H. Crawford, Co-Supervisor

Carolyn C. Seepersad

Preston Wilson

Sharon Wood

Innovative Energy Harvesting Technology for Wireless Bridge Monitoring Systems

by

Jason Michael Weaver, B.S., M.S.E.

Dissertation

Presented to the Faculty of the Graduate School of

The University of Texas at Austin

in Partial Fulfillment

of the Requirements

for the Degree of

Doctor of Philosophy

The University of Texas at Austin

August 2011

Dedication

For my great-grandfather, T. Henry Moray, whose “radiant energy”
would have made our jobs a lot easier.

And to my parents, who taught me to love learning.

Acknowledgements

This dissertation is the result of many people's hard work throughout the years. My parents have been a constant source of support and encouragement as I have ventured into the real world and the not-so-real world of higher education. My wife, Annamaria has been a loving, patient, but motivating influence to push forward each day. She is the greatest joy in my life. My three sons, Luke, Ezra, and Isaac, excel at letting me know it is time to call it a day and come back to what is truly important.

I would like to thank the many professors who have assisted in this research, including my supervisors Kristin Wood and Richard Crawford; colleagues from Civil and Electrical Engineering Sharon Wood, Karl Frank, Todd Helwig, and Dean Neikirk; members of my committee Preston Wilson and Carolyn Seepersad; and Dan Jensen from the United States Air Force Academy. Thanks also to David Potter and his team at National Instruments and Richard Lindberg at Wiss, Janney, Elstner Associates. Many graduate and undergraduate students have also been integral to this research, including Eric Dierks, Travis McEvoy, Jeremiah Fasl, Vasilis Samaras, Praveen Pasupathy, Ali Abu Yousef, Matt Reichenbach, Krystian Zimowski, Sumedh Inamdar, Rob Secker, Kimberly Souers, Leo Zhang, and Jedmond Tacardon.

Finally a special thanks to the Cullen Endowed Professorship in Engineering, the NIST Technology Innovation Program, and the Barnard P. Dietz Endowed Graduate Fellowship in Engineering for their invaluable support, as well as the Department of Engineering Mechanics at the U.S. Air Force Academy and the Manufacturing and Design Laboratory at The University of Texas at Austin for their support and guidance.

Innovative Energy Harvesting Technology for Wireless Bridge Monitoring Systems

Jason Michael Weaver, Ph.D.

The University of Texas at Austin, 2011

Supervisors: Kristin L. Wood and Richard H. Crawford

Energy harvesting is a promising and evolving field of research capable of supplying power to systems in a broad range of applications. In particular, the ability to gather energy directly from the environment without human intervention makes energy harvesting an excellent option for powering autonomous sensors in remote or hazardous locations.

This dissertation examines the possibility of using energy harvesting in new and innovative ways to power wireless sensor nodes placed in the substructures of highway bridges for structural health monitoring. Estimates for power requirements are established, using a wireless sensor node from National Instruments as an example system. Available power in a bridge environment is calculated for different energy sources, including solar radiation, wind, and vibration from traffic. Feasibility of using energy harvesting in such an application is addressed for both power availability and cost

as compared with grid power or primary batteries. An in-depth functional analysis of existing energy-harvesting systems is also presented, with insights into where innovation would be most beneficial in future systems.

Finally, the development of a suite of complementary energy-harvesting devices is described. Because conditions on bridges may vary, multiple solutions involving different energy domains are desired, with the end user able to select the harvester most appropriate for the specific installation. Concept generation techniques such as mind-mapping and 6-3-5 (C-Sketch) are used to produce a wide variety of concepts, from which several promising concept variants are selected. The continued development for one concept, which harvests vibration using piezoelectric materials, is described. Analytical modeling is presented for static and dynamic loading, as well as predicted power generation. Two proof-of-concept prototypes are built and tested in laboratory conditions. Through the development of this prototype, it is shown that the example wireless sensor node can successfully be powered through energy harvesting, and insights are shared concerning the situations where this and other energy harvesters would be most appropriate.

Table of Contents

List of Tables

List of Figures

Chapter 1: Introduction

1.1 Energy Harvesting

To power most electromechanical systems, electricity is generated on a large scale (e.g., coal-fired plants, hydroelectric dams, or wind farms) and then distributed to the individual systems (El-Khattam & Salama, 2004; Nishimura, Tabors, Ilic, & Lacalle-Melero, 1993). This distribution usually occurs either as AC power delivered on the electrical grid or DC power stored in batteries. However, there are many instances when both grid power and user-replaceable batteries may limit the effectiveness of an application. These instances represent opportunities for innovation.

One such application is the use of distributed sensor networks. With recent advances in small- and micro-scale electronics and sensors, using arrays of autonomous sensors to measure strain, temperature, and other characteristics is becoming more widespread. Such sensors can supplement or even eliminate the need for in-person inspection. The preferred locations for these sensors are often in remote or difficult-to-reach areas, such as inside aircraft wings, on the underside of bridges, or within structures. Extensive wiring to reach grid power is often infeasible, and batteries severely limit the available operational life or require periodic replacement. Data transmission can be accomplished wirelessly through communication protocols such as Wi-Fi or ZigBee (Kinney, 2003). The ability to similarly power the sensor nodes without wires or periodic battery replacement would allow for fully independent, long-term sensor nodes that could be placed virtually anywhere in a system. This capability is now becoming possible through the generation of electricity directly from the immediate environment, often called “energy harvesting” or “energy scavenging.”

Energy harvesting can be described as any process by which freely available energy from external sources is captured *in situ* (or on location) and converted into usable electrical energy for local use. Such processes harness energy that otherwise would have been wasted. Many types of *in situ* energy sources may be used; the most common types of energy harvesters are wind turbines and solar harvesters (photovoltaic panels and solar heat engines). Other harvesting technologies under development include systems for harnessing vibration or movement (from machinery, human movement, structures, etc.), thermal gradients, acoustic energy, and electromagnetic energy (primarily incident radio waves) (Roundy, Wright, & Rabaey, 2004). Example products in these energy domains are shown in Fig. 1.1. With the exception of solar power and large-scale wind power, the energy sources described here do not provide enough power to operate typical mechanical or electromechanical systems. They are, however, capable of supporting many low-power electronic systems like the sensors networks described above.

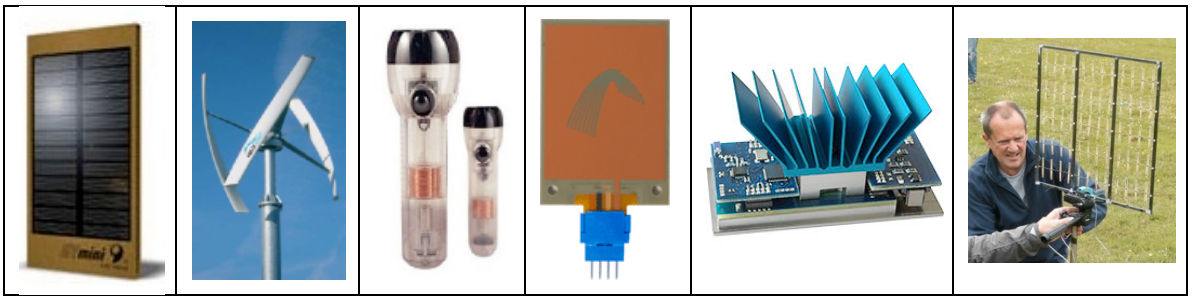

Figure 1.1 Energy harvesters capturing solar rays, wind, vibration (inductive and piezoelectric), thermal gradients, and radio waves

1.2 Specific Application

In the approximately fifty years since the interstate highway system was proposed (Weingroff, 1996), the number of bridges and overpasses in the United States has grown tremendously. There are currently over 600,000 highway bridges identified by the US

government (Memmott, 2007). Many of these are approaching the end of their expected fatigue lives. Others are not built to today's more rigorous engineering standards. A single structural-element failure within these bridges can sometimes lead to sudden, catastrophic failure of the entire structure, as occurred on the Minneapolis I-35W bridge in 2007 (Collapse, 2008).

Because of these considerations, every bridge must be visually inspected at least every other year. These inspections can be costly and dangerous, requiring specialized equipment to reach remote areas of the bridge and disrupting normal traffic. These factors make long-term fatigue monitoring of bridges a prime candidate for wireless sensor networks.

Maintaining the status quo of fixed-interval inspections proves to be an expensive and risky approach. A bridge that is in good repair and has a long expected life is likely inspected far more frequently than is actually needed. Each unnecessary inspection takes time, money, and resources away from already stressed departments of transportation. On the other hand, not identifying a potential problem on a bridge can be disastrous. In addition to the tragic loss of life caused by the I-35W bridge collapse, the direct costs for replacing the bridge were estimated at $235 million, with additional costs to displaced motorists and struggling downtown businesses exceeding $400,000 each day until the replacement bridge could be built (Hoppin, 2007). This bridge had passed its required inspection less than a year earlier, but a design flaw accelerated the growth of unseen fractures until sudden failure occurred throughout the bridge. Continuous monitoring could have identified the problem as it occurred, instead of waiting until the next inspection. The additional capabilities and insight offered by continuous monitoring would allow for a more flexible and robust inspection schedule, ideally permitting

inspectors to lengthen the time between in-person inspections on healthy bridges and identify early warnings signs on problem bridges, such as changes in traffic patterns or stress levels, signs of crack propagation, and other situations that may require immediate inspection or repair.

1.3 Motivation for Pursuing Energy Harvesting

The most widely available sources of power are AC grid power and DC power from batteries. A brief overview will show that for long-term monitoring of bridges, neither technology meets the desired capabilities.

The primary concern for the use of grid power is the cost and manpower required to install and protect the extensive amounts of wiring. Highway bridges can be thousands of feet or even miles in length. The actual length of wire and conduit required would be even greater, due to the need to route wires around obstacles and bridge geometry to avoid damaging equipment and obstructing traffic. Figure 1.2 shows a conceptual cross section of a bridge and the convoluted wiring path required to connect an existing source to a single sensor on the opposite side of the bridge. As a real-life example, the Fred Hartman Bridge in La Porte, Texas was recently fitted with a sensor system powered by wired grid power. The bridge is 2.6 miles long, but the installation required over 47 miles of electrical conduit to reach the sensors. The resulting cost of installation for equipment and labor was $1,025,000 (Development, 2009).

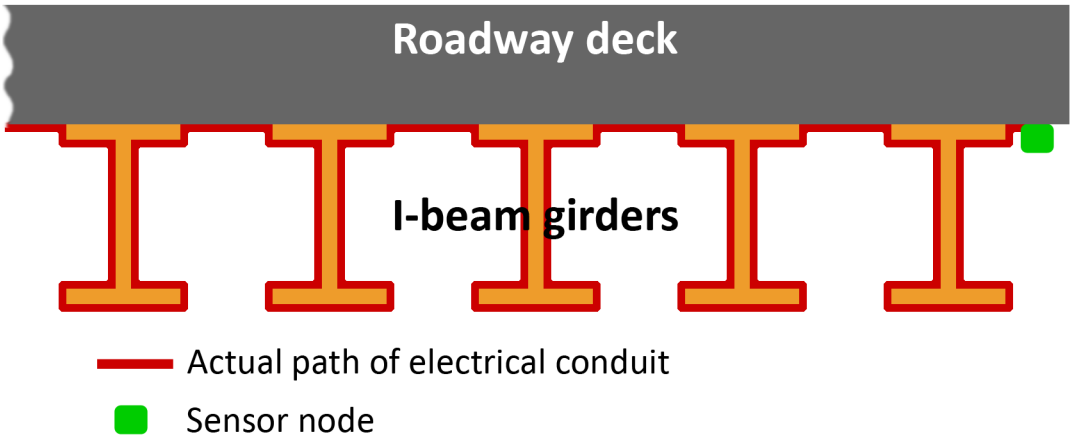

Figure 1.2 Conduit path to a wired sensor on a typical I-beam-girder bridge

Battery power is the most commonly used power source for existing sensor networks on bridges and similar structures. Batteries are very attractive, especially for short-term, temporary sensor installation. High-power systems can be operated with marine or auto lead-acid batteries, and low-power systems can often use disposable AA or watch/calculator-type batteries. Such batteries are widely available, inexpensive, and have well-documented characteristics. However, relying solely on disposable batteries supplied at initial installation places firm limits on the operational lifespan of the sensor system. For example, the National Instruments WSN-3202 sensor node requires four AA batteries (Wireless, 2011). At the lowest published duty cycle (1 measurement/minute), the WSN-3202 can be expected to last only two to three years on alkaline batteries. By using more expensive disposable lithium batteries, the lifespan can be extended to four to five years (Weaver, Wood, Crawford, & Jensen, 2010). The desired operational life for the long-term monitoring evaluated in this project, however, is a minimum of ten years. A more feasible approach is to use rechargeable batteries or ultra-capacitors that are periodically or continually recharged through energy harvesting.

1.4 PURPOSE OF DISSERTATION

This dissertation documents the development of new energy-harvesting technology for use with wireless sensors in a bridge environment. The primary goal of this research is to investigate the following hypothesis:

Research Hypothesis: *Energy-harvesting systems can power wireless sensor nodes in a typical bridge environment with greater efficiency and longer life than currently exists in the state-of-the-art.*

To support this investigation, several avenues of research are followed. Power and cost feasibility are assessed for common types of harvesters, and energy sources feasible for energy harvesting on a bridge are identified. Opportunities for innovation are identified through functional modeling of existing energy harvesters. Concepts for energy harvesters in these energy domains are then developed through structured concept-generation processes. The practical assessment of the research hypothesis is the development of a working prototype energy harvester, which is tested in both laboratory and field tests.

1.5 ORGANIZATION OF DISSERTATION

Chapter 2: Literature Review

Chapter 2 summarizes the available literature on energy harvesting, bridge monitoring and relevant design tools. A brief history of energy harvesting is given, including research milestones and recent developments in each field. An overview of remote health monitoring on highway bridges is also given, including a description of the current state-of-the-art. Finally, several design methods used in this dissertation are described, including functional modeling and concept generation techniques.

Chapter 3: Power Requirements for an Example Wireless Sensor Node

Chapter 3 estimates the power needs of an individual wireless sensor node, using the example of National Instruments' WSN-3202 node. Power usage data measured by National Instruments for two duty cycles are used to extrapolate power needs for a variety of more realistic duty cycles of interest in bridge monitoring. Three duty cycles of interest are selected for subsequent analysis: router mode (high power draw, radio transmitting continuously), continuous sampling (medium power draw, measurements at 30 Hz), and intermittent sampling (low power draw, measurements once per hour).

Chapter 4: Available Power Density in a Bridge Environment

Chapter 4 examines the availability of *in situ* energy on and around highway bridges. Typical energy sources are discussed, with analytical models used to estimate the theoretical power available from each source. These estimates are normalized by harvester size to yield power density, which can be more easily compared across domains. These theoretical limits are compared to the output of actual harvesters in the literature, as well as solar, wind and vibration data gathered from bridges in central Texas.

Chapter 5: Power and Cost Feasibility of Energy Harvesting

Chapter 5 compares the system power requirements in Chapter 3 to the available power densities in Chapter 4. Size estimates for feasible energy-harvesting systems are given, as well as likely constraints and limitations. The cost of installing and using these systems to power bridge-mounted wireless sensor networks is compared to the estimated installation and maintenance costs of using grid power or replaceable batteries to operate an equivalent network.

Chapter 6: Innovation Opportunities in Energy Harvesting

Chapter 6 examines innovation insights that can be gained in energy harvester design through the use of functional modeling. Several existing energy harvesters in different domains are modeled and compared. The resulting functional models are compiled into a binary product-function matrix, which is manipulated through vector-space analysis to yield product-product and function-function matrices. Through quantitative and qualitative examination of these results, archetypical functional models for each energy domain are described, and a set of generalized driving functions for energy harvesting is proposed. From these driving functions, several opportunities for innovation are identified and discussed.

Chapter 7: Concept Generation for an Energy Harvester Portfolio

Chapter 7 outlines the concept generation processes used to develop a portfolio of energy harvester designs. The specific design problem is addressed, as well as known customer needs and key functionalities. Concept generation sessions by several teams and individuals are described, as well as the resulting ideas and innovations. From these resulting concepts, a portfolio of concept variants is chosen for further development.

Chapter 8: Embodiment and Development of a Vibration Harvester

Chapter 8 describes the development of one of the chosen designs, a piezoelectric vibration harvester. Analytical models predicting static and dynamic behavior are given, comparing several parameter and material options. CAD mock-ups are created, leading to the construction of a proof-of-concept prototype. An experimental method is laid out for laboratory and field tests, and results from these tests are discussed.

Chapter 9: Recommendations and Conclusions

Chapter 9 contains recommendations for the further development of energy-harvesting technology for bridge monitoring. Next-generation design iterations of the piezoelectric vibration harvester and other concepts are discussed. Insights and recommendations regarding the bridge-monitoring project and energy harvesting in general are given, as well as some final thoughts on the future of the field and of design methodology development.

Chapter 2: Literature Review

2.1 Energy Harvesting

Energy harvesting can be described as any process by which freely available energy from external sources is captured *in situ* (or on location) and converted into usable electrical energy for local use. This is in contrast to most electrical power production, where energy is captured on a large scale through centralized fossil fuel, hydroelectric, or nuclear plants and then distributed through the AC grid power or batteries. Energy harvesting harnesses energy that otherwise would have been wasted. Many types of *in situ* energy sources may be used. Among the most common types of energy harvesters are wind turbines and solar harvesters (photovoltaic panels and solar heat engines). Other types under development include systems for harnessing vibration or movement (from machinery, human movement, structures, etc.), thermal gradients, acoustic energy, and electromagnetic energy (primarily incident radio waves).

Energy harvesting is usually interpreted to refer to relatively small, localized energy production. Though large solar and wind farms can produce power on the order of megawatts, energy-harvesting applications in these domains rely on smaller panels or wind turbines that can be placed near the system to be powered. Power levels available from energy harvesting range from microwatts to several watts. Solar harvesting lies at the upper end of the spectrum, with wind and vibration midrange (typically milliwatts) and the domains of thermal gradients, acoustic energy, and electromagnetic waves currently able to provide a few microwatts at best.

2.1.1 Why use energy harvesting?

Most energy harvesting processes (other than solar) provide power levels too low to power typical mechanical systems. However, their power output is sufficient for a wide variety of small electrical systems like sensors, controls, or lighting. In addition, the harvested energy can be stored until enough charge is available to operate a system for a short period of time.

As discussed in Chapter 1, one application of interest is the use of distributed wireless sensor networks. Such sensors can be placed in remote or dangerous locations to measure local conditions, supplementing or eliminating the need for in-person inspection. Other applications are also possible, especially when energy is stored and used intermittently. Possible applications include harvesting energy to power MEMS devices, radios, cell phones, flashlights, wristwatches, microcontrollers, traffic lights, pacemakers and other bio-embedded devices, thermostats, and even prosthetic limbs. As further development leads to increased power output from harvesters and decreased power requirements from electromechanical systems, more and more low-power applications become feasible.

2.1.3 A Brief History

The different domains of energy harvesting have very distinctive histories. The historical development of some major energy harvesting domains is summarized below.

Solar harvesting has a long history through the millennia. Energy from the sun has been used since ancient times for lighting and heating activities like drying clothes and food, heating homes and water, cooking, and purifying water through distillation (Civil Engineer, 2011). More sophisticated methods of capturing solar energy were discovered in the late 1800s (Smith, 1995), with the first solar-powered steam engine

developed in 1866 (Gordon, 2001), the first parabolic-trough solar steam engine in 1870 (A genuine, 1975) and the first selenium-based photovoltaic cell built in the 1880s (Sun, Fan, Wang, & Haliburton, 2004). Research continued throughout the early 1900s, but little progress was made until silicon-based photovoltaics were discovered in the 1950s (Civil Engineer, 2011).

Photovoltaic cells finally found a practical application as a backup power supply on satellites in the late 1950s and 1960s (Civil Engineer, 2011). The energy crisis of the 1970s and improved silicon manufacturing processes spurred on by the computer industry led to a decade of rapid development, but lower oil prices in the 1980s led to another plateau in development. Interest in photovoltaic panels renewed in the mid 1990s, with much of the current leading research taking place in Japan and Europe, although the US is starting to catch up. Many varieties of photovoltaic cells are available, with varying efficiencies, wavelength sensitivities, costs, and other advantages. Some of the more common types include monocrystalline silicon, polycrystalline silicon, cadmium telluride, and amorphous silicon (thin film) (Green, Emery, Hishikawa, & Warta, 2010).

At the same time, technology for solar heat engines also continued to develop. Variations of solar heat engines often use a Stirling engine or a steam engine to convert solar heat into electricity. The solar radiation is usually concentrated through mirrors or lenses. Parabolic mirrors are the most effective means for concentrating light, but are still expensive to manufacture. Current research is developing alternate methods such as the use of Fresnel lenses or parabolic assemblies of thin flat mirrors (Mariyappan, 2001).

Wind harvesting has a history similar in many ways to solar harvesting. Wind harvesting originates from the basic use of sails to transform wind energy into a means of transportation. Windmills began to be used in the 7th century for both pumping water and

milling grain (Hill, 1991). Throughout the late Middle Ages, windmills became prevalent throughout Europe, particularly in the Netherlands. In the 1800s, windmills became an integral part of developing the western United States, allowing wells to be drawn, grain to be processed, lumber to be cut, and water for steam locomotives to be pumped (White, 1962). With the development of electromagnetic generators, wind turbines began to be used to generate electricity in the late 1800s (Price, 2005). Wind turbines gradually became bigger, more sophisticated, and more popular until 1979, when several Danish companies began mass production of the long, slender turbines now widespread (Gipe, 1995).

Much research during the 1980s and 1990s was directed at improving these large wind turbines, with a single turbine now capable of generating up to seven megawatts (Thomas, 2008). The domain of smaller, more compact turbines is still relatively undeveloped (Carbon Trust, 2008). In recent years, more focus has been given to the design of turbines suitable for use on residential or commercial property, but even these typically have blade lengths of several feet (Olson, 2010). The market for turbines smaller than a foot or two in radius is still dominated by novelty toys and do-it-yourself kits (KidWind, 2011).

Vibration harvesting is a relatively recent development. There are currently four technologies that can be harnessed to capture vibration energy: coil/magnet induction (through Faraday's Law), piezoelectric materials, magnetostrictive materials, and variable-thickness capacitors.

In induction, a coil experiences a change in magnetic field due to motion relative to a magnet. This in turn induces a current in the coil, transforming the kinetic energy into electrical energy. The principle of induction has been understood since the work of

Faraday beginning in the 1830s and continued by Maxwell in the 1860s and 1870s (Maxwell, 1865). This principle is of course the foundation of all our electromagnetic motors and generators. The conversion between linear motion or vibration and electricity has been in practice for much of the 20th century, including linear actuators, speakers, accelerometers, and seismographs. However, the conversion from vibration to electricity (as in accelerometers and seismographs) has typically been focused on accuracy for sensing and measurement, not on power output or efficiency. The specific use of induction to generate power from vibration is a development of the past two or so decades, with much of the design growing directly out of typical speaker or accelerometers (Olson, 2002). Today, induction-powered vibration harvesting can be found in motion-powered wristwatches (Seiko, 2007), shaker flashlights (AIT, 1997), and many types of microgenerators that can power sensors from the vibration of industrial machinery (Perpetuum, 2011).

In the piezoelectric effect, which was first demonstrated in the 1880s (Piezo Institute, 2011), certain materials show a relationship between strain and voltage. If a changing mechanical strain is imposed on the material, an electric potential is induced across the material. Conversely, an applied voltage to the material will cause a change in shape due to induced strain. Modern piezoelectric materials such as lead zirconate titanate (PZT) began to be developed in the 1950s. For many years, research in the US faltered due to post-war secrecy, but advances flourished in Japan. This led to the design of inventions like piezoelectric filters for radio and television signals and piezoelectric igniters for small combustion engines, gas stoves, and lighters.

Some of the first experiments for using piezoelectric materials to generate power proposed their use *in vivo* to power artificial organs and pacemakers. Enger and Kennedy

(1964), Lewin, et al. (1968), and Ko (1969) examined harvesting energy from the movement of the heart or aorta, placing piezoelectric material either directly on the organ surface or on a cantilever structure embedded nearby. In 1984, a piezoelectric strip was inserted into the ribcage of a dog (Hasler, Stein, & Harbauer, 1984), but the resulting power was only one fiftieth of what was expected. In the late 1990s, several teams experimented with generating power from human movement, particularly foot impacts during walking. Antaki, et al. (1995) investigated this field for the application of charging batteries for artificial organs. Starner (1996) calculated the power theoretically available from many types of body motion and concluded that energy from foot impacts could be used to power microelectronics. A research team at MIT (Kymissis, Kendall, Paradiso, & Gershenfeld, 1998; Shenck & Paradiso, 2001) pursued several prototype harvesters attached to the heels of shoes. They concluded that their electromagnetic concepts were too unwieldy for practical use, but that a piezoelectric stack could effectively be imbedded in the sole. This was later improved by Rocha, et al. (2010) by embedding a piezoelectric structure resembling a leaf spring that both improved the power efficiency and retained a more natural bounce to the shoe.

In the late 1990s and early 2000s, improvements in microelectronics and wireless communication led to widespread development of wireless sensor technology. Energy harvesting quickly became a popular topic of research as well, as the development of reliable, independent, long-term power sources would greatly increase the potential for wireless sensor networks (WSN). Much of the prominent research on vibration harvesting during this time was carried out by teams at the University of California (Berkeley) and Virginia Tech.

Research at Berkeley focused on the ability to harvest energy from sinusoidal vibration inherent in AC motors. Because these motors match the frequency of the incoming AC current, they typically exhibit vibration at 50, 60, 100, or 120 Hz. In their initial study, Roundy, Wright, and Rabaey (2004) examined the use of electromagnetic (inductive), electrostatic (capacitive), and piezoelectric systems to harvest energy. They determined that a piezoelectric energy harvester would be the best choice for a 60-Hz, low-amplitude vibration source (their specific example was a microwave oven). They also built several prototype harvesters on the scale of one cubic centimeter in volume. Their later papers (Roundy, Wright, & Rabaey, 2003; Roundy & Wright, 2004; Roundy, Steingart, Frechette, Wright, & Rabaey, 2004) developed these concepts and examined the specific needs of WSN.

At Virginia Tech, Sodano, et al. (2002) examined the feasibility of using piezoelectric materials to harvest vibration by using a strip of PZT bonded to an aluminum cantilever in conjunction with either a capacitor or a NiMH battery and exposed to 63-Hz vibration. They determined that using a battery resulted in better power efficiency and storage. A later paper (Sodano, Inman, & Park, 2005) compared several harvester designs and examined how to further optimize such piezoelectric harvesters for charging batteries.

In the late 2000s, significant research in piezoelectric harvesting was done at the University of Southampton. Much of their work, led by Beeby, et al. (Beeby, Tudor, & White, 2006) focused on the development of piezoelectric vibration harvesting at the micro scale and the manufacture of such harvesters integrated into MEMS devices and circuitry.

The other two types of vibration harvesting are still in developmental stages. Piezomagnetism and magnetostriction (a related property) function similarly to the piezoelectric effect in that there is a relationship between strain and magnetic field. Actuators and sensors based on these properties are beginning to become more common, but the technology available is not yet sufficient to produce energy harvesting at a useful level (Wang & Yuan, 2008). The final category, capacitive vibration harvesting, has met with more success. In this type of energy harvesting, a capacitor with movable plates is subjected to the vibration, causing the distance between the plates to change. This results in an induced change in voltage across the capacitor (Roundy, Wright, & Rabaey, 2004). This principle has been used, like induction and piezoelectric materials, in speakers, microphones, actuators, and sensors. The primary drawback is that the capacitor must first be charged, requiring an additional source of power. Even so, capacitive energy harvesters are being developed and may find practical use in the near future (Yen & Lang, 2006).

Much of the necessary research in piezoelectric vibration harvesting consists of producing accurate analytical models of the electromechanical system and optimizing the power conditioning and load circuits. One of the first breakthroughs occurred in 1996, when William and Yates (1996) created a basic analytic model for calculating the power output from a cantilever vibration harvester. Meninger, et al. (2001) modeled power-conditioning circuits and experimentally tested their effectiveness. Subsequent work in modeling harvesting systems and predicting their output was described by Ottman, et al. (2002; 2003), Sodano, et al. (2004), Lu, et al. (2004), Roundy (2005), Roundy, et al. (2005), and Ertuk and Inman (2008; 2009).

Specific use of vibration harvesting for structural health monitoring on highway bridges requires an understanding of the vibration patterns on bridges and other characteristics and limitations of the environment. Several studies have been done (Wang, Huang, & Shahawy, 1999; Yin, Fang, Cai, & Dang, 2010) to create models of bridge vibrations from traffic, showing vibration patterns predominantly in the 1-15 Hz range. Work done with vibration harvesting at Clarkson University (Sazonov, Janoyan, & Jha, 2004; Sazonov, et al., 2006) confirmed this experimentally, measuring a dominant frequency of 3 Hz on their test bridge. Doebling, et al. (1996) and Salawu (1997) have shown possible ways to even use small changes in vibration frequency to detect structural changes that may indicate damage to the bridge.

The vibration signatures of bridges may vary considerably among different structures, and may change with time. Because of this variation, the ability to change the resonant frequency of the harvesting system or access a wider band of frequencies would be beneficial to the application. Some techniques have been proposed to increase the bandwidth through nonlinearity and allow various degrees of frequency tuning, but the problem is still largely unresolved (Challa, Prasad, Shi, & Fisher, 2008; Cornwell, Goethal, Kowko, & Damianakis, 2005; Davis & Lesieutre, 2000; Guyomar, Badel, Lefeuvre, & Richard, 2005; Jung & Yun, 2010; Kozinsky, 2009; Okamoto, Onuki, Nagasawa, & Kuwano, 2009; Wickenheiser & Garcia, 2010).

In addition to the resources cited above, the reader is directed to several excellent review papers covering the history, development, and current state of the art in vibration energy harvesting. These include papers by Mitcheson, et al. (2004), Sodano, et al. (2004), Paradiso and Starner (2005), Lynch and Loh (2006), Anton and Sodano (2007), Priya (2007), and Harb (2010).

Thermoelectric harvesting is primarily accomplished through the thermoelectric (Seebeck or Peltier) effect. In the Seebeck effect, a temperature gradient in a semiconductor induces a voltage between the different junctions. The Peltier effect describes the reverse process, where an applied voltage leads to heating or cooling of the material faces. Both of these effects were discovered in the mid 1800s by their respective namesakes (Rowe, 2006). The thermoelectric effect has found wide use in thermocouples and digital thermometers (Thermocouples, 2008). Thermoelectric generators are often placed on spacecraft, where the temperature gradient between heat from a radioactive material and the cold exterior of the craft make an excellent source of energy (Thermoelectric Generators, 2010). Thermoelectric generators are often used in microelectronics, where large differences in temperature exist and space is too limited for conventional heat engines like Stirling or steam engines (Rowe, 2006).

Acoustic harvesting is essentially a subtype of vibration harvesting, but with much lower input energy available. This means of harvesting may be currently feasible in specific applications where intense acoustic energy is concentrated, but is currently infeasible for use with ambient noise in typical environments (Wu, Chen, & Liu, 2009). However, the universal appeal of possible applications continues to spur research, with possible advances in the near future.

Electromagnetic radiation harvesting finds its roots in the first commercially popular radio receiver – the crystal radio (or cat's whisker radio). This type of radio has no external power supply, but uses the actual energy of the incoming radio waves to convert the radio signal into electricity and then into sound through a headphone. The crystal radio was popular from the 1900s until the 1920s, when it was replaced by vacuum tubes capable of amplification. During the two world wars, additional research

produced passive devices such as the IFF (identification, friend or foe) transponder for aircraft and covert listening devices, both of which use the power from incoming radio waves to broadcast their own signals (Landt, 2005). Current research is capable of extracting a usable amount of power from a high-intensity microwave beam or from radio frequency radiation from power lines (Merabet, et al., 2009). Obtaining usable amounts of electricity from ambient radio waves (from radio broadcasts and environmental sources) is still in developmental stages, but may soon be possible through the use of the "rectenna," or rectifying antenna (Visser, Theeuwes, Van Beurden, & Doodeman, 2007).

2.1.4 The Future of Energy Harvesting

Much of the future of energy harvesting simply involves the continued gains in efficiency of both harvesters and electronics so that more applications with higher power requirements become eligible for power from energy harvesting. However, there are also many new technologies, materials, and techniques currently under development, each of which would significantly advance energy-harvesting capabilities:

Solar

- Flexible film photovoltaics that can be installed on curved or even movable surfaces (Shah, Torres, Tscharner, Wyrsch, & Keppner, 1999)
- Photovoltaic paint (Javier & Foos, 2009)
- Transparent photovoltaics for installation on windows (Miyazaki, Akisawa, & Kashiwagi, 2005)
- Photovoltaic panels optimized for high efficiency in the shade or indoors (Phani, Tulloch, Vittorio, & Skryabin, 2001)
- Small-scale solar heat engines using Stirling engines (Kongtragool & Wongwises, 2003)

Wind

- Small-scale turbines optimized for low speeds and turbulent flow near buildings (Bahaj, Myers, & James, 2007)
- Hybrid systems that combine wind turbines and photovoltaic panels (Yang, Lu, & Zhou, 2007)
- Turbines that incorporate piezoelectric materials rather than electromagnetic motors (Tan & Panda, 2007)
- Counter-rotating turbines that boost relative velocity in the generator by rotating two rotors in opposite directions (Appa, 2000)
- Clutched turbines that provide multiple levels of harvesting for different wind speeds (Brune, Spee, & Wallace, 1994)

Vibration

- The use of nonlinear systems to capture vibration at a wider bandwidth (Zhu, Tudor, & Beeby, 2010)
- Tunable systems that can be adjusted to resonate at different frequencies (Zhu, Tudor, & Beeby, 2010)
- "On-the-fly" tunable systems that can periodically adjust the natural frequency automatically to match changing conditions (Zhu, Tudor, & Beeby, 2010)
- Hybrid harvesters that incorporate piezoelectric, inductive, magnetostrictive and/or capacitive elements (Dong, Zhai, Li, Viehland, & Priya, 2008; Zhang, Yang, & Chen, 2010)
- Conversion of incoming vibration to more appropriate higher or lower frequencies (Jung & Yun, 2010; Kulah & Najafi, 2008)

Thermoelectric

- Combination photovoltaic cells (harvesting higher-frequency optical light) and thermogenerators (harvesting lower-frequency infrared light/heat) (Kraemer, Hu, Muto, Chen, Chen, & Chiesa, 2008)
- Systems optimized for applications such as clothing (skin temperature/environment) automobile exhausts, and jet engines (Leonov & Vullers, 2009)

Acoustic

- Nano/micro-scale harvesters that can be arranged in networks to increase power output in typical ambient noise levels (Wu, Chen, & Liu, 2009)

Electromagnetic Radiation

- Miniaturization of rectenna to harvest radio frequency radiation (Motjolopane & van Zyl, 2009)
- Further miniaturization into "nantenna" capable of harvesting visible light at much higher efficiency than photovoltaic cells (Kotter, Novack, Slafer, & Pinhero, 2008)

2.2 STRUCTURAL HEALTH MONITORING OF HIGHWAY BRIDGES

Highway bridges, as with any structure, eventually fail if kept in service. Failure begins with damage at the material level (whether from design defects or inherent material flaws) and can be accelerated by excessive loading and environmental factors like corrosion, water seepage, and temperature changes (Farrar & Worden, 2007). This continual process, if unchecked, leads to failure, which is the point where the level of damage becomes unacceptable to the user. If, however, the damage levels on a structure

are sufficiently monitored and understood, failure can more easily be predicted or prevented.

2.2.1 Need For Structural Health Monitoring

The periodic inspection of a structure and the means for identifying damage is referred to as structural health monitoring (SHM). There are three main modes of SHM. In short-term SHM, observations take place periodically over a relatively short time period (days, weeks, or months). This may be done to verify performance after installation, after major changes, or when an area of concern is discovered. In long-term SHM, observations are scheduled over a long time period, typically the life of the structure. For example, highway bridges are visually inspected every two years for as long as they are in operation. A third variation, extreme-event monitoring, is the observation of the structure during and after an abnormal event such as a hurricane or earthquake. It is typically developed out of existing short-term or long-term protocols and is intended to provide reliable real-time safety and performance information (Farrar & Worden, 2007).

Structural Health Monitoring may include visual inspections (e.g., looking for cracks), in-person measurements (e.g., acoustic or half-cell measurements to identify rebar corrosion), and remote sensing (e.g., strain, vibration, or temperature measurements). Until recently, most SHM protocols dealt primarily with in-person inspections and measurements. However, the combination of improved remote sensing technology and several high-profile bridge failures (unanticipated despite recent in-person inspections) has led to an increased interest in continual, long-term remote sensing.

The current mandated systems for inspecting bridges every two years do much to ensure proper maintenance and prevent failure. However, many examples exist where these biennial inspections are insufficient to identify damage in a timely manner. In 1998, the possible collapse of a bridge in Rhode Island was averted only when a driver noticed extensive cracking in a load-bearing girder. Experts determined that the cracks had developed over the course of only three days (Castellucci, 1988; Mazurek & DeWolf, 1990; R. I. shores, 1988). More recently, the I-35W Bridge in Minneapolis suffered a complete catastrophic collapse in 2007. It had undergone an extensive visual inspection less than a year before, yet a critical design flaw remained unnoticed because no damage was detected (National Transportation Safety Board, 2008). In both of these cases, even a rudimentary system for continuous, autonomous monitoring may have identified the growing damage in between visual inspections. With the introduction of low-cost, reliable long-term sensing, the health of bridges can be assessed with more regularity and flexibility than is possible with current inspection procedures.

2.2.2 Early Structural Health Monitoring Research

During the 1970s and 1980s, a large focus of research in SHM was the development of global methods for damage identification. The predominant method for identifying system-wide signals of possible damage was through the analysis of vibration characteristics of the structure (Doebling, Farrar, Prime, & Shevitz, 1996). This method was tested, with mixed results, primarily on offshore oil platforms. For example, Vandivar (1977), Loland and Dodds (1976), and Cawley and Adams (1979) each were able to successfully correlate damage or structural changes to changes in resonant frequencies. However, the majority of studies found that, in most real-world applications, the variations in frequencies resulting from normal operation and changes in the

environment (such as changes in temperature, loading, etc.) were indistinguishable from variations in frequencies resulting from damage or even structural failure (Begg, Mackenzie, Dodds, & Loland, 1976; Coppolino & Rubin, 1980; Duggan, Wallace, & Caldwell, 1980). By the 1990s, it had been determined that looking at frequency changes alone was seldom sufficient for accurately identifying the presence of damage (Doebling, et al., 1996). However, research continued on the possibility of using vibration mode shapes, forced vibration tests, and eigenparameters in global damage identification. Doebling, et al. (1996) cite many examples where these methods were successful in controlled laboratory settings, but application in the field was largely limited to systems where loading and environmental conditions are constant and well-understood, such as rotating machinery.

During the 1980s, quantitative damage detection techniques specifically for highway bridges also began to be developed. A study in 1981 found some success using changes in stiffness and vibration signatures to identify deterioration during a fatigue test on a bridge (Salane, Baldwin, & Duffield, 1981). Other studies using simplified analytical models and scale bridge models reached similar conclusions, though these changes were typically very small, in the range of 5% or less even for critical damage (Spyrakos, Chen, Stephens, & Govidaraj, 1990; Turner & Pretlove, 1988). As with other structures, it gradually became apparent that frequency changes alone were usually insufficient for damage identification. Analyzing modal shapes yielded much more promising results (Farrar, et al., 1994; Tang & Leu, 1991), but such techniques were still not reliable enough for actual field use (Farrar & Cone, 1995; Raghavendrachar & Aktan, 1992).

2.2.3 Recent Advances in Structural Health Monitoring Technology

With the advent of wireless protocols and low-power electronics, the use of wireless sensor networks became a viable alternative to the wired sensors used previously. With reduced cost and increased ease of installation, it suddenly became much more feasible to install large numbers of sensors throughout entire bridge structures. Many notable bridges have now had successful large-scale SHM systems installed (Ko & Ni, 2005).

Due to the challenges of successful data transmission in a bridge environment, many first-generation wireless networks were simple single-hop configurations (Xu, et al., 2004). However, improved wireless protocols specialized for longer transmission ranges and lower power consumption, such as Wisden (Xu, et al., 2004) and ZigBee (Kinney, 2003), have made more extensive networks possible in more recent installations. MicroStrain has successfully installed long-term WSN on several bridges, including a battery-powered system on the Benjamin Franklin Bridge between Pennsylvania and New Jersey (Galbreath, Townsend, Mundell, & Arms, 2003) and solar-powered systems on bridges in Corinth, Greece and New London, Connecticut (Arms, et al., 2009). A recent short-term installation on the Golden Gate Bridge in San Fransisco, California incorporated a 46-hop system with 64 nodes to measure vibration across the structure (Kim, et al., 2007).

Current research in using WSN for SHM appears to focus on three primary objectives. The first objective continues the work described in the previous section, developing new algorithms and statistical tools for measuring and manipulating data and extracting useful and accurate information on bridge health. This involves both global damage identification methods and localized damage tracking. In addition to the studies

mentioned previously, other significant literature in this field includes papers by Catbas, et al. (2008), Deraemaeker, et al. (2008), Farrar and Lieven (2007), Friswell and Adhikari (2010), Ntotsios, et al. (2009), Ou and Li (2010), Salawu (1997), Sohn, (2007), Wang, et al. (2007), and Worden, et al. (2007).

The second objective seeks to maximize the potential of wireless systems by improving the efficiency and reliability of the data processing and transmission. This includes exploring different software options for on-chip and off-chip data analysis, data fusion and compression, and increasing the range of reliable wireless transmission through interference-dense structures like steel and concrete bridges. Significant papers in this area include work by Abbasi and Younis (2007), Akkaya and Younis (2005), Gungor and Hancke (2009), Lynch, et al. (2003), Meguerdichian and Potkonjak (2003), Muruganathan, et al. (2005), Pandey, et al. (2010), Sohrabi, et al. (2000), Varshney (1996), Wan, et al. (2002), Wang, et al. (2003), Woo, et al. (2003), Xu, et al. (2004), and Yick, et al. (2008).

The third objective, and the most relevant to this dissertation, seeks to lower cost and increase operating life by improving the power flow through the system. This includes hardware advances in low-power computing and radio transmission, improved battery technology, and energy harvesting from the environment. Recent research in power reduction includes work by Cardei and Du (2005), Decotignie, et al. (2010), Nedevschi, et al. (2008), and Polastre, et al. (2004). Advanced battery technology is available from companies like A123 Systems (A123 Systems: About us), BetaBatt (Cascio, 2005), Oak Ridge National Laboratory (Dudney, 2009), Tadiran Batteries (Gadomski), and Quallion (Road transportation batteries).

The study of energy harvesting specifically for SHM and WSN has only begun in the last few years, but is gaining more traction. Roundy, et al. (2004) investigated the possibility of using using 60-Hz vibration from motor-driven devices like microwave ovens to power sensors on the walls of buildings and other structures. They successfully manufactured a piezoelectric harvester consisting of a cantilever bimorph and tip mass 3 cm in length capable of harvesting 300 mW from a 60-Hz sine wave with amplitude of 0.23 g acceleration. They also summarized the power availability from the other major sources of environmental energy, including solar, wind, and thermal energy.

Elvin, et al. (2006) studied the feasibility of powering sensors for structural monitoring using vibration from traffic on bridges, wind on tall buildings, and earthquakes. They determined that bridge vibration is typically below 5 Hz with maximum accelerations between 0.01 and 0.1 g. They built prototype harvesters of about 3-cm length with two piezoelectric materials, PVDF and PZT. They had significant difficulty powering their sensor: the PVDF did not generate enough power even from the earthquake vibration, and they were unable to parameterize their PZT harvester to resonate below 7 Hz without overstressing the piezoelectric material. They suggested that, if the strength limitations of the PZT ceramic could be overcome, several millijoules could be generated from a harvester of 0.1-1.0 kg.

Microstrain (2007), as mentioned above, has installed WSN networks on bridges in Greece and Connecticut that are completely solar powered. They also have done research on harvesting vibration, predominantly using piezoelectric materials (Churchill, Hamel, Townsend, & Arms, 2003). However, they only studied vibration in the range of 60-180 Hz and have not as yet introduced commercial products for vibration harvesting on bridges.

Park, et al. (2008) provided a detailed overview of research previously done in each of the major energy-harvesting domains and examined how these technologies could be used for powering WSN for SHM. Particular attention was given to previous research in vibration harvesting due to its parallel with using vibration in global condition monitoring.

Sazonov, et al. (2009) described research at Clarkson University regarding the development of a low-power wireless sensor node, afterwards marketed by Ambiosystems, and several prototype vibration harvesters that use electromagnetic induction coils to harvest vibration on bridges. They were able to successfully power their sensor node, using only vibration from traffic, with sufficient power to send a wireless signal several times an hour, depending on traffic. They tuned their harvesters to resonate at 3 Hz, which matched the vibration they observed on their bridge in New York.

Steingart (2009) provided insight into the overall problem of powering wireless sensors. He examined power needs under different WSN functions, different battery and storage technologies, and attractive options for energy harvesting. He concludes that, where possible, primary batteries be used for expected lifecycles of 5 years or less, solar power should be used for long-term outdoor applications, and thermal harvesting may be attractive for industrial applications with sufficient heat differentials. About vibrational energy harvesting, he noted that it was "attractive in theory, but mechanical coupling issues and narrow-band frequency response remain obstacles to widespread implementation." He also noted that energy harvesters in general remain larger than their equivalent battery systems.

2.3 DESIGN METHODOLOGIES

Formal methodologies for product design have been described in detail in numerous texts, including Cagan and Vogel (2002), Otto and Wood (2001), Pahl and Beitz (1996), Ullman (2002), and Ulrich and Eppinger (2004). These methodologies speak in detail about each step in product design and development, from initial decisions of scope and project definition to the final actions needed to ramp up full-scale production.

The primary phases of this design process, as defined by Ulrich and Eppinger (2004), are as follows:

Phase 1. Planning

(includes project mission statement, business goals, etc.)

Phase 2. Concept Development

(includes identifying customers and customer needs, researching and benchmarking competitive products, feasibility studies, product specifications, concept generation and selection, and experimental prototyping and testing)

Phase 3. System-Level Design

(includes definition of product architecture, decomposition into components and sub-systems, and geometric layout and assembly decisions)

Phase 4. Detail Design

(includes complete specification of unique parts and identification of standard parts and suppliers, process and tool planning, and control documentation)

Phase 5. Testing and Refinement

(includes alpha and beta prototypes using materials, fabrication, and assembly increasingly similar to that intended in final production, focusing on verification of expected performance and reliability)

Phase 6. Production Ramp-Up

(includes using the intended production process to make the product in smaller quantities, training staff, diagnosing problems in the production process, and seeking customer feedback before widespread launch)

The majority of the work covered in this dissertation falls under Phase 2 of this process, Concept Development. Phase 1, Planning, was accomplished primarily in the proposal submitted to NIST by The University of Texas (Development, 2009). Phases 3-6 will be completed by subsequent research according to the schedule indicated in the proposal.

Concept development is composed of several parts, each of which have been covered extensively in the literature. Several key components relevant to this dissertation are described below.

2.3.1 Understanding the Opportunity

The first part of concept development has been described variously as "understanding the opportunity" (Otto & Wood, 2001; Ullman, 2002), "clarification of the task" (Pahl & Beitz, 1996), or the "front end" of the design process (Cagan & Vogel, 2002). Primary goals in this area include identifying customer needs and translating these

needs into product specifications. Specific steps may include identification of "lead users" (customers often on the leading edge of technology or with specific needs), interviews and focus groups to discover both stated and unstated expectations of the customer, assigning importance rankings to these needs, creating activity diagrams to determine typical customer behavior, researching literature, benchmarking similar products, mapping customer needs to predicted engineering specifications through tools such as The House of Quality or Value Analysis, and creating product specification sheets (Otto & Wood, 2001). The importance of thoroughly exploring these areas cannot be overstated, as an increase in understanding of the product early on leads to more efficient design and much reduced costs later in the process. Specific instruction regarding these steps can be found in the sources above, as well as many other design textbooks.

2.3.2 Functional Modeling

Functional Modeling is an additional step that can greatly add to the designer's understanding of what the desired product should accomplish. Functional modeling has roots in the field of Value Engineering, where percentages of the total product cost can be ascribed to each key function (Akiyama, 1991). Subsequent research attempted to establish classification systems and common vocabulary for system functions, including work by Collins, et al. (1976), Hundal (1990), Kirshman and Fadel (1998) Koch, et al. (1994) and Pahl and Beitz (1996).

Functional modeling creates a "form-independent blueprint" for a product (Stone & Wood, 2000). Such a model can describe *what* a product does or should do without specifying and limiting *how* it accomplishes these functions. One method for comprehensively modeling functionality, described by Otto and Wood (2001), involves

breaking apart the overall product function into smaller and smaller subfunctions. One first starts with a simple black box diagram for the product, then analyzes what functions must occur inside the black box to accomplish the overall effect. This results in a heirarchy of functions of varying degrees of specificity, which can then be reassembled into a structure with parallel and series-based organization. This can be considered a top-down approach. Alternately, the function structure can be constructed from the bottom up. It is still suggested that the designer starts with a black box diagram for the product. This allows the designer to identify all the "flows" (materials, energies, and information) going in and coming out of the system. Next, the previously identified customer needs and typical customer activities are examined. If these needs and activities relate somehow to an identified flow, this relationship can likely be expressed as one or more functions performed on the flow. It is also possible that some needs and activities may not show direct correlation with the flows and functionality; in these cases, they would be satisfied by environmental or product-wide constraints instead. For each customer need/flow interaction, a small function structure can be assembled. These sub-structures can then be assembled into a complete function structure by following the path of each flow from its initial entry into the system, through the need-based sub-structures, to its final exit from the structure. Assessing the function structure as it arises from customer needs can give great insight into the design process, including the questions:

- Do the listed customer needs completely describe all the expectations of the customer? Can they each be concretely satisfied by specific functions and constraints?
- Are there non-obvious flows or functions that must be added in order to satisfy customer needs and other requirements?

- Are there flows or functions in the function structure that do not seem to relate to given customer needs? If so, what purpose do they serve? Are they necessary?
- Does the organization of functions and the movement of flows through the function structure give insight into the physical organization of the final product, such as modules, subsystems, architecture, and assemblies?

An example of functional modeling is shown below. Figure 2.1 shows an example product, a NERF air-dart gun. Figure 2.2 shows a black box diagram constructed for the product. A completed function diagram for the product is shown in Fig. 2.3.

Figure 2.1 Nerf Missilestorm air-dart gun (Nerf Missilestorm)

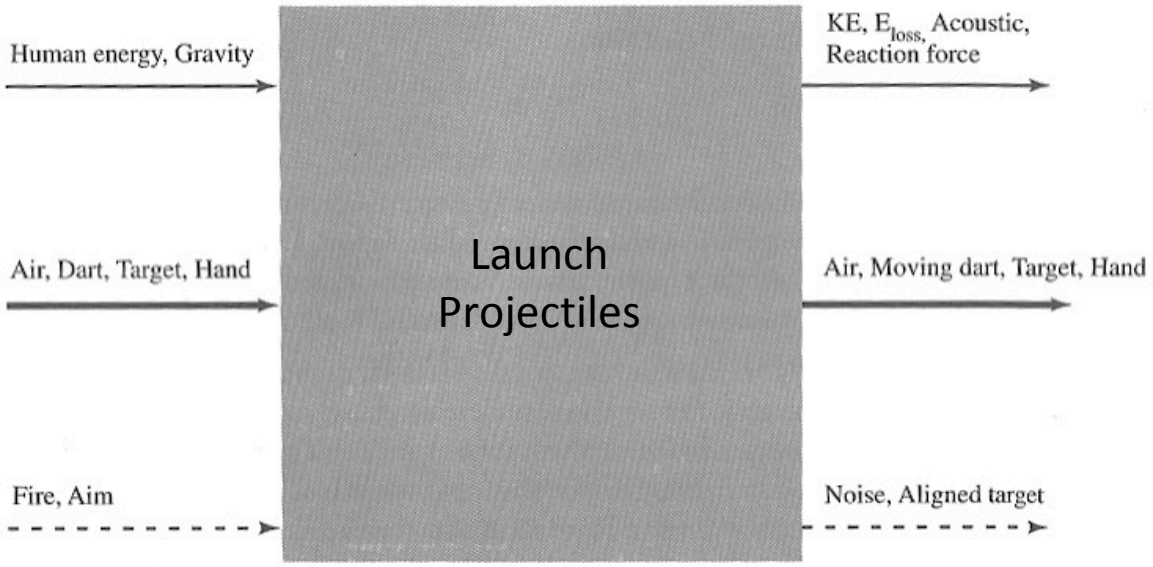

Figure 2.2 Nerf Missilestorm black box diagram (Otto & Wood, 2001)

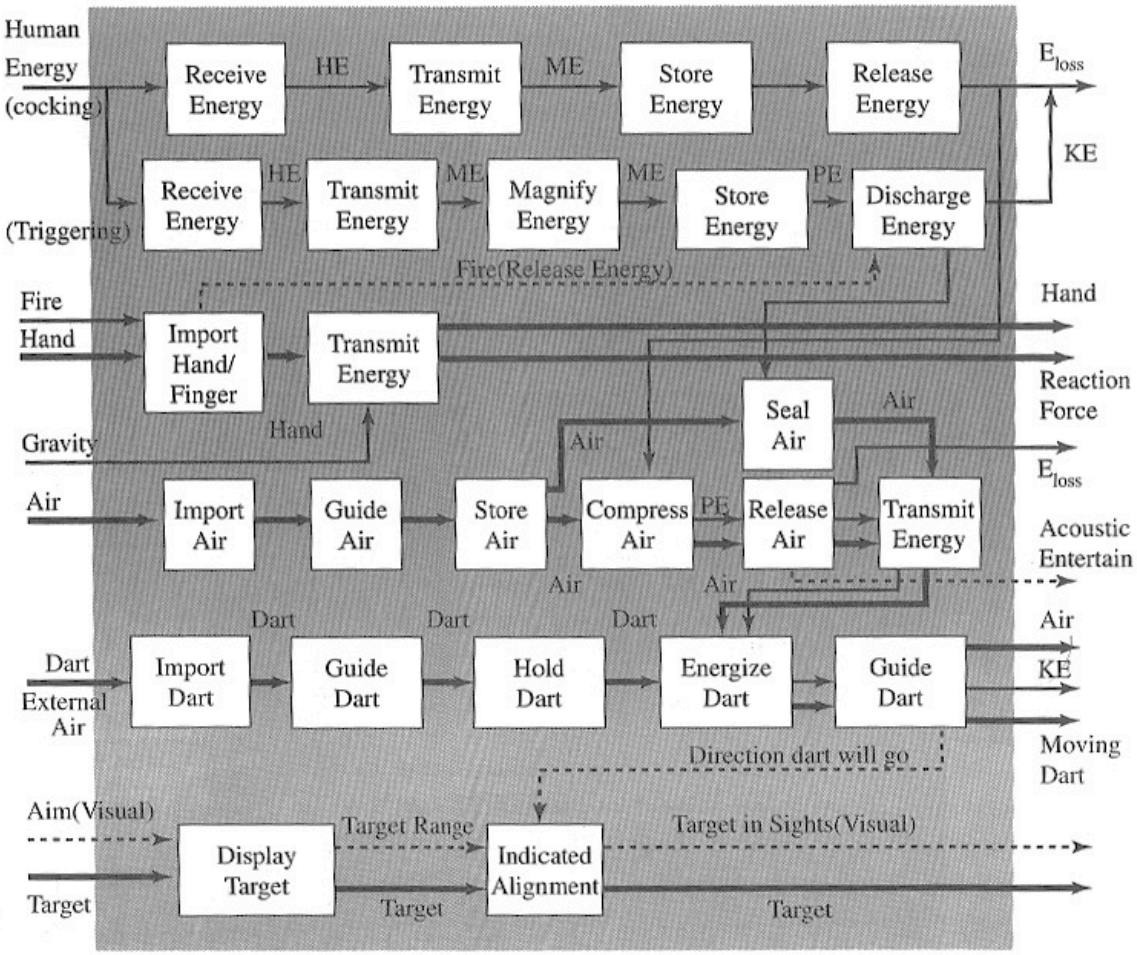

Figure 2.3 Nerf Missilestorm functional model (Otto & Wood, 2001)

One major limitation to functional modeling can be a lack of universality. Different designers may look at the same product and explain its functionality with different vocabulary, degree of specificity, and even order of functions. To help alleviate this problem, efforts have been made to describe a common vocabulary basis for describing functionality at its simplest levels (Little, Wood, & McAdams, 1997; Stone & Wood, 2000; Szykman, Racz, & Sriram, 1999). Several independent studies have been reconciled into a combined taxonomy referred to as the "functional common basis"

(Hirtz, Stone, McAdams, Szykman, & Wood, 2002). This functional common basis is presented in Appendix A.

Functional modeling can be used in several ways in the design process. Otto and Wood (2001) mention using functional modeling to identify analogous products for benchmarking, creating product families, generating alternative modular architectures, and as a starting point for concept generation and analytical modeling. In addition, Stone, et al. (1999) describe a process for using functional modeling quantitatively, tallying the functions of each product and performing a vector space analysis to identify relationships among products. This process will be explored in more depth in Chapter 6.

2.3.3 Concept Generation

Concept generation is a stage of product development that has received extensive attention, and yet is too often pursued informally or casually. It is easy for a designer to just sit and try to think up new ideas off the top of his or her head; however, concept generation is much more effective and efficient when following a step-by-step model. Ulrich and Eppinger (2004) describe a five-step process:

1. Clarify the Problem
    a. Decompose into Simpler Sub-Problems
    b. Focus Initial Efforts on Critical Sub-Problems
2. Search Externally
    a. Interview Lead Users
    b. Consult Experts
    c. Search Patents
    d. Search Published Literature
    e. Benchmark Related Products

3. Search Internally
    a. Individual and Group Sessions
4. Explore Systematically
    a. Concept Classification Trees
    b. Concept Combination Tables
5. Reflect on the Result and the Process

As can be seen, the first two steps listed reflect portions of the "understanding the opportunity" phase described previously. The crux of the concept generation process is Step 3, but Ulrich and Eppinger give little structure into how time spent by the designers is converted into quality ideas of sufficient breadth, novelty, and feasibility. Otto and Wood (2001) and Pahl and Beitz (1996) give more insight into possible methods that can be used to aid ideation.

Otto and Wood (2001) state, "the underlying goal of concept generation is to develop as many ideas as possible." The likelihood of finding a promising concept increases as the overall number of concepts increases (Bouchard, 1969; Shah, Kulkarni, & Vargas-Hernandez, 2000; Shah, Vargas-Hernandez, & Smith, 2003). Hence, a main goal of any concept generation technique is to produce a large number of ideas across a wide and varied design space.

Concept generation techniques can be grouped into two categories: intuitive and directed or logical (Shah, 1998). Intuitive methods focus on removing barriers to divergent thinking and creating alternate ways of looking at a problem so that new analogies and bridges to possible solutions can be identified. Various intuitive methods can be utilized by individuals or groups, and may involve communication through talking, writing, or sketching pictures. These ideation sessions are relatively unguided,

allowing the designers to explore whatever portion of the design space catches their attention. In any intuitive method, two key components are suspending judgement (recording and encouraging all ideas no matter how far-fetched) and expanding the breadth of the examined design space. Some popular intuitive methods include conventional brainstorming, mind mapping, and 6-3-5/C-Sketch (Otto & Wood, 2001).

Brainstorming is an activity where team members communicate ideas verbally, focusing on functional needs and architecture. The main focus of brainstorming is to build upon each other's ideas, making intuitive jumps to new concepts and relations. A companion tool often used with brainstorming is mind mapping. Mind mapping is a graphical technique where related ideas are organized in a web structure. Typically, a facilitator records the problem statement in the middle, then quickly records all ideas as they are proposed, linking each one back to either the original problem statement or a previously mentioned idea. The resulting mind map organizes the disjointed thoughts of all the teammates into a logical framework of related ideas.

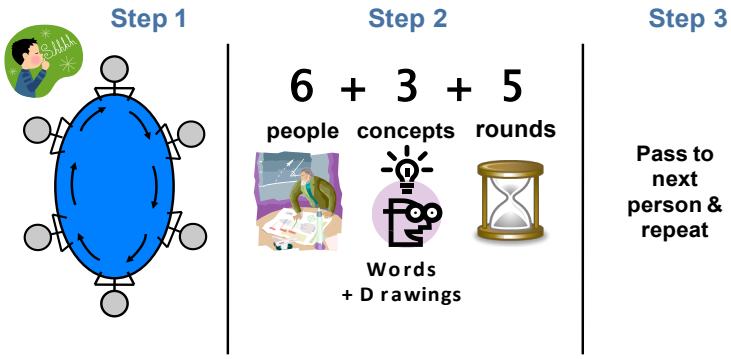

Figure 2.4 Concept generation process for 6-3-5

6-3-5, or C-Sketch, is an alternative approach to brainstorming that draws upon possible strengths not utilized with verbal methods. In this method, illustrated in Fig. 2.4, team members gather around a table, each with a sheet of paper. Each member sketches

three ideas on their paper, with only limited use of key words or descriptions. Speaking aloud is discouraged. After a set amount of time, the team members pass their papers to the members next to them. During the second and subsequent lengths of time, each member works on their new papers to modify the existing ideas or record new ones. One round is complete after the papers have passed all the way around the table. Otto and Wood (2001) recommend going through five complete rounds in order to yield the maximum number of new ideas. The use of sketches and the discouragement of verbal communication encourages new ideas and points of view as the team members interpret each other's drawings, perhaps in ways not intended by the original artists. This in turn allows a flow of ideas and an end result that differs from one limited by verbal communication.

Directed methods seek to guide the designer to a solution by starting with the design problem and exploring specific portions of the design space in a systematic manner. Using physical principles, design guidelines, or known solutions in other fields, the designer discovers what types of solutions would be the best avenues for continued study. Directed methods may include studying analytical models and identifying variables that can be adjusted to satisfy customer needs, as well as systematically looking at the different technologies available for a particular function.

Perhaps the most fleshed-out directed method is the Theory of Inventive Problem Solving (TIPS, or TRIZ in the original Russian). TIPS was developed by Genrikh S. Altshuller and his team in the U.S.S.R. by studying millions of patents. Their efforts led to the description of several guidelines and trends in design. These include the classification of different levels of invention (from routine parametric changes to drastic functional changes), observations on the typical evolution of an engineering system, a

thorough analysis of typical engineering conflicts (such as trying to make a system both lightweight and high in strength), and a method for systematically finding solutions to these conflicts through known design principles (such as using composite materials, counterweights, or removable parts). In this way, the designer is guided toward the general design principles that will be most helpful to solving the design problem without becoming fixated on a single actual solution.

A successful design process will likely incorporate several of these or other concept generation techniques. As Otto and Wood (2001) remind us, "Final product concepts are not the first ones generated. Many concepts must therefore be explored, seeking continual additions and refinements."

2.4 Conclusions From Literature Review

The fields of structural monitoring and energy harvesting have both seen considerable progress in recent years. As efficiencies have improved in both energy harvesting and sensor node technologies, the two fields have reached the point where low-power wireless sensor networks can feasibly be powered directly from the environment. Today, the use of solar power, wind, and vibration is growing as a viable alternative to grid power or batteries in small, distributed electronic devices.

Solar power is by far the most energy dense source of environmental energy suitable for bridge monitoring. Recent and current research that may improve solar harvesting on bridges includes flexible film photovoltaics, panels optimized for better efficiency in the shade, and alternative means of solar harvesting like heat engines. Where solar is not feasible due to location, wind and vibration present alternative sources of energy. Other sources of energy, such as thermal gradients and EM radiation, are promising but remain in early experimental phases.

Wind power on a small, distributed scale and in an urban setting like a bridge is still relatively undeveloped. Current research is examining the difficulties and opportunities of harvesting wind in an urban setting, which may include increased turbulence, lower wind speed, and space limitations. Several new systems under development address these issues with new technology such as hybrid wind/solar systems, the use of piezoelectric generators, and novel turbine and generator architectures.

Vibration harvesting is the newest of the three forms of energy harvesting. Possible applications for vibration harvesting are ubiquitous, but researchers have had significant difficulty harnessing this energy due to its variability. Currently, most vibration harvesters use inductive, piezoelectric, or capacitive components that naturally resonate at the same frequency as the predominant vibration input. This greatly increases the amount of power that can be harvested from consistent vibration, but only within a narrow frequency bandwidth. To overcome this limitation, much of the current research in vibration harvesting focuses on using non-linearity, tunability, and frequency transformation to widen the bandwidth or adjust the device to match the incoming vibration.

Chapter 3: Power Requirements for Example Wireless Sensor Node

3.1 Introduction

Power requirements can often be the limiting factor in designing for a product's lifecycle. Until recently, the two viable alternatives for long-term power in most situations were grid power (which limited location and mobility) and batteries (which limited available power and longevity). Over the last decade, however, advancements in both low-power electronics and the efficiency of energy harvesting technology have opened the possibility of powering many low-power systems directly from the environment for extended periods of time.

This chapter considers the power needs that must be met to undertake wireless sensing on a bridge. We examine a sample wireless sensor node from National Instruments and estimate peak and average power requirements under various sample rates typical of bridge operation. In the following chapter, this information will be compared to the theoretical power available through energy harvesting, yielding an initial assessment of the proposed system's feasibility from a power viewpoint.

3.2 Design Feasibility Methodology

The methodology followed in this and the following chapter to determine power feasibility is shown in Fig. 3.1. The first step is to identify the specific application for the wireless sensors. Then, we must specify the parameters to be monitored and how frequently the node will perform functions such as taking measurements, processing data, performing calculations, transmitting data, etc. A specific wireless sensor system must be identified, and the power requirements for the chosen duty cycles must be calculated. We can then compare these power requirements to the available power densities of various

energy harvesters. In determining harvester power densities (considered in Chapter 4), we must first estimate the available power in the environment (vibration signatures, solar irradiation, wind speed) and then calculate the power that the harvester can supply to the sensor node. Finally, the possible need for energy storage should be addressed, and the system can be finalized.

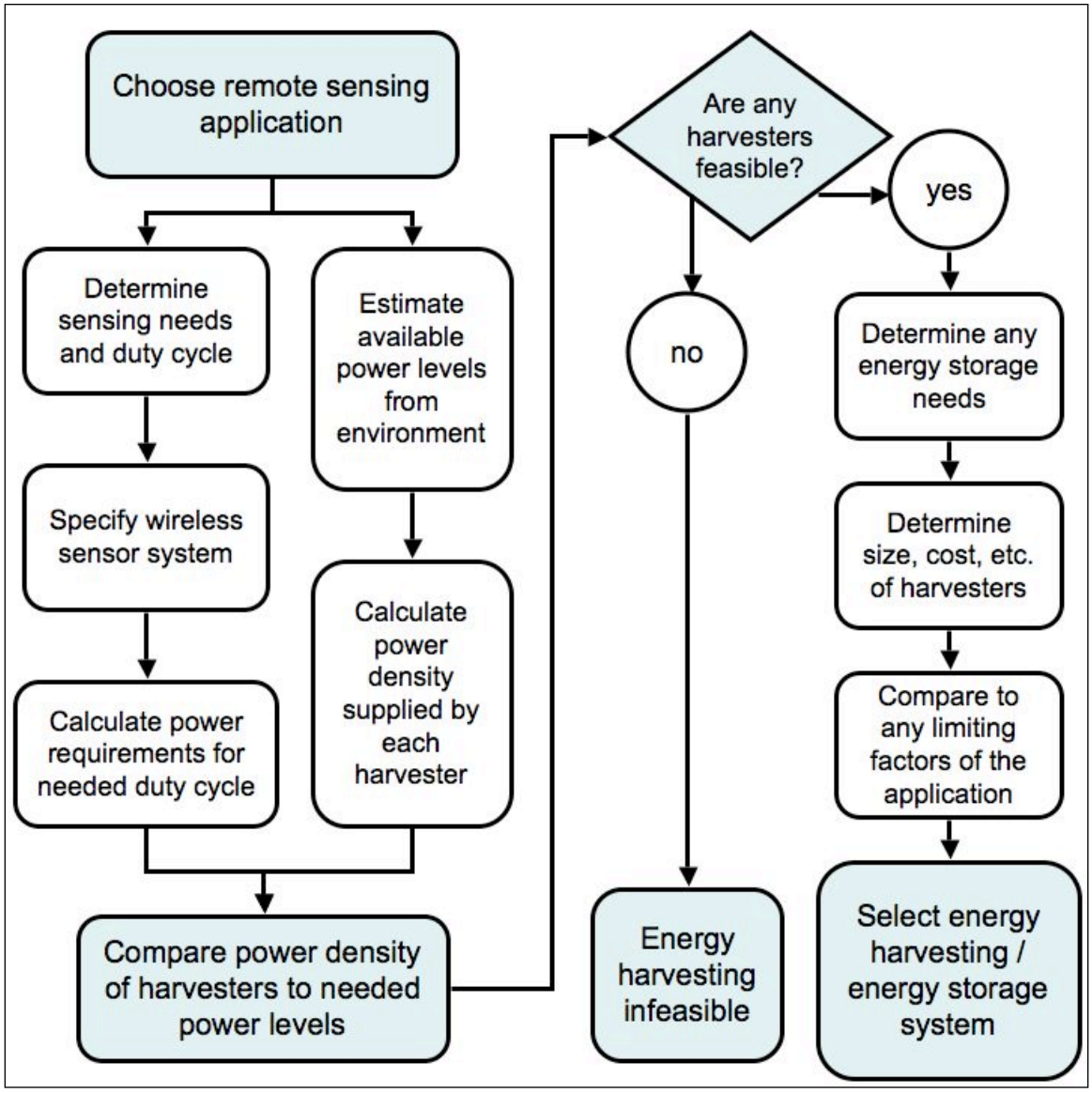

Figure 3.1 Power feasibility methodology for energy harvesting in WSN applications

3.3 POWER REQUIREMENTS

Following the methodology described above, we determine the power requirements for the system by (a) specifying the sampling and transmission rates for the sensor node, (b) determining the rated power consumption for a specific example sensor system, and (c) calculating the peak and average power consumption at the desired duty cycle.

3.3.1 Sensing Needs and Desired Duty Cycles

When monitoring a structure such as a bridge, a variety of sensing needs may exist. For example, to measure long-term strain or crack propagation, it may be appropriate to take a sample periodically at a rate of once per hour, day, or even month. On the other hand, to measure vibration signatures or continuous strain energy, it may be more appropriate to sample in real-time at tens or hundreds of hertz. Finally, some of the nodes may need to be active all the time so they can act as routers, passing information from low-power end nodes back through the network for data processing or storage.

We will examine the power requirements for a sample wireless sensor node at the following duty cycles:

- Router mode (radio always on)
- 30 Hz sampling, with radio transmission hourly
- One sample and radio transmission per second
- One sample and transmission per minute
- One sample and transmission per hour
- One sample and transmission per day
- One sample and transmission per month

External sensors will also require power during each sample cycle. However, in some cases, this additional load can be neglected. For example, one typical sensor configuration is four strain gauges arranged in a Wheatstone bridge. By using high resistance strain gauges, a low supply voltage, and a very brief sample pulse, the power draw can be minimized. Using four 1 kΩ gauges, a supply voltage of 2 V, and sample duration of 1 ms, the additional load would be 4 mW during the 1 ms pulse. For a 60 second sample interval, this sensor load only adds 4 μW to the average power each cycle, which as we will see is less than 1% of the overall power required by the wireless node at that sample interval. In this chapter, we will only consider the power requirements of the wireless node itself, with the understanding that the additional needs of specific sensors can easily be added to the analysis once they are known.

3.3.2 Rated Power Draw of Example System

The example wireless sensor node chosen for this chapter is the National Instruments WSN-3202 device, shown in Fig. 3.2. The WSN-3202 can be run from either a 24-V DC source or from 4 AA batteries (6 V DC, total). The manufacturer has documented typical power consumption at two duty cycles: one sample every second and one sample every 60 seconds (Table 3.1).

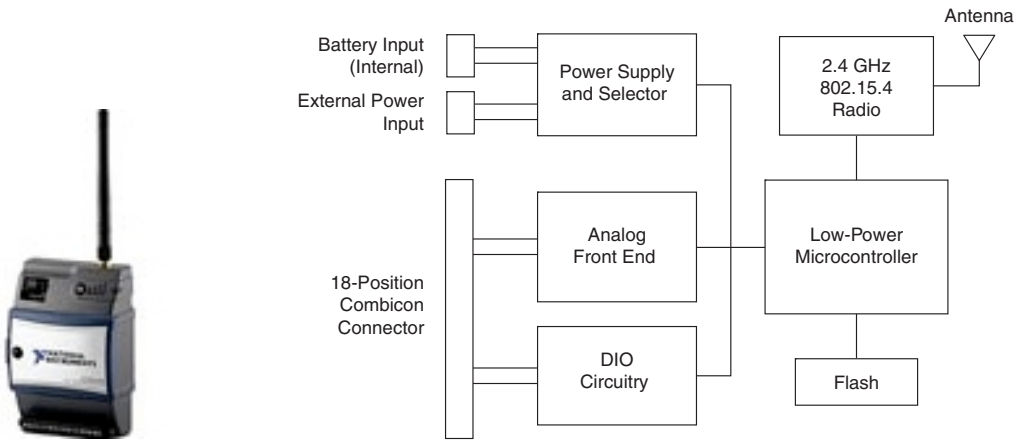

Figure 3.2 National Instruments WSN-3202 module (Wireless, 2011)

Table 3.1 Rated power consumption of example node (National Instruments, 2009)

Input voltage	**1 sample / second**	**1 sample / minute**
6 V DC Input	13.3 mW	0.5 mW
24 V DC Input	33 mW	16 mW

Naturally, for our specific application, we will want to minimize the power draw, so we would want to use the lower voltage. The node is actually capable of performing with an input voltage of as low as 3.6 V with customization, but for the sake of consistency we will use a standard input of 6 V DC throughout the remainder of the chapter.

Figure 3.3 shows a waveform of the current draw during a sample cycle, using 6-V battery power and a 1-second sample interval. The power usage is broken down by activity in Table 3.2.

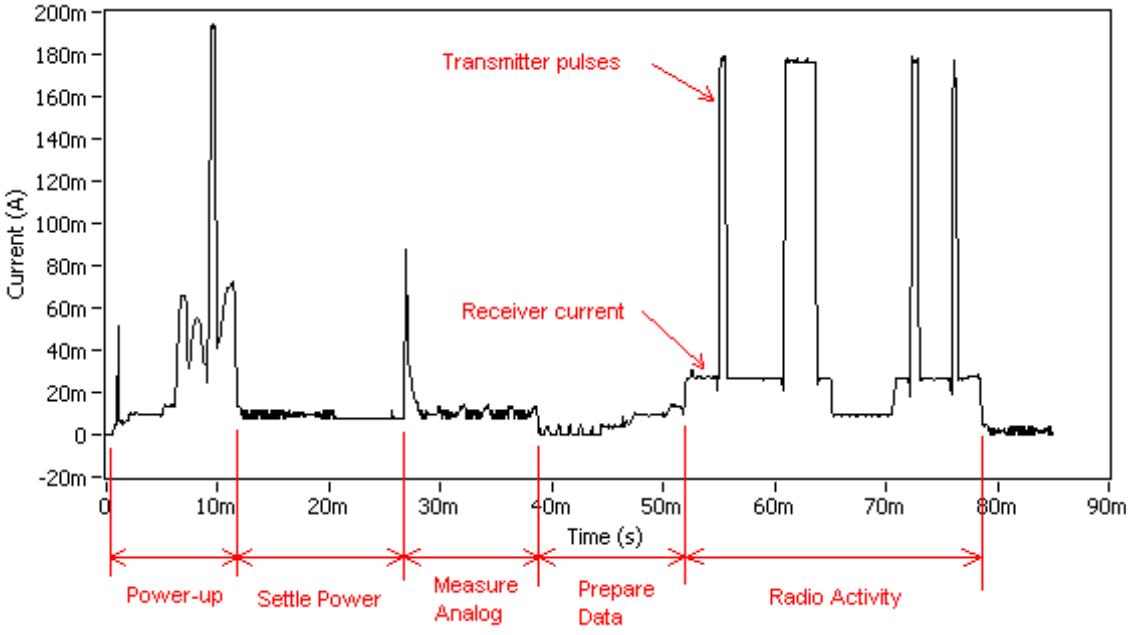

Figure 3.3 Waveform of power consumption during sampling (National Instruments, 2009)

Table 3.2 Break-down of power consumption (National Instruments, 2009)

Function	**Power (mW)**	**Δt (ms)**
Power-up	200	12.4
Settle power	52.5	14.5
Measure analog	73.4	13.0
Prepare data	37.9	12.0
Radio activity (transmit/ack data)	207	29.0
Total – active period	154 (average)	81
Sleep period	0.3	variable

3.3.3 Power Draw at Desired Duty Cycles

With the power consumption for each activity in the sample cycle known, we can extrapolate the overall power draw over different sample periods as well. We assume for these calculations that for typical operation, where each sample cycle includes both a measurement and a radio transmission, the waveform for the active period remains the

same, with the duration of the sleep period the only change. Table 3.3 shows an example of this calculation, where an hourly sample rate is considered.

In this scenario, the average power draw is approaching the lower bound of 0.3 mW imposed by the level of power needed for the current "sleep" mode. Increasing the time between samples beyond this point will not yield any further energy savings. To decrease the average power required, we must now focus on decreasing the power level while the system is idle.

Table 3.3 Power consumption at 1 sample per hour

Function	**Power (mW)**	**Energy (mJ)**	**Δt (ms)**
Power-up	200	2.5	12.4
Settle power	52.5	0.8	14.5
Measure analog	73.4	1.0	13.0
Prepare data	37.9	0.5	12.0
Radio activity	207	6.0	29.0
Sleep period	0.3	1,008.0	3,599,919
Complete Cycle	0.3	1,018.6	3,600,000

The NI WSN-3202 is currently programmed to use the Zigbee wireless protocol for communicating with other nodes in the network. The Zigbee protocol includes a "heartbeat" signal that is transmitted approximately once per minute. This precludes the possibility of using an extended "deep-sleep" mode between measurements. National Instruments is currently investigating the possibility of reprogramming the node to allow for such a deep-sleep mode, which would draw far less power than its current configuration. For comparison, the Ambiomote24 (Ambiosystems, 2010) is a similar system that can go into a deep-sleep mode consuming only 9 μW (Sazonov, 2004). If a similar result could be obtained with the example node, the overall power consumption would approach this new limit with sample intervals of a day or more. Completely

turning off the module between samples would result in even more energy savings. However, it is more likely that some functions, like the clock, would need to be on continually to ensure proper timing of the samples.

In some instances, it may be necessary to take measurements more frequently than once per second or minute. To measure vibration, cyclical strain, and other time-dependent characteristics, we would want to record continuously for an extended period of time. As an example, we may want to take samples at a rate of 30 Hz, perform on-chip analysis, and then send a sum or other data analysis or transformation once per hour. The power consumption in this case, sometimes called "rainflow analysis," is outlined in Table 3.4.

Table 3.4 Sampling at 30 Hz, then transmitting once per hour

Function	**Power (mW)**	**Energy (mJ)**	**Δt (ms)**
Power-up	200	N/A	N/A
Settle power	52.5	115,288	2,195,959
Measure analog	73.4	103,054	1,404,000
Prepare data	37.9	0.5	12.0
Radio activity	207	6.0	29.0
Sleep period	0.3	N/A	N/A
Complete Cycle	60.7	218,348	3,600,000

In this scenario, the node spends a large part of the cycle measuring data. There is not enough extra time to cycle through the sleep/power-up functions repeatedly, so the node spends most of the rest of the time in the "settle power" function. At the end of each hour, the node prepares the data and sends a single data transmission. This scenario results in an overall power consumption of 60.7 mW, much higher than our calculations for previous sample rates.

The average power consumption for a variety of sample rates (including the ones discussed) is shown in Fig. 3.4. Each sample rate has three bars showing scenarios where (a) the node uses its current configuration of staying on and consuming 0.3 mW when idle, (b) the node enters a "deep-sleep" mode that only consumes 9 μW, and (c) the node turns completely off between samples and consumes no power. In addition to the sample rates described previously, the chart below includes a router mode, where the radio is transmitting continuously, and sample rates of once per day and once per month.

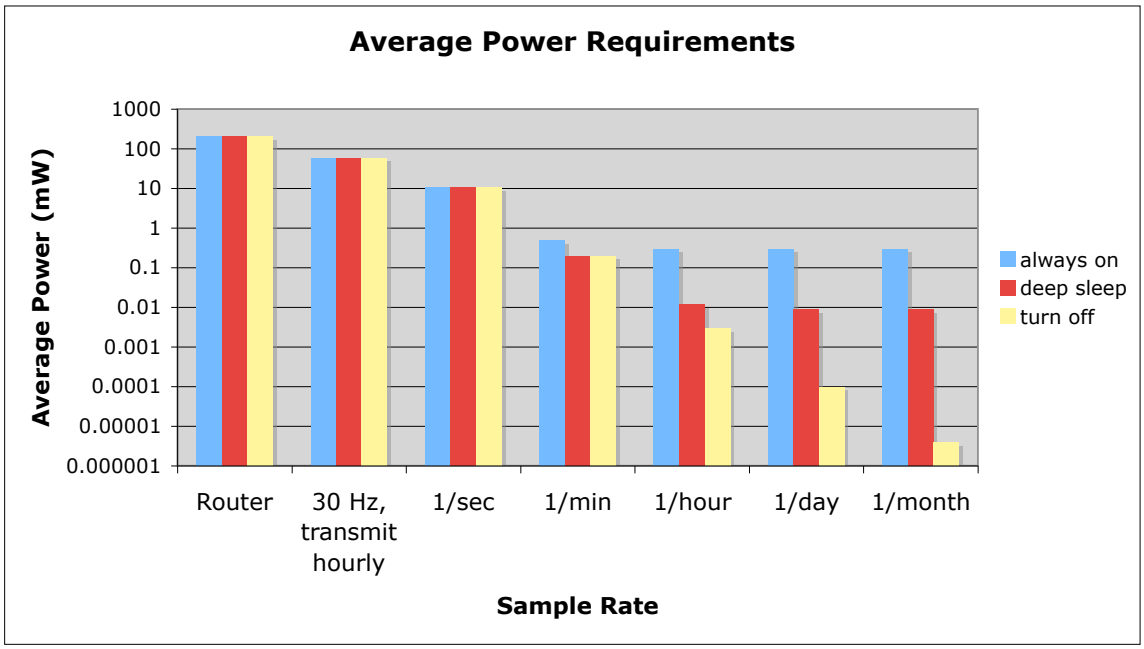

Figure 3.4 Average power consumption by sample rate

To consider this information from a different perspective, it can be translated into the equivalent energy consumption for one year of operation. Figure 3.5 shows the energy required for each scenario. In this figure, the 30 Hz sample rate is examined in two ways. Continuous monitoring throughout the entire year will usually not be necessary. Instead, the node may monitor continuously for a limited amount of time, then

operate at a lower sample rate the remainder of the year. In Fig. 3.5, numbers are given for the scenarios of (a) running at 30 Hz for 10 weeks, then at once per hour the rest of the year, and (b) running at 30 Hz for 2 weeks, then hourly for the remainder.

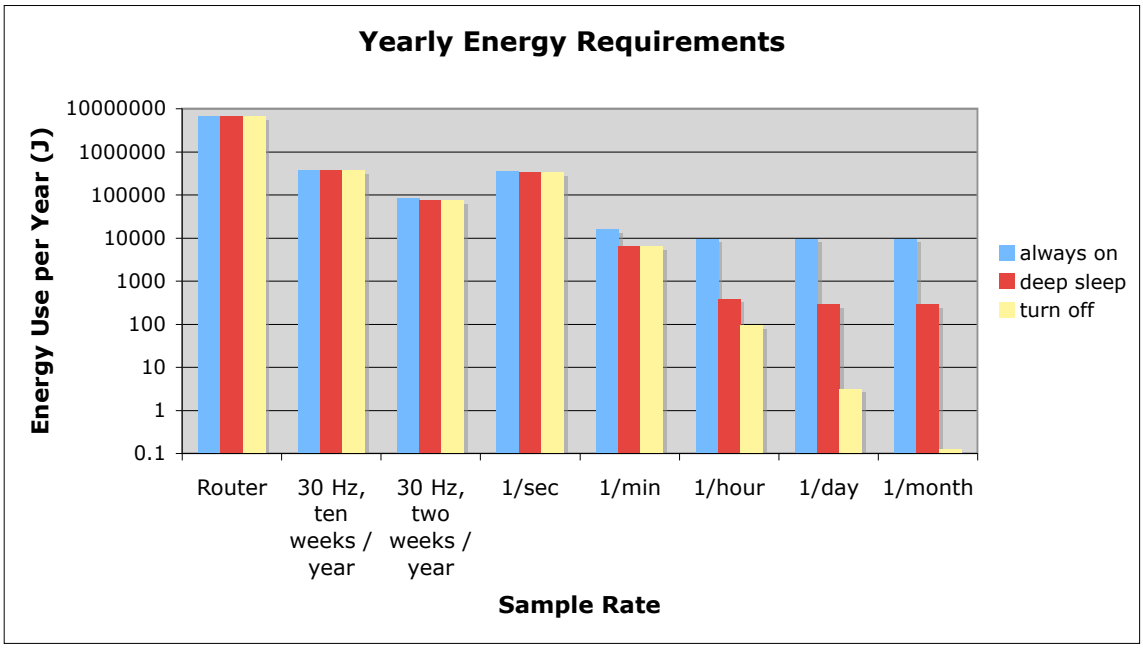

Figure 3.5 Yearly energy consumption by sample rate

The power and energy consumption of each sample rate is shown more fully in Appendix B. We can see that there is a wide range of power levels necessary for different sample rates, from about 200 mW to operate as a router on the high end to 0.3 mW, or possibly even lower, as the sample rate decreases. To examine the feasibility of powering this node with energy harvesting technology, we will focus on three typical scenarios: running the WSN-3202 in router mode (high power), running at 30 Hz for 10 weeks and once per hour the rest of the year (medium power), and taking measurements once per hour the entire year (low power). In addition, we will also consider the possibility of lowering power requirements by sampling once per day and implementing a deep-sleep

mode (like the Ambiomote24), as well as the much higher power required to power a central gateway/modem (such as a CompactRIO or NI 9792 gateway node). The power and energy requirements for these five scenarios are summarized in Table 3.5.

Table 3.5 Power and energy consumption for test scenarios

Scenario	Description	Average Power	Yearly Energy	
Router mode	Radio always transmitting	207 mW	6.53 MJ	1.81 kWh
Rainflow mode	Sampling at 30 Hz (10 weeks) / hourly rest of year	60.7 mW (30Hz) 0.3 mW (hourly)	375 kJ	104 Wh
Hourly mode	One sample / hour	0.3 mW	9.47 kJ	2.63 Wh
Deep sleep mode	One sample / day (with deep sleep)	0.009 mW	284 J	79 mWh

Scenario	Description	Average Power	Yearly Energy	
Gateway	CompactRIO or NI 9792 gateway node	10 W	315 MJ	87.6 kWh

3.4 Independent Verification of NI Measurements

The measurements reported by National Instruments were verified by conducting a similar experiment with our own NI hardware. This was done by measuring the current draw in an NI WSN-3202 node as the node measured and transmitted at a 5-second duty cycle (its default setting). A 10-Ω resistor was placed in series with the 4 AA batteries (6 V DC total) as they powered the node. The node was configured to take a measurement of the voltage across the batteries every five seconds in order to have data to transmit.

While the node was operational, the voltage across the 10-Ω resistor was measured at 1 kHz by a CompactDAQ and recorded in LabVIEW. By dividing the recorded voltage by the added resistance, the current in the circuit was measured, resulting in the current waveform in Fig. 3.6. Figure 3.7 focuses on a single active period

and reveals a waveform similar to that provided by National Instruments, both in shape and magnitude. By multiplying the current by the total voltage across the load (measured consistently as 5.9 V), the resulting power waveform was calculated (Fig 3.8-3.9).

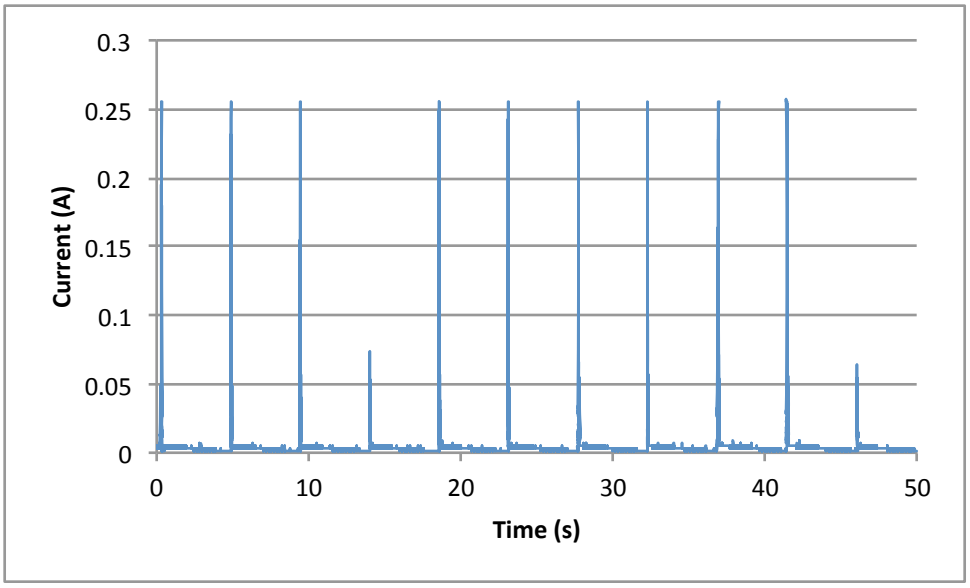

Figure 3.6 Measured current to NI WSN-3202 at 5-second duty cycle

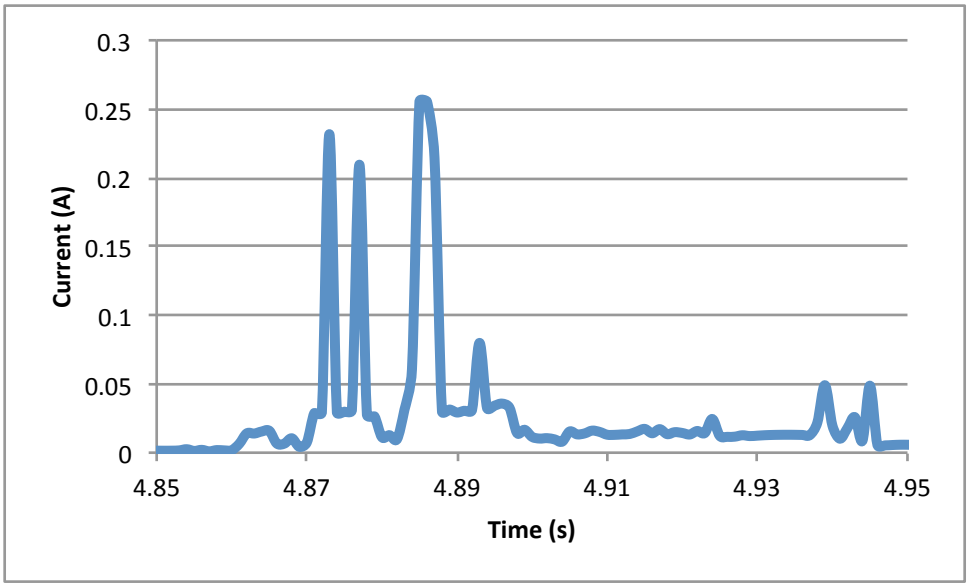

Figure 3.7 Current measured during one active period (10-Ω resistor)

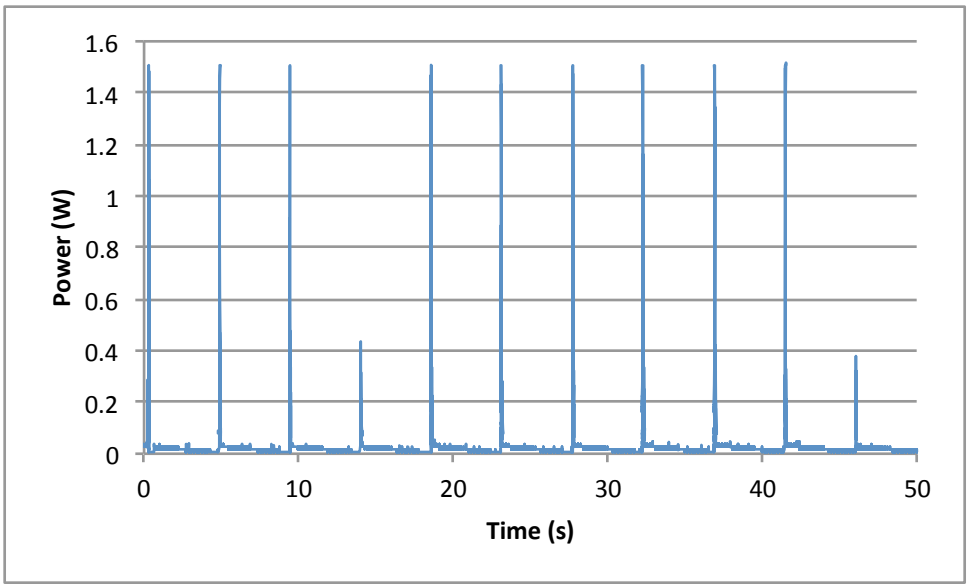

Figure 3.8 Measured power to NI WSN-3202 at 5-second duty cycle

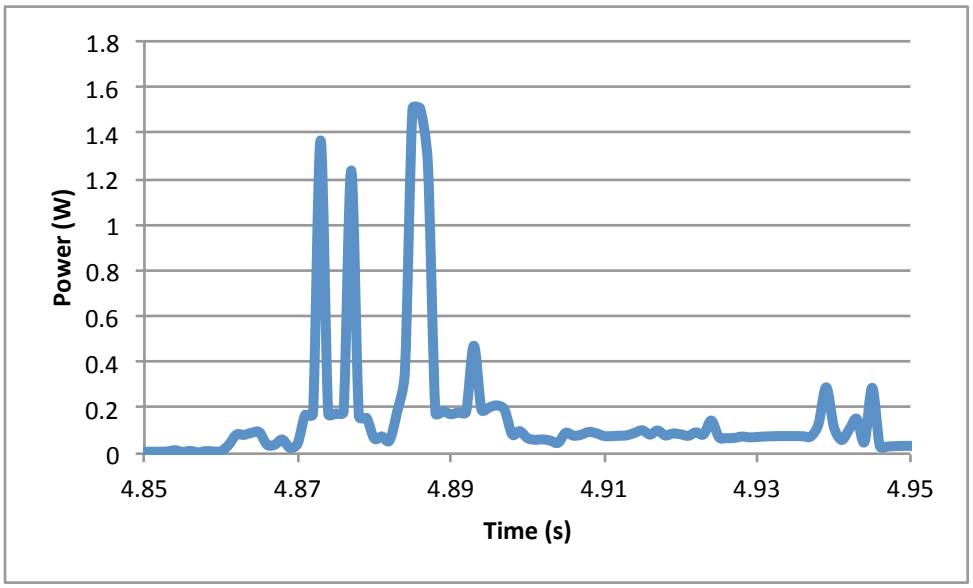

Figure 3.9 Power measured during one active period (10-Ω resistor)

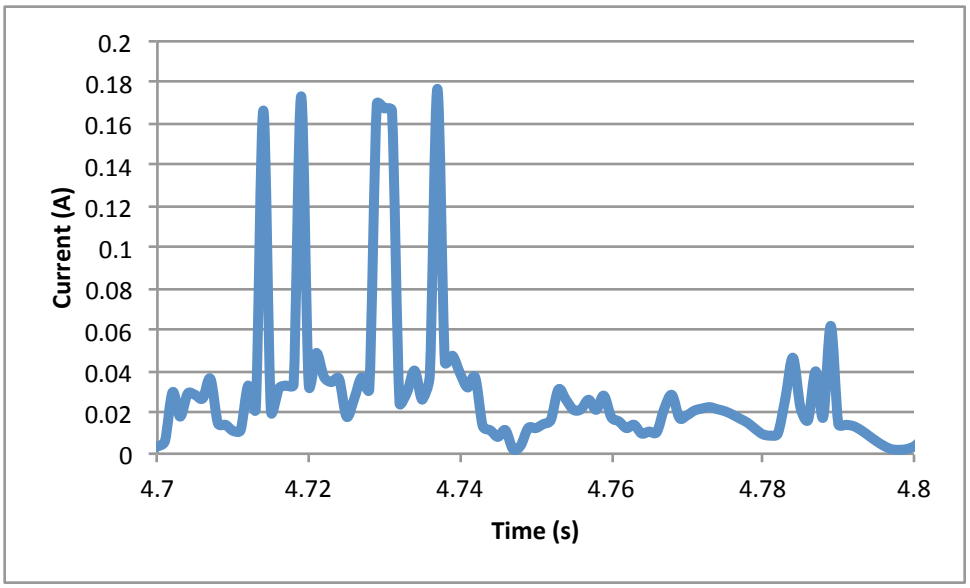

Figure 3.10 Current measured during one active period (1-Ω resistor)

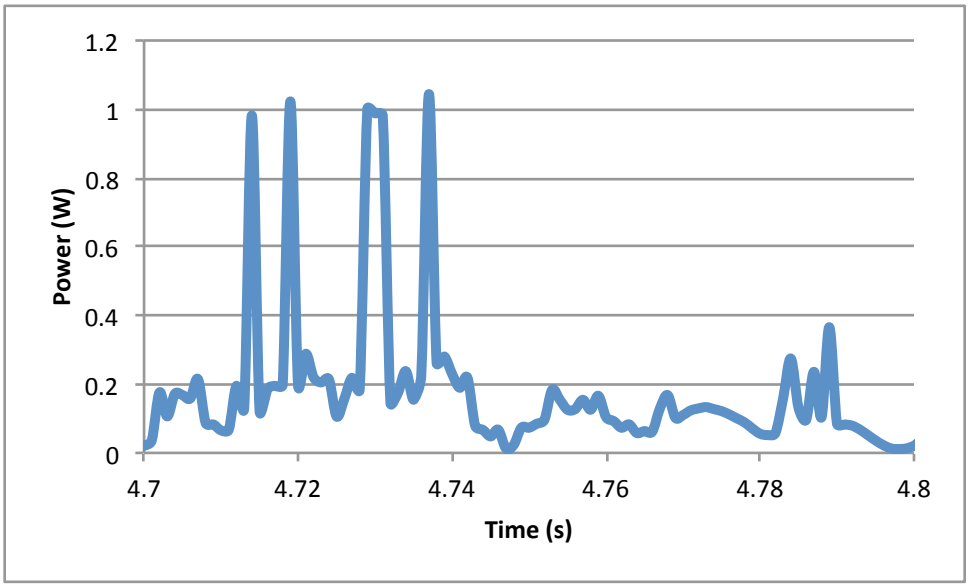

Figure 3.11 Power measured during one active period (1-Ω resistor)

The experiment was repeated using a 1-Ω resistor, with similar results. The measured voltage was one tenth of that measured with the 10-Ω resistor. This yielded a current and power draw roughly equivalent to that of the first test (Fig. 3.10-3.11). Using

the 1-Ω resistor resulted in a slightly lower peak current during the power-up and radio functions, more closely matching the waveform reported by NI. This lower impedance also exhibited a higher current during the low power and sleep functions, but this appears to have resulted from sinusoid noise in the testing equipment.

Finally, the wireless sensor node was also tested with increased interference blocking the signal. The intent was to determine if lower signal strength would lead to an increase of power usage, either through routing more power to the radio transmission or by transmitting more frequently. By placing the sensor node in a separate room from the gateway node and placing it within a metal enclosure, we were able to lower the measured signal strength from 99% to 45%. Even at this level, power usage increased only slightly, with peak current increasing from 0.17 A (with the 1-Ω resistor) to 0.19 A. Very low signal strength may lead to a noticeable increase in power consumption, but it should be minor compared to the overall power requirements of the system.

3.5 Conclusions From WSN Power Requirements

Power requirements for the NI WSN-3202 vary significantly with different duty cycles. The average power requirements of primary interest are 207 mW for router operation, 60.7 mW for measurements at 30 Hz, and 0.3 mW for measurements once per hour. Typical usage may involve 30-Hz measurements for 10 weeks and hourly measurements the remainder of the year, resulting in a yearly energy usage of 375 kJ / 104 Wh (long-term average power of 11.9 mW). These calculations are based on current draw measured by National Instruments with a 60-second duty cycle. Independent measurements at a 5-second duty cycle were made to validate the NI measurements;

however, actual power usage at these duty cycles may vary slightly from the predicted values.

In addition, a central gateway node will also be needed, which would require a constant power source of approximately 10 W. Due to its much higher power requirements, it is not the primary focus of this dissertation. Depending on the location, this gateway node could be powered by a large solar panel. If this is not possible, then grid power or batteries would be required. This is not, however, a major issue, as the location of the central gateway can be selected based on the required power input.

Chapter 4: Power Feasibility in a Bridge Environment

4.1 Discussion of Energy and Power Density

With a better understanding of the power needs of the system, we can compare these requirements to the power available from energy harvesting. For most energy-harvesting technologies, power is directly related to the size of the harvester. For example, a solar panel two square feet in area will produce twice the power of a one-square-foot panel of the same type. Because of this scalability, it is most convenient to consider the output in terms of *power density* or *energy density*.

Power density normalizes the power output by length, area, volume, or mass, depending on what is most appropriate. For example, the power density of a solar panel would be expressed in units of watts per unit area. Energy density expresses the normalized energy production in joules per unit length, area, volume, or mass. Energy density per year is a convenient way to consider the long-term energy production of energy harvesters, which often are irregular in their levels of power generation.

Many technologies exist to scavenge energy from the surroundings. We consider three of the most common and well developed: photovoltaic cells, wind turbines, and vibration harvesters.

4.2 Solar Energy: Photovoltaic Cells

Solar energy is becoming a reliable alternative to batteries or grid power in many applications. Solar-powered sensors have recently been installed on bridges in Corinth, Greece and New London, Connecticut (MicroStrain, 2007). Photovoltaic cells are the most common method for capturing solar energy, with higher power density than most

other energy harvesting technologies (Raghunathan, Kansal, Hsu, Friedman, & Srivastava, 2005).

4.2.1 Solar Data from Literature

Electromagnetic radiation from the sun reaches Earth with a flux density of approximately 1,366 W/m^2, depending on the Earth's distance from the sun (Wilson & Mordvinov, 2003). As the radiation passes through the atmosphere, it is attenuated by about 17% through scattering and absorption, particularly by water vapor. In addition, the light must pass farther through the atmosphere as latitude increases, leading to what is called the "air mass" effect. Thus, the power available even from direct sunlight varies considerably with season, latitude, and altitude, even before weather is considered. Typical baseline irradiances (the power per unit area at a surface) range from 1,130 W/m^2 in the tropics to the mid 900 W/m^2 in high latitudes. The international standard irradiance is set at 1,000 W/m^2, which corresponds to an air mass of 1.5 and is similar to the conditions in San Francisco in the spring.

Irradiance is also greatly influenced by the weather and environment. Clouds may obscure light, or they could reflect light down and actually make it brighter. Reflections from snow, water, sand, and man-made structures can also influence the end effect. Nearby structures or geographic features may shade the area. The following estimates are provided to give an idea of expected irradiance in different weather, assuming a baseline irradiance of 1,130 W/m^2 (Magee, 2010):

- Clear, sunny skies – 1,130 W/m$^{2:}$
- Thin cirrus clouds – 1,000 W/m^2
- Thick cirrus clouds – 750 W/m^2
- Thin cloud cover – 500 W/m^2

- Thick cloud cover – 250 W/m^2
- Cloud cover sufficient to eliminate shadows – 100 W/m^2
- Tall broken clouds reflecting light downward – 1,500 W/m^2

To combine average behavior of all these effects for a given location, the idea of "insolation" is often used. Insolation relates the total solar energy delivered over the course of a day to an equivalent number of hours of sunlight at the standard irradiance of 1,000 W/m^2. For example, a given location may have eight hours of daylight, with irradiance levels ranging from 1 W/m^2 at dawn and dusk to 1,100 W/m^2 at noon. The total energy gathered over the course of the day might be equivalent to four hours of sunlight at 1,000 W/m^2. Insolation is typically calculated for both summer and winter, and can range in the US from 0.21 hours (Anchorage, AL in January) to 7.77 hours (Phoenix, AZ in June), with yearly averages ranging from 2 hours (Alaska) to 6 hours (Hawaii) (Solar Panels Plus, 2007). Insolation in central Texas ranges from 4.65 hours in the winter to 5.88 hours in the summer (Advanced Energy Group, 2005).

4.2.2 Measurements on Existing Bridges

Typical solar irradiation levels from the literature were compared to levels around several bridges in central Texas. To make these measurements, a Mastech LX1010B lux meter was used. At each bridge, measurements were taken at several locations in both the sun and shade, with the average measurements at each location recorded in lux. Lux is a unit of measuring perceived brightness, which is dependent on the frequency of the light measured. To convert the lux measurements to watts per square meter, a standard conversion for sunlight was assumed at 93 lux per W/m^2 (Littlefair, 1988). These converted values are given in Table 4.1.

Table 4.1 Solar irradiation on central Texas bridges

I-35/US-290 Bridge, Austin TX, 10/10/09, 9:00 AM	
Direct sun, sensor facing sun	1,100 W/m^2
Direct sun, sensor facing up	600 W/m^2
Direct sun, facing away from sun	200 W/m^2
Shade, open area under bridge	100 W/m^2
Shade, 5-10 inches from structure	30 W/m^2
I-45 Bridge, Conroe TX, 11/17/09, 2:00 PM	
Direct sun, sensor facing sun	1,132 W/m^2
Direct sun, sensor facing up	824 W/m^2
Direct sun, facing away from sun	165 W/m^2
Shade, open area under bridge	55 W/m^2
Shade, 5-10 inches from structure	22 W/m^2
US-71/US-183 Bridge, Austin TX, 3/9/10, 2:00 PM	
Direct sun, sensor facing sun	1,132 W/m^2
Direct sun, sensor facing up	1,121 W/m^2
Direct sun, facing away from sun	102 W/m^2
Shade, open area under bridge	15 W/m^2
Shade, 5-10 inches from structure	3 W/m^2
I-35/I-410 Bridge, San Antonio TX, 8/17/10, 2:00 PM	
Direct sun, sensor facing sun	1,110 W/m^2
Direct sun, sensor facing up	421 W/m^2
Direct sun, facing away from sun	151 W/m^2
Shade, open area under bridge	112 W/m^2
Shade, 5-10 inches from structure	54 W/m^2

These measurements align well with the standard irradiance level of 1,000 W/m^2, with direct sunlight at these bridges averaging about 1,100 W/m^2. It can also be seen that irradiance drops off rapidly in the shade, down to as little as 0.3% of the maximum level.

4.2.3 Theoretical Power Density

The theoretical power available from a PV cell can be determined from the light irradiance available (E, in watts per square meter), the area of the cell (A_{cell}, in square meters), and its energy conversion efficiency (η):

$$P_{\max} = \eta E A_{cell} \qquad \text{Eq. 4.1}$$

The standard test condition for measuring efficiency is an irradiance of 1,000 W/m^2. Efficiencies can range from 5% to 40% (Woyte, Nijs, & Belmans, 2003), with most commercially available cells falling around 8-15%. For a cell with 10% efficiency, this translates into an approximate power density of 100 W/m^2, or 10 mW/cm^2.

Because of the aforementioned variations in irradiance with weather and seasons, insolation must also factor into the equation. Austin, Texas has an insolation of 5.88 hours during the summer and 4.65 hours during the winter (Advanced Energy Group, 2005). Combining the winter insolation with the previous calculation yields the following equation:

$$\text{Power Density} = P/A = \eta Q_{\text{insol.}} E = (0.10)(\tfrac{4.65}{24})(1{,}000\ \text{W/m}^2) \qquad \text{Eq. 4.2}$$

A solar cell with 10% efficiency and 4.65 hours of insolation would be able to provide a yearly average of at least 1.9 mW/cm^2. This translates into a yearly energy production in the range 60 kJ (17 Wh) per square centimeter.

4.2.4 Power Feasibility of Solar Energy

Comparing this energy production to the three primary duty cycle scenarios listed in Table 3.5, we find that the hourly-measurement configuration requires 9.47 kJ per year. This could easily be provided from just one square centimeter of PV paneling, provided it received direct sunlight and had sufficient energy storage to power the sensor through the night. To continuously provide peak power for the 30 Hz duty cycle (60.7

mW) would require at least 32 cm^2, but because the duty cycle is only needed for part of the year, a smaller panel of 7 cm^2 could be used and excess energy stored. To run the sensor in router mode, a panel of at least 110 cm^2 and direct sunlight would be required.

Because of the constraints in location on the bridge, it is highly likely that PV panels would not be exposed to direct sunlight the entire day. Unless a tracking system is included in the hardware, the panels would, at best, receive full sunlight at varying angles throughout the day, with many installations encountering shade for at least part of the day as well. Solar irradiance in the shade averages in the neighborhood of 10-100 W/m^2, meaning that the power out could be cut by a factor of ten to one hundred. In addition, the underlying physics of photovoltaics makes panel efficiency drop under partial shading or low lighting (Deline, 2009; Hande, Polk, Walker, & Bhatia, 2007; Woyte, Nijs, & Belmans, 2003). This could necessitate the use of larger panels (up to 1 m^2), but even these would often be within the feasible scope for use on bridges. Table 4.2 shows the estimated panel sizes needed for the power requirements of interest, assuming 10% efficiency, no shading, and a winter insolation of 4.65 hours in central Texas.

Table 4.2 Solar panel sizing for powering WSN on central Texas bridges

	Gateway (10 W)	Router (207 mW)	Rainflow (11.9 mW)	Hourly (0.3 mW)
Minimum panel size	5,260 cm^2	110 cm^2	7 cm^2	1 cm^2

4.3 WIND ENERGY: TURBINES

Wind energy has long been used as a power source in areas where reasonably constant behavior could be expected, such as on rural farmland, expansive plains, and coastlines. However, the possibility of using wind turbines in an urban setting has only recently received focus. Urban wind harvesting is often seen as a complement to solar

power: times when solar irradiance is lower (e.g., night time, storms, winter) are the same times when wind speed typically increases (SECO, 2007).

4.3.1 Wind Data from Literature

As will be shown in Section 4.3.3, wind power is proportionate to the cube of wind speed. Because of this, the vast majority of power is harvested from short bursts of higher wind speed. For example, one report discovered that half of the captured energy at their site arrived in just 15% of the operating time (Global, 2002). Such high velocities are most likely to be consistently maintained in open, rural areas and at greater heights above the ground and nearby structures. Thus, large capacity wind turbines are almost exclusively found on top of large towers in open spaces.

This contrasts significantly from the environment of highway bridges and other urban situations. Inside bridges and between tall buildings, an "urban canyon" effect is often experienced, where wind is channeled into a small path and wind speed is elevated (Chang & Meroney, 2003). However, this wind is highly turbulent, intermittent, and unpredictable. Such gusts can be dangerous if they exceed predicted wind behavior, possibly damaging or even tearing apart the turbines (Olson W., 2010). At other times, wind levels may be unexpectedly low, preventing the turbine from engaging and generating any power. In general, a wind speed of at least 7 mph (3.1 m/s) is needed to activate most wind turbines (Wind Speed, 2008). For comparison, the average wind speed on the ground in Austin, Texas is 8 mph (3.6 m/s), with maximum levels often around 25-30 mph (11-14 m/s) (Wolfram Alpha, 2011).

To make the most of available wind in an urban environment, it is often recommended to place a wind turbine 30 feet (9 m) higher than any surrounding structure. Successful implementation of turbines in such a configuration includes

wind/solar-powered light poles (Green Column, 2009). Turbines not elevated above surrounding structures, such as those placed right on residential roofs, are often not effective (Leake, 2006). However, even these "micro" wind turbines are typically several feet in diameter and rated for several kilowatts. On a highway bridge, wind speeds may be low and sporadic, but the required power output is also much lower.

4.3.2 Measurements on Existing Bridges

We measured wind speed at three bridges in central Texas. The first bridge, the I-35/US-290 Interchange in Austin, Texas, extends over an empty grassy median as it connects the two highways, so there is little limitation on where on the structure to attach a wind turbine. Wind speed measurements were taken near the bridge with an Inspeed Vortex handheld anemometer on October 10, 2009 at 9:00 AM. Wind speeds were typically 4-12 mph (1.8-5.4 m/s), with the highest speeds right off the edge of the upper deck.

Measurements were taken for several hours on the I-45 bridge in Conroe, Texas on November 17, 2009. These measurements were taken by three Young Wind Monitor anemometers at three locations in the girders of the bridge. The data was logged by a National Instruments CompactRIO. Because the bridge extends over traffic, the anemometers were positioned flush with the bottom of the girders, not extending below the structure. Figure 4.1 shows the recorded wind speeds over approximately six hours. Figure 4.2 shows periodic measurements taken at the Conroe airport nearby. These figures indicate that wind behavior under the bridge corresponded well with recorded behavior in the open nearby, with speeds reduced by about 5 mph (2.2 m/s). With wind speed often between 4 and 8 mph (1.8-3.6 m/s), special design may be needed to encourage a wind turbine to engage at such speeds.

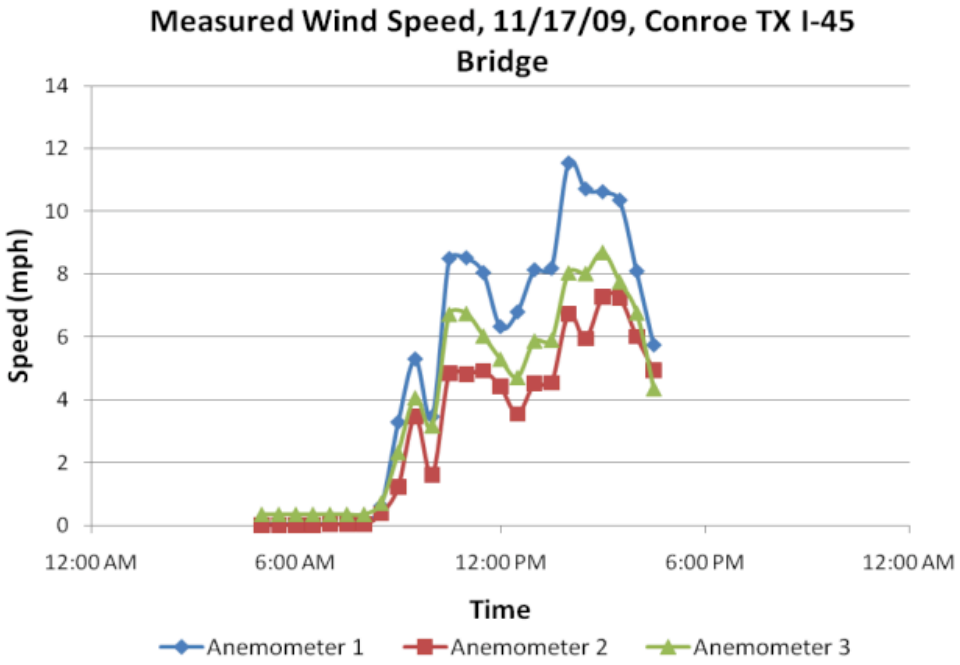

Figure 4.1 Wind measurements on I-45 Bridge, Conroe TX

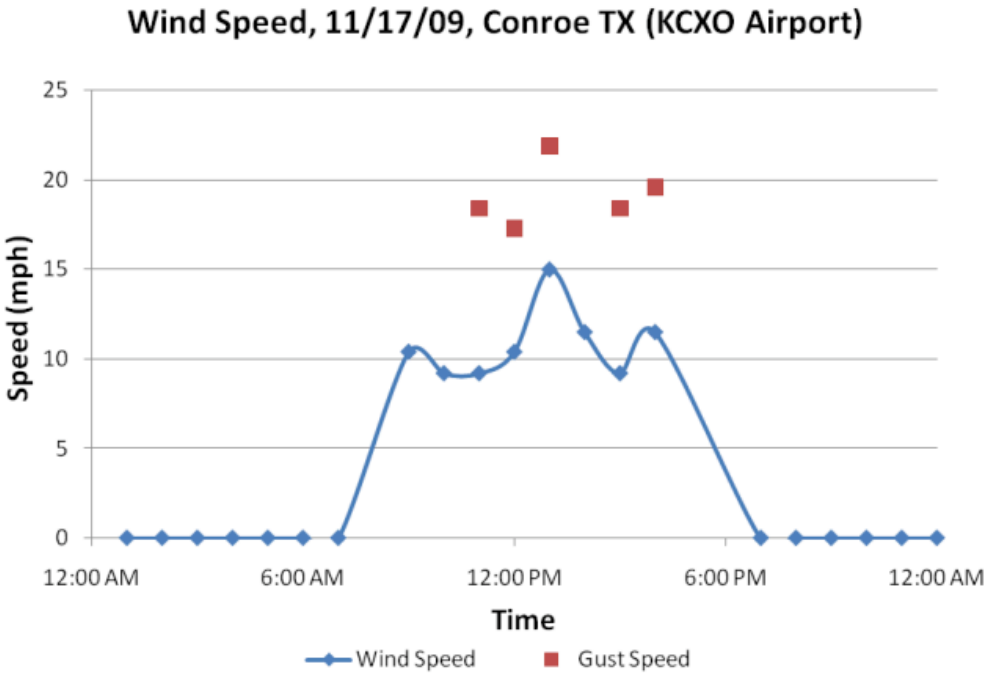

Figure 4.2 Weather Underground data at Conroe airport (Weather, 2009)

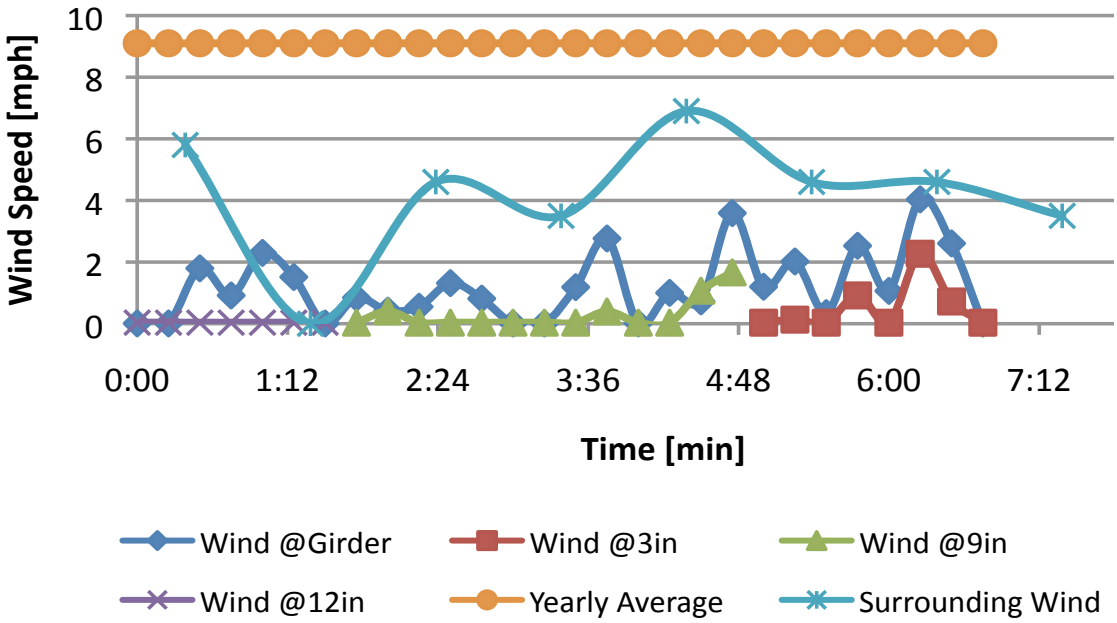

Figure 4.3 Wind measurements on I-35/I-410 Bridge, San Antonio, Texas

A third test was conducted at the I-35/I-410 Bridge in San Antonio, Texas on August 17, 2010. Seven hours of measurements were taken in the same manner as on the bridge in Conroe (Fig. 4.3). In this test, two anemometers were placed near each other, with one positioned flush with the bottom of a girder and the other placed up between the girders at various heights. Wind speed at this location was significantly lower than Conroe, with wind at a nearby weather station at 4-7 mph (1.8-3.1 m/s) and wind at the bottom of the girder only reaching 4 mph (1.8 m/s). This test also showed that wind speed drops off rapidly as one goes up inside the girders. Wind harvester design should allow the turbine blades to be as low as possible while still meeting safety constraints for the bridge.

4.3.3 Theoretical Power Density

The theoretical power available from a wind turbine can be determined from the air density (ρ), turbine area (S), intake air velocity (v_1), and the coefficient of performance (C_p):

$$P = \tfrac{1}{2}\rho S v_1^{\,3} C_p \qquad \text{Eq. 4.3}$$

The theoretical maximum to the coefficient of performance, known as the Betz Limit, is 0.593. Many commercial products have coefficients in the range of 0.3-0.5. As is evident by the governing equation, the power is proportional to the cube of the wind speed, meaning that a great deal more power is available at higher velocities than lower velocities. If we were to use a coefficient of 0.3, the power density of a turbine at an air velocity of 2 m/s (4.5 mph) would be only 0.14 mW/cm^2, but a velocity of 5 m/s (11 mph) would yield 2.25 mW/cm^2, and 10 m/s (22 mph) would yield 18 mW/cm^2. Figure 4.4 shows the relationship between wind speed and output power, again assuming a coefficient of performance of 0.3.

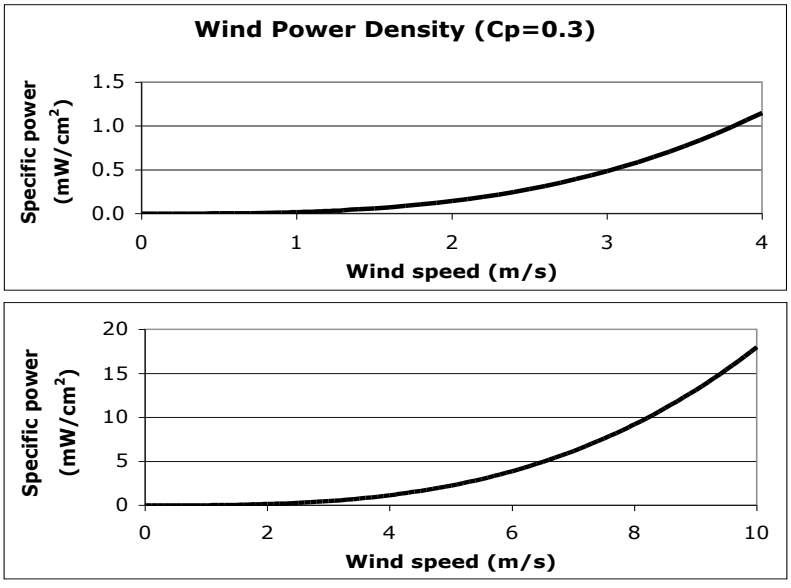

Figure 4.4 Power density of turbine by wind speed

This result is also highly dependent on the constancy of the wind in the area of interest. Studies of one bridge at multiple points and elevations revealed a distribution peaking at 5 m/s (11 mph), with speeds generally between 2 and 15 m/s (4.5-34 mph) (Jo, Park, & Kim, 2005). On the other hand, studies of several micro-turbines installed in initially promising locations showed the same distribution when there was wind, but the turbines were also idle 30-70% of the time (Corbus, Newcomb, Baring-Gould, & Friedly, 2002).

4.3.4 Power Feasibility of Wind Energy

If, for simplicity, we assumed a relatively constant wind speed of 5 m/s (11 mph) and a coefficient of performance of 0.3, the power density available from a wind turbine would be 2.25 mW/cm^2. Thus a turbine as small as 1 cm^2 would theoretically be sufficient to power either of the lower-power duty cycles, and a turbine of 92 cm^2 (14 in^2) at constant speed could power the node in router mode. Naturally, due to both practicality and the unpredictability of wind patterns, a larger turbine size than one square centimeter would be desired. Even a turbine significantly larger would still be quite feasible for use in a bridge environment. As a comparison to these values, Xu, et al. (2010) tabulated the power density of several small wind turbines, shown in Table 4.3.

Table 4.3 Reported power densities of similar small wind turbines

Author(s)	Number of blades	Rotor tip diameter (*cm*)	Air speed (*m/s*)	Maximum power (*mW*)	Maximum efficiency (%)	Power density (mW/cm^2)
Federspiel and Chen (2003)	4	10	2.5	8	10%	0.10
Holmes *et al.* (2005)	24	0.75	40	1.1	0.4%	2.26
Hirahara *et al.* (2004)	4	50	9.4	2965	28%	1.51
Priya *et al.* (2007)	12	10.2	4.4	5	1.1%	0.06
Rancourt *et al.* (2007)	3	4.2	11.8	130	9.5%	9.39

Because of the cubic relationship between wind speed and power, simply knowing the average wind speed will not typically be sufficient to accurately size the wind turbine. Instead, some idea of the wind-speed distribution should be gathered. Distribution of wind speed is usually skewed from normal, and it instead can be modeled by a Weibull or Rayleigh (simplified Weibull) distribution (Jowder, 2006), as shown in Fig. 4.5. If data of the actual distribution is not know, however, a Rayleigh shape factor of two can be assumed, which is average for wind patterns in much of North America and Europe (Met Office, 2008).

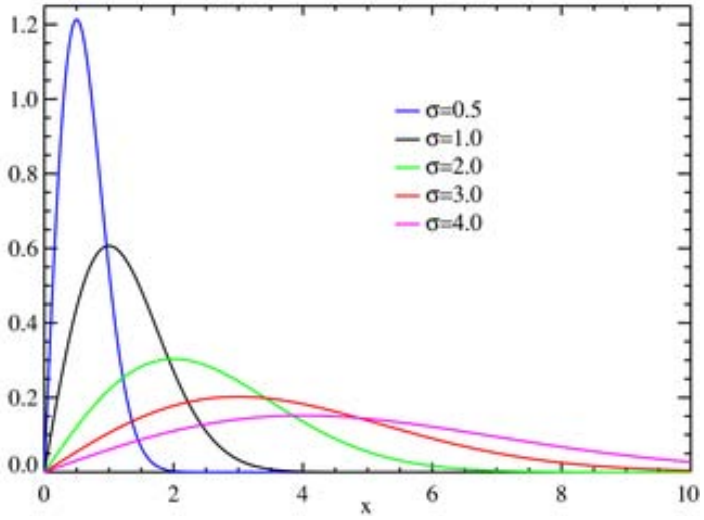

Figure 4.5 Rayleigh distributions (Met Office, 2008)

4.4 VIBRATION ENERGY: PIEZOELECTRIC & INDUCTIVE HARVESTERS

On many bridges, the very locations we are most interested in monitoring are the ones that are the hardest to access. In many cases, these locations may not have easy access to sunlight or consistent wind. It is in these scenarios that vibration harvesting is most attractive.

4.4.1 Vibration Data from Literature

Bridge vibration primarily comes from three sources: wind, ground vibration (seismic), and traffic, with traffic by far being the most substantial (Brownjohn, Dumanoglu, Severn, & Taylor, 1987). Many studies have examined vibration patterns on bridges. For example, a study of the Golden Gate Bridge in San Francisco, California identified 91 modal frequency shapes in the bridge, all below 1.5 Hz (Abdel-Ghaffar & Scanlan, 1985). Measurements taken on the Humber Bridge in England found several modes ranging from 0.2 Hz to 6 Hz (Brownjohn, Dumanoglu, Severn, & Taylor, 1987). The largest of these modes was only 0.001 g acceleration. A study by Williams, et al. (1999) compared two bridges in England and found that one had large spikes at 6 Hz and 12 Hz, while the other exhibited spikes at 4.5 Hz and 14.5 Hz. The maximum accelerations on these bridges were about 0.02 g and occurred when a large truck (lorry) passed over the bridge. Vibration from passenger cars was just 10% of this level. Time-domain and frequency-domain results for the second bridge with a truck passing are shown in Fig. 4.6-4.7.

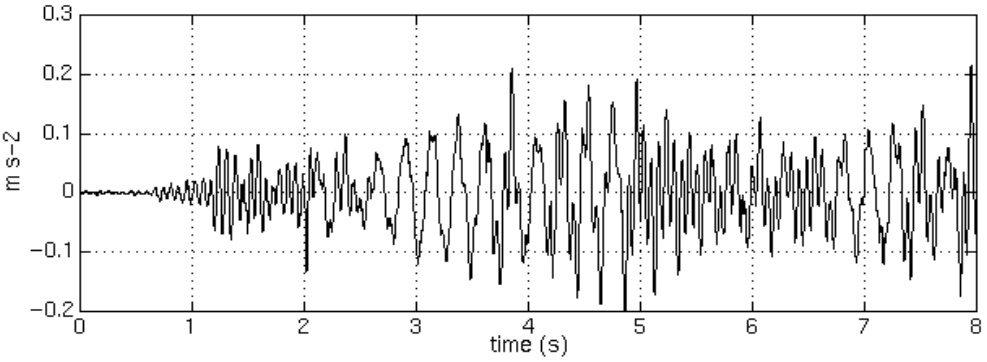

Figure 4.6 Acceleration on a bridge in Sheffield, England (Williams, et al., 1999)

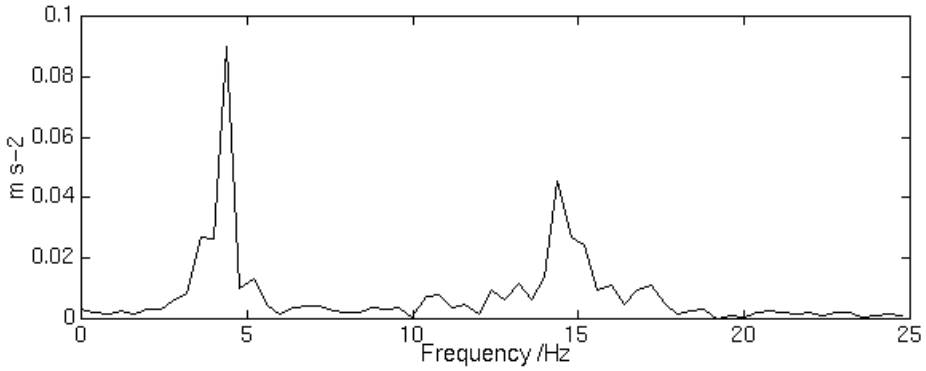

Figure 4.7 Vibration power spectrum (Williams, et al., 1999)

Clarkson University studied a bridge in rural New York and found a predominant resonant frequency at 3 Hz (Sazonov, Jha, Janoyan, Krishnamurthy, Fuchs, & Cross, 2006). Accelerations on this bridge occasionally reached as high as 0.1 g. Measurements from this bridge are shown in Fig. 4.8-4.9. From these and other studies (Chatterjee, Datta, & Surana, 1994; Turner & Pretlove, 1988), it appears that vibration characteristics can vary significantly from bridge to bridge, but are generally in the range of 1-15 Hz and under 0.1 g.

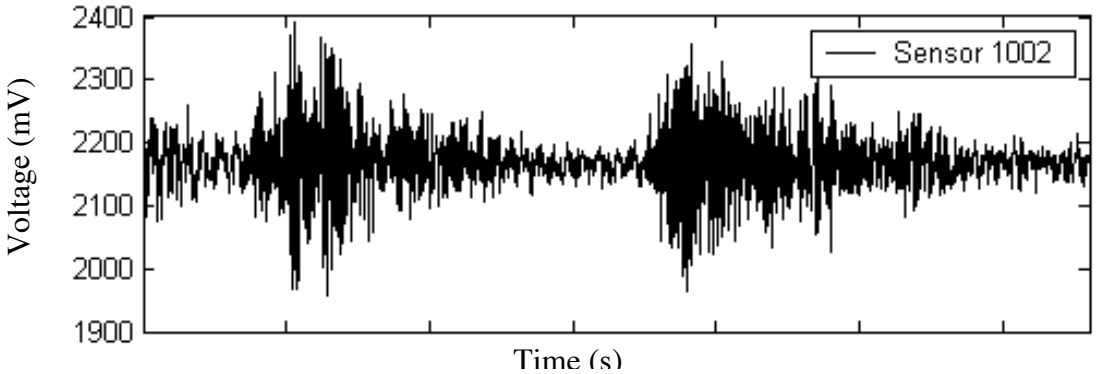

Figure 4.8 Acceleration on a bridge in New York (Sazonov, et al., 2006)

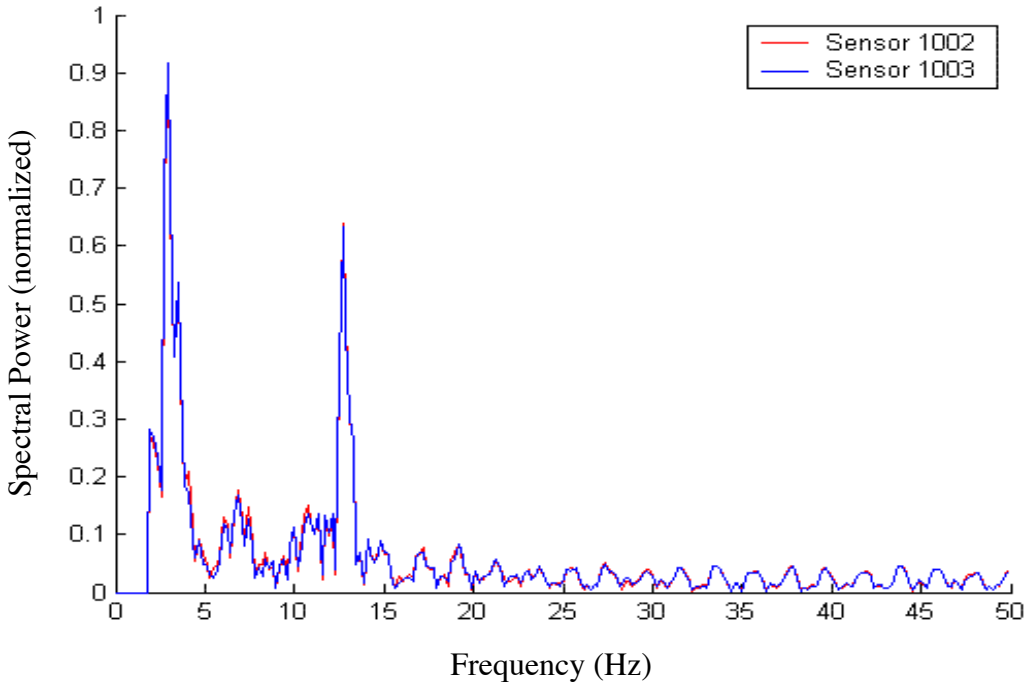

Figure 4.9 Vibration power spectrum (Sazonov, et al., 2006)

4.4.2 Measurements on Existing Bridges

Acceleration measurements were taken on two of the same bridges as the solar and wind measurements. The first bridge analyzed was the I-35/US-290 Interchange in Austin, Texas (Fig. 4.10). This box-girder bridge, which is an onramp between two highways, was fitted with ten accelerometers at regular intervals along the length of the span. Measurements were taken for five hours, during part of which, traffic was being visually monitored as well. Results from this test confirm that the passage of large trucks and buses induced significant vibration in the bridge, (Fig. 4.11) but passenger cars had no noticeable effect.

Figure 4.10 I-35/US-290 bridge, Austin, Texas

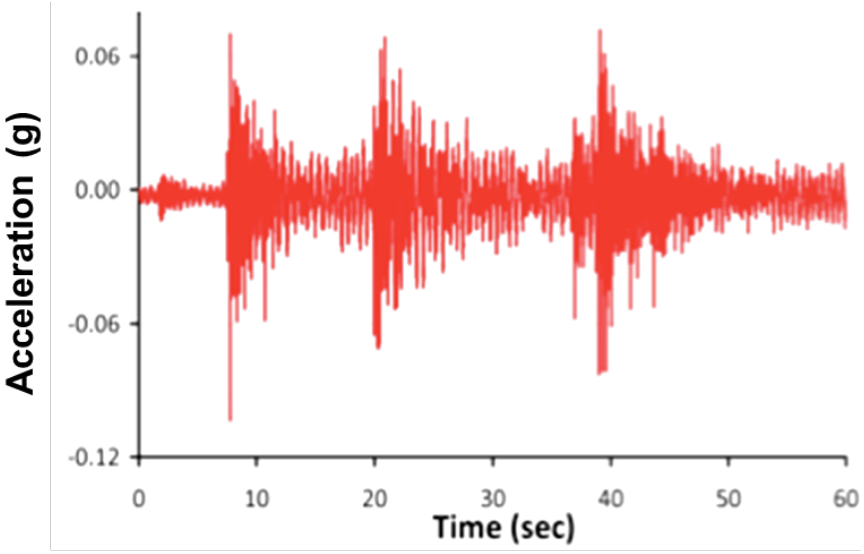

Figure 4.11 Vibration as three trucks pass over the I-35/US-290 bridge

Analysis of the data from this bridge showed maximum accelerations of about 0.1 g, with spectral power spikes at several frequencies, including 2 and 4 Hz (Fig. 4.12). In addition, the use of multiple accelerometers demonstrated the differences in vibration characteristics along the length of the bridge (Fig. 4.13). The portion of the bridge considered consists of two spans. The first span begins at ground level and rises to a support at the other end. The second span continues from the support and is completely elevated, ending at a second support. Measurements indicate that vibrations were significant throughout the first span, with highest levels at the midpoint. Vibration levels on the second span were significantly lower. This shows that, like solar and wind power, vibration harvesting is sensitive to the location of the harvester on the structure.

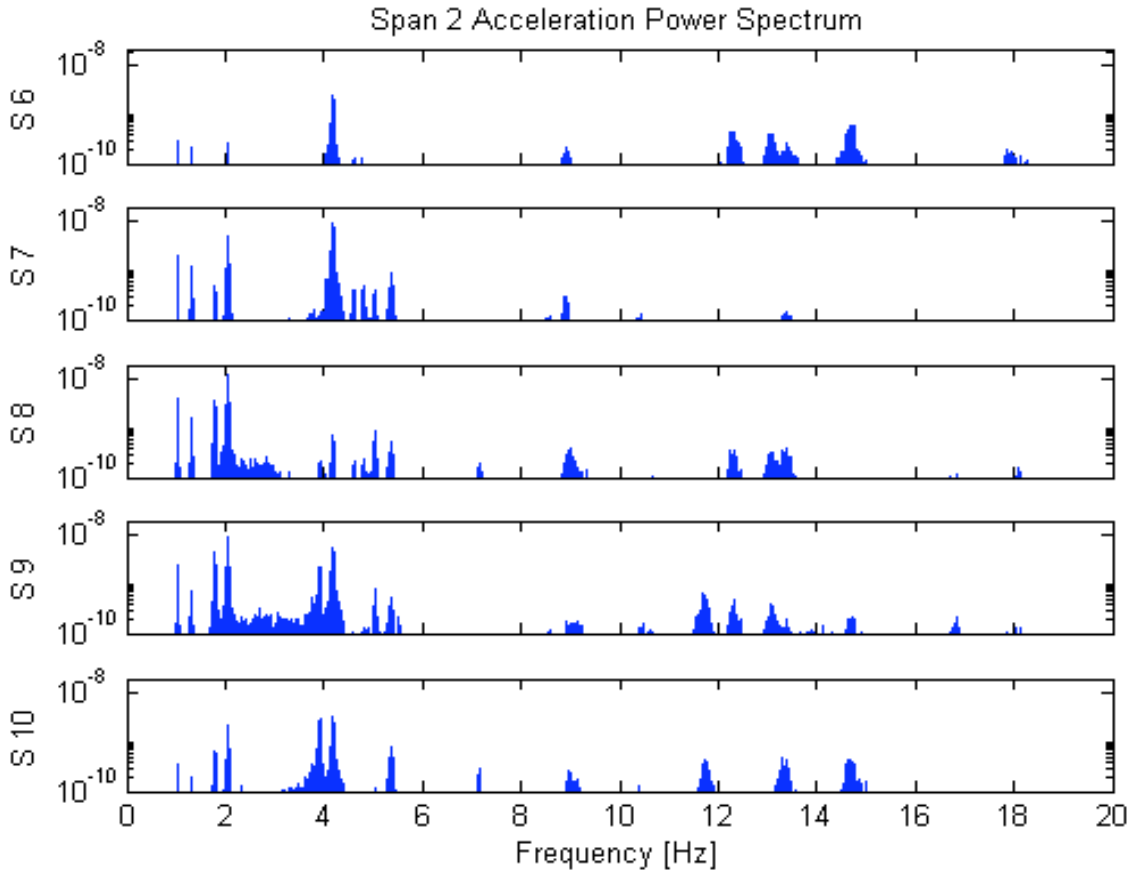

Figure 4.12 Power spectrums for several accelerometers along the span

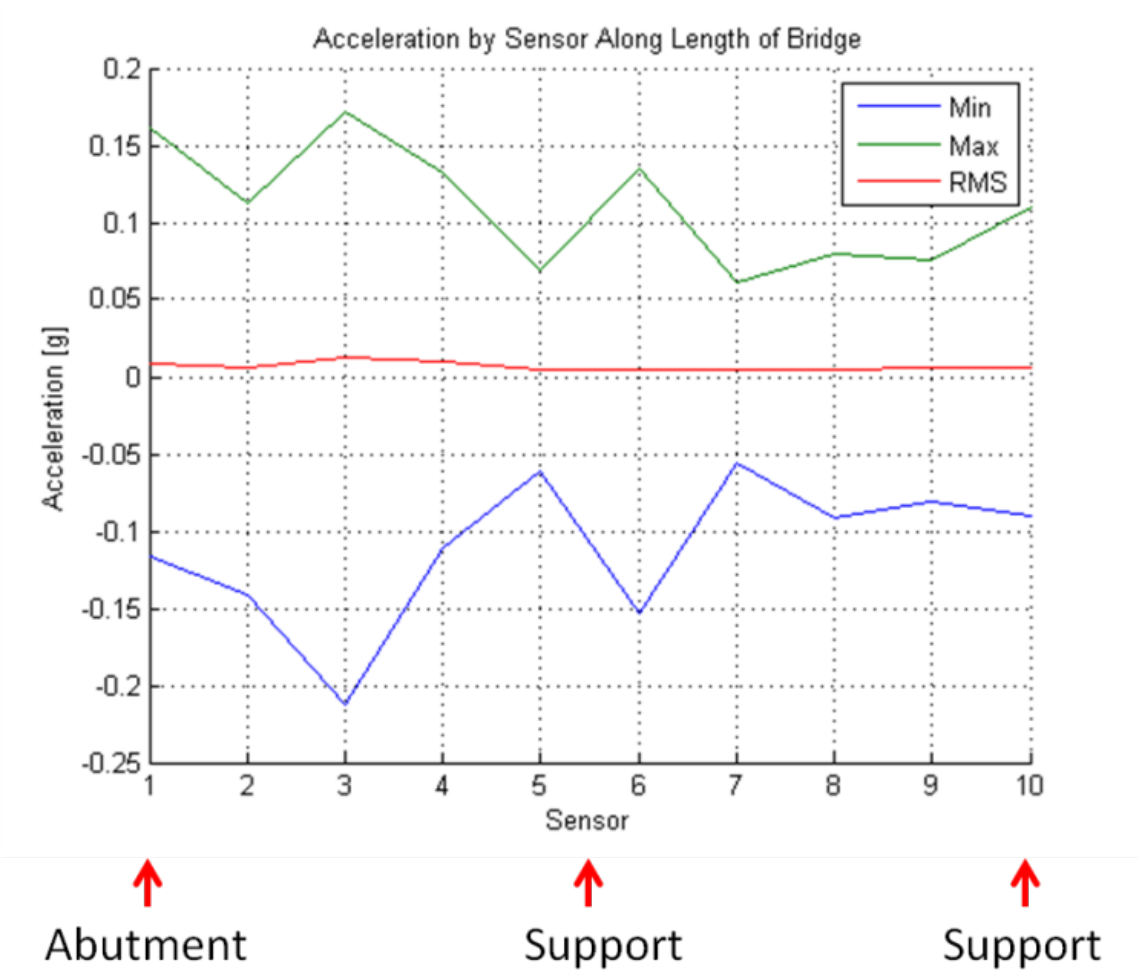

Figure 4.13 Variation of vibration magnitude with position

The second bridge considered is the I-35N Medina River Bridge in San Antonio, Texas (Fig. 4.14). This fracture-critical bridge is older and approaching the end of its expected fatigue life, making it typical of bridges most urgently in need of structural health monitoring.

Figure 4.14 I-35N Medina River Bridge, San Antonio, Texas

Analysis of measurements on this bridge revealed accelerations up to 0.18 g, 80% more than the vibration levels on the first bridge (Fig. 4.15, Table 4.4). Performing Fast-Fourier Transforms on the data yields power spectra for the accelerometers (Fig. 4.16). These spectra show a wide band of increased vibration from 8 Hz to about 20 Hz.

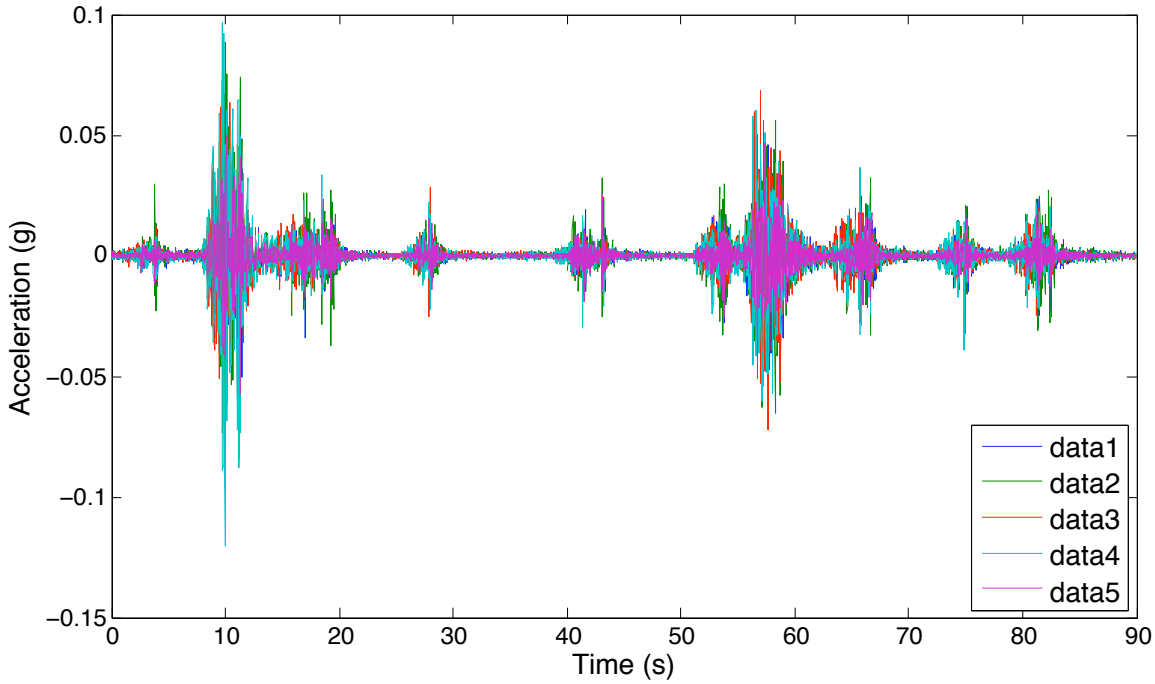

Figure 4.15 Vibration from truck traffic on the Medina River Bridge

Table 4.4 Vibration by accelerometer for the Medina River Bridge

	Ch 4	Ch 5	Ch 6	Ch 7	Ch 8
Max acceleration	0.1054 g	0.1540 g	0.0950 g	0.1801 g	0.0863 g
Min acceleration	-0.1038 g	-0.1555 g	-0.1144 g	-0.1742 g	-0.0994 g
RMS acceleration	0.0095 g	0.0134 g	0.0096 g	0.0128 g	0.0070 g

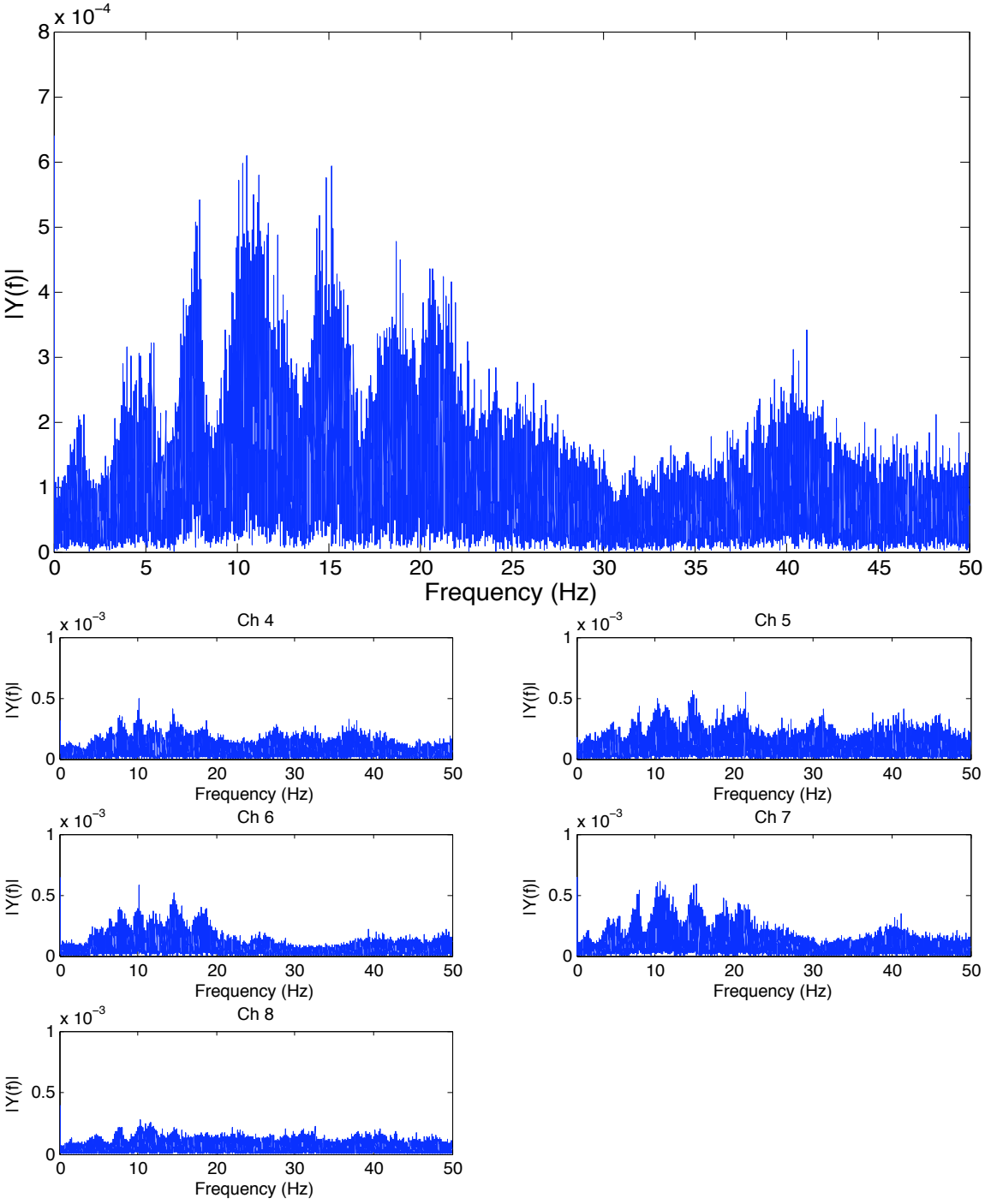

Figure 4.16 Power spectra for accelerometers on Medina River Bridge

Further insight can be gained by comparing vibration patterns during different times of the day. Reichenbach (2011) isolated several instances of free vibration on the bridge at different times of the day, such as the examples in Fig. 4.17. Performing FFT on these individual occurrences reveals substantial shifts in natural frequency throughout the day, emphasizing the need for either wideband or tuning capabilities (Fig. 4.18).

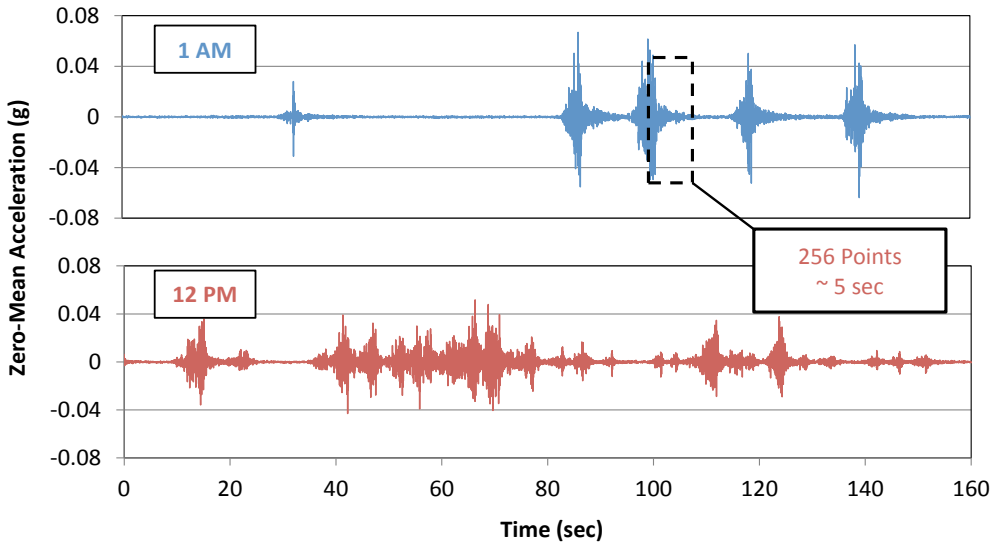

Figure 4.17 Accelerations on Medina River during day and night (Reichenbach, 2011)

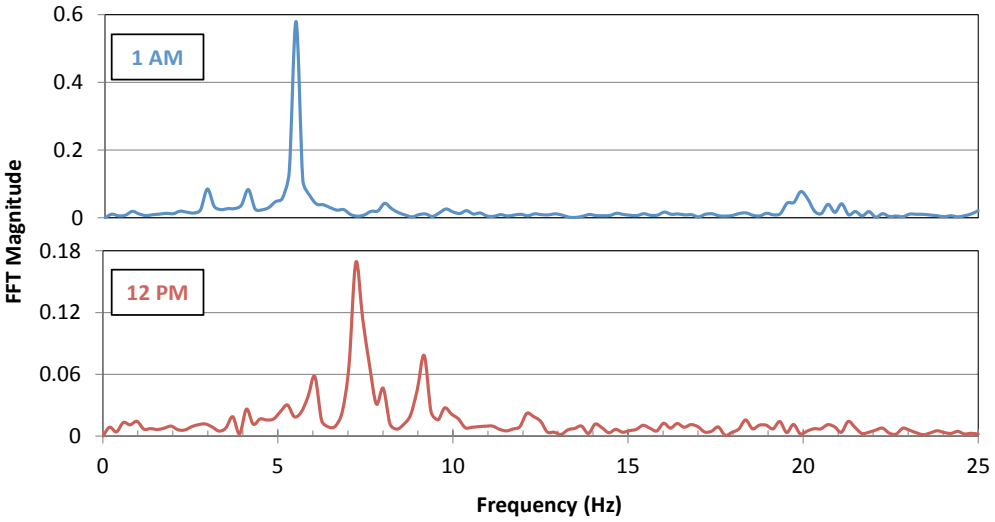

Figure 4.18 Power spectra for Medina River accelerations (Reichenbach, 2011)

4.4.3 Theoretical Power Density

The theoretical power available from vibration relates to the kinetic energy of moving masses, but the governing equations can vary depending on the mechanics and the geometry of the system. One governing equation for a cantilever beam embedded with piezoelectric material (Steingart, 2009) involves the proof mass (m), the acceleration involved (A), the vibrating frequency (ω), and the coefficients for mechanical and electrical damping (ζ_M and ζ_E):

$$P = \frac{m\zeta_E A^2}{4\omega\left(\zeta_E + \zeta_M\right)^2} \qquad \text{Eq. 4.4}$$

This equation shows the power present during harmonic motion, assuming that the input vibration is the same frequency as the resonant frequency of the cantilever beam. As this equation shows, we can maximize power by increasing the mass of the vibrating tip, increasing the acceleration it experiences, and working in lower frequencies. This relationship also assumes the system has been tuned to resonate at the same frequency it experiences.

4.4.4 Power Feasibility of Vibration Energy

Because of the dependence of the governing equation on system damping coefficients, it can be difficult to accurately predict power output without a good estimate of damping. However, comparable vibration harvesters can be benchmarked to get a sense of power feasibility. Several ready-to-install vibration harvesters are available, though most of them are tuned to frequencies higher than those predominant on a bridge. The Perpetuum PMG27 (Perpetuum, 2009) is tuned to 17 Hz. With a continuous vibration of 0.05 g (0.5 m/s^2), this system can generate 4 mW. With a continuous vibration at 1 g (9.8 m/s^2), the power increases to 90 mW.

Vibration on a bridge is frequently lower, in the range of just a few hertz, with maximum accelerations from 0.01 g to 0.2 g. By taking advantage of the additional power available at low frequencies and increasing the proof mass, a similar system should be capable of powering the wireless node even with intermittent traffic. As an example of feasible vibration harvesting for bridge monitoring, Clarkson University installed a wireless node powered by an inductive (magnet and coil) vibration harvester on a rural bridge in New York in 2007 (Sazonov, 2007). Even with sporadic traffic patterns and prototype equipment, they were able to take measurements about five to ten times an hour during the day (the system was programmed to immediately take a sample if it had enough power to do so, instead of storing energy for later use, thus the sample rate was much lower during the night).

4.5 Other Energy-Harvesting Domains

The power density of the three primary forms of energy harvesting – solar, wind, and vibration – can be compared to the power density of the other, more experimental forms discussed in Chapter 2. Table 4.5 summarizes the maximum estimated power densities available from each source.

For each domain, a mathematical model for power density is given, along with the theoretical maximum power density available according to this equation. In most cases, this theoretical maximum is much higher than the practical maximum given, which is based on typical environmental conditions and realistic efficiencies. Where possible, the parameters considered for these results are listed as well. In addition to the primary harvesting domains of solar, wind, and vibration, power density estimates are also given for rain, thermal gradients, solar power in the shade, pressure gradients, radio waves, radioactivity, and acoustic energy.

Table 4.5 Power densities of energy-harvesting domains

Domain	Model	Theoretical Max	Practical Max	Parameters
Solar (direct)	$P=\eta EA$	100 mW/cm^2	3,750 μW/cm^2	1 kW/m^2 irradiation, 15% efficiency, 6 hours insolation
Wind	$P=0.5\rho Sv^3C$	4.5 mW/cm^2	380 μW/cm^2	5 m/s, 5% conversion eff.
Vibration	$P=m\zeta_e A^2/4\omega\zeta_T^2$	19 mW/cm^3	300 μW/cm^3	Tungsten mass, 1 Hz, .01 ζ_e, 0.02 ζ_t
Rain	$P=0.5\rho Sv^3C$	3.7 W/cm^2	670 μW/cm^2	5 m/s, 5% conversion eff.
Thermal*	$P=\eta_C k\Delta T/L$	117 mW/cm^2	40 μW/cm^2	5°C differential, silicon, 1 cm length
Solar (shade)	$P=\eta EA$	5 mW/cm^2	10 μW/cm^2	Shade reduces both irradiation and efficiency
Varying Pressure*	$\Delta E=mR\Delta T$	17 μW/cm^3	3 μW/cm^3	Helium, 10°C temp change/day
RF*	$P=P_0\lambda^2/4\pi R^2$	50 μW /receiver	2 μW /receiver	1 W transmitter, 5 m away, 2.4 GHz
Radioactivity*	$P=A_cE_e$	1.6x10^6 W/cm^3	0.52 μW/cm^3	^{63}Ni activating an oscillator
Acoustic*	$I=P_{ac}/4\pi R^2$	0.96 μW/cm^2	0.1 μW/cm^2	100 dB

* Values taken from Roundy, et al. (2004)

Estimates for power from falling rain were calculated using the same form of equation as wind power. The density of water is much higher than that of air, which would increase the possible power available. The terminal velocity of rain is often between 2 and 8 m/s. However, the actual effective mass density of rain passing through a swept area is surprisingly low, 0.2% or lower of the density of water. The power density available from rain can exceed that from wind, but not by much. The presence of rain is much more variable than wind; there could be weeks or even months between

rainfall. For this reason, relying solely on rainfall would not be recommended, although a hybrid wind/rain harvester may be beneficial.

The use of the thermoelectric effect to harvest thermal gradients is promising, but is not to the point where it could be used commercially in a bridge environment. Large temperature differences can be found between sun and shade on a bridge, but these gradients are not reliably fixed in location and concentrated over just a few centimeters. As mentioned in previous sections, solar power in the shade yields much less power than direct sunlight because of the combined effects of lower light intensity and shading effects on the internal electronics and photovoltaic physics.

The remaining domains are still highly experimental and far below the power threshold needed for feasibility in this application. A review of current research in these areas is available by Roundy, et al. (2004).

4.6 Energy Storage Types

Remote monitors must be able to perform as needed throughout their lifecycle, without suddenly running out of power at a critical moment. Because of this need, energy storage is a vital component of the overall design. Energy storage can be used in two ways. First, the designer may simply include enough stored energy at the outset to last the entire life of the system, or at least until it can be conveniently replaced manually. Alternatively, the designer may incorporate a rechargeable system that is replenished periodically or continually. The first approach is that of primary (one-time-use) batteries, which is currently the industry standard for wireless systems. The second approach is that of rechargeable storage, such as rechargeable batteries, capacitors, and fuel cells. This section will briefly touch upon how each of these approaches influences the feasibility of energy harvesting in our design.

4.6.1 Primary (Disposable) Batteries

Energy harvesting is only attractive if it compares favorably to the alternative means of powering the system. For a sensor network where wired power from the grid is not desired, battery power is, by far, the primary source of power. Such batteries may be replaceable by the user, or they may be designed to last the life of the product and then disposed of together. Disposable batteries are relatively inexpensive, and their standardization makes them very convenient. Their predicted shelf life, energy capacity, and discharge rates make them easy to design around. As mentioned before, the example sensor node considered for this chapter is designed to use four AA batteries. If energy harvesting does not show some advantage over disposable batteries, then there is no reason to consider it further.

The most widespread type of primary battery is the alkaline battery. The Energizer E91 battery (AA, alkaline) is rated at a capacity of 2.8 Ah when discharged from 1.5 V to 0.8 V at a constant 25 mA (Energizer, 2008). Total capacity for four batteries would be 16.8 Wh. This would theoretically power the sensor in router mode for 3 days, in rainflow mode for 4-5 months, and in hourly mode for up to 5 years (limited by the battery's shelf life). The actual usable capacity is slightly lower, because the voltage drops as the batteries discharge. However, a life of 2-4 years seems a reasonable estimate for this system under the lower-power duty cycles.

A better choice for a primary battery would be the lithium iron disulfide battery, marketed by Energizer simply as "lithium." Compared to alkaline, lithium has a longer shelf life (16 years vs. 7 years) and lower self-discharge rate (0.6% per year vs. 3%) (Energizer, 2009). Lithium batteries also have greater energy capacity than alkaline: 3.2 Ah, for a total of 19.2 Wh for four batteries. Lithium batteries would power the node for

4 days in router mode, 6 months in rainflow mode, and perhaps up to 6-7 years in hourly mode. If the deep-sleep mode is possible, a life in excess of 10 years may be possible.

Because of the success already available with primary batteries and their low cost relative to many energy harvesting systems, energy harvesting may not be needed for shorter lifecycles or if the power requirements can be reduced sufficiently. Three scenarios do present themselves where energy harvesting would be appropriate:

- The required power level is larger than that available from batteries, but still within the scope of energy harvesting (such as the wireless node in router mode).
- The desired lifetime is much longer than what is available from primary batteries, due to the limited energy capacity and shelf life.
- Energy harvesting can be accomplished in a way that the overall cost over the lifetime of the product is less expensive than the cost of using primary batteries.

4.6.2 Rechargeable Energy Storage

Regardless of the means of energy harvesting selected, the system will most likely include some means of rechargeable energy storage. This storage serves three functions. First, it allows a steady, well-conditioned flow of electricity to the system, instead of the noisy, variable power generated from the environment. Second, it allows excess energy from peak generation to be stored for use when generated power falls below the level required by the system, such as at night. Third, it allows the peak power draw to be greater than what may be available from the harvested energy rates.

A wide variety of rechargeable solutions are available, such as rechargeable batteries (Lead acid, NiCd, NiMH, Li ion, etc.), capacitors, fuel cells, and hybrids of these categories (e.g., ultracapacitors). Lithium ion batteries are widely used for similar applications (Li, Yu, Su, & Shang, 2008; Corke, Valencia, Sikka, Wark, & Overs, 2007),

but many options may be most appropriate for a given application. In selecting a rechargeable energy storage system, the following must be considered:

- The life of the energy storage, as well as the harvester, must meet the desired operational life for the system.
- The energy capacity must be able to supply continuous power through the longest expected period of time where energy harvesting will be unavailable (e.g., bad weather for several weeks).
- The voltage of the energy storage must be appropriate to both power the wireless node and be charged by the generated power from the harvester.
- The maximum level of current (or power) available from storage must exceed the peak current (or power) required by the node.
- The energy storage system must be appropriately designed to meet the challenges and constraints of the application, including temperature, humidity, possible impact, etc.
- The energy storage system must meet the designer's needs for lifecycle considerations, including a means of safe disposal or recycling at the end of life.

4.7 CONCLUSIONS FROM POWER FEASIBILITY

Initial analysis shows that all three energy-harvesting techniques considered are feasible for powering wireless nodes for a bridge sensor network. Of the three, solar and wind power are more developed and in use commercially, while vibration is still largely in the research phase (although many commercial products are beginning to be available).

Both solar and wind are similar in their power densities during optimal conditions (direct sunlight, constant wind), but die off quickly where light or wind is of low magnitude or inconsistent. In addition, they also both must include exposed parts (PV

panels, turbine blades) that may require careful design, blending with the surrounding environment, and occasional maintenance or cleaning. This is especially true in the harsh environment of a roadway, where oil, grime, animal droppings, garbage, vandalism, and severe weather may pose a danger.

Vibration harvesting systems, in contrast, are largely maintenance-free and can be entirely isolated from the environment. However, they typically can only operate over a narrow range of frequencies, which can vary from bridge to bridge. As will be discussed in the next chapter, they also are currently more expensive than solar or wind systems. A large portion of this cost is the power processing of the generated AC electricity into a steady DC voltage capable of powering the system or charging a battery.

Solar, wind, and vibration harvesting each have different strengths, and each is best suited to different situations. In fact, different types of harvesters may be appropriate even for sensors on different parts of the same bridge. From a power feasibility standpoint, it is recommended that all three technologies be developed, so that the optimal technology can be used to maximize power for any bridge and sensor.

For the wireless node considered, primary (disposable) batteries may already give a life in the neighborhood of five years in the hourly measurement duty cycle, with life possibly in excess of ten years if the power requirements are drastically reduced. However, energy harvesting remains a promising alternative to extend the operational lifespan and allow operation at the higher power levels needed for rainflow and router modes.

Chapter 5: Cost Feasibility of Energy Harvesting

5.1 Discussion of Cost Feasibility

In addition to being feasible from a power perspective, energy harvesting must also exhibit cost feasibility. Wireless sensors on highway bridges can be powered by grid power, by replaceable batteries, or by energy harvesting. In order to be pursued, energy harvesting must demonstrate a lower overall lifecycle cost than either of the alternatives.

5.2 Estimated Costs for Grid Power

With grid electricity priced in the range of 6-20 cents per kilowatt-hour (Energy Information Administration), the price for the actual flow of electrons to the wireless node is literally negligible. An average power of 0.6 mW translates into a yearly consumption of 0.0053 kWh, for a yearly cost of under a tenth of a cent. The primary cost of using grid electricity stems from routing the electricity to the nodes.

If the nodes on a bridge are spaced evenly, every 30-50 feet, the wiring needs can be divided into two groups. First, a length of cable is needed to link each sensor to the previous one, creating a long chain from of a single power source. Three-wire cable this length, either insulated for outside use or contained in a metal conduit, will cost $50-$100 per node (Allied Tube and Conduit). Boxes will also be needed at each point where the sensor wiring connects to the main cable.

The second part of the cabling must connect this whole system to the grid. On some bridges, power is readily available on or near the deck from lighting or traffic signs. In this case, routing power from an existing source to the chain of sensors may only cost a few hundred dollars. However, if no power is currently available on the bridge, the cost could easily jump to additional thousands to tens of thousands of dollars to extend power

from existing lines to the bridge and up to the chain of sensors. Federal and state guidelines would also have to be followed for any permanent wiring on the bridge (Campbell, 2008).

5.3 Estimated Costs for Battery Power

Battery power is currently used for a large number of short-term bridge monitoring systems, and a few that are more long-term (Johnson, 2007). Specifications for the WSN-3202 show that using four alkaline AA batteries (for an input of 6 VDC) will give a life of three years with a 60 second sample interval (Wireless, 2011). We can compare this to the listed capacities of specific batteries.

As discussed in Chapter 4, the Energizer E91 battery (AA, alkaline) is rated at a capacity of 2.8 Ah when discharged from 1.5 V to 0.8 V at a constant 25 mA (Energizer, 2008). Total capacity for four batteries would be 16.8 Wh, which would power the wireless sensor node for up to 5 years in hourly mode. Attempting to use the node in router mode or rainflow mode would reduce battery life to only 3 days or 5 months, respectively. Four batteries typically cost $5-$6 (Wal-mart, 2009).

A better choice for a primary battery would be lithium iron disulfide batteries, which would power the node for 6-7 years in hourly mode, 6 months in rainflow mode, and 4 days in router mode. A set of four lithium batteries costs about $9 (Wal-mart, 2009).

The predominant cost of primary batteries is therefore not the batteries themselves, but the labor to replace them periodically. If the capability to operate in router mode or rainflow mode is required, primary batteries would not be cost effective. However, if hourly measurements only are required and technicians visit the site to

inspect the bridge every two years anyway, the additional cost to replace batteries may be small.

Secondary (rechargeable) batteries would not be recommended as a sole power source. Their self-discharge rates are much higher than primary batteries (5-20% per *month*) and their energy density is slightly lower (Buchmann, 2006). Their shelf life is also shorter than primary batteries, typically 2-5 years. However, there are lead-acid and lithium-ion batteries that can last 10 years (Edwards, 2010). New generations of lithium-ion and lithium-polymer batteries claim a life of 20-25 years, although this is largely untested (Quallion, 2009). They still have self-discharge rates of 5% per month, but could be used for energy storage in conjunction with one of the energy harvesting technologies under consideration, as could maintenance-free lead acid batteries.

5.4 Comparison to Energy Harvesting – A Case Study

Because each bridge has a different environment, it is useful to look at one bridge in detail as a specific example. The interchange in Austin, Texas connecting northbound I-35 to eastbound US 290 (Fig. 4.10) is a bridge about 2,000 to 3,000 feet long. The deck is supported by two steel trapezoidal box girders running the length of the bridge. Sensors would be placed primarily within these girders, but may be placed on their exterior walls as well. Seventy sensors would be a good estimate of this bridge's need.

5.4.1 Cost of Grid Power on I-35/US-290 Interchange

No bridge-wide lighting system is installed on the deck, but one small service light is located on one of the supports. It would take about 200 feet of cable and a small hole drilled in the underside of each girder to deliver the electricity to the interior of the girders. In total, about 3,700 feet of cable would be needed, for a material cost of $3,000

to $4,000, plus about $1,000 for other hardware and installation labor. Labor costs on this particular bridge would be much less than many bridges because of the access to the box girders. Workers on this bridge would be able to gain access through a ladder and lay cable straight down the length of the girder, whereas many other bridges would require man-lifts or other expensive equipment and additional labor to route the cabling around the girders, as illustrated in Chapter 1 (Fig. 1.2). These installation costs, however, would still likely be much higher than the installation costs for independent energy harvesters. Once installed, there would be little additional cost.

5.4.2 Cost of Primary Battery Power on I-35/US-290 Interchange

To equip the same network with batteries for ten years would cost about $2100 (for alkaline) or $1800 (for lithium) for the batteries. The initial installation would not require any additional work beyond installing the sensors themselves. If the nodes only operate in hourly mode, lithium batteries would need to be replaced two or three times over a ten-year life. For many bridges, this replacement process would be labor intensive, but the likely locations for sensors on this bridge are easily accessible by inspecting technicians, and replacing the batteries would only add one or two additional man-hours of work. However, as mentioned, the use of router mode or rainflow mode would likely cut the battery life to only days or months, which would be unattractive for prolonged health monitoring on the bridge.

5.4.3 Cost of Solar Power on I-35/US-290 Interchange

The I-35/US-290 Interchange is a box-girder bridge, where most of the sensing needs would be within the enclosed box girder. The use of solar panels would only be practical for sensor nodes attached to the exterior of the girder or in locations where

access holes between splice plates can be used to run wiring to the interior. Calculations in Chapter 4 estimated an expected power density from solar harvesting of 1.9 mW/cm^2, which translates to a yearly energy production of 60 kJ (17 Wh) per square centimeter. This estimate assumes an unshaded panel location, 10% panel efficiency, and solar irradiance levels typical of Austin, Texas in the winter (to be conservative). To consistently meet the power requirements summarized in Table 4.2 throughout the year, including winter, a solar panel should be rated five times the needed power (an insolation level of 4.65 hours out of 24 hours means a long-term average of 0.19 times the rated power output at the standard irradiance of 1,000 W/m^2). By these calculations, the hourly mode would require a rating of at least 2 mW, rainflow mode would require a rating of 60 mW, and router mode would require a rating of 1 W.

Any of these power levels could easily be met by a 1-W-rated panel, which would average 200 mW over the long term. A six-volt panel rated at 1 W is available for $8.99 retail (Parallax, 2011) and likely a small fraction of that in high volumes. In addition, each panel would require a battery and a charge controller. Six-volt lead-acid batteries are available for $6 (Rage Battery, 2009), and equivalent lithium ion batteries are available for about $30 (Only Batteries, 2011). A charge controller, which ensures maximum charging efficiency and prevents draining or overloading the battery, costs about $15 (Silicon Solar, 2010). Support of a gateway node would likely require a panel rated for 50 or 60 W, which with battery and charge controller would cost about $300 (Costco, 2011).

Using these price estimates, powering each node would cost $30 with lead-acid batteries, or $55 with lithium-ion batteries. The total material cost to power 70 nodes would therefore be $2,100 to $3,150. Labor costs would also have to be considered, with perhaps a total of 30-40 man-hours needed for the entire bridge. Periodic cleaning of the

panels may also be necessary, although proper design and sufficient rainfall can alleviate much of the problem.

5.4.4 Cost of Wind Power on I-35/US-290 Interchange

As with solar panels, the use of wind turbines would be practical for this bridge only for exterior sensors or if access holes are available for routing wiring to the interior of the box girder. Chapter 4 illustrated that using wind harvesting to power the example sensor nodes would be possible with a swept area of only a few centimeters in diameter. This assumed a constant wind speed of 5 m/s (11 mph) and a coefficient of performance of 0.3. Efficient wind turbines of this size are not as common as larger turbines, but several examples can be used to estimate costs.

One available wind turbine (USA Wind Generators, 2011) can produce up to 30 W at wind speeds of 25 mph (11.2 m/s). It is designed to start turning at as low as 4 mph (1.8 m/s). It has a swept area of 5,000 cm^2 (diameter of 32 inches) and costs $50. An educational wind turbine kit (PicoTurbine, 2011) is available for $39 that produces 150 mW in 12-mph winds. The $50 HYmini micro wind power generator (HYmini, 2011) can generate up to 350 mW in winds of 9-45 mph.

If we assume a price of $50-$100 for an appropriately sized turbine, along with the battery and charge controller used for the solar panel system, the total cost per node would be about $70-$150. This translates to a total material cost for the bridge of $5,000-$11,000. In addition, installation and maintenance labor costs would be very similar to that of using solar power.

5.4.5 Cost of Vibration Power on I-35/US-290 Interchange

To get a sense of the cost involved for vibration harvesting, we can consider several commercial harvesters similar to the proposed system. Perpetuum (2011) provides electromagnetic (coil/magnet) vibration harvesters tuned at several frequencies. Most of these models are designed for use with electric machinery vibrating at 50, 60, 100, or 120 Hz. However, they also offer lower frequencies for trains and aerospace, the lowest being 17 Hz (Perpetuum, 2009). These Perpetuum harvesters are available starting at $400. Another company, MIDE, (2011) offers piezoelectric vibration harvesters, primarily within the same frequency range. Complete tuned harvesting systems are available for $400. Also available separately are the piezoelectric bimorph ($80), the tuning mass ($20), and the power-conditioning circuitry ($100). Enocean (2011) offers motion harvesters of a different kind, which use magnet/coil induction to convert the motion of flipping a light switch or pushing a button into enough power to send a short, low power radio transmission. These systems are available for around $30, including the radio transmitter. The output from these systems would be too low for our application, but demonstrate the cost scalability of vibration harvesting.

If we assume a harvester cost of $400 per node, plus the same batteries used previously, the total material cost for outfitting 70 nodes with vibration harvesting would be very high, about $28,000. However, if low-cost harvesters can be designed closer to $150-$200 per node, the cost would be a more reasonable $11,000-$15,000. Although the material cost per node is still significantly higher than the alternatives, vibration harvesting may still be the most feasible option where solar and wind are unavailable, routing grid power is prohibitively expensive, and replacing batteries is unwanted.

5.8 Conclusions From Cost Feasibility

The optimal power source to use with a bridge sensor network is highly dependent on the bridge environment. If inspections of a bridge still take place every two years and technicians have relatively easy access to the sensors, using replaceable batteries appears to be the simplest, cheapest, and most reliable option for low-power end nodes only transmitting hourly. However, routing and other higher-power functions would be unavailable with this option. If the sensors are not easily accessible, but are located on the exterior of the bridge, solar or wind energy may be the best fit, provided that an accurate prediction of light/wind patterns can be determined and that the hardware can be designed and installed so that future maintenance can be minimized. If the sensors are placed in locations where sunlight or wind is not available and no future maintenance is available, vibration harvesters are excellent candidates for consistent, self-contained power, though they are more expensive.

Surprisingly, the bridge chosen for this study indicated reasonable costs for outfitting it with grid power, as it is a relatively short bridge with easy technician access and no need for excessive routing of wires around obstacles. In general, though, the prohibitive cost of laying new wiring for such a small power need makes grid power unattractive for installation on existing bridges. On new bridge construction, where power lines may be placed in a convenient location for both sensors and lighting, grid power may be a viable option for permanent, reliable sensing.

Under current regulations, biennial inspections would still be required for all bridges, even those with sensor networks in place. Battery power would often be sufficient in such a situation. The long-term goal for this research, however, is to allow longer intervals with minimal in-person inspection. Thus, the development of

technologies capable of lasting much longer than two years is desirable. Developing a portfolio of both improved battery technology and the various energy harvesting technologies will be the best path to enabling long-term, autonomous monitoring of any bridge, optimized to the bridge's individual characteristics.

Chapter 6: Innovation Opportunities in Energy Harvesting

6.1 INTRODUCTION

The concept of "innovation" currently receives much attention in the popular media, in policy statements (The White House), and in the design research community (Markman & Wood, 2009). Innovation can be defined in multiple ways. For this dissertation, we define innovation as the process by which a novel product or system is conceived and realized intentionally to address a human need. In the innovation of new technologies and products, many techniques are available to assist the designer. Some techniques facilitate a better understanding of the design problem, customer needs, and technical specifications, such as QFD (Otto & Wood, 2001). Others identify and offer solutions to inherent conflicts or tradeoffs, such as the Theory of Inventive Problem Solving (TIPS) (Altshuller, 1984; Sushkov, Mars, & Wognum, 1995). This chapter examines how design in energy harvesting can be aided through functional modeling. Generalizations regarding functional modeling are developed based on this examination.

6.1.1 Energy Harvesting

Energy harvesting is any process by which freely available energy from external sources is captured *in situ* (on location) and converted into usable electrical energy for local use. This process is in contrast to most electrical power production, where energy is captured on a large scale through centralized fossil fuel, hydroelectric, or nuclear plants and then distributed through AC grid power or replaceable batteries. Energy harvesting harnesses power that otherwise would have been wasted. Among the most common types of energy harvesters are wind turbines and solar harvesters (photovoltaic panels and solar heat engines). Other types under development include systems for harnessing vibration or

movement (from machinery, human movement, structures, etc.), thermal gradients, acoustic energy, and electromagnetic energy (primarily ambient radio waves).

6.1.2 Innovation and Driving Functions

Substantial research has been conducted regarding how to forecast or predict innovation (Christensen, Anthony, & Roth, 2004; Daim, Rueda, Martin, & Gerdsri, 2006; Martino, 2003; Porter, Roper, Mason, Rossini, & Banks, 1991; Watts & Porter, 1997). Industry leaders can make fortunes based on their understanding of when and where innovation is likely to take place. Innovation can occur at varying degrees of significance. Altshuller (1984) identified several "Levels of Invention," ranging from minor parametric changes to new discoveries in underlying science. In developing energy harvesting, one of two design paths may be followed. The designer may seek to innovate original or novel core technologies, such as a drastically more efficient photovoltaic panel from a never-before-seen material. This direction of research can lead to cutting-edge advances in overall technology, with both high cost and high pay-off. Another avenue of design that is often attractive is to utilize existing core technology and focus solely on the driving system functions. These driving functions typically call for inventive ideas or make use of more established technology, allowing the designer to entertain design changes with greater freedom and at lower cost. Although the resulting concept will be limited by the fundamental restrictions of the core technology, it will still be capable of great advances in efficiency and functionality, which can then be further improved over the long term by subsequent improvements in the core technology. These possible opportunities of innovation in driving functions are low-hanging fruit that can be quickly and easily incorporated into design without the need for extensive research.

Before conducting the research outlined in this chapter, we hypothesized the following as the primary driving functions of an energy-harvesting system:

- Concentrate/Direct
- Capture/Collect
- Transform/Amplify
- Convert to Electrical Energy (core function)
- Rectify/Process
- Condition
- Store (short-term and long-term)
- Attach to Environment
- Blend with Environment (visually, etc.)

Each of these driving functions may present numerous opportunities for innovation and improvement. These functions can often be broken down into groups of sub-functions, which may vary substantially from system to system. By identifying these sub-functions and how they can be improved, modified or rearranged, the designer gains access to a set of specific areas that can be targeted for redesign and innovation.

6.1.3 Functional Modeling

Functional modeling is a process whereby the overall intended behavior of a system is broken down into an architecture or schematic of sub-functions. Functional models can vary in their resolution, from generalized black-box diagrams identifying the input, primary function, and resulting output of the system, to specific diagrams outlining every component, physical phenomenon, and action.

Functional modeling has been identified as a critical step in the design process (Hubka, 1996; Pahl & Beitz, 1996) and has been included in many well-known design

methodologies (Otto & Wood, 2001; Ullman, 2002; Ulrich & Eppinger, 2004) as a means to understand the underlying mechanics of complicated systems, how the sub-functions relate to customer needs and constraints, and how to improve these relationships in future design. To facilitate commonality and better communication among designers using functional modeling, a common basis or taxonomy can be used. The functional common basis developed from efforts by Stone, Wood, Szykman, and others (Bryant, Stone, McAdams, Kurtoglu, & Campbell, 2005; Caldwell & Mocko, 2010; Otto & Wood, 2001; Stone & Wood, 2000; Szykman, Racz, & Sriram, 1999) gives a set of generalized terms describing energies, materials, signals, and functions applicable to any system of interest. The use of these generalized descriptors allows consistent comparisons of different systems and the models of different designers.

By using functional modeling to analyze energy-harvesting systems, we can identify the functions that comprise the systems' core technologies (primarily the method of energy conversion to electricity). The other functions in the models can then be identified as driving functions ripe for innovation, and designers can focus on rearranging or altering the existing framework to enhance or create new functionality.

6.2 Functional Analysis Methodology

This chapter addresses several ways functional modeling can be used in the design process, as applied to the field of energy harvesting. First, representative energy-harvesting products were selected, and functional models were created for each system in the set. These models were used to gain insight both quantitatively and qualitatively.

The functional models were evaluated quantitatively by compiling the results in a vector-space repository (McAdams, Stone, & Wood, 1999; Stone, Wood, & Crawford, 1999; Weaver, Wood, & Jensen, 2008). By performing normalization and matrix

manipulation steps, matrices were formed that illustrate correlations among products and among functions.

The functional models were also evaluated qualitatively by comparing their organization and identifying key modules and functions characteristic of different types of harvesters and of harvesters in general.

6.2.1 Choice of Energy Harvesting Systems

Thirty-nine energy-harvesting systems were chosen for this study. They consist of nine inductive (electromagnetic) vibration harvesters, six piezoelectric vibration harvesters, six wind harvesters, three ocean-current or wave harvesters, six solar harvesters, five thermal harvesters, and four hybrid harvesters that make use of two or more of the other technologies. These systems are a mix of existing commercial products and research prototypes in development. An effort was made to include a representative sampling of typical harvester designs. For example, the selected systems for wind harvesting include two different vertical-axis wind turbines, two horizontal-axis wind turbines, and two systems that use vortices to exploit a flapping or vibrating action.

6.2.2 Generating Functional Models

Following the selection of sample energy-harvesting systems, functional models were created using the functional common basis. By using this terminology, we can convert application-specific terminology into standardized descriptions. For example, one might describe some of the functions of a kinetic flashlight (which uses induction to harvest vibration) as the following:

- Accept the user's hand
- Convert motion from the hand into relative motion between the magnet and coil

- Convert kinetic energy into a changing magnetic field and then into a voltage
- Condition the voltage by storing it in a capacitor
- Convert the electricity into light
- Transmit the light

These same functions, converted to the functional common basis, would read as the following:

- Import human
- Convert human energy to translational mechanical energy
- Convert translational ME to magnetic energy
- Convert magnetic energy to electrical energy
- Change electrical energy
- Store electrical energy
- Supply electrical energy
- Convert EE to electromagnetic energy
- Transfer electromagnetic energy
- Export electromagnetic energy

This yields a function structure with components that are not application-specific and can be more readily compared with functional models for systems across diverse domains.

6.2.3 Product Repository

A typical functional model may contain a large number of different functions, and it may even contain the same function numerous times in slightly different capacities. To distill this large amount of information, the functions of each system can be summarized in vector form. For example, if the possible functions are {import, export, transfer,

change, convert, position} and a particular system contains the functions {import, export, convert}, then a binary vector representation of this system would be {1,1,0,0,1,0}. This simple binary representation was used in this study. Additional insights may be gained through more in-depth breakdown of the functions, such as delineating the object of the function (e.g., "transfer mechanical energy" versus "transfer electrical energy") or by weighting the functions based on the strength of their relationships with key customer needs (Stone, Wood, & Crawford, 1999).

A product repository was formed by compiling the binary vectors for all 39 systems. This resulted in a matrix with each row listing an energy-harvesting system and each column listing a function, material, energy, or signal from the functional common basis. For brevity and clarity, only those members of the basis that were found in at least one harvester were included in the matrix (i.e., no columns were empty).

6.2.4 Vector Space Analysis

To analyze the product repository, we used a vector space analysis similar to that used previously by Stone, et al. (1999), McAdams, et al. (1999), and Weaver, et al. (2008). Two techniques were used in this analysis. For the first technique, each row was normalized by the square root of the number of functions in the system. This prevented skewing from systems with abnormally large or small numbers of functions. By post-multiplying this matrix by its transpose, a square matrix was formed that has the list of products on both the rows and the columns. Because of the square-root normalization, the diagonal entries became unity, and the off-diagonal entries describe the relative similarity between the functional models of the energy harvesters in corresponding rows and columns. This procedure is illustrated in Eq. 6.1, where A_{ij} is the repository's entry in the i^{th} row and j^{th} column, and P_{ij} is the corresponding entry in the final matrix.

$$P_{ab} = \frac{1}{W_a}\frac{1}{W_b}\sum_{i=1}^{n}(A_{ai}A_{bi}), \quad where \quad W_a = \sqrt{\sum_{k=1}^{n}(A_{ai})}, W_b = \sqrt{\sum_{k=1}^{n}(A_{bi})} \qquad \text{Eq. 6.1}$$

For the second technique, each column was normalized by the square root of the number of systems exhibiting the function. Then, by pre-multiplying the matrix by its transpose, a square matrix was formed that lists the functions, materials, energies, and signals along both the rows and columns (Eq. 6.2). As in the previous example, the diagonal entries became unity. Each off-diagonal entry gives the correlation between the two functions or flows, i.e., how often the pair of descriptors appears together in the same system.

$$F_{ab} = \frac{1}{W_a}\frac{1}{W_b}\sum_{i=1}^{n}(A_{ia}A_{ib}), \quad where \quad W_a = \sqrt{\sum_{k=1}^{n}(A_{ia})}, W_b = \sqrt{\sum_{k=1}^{n}(A_{ib})} \qquad \text{Eq. 6.2}$$

The result of these two techniques is two large matrices that provide insights into the relationships among the examined systems. The first matrix illustrates the functional similarities among the energy harvesting systems, and the second matrix shows typical relationships among the functions and flows found in the systems.

6.2.5 Finding Key Modules and Functions

In addition to the quantitative procedure described above, the functional models were evaluated qualitatively to identify observable trends in how functions, modules (groups of functions acting together on a common material, energy, or signal flow), and overall functional architectures are used in energy harvesting. In particular, the completed functional models were compared to the list of hypothesized driving functions described in Section 6.1.2.

6.3 Discussion of Results

A product repository was formed from 39 energy-harvesting systems and their included functions and flows. The sampled systems have very diverse functions and flows. Out of 14 possible types of energy, 6 types of materials, 2 types of signals, and 21 distinct functions, the product repository included examples of 10 energies, 4 materials, and all possible signals and functions. Thus the total dimensionality of the repository was 37 out of a possible 43 descriptors. The energy-harvesting systems tended to individually be complex as well. The simplest harvester, a thin-film photovoltaic panel with no power conditioning or storage capabilities, utilized 8 distinct functions, several of which appeared multiple times. One of the most complex systems, the HYmini (Fig. 6.1), included 18 distinct functions, 3 types of materials, 7 types of energy, and both types of signals. This system appears simple, but involves several parallel charging options (wind turbine, solar panel, hand crank, bicycle-powered dynamo, and plugging into AC or DC power sources), each with its own power conversion functionality.

Figure 6.1 HYmini universal charger (HYmini, 2011)

Of the functions involved in energy harvesting, the following functions were used at least once in every system: import, export, separate, transfer, and convert. Other frequently used functions include change, position, guide, and secure. Commonly used materials include solid objects, humans, and gas. Common forms of energy include light energy (solar power, status signals, and visual appearance) and electrical energy (the necessary output of energy harvesting), with an even distribution of many other forms of energy like magnetic energy, mechanical energy, pneumatic energy, and human energy.

6.3.1 Functional Similarities

Normalizing the product repository and post-multiplying by its transpose yields a 39x39 matrix correlating each energy-harvesting system to the other systems. This product-product matrix is found in Appendix C. Off-diagonal entries show the functional similarity between two systems. In the sample systems, this degree of similarity ranges

from 50% to 97%. From this product-product matrix, the following conclusions can be drawn:

- Wind harvesters showed high degrees of functional similarity with other wind harvesters, ranging from 80% to 96%.
- Thermal harvesters showed high levels of similarity as well. With one exception, similarities ranged from 83% to 97%. The exception, the Seiko Thermic watch, shared similarities of 69% to 73% with other thermal harvesters, but showed higher similarity with other human-related products, such as kinetic and solar-powered watches, kinetic flashlights, and hand-held harvesters like the HYmini.
- Vibration, wave, and solar harvesters exhibit a wider range of high and low similarity within their respective domains. These levels range from 60% to 96%.
- High degrees of similarity between differing domains include the following combinations:
    - Solar harvesters with hybrid systems (which all include solar capability)
    - Wind harvesters with hybrid systems (one hybrid system includes a gas-based Stirling engine heated from solar power; the others include wind turbines)
    - Human-related harvesters (watches, flashlights, and handheld wind turbines)
- Low degrees of similarity between differing domains include the following combinations:
    - Wave harvesters and vibration harvesters
    - Solar harvesters and wave harvesters
    - Solar harvesters and wind harvesters

- Vibration harvesters and thermal harvesters

6.3.2 Function and Flow Combinations

Normalizing the product repository and pre-multiplying by its transpose yields a 37x37 matrix relating the relevant members of the functional common basis (Appendix D). In this function-function matrix, as in the previous example, the diagonal terms have been normalized to unity. The off-diagonal terms indicate the relative strength of correlation between the row and column functions or flows, i.e., how likely they are to appear together in a functional model. As described previously, several functions are near universal among the sampled systems, such as "import," "export," "transfer," and "convert." This prevalence creates strong correlation among all these functions that can overshadow other relationships shown in the function-function matrix.

In addition to these most common functions, several common groupings can also be identified that often occur together:

- Store, supply, sense, indicate, actuate, regulate, and signal
- Guide, secure, sense, position, secure, and solid
- Human and human energy
- Gas and pneumatic energy
- Liquid and hydraulic energy

The interactions among the materials and energies were below the average for function correlations, meaning that the individual flows were less likely to be found with other flows. The combinations identified above are exceptions to this, as is solid material, which occurred with other materials and energies slightly more than average.

6.3.3 Common Modules and Comparison to Hypothesized Driving Functions

Examination of the functional models created for the ensample energy-harvesting systems produced several insights. Within each domain (e.g., vibration harvesting), functional models follow very similar structures. The predominant changes are addition or subtraction of beneficial but non-essential functionality. In addition, these structures largely remain consistent when comparing across differing domains, as well. Here, the major shifts occur by substituting different material and energy flows into similar function architectures.

As an example, we can consider three example systems: the Seiko Kinetic watch (inductive vibration harvesting), a prototype harvester inside the heel of a shoe (piezoelectric vibration harvesting) and the Enviro-Energies vertical-axis wind turbine (wind harvesting). Functional models for these three systems are included in Appendix E.

In the Kinetic watch (Fig. 6.2), the material flow of interest is the human hand, which carries with it mechanical energy from its motion. Functions acting on this flow include importing the hand, guiding it (through the wristband), positioning it (so the watch is on the wrist facing the right way), separating out some of the mechanical energy for harvesting, and distributing the rest evenly back into the human as reaction forces. Additional functions that occur include guiding the hand back out of the wristband, separating from it, and exporting the hand from the system. The mechanical energy extracted is transmitted to the components of the watch, where it is converted from oscillating motion to rotary motion. A gear system changes the mechanical energy by increasing the rotational velocity and decreasing the torque, after which the mechanical energy is converted to electrical energy by an electromagnetic generator. After the electrical energy is conditioned and smoothed, it is stored and supplied as needed in a

battery, with the measured voltage being displayed visually as a battery life gauge. Electricity is then transmitted to the motor and converted back into rotational mechanical energy, which is then changed through the complicated workings of the watch into rotation of the hands on the face. In addition to this entire process, a separate structure exists to describe the visual appearance of the watch, addressing such functions as blending and aesthetics. These functions can be grouped into general modules, including attaching to the environment (the hand), capturing the mechanical energy, directing or filtering it into a two-dimensional oscillation, transforming it into rotational mechanical energy at higher velocity, conversion to electricity, conditioning, storage, blending with the environment, and the application functionality of displaying time.

Figure 6.2 Seiko Kinetic wristwatch (Seiko, 2007)

In the heel-impact shoe vibration harvester (Fig. 6.3), two material flows are imported: the human foot and the ground. Like the watch, this system uses functions like guide, secure, stabilize, distribute, and separate to describe attachment to the environment (the foot and the ground) and effective collection of mechanical energy for harvesting. After the mechanical energy is isolated, it is transformed by a function sequence very similar to the watch, with the energy directed in the appropriate direction for the piezoelectric ceramic, converted to electricity, rectified and smoothed, stored temporarily, and then exported for use powering low-power electronics or similar

applications. The blend functionality is also important here, both visually and indirectly through the even distribution of reaction forces to the foot.

Figure 6.3 Shoe-mounted piezoelectric harvester (Shenck & Paradiso, 2001)

In the Enviro-Energies wind turbine (Fig. 6.4), the primary material flows are the roof (or other solid structure) and the air, a gas. The roof is subjected to the same attachment oriented functions as in the previous examples, including positioning, securing to, and eventually separating from the roof. The gas is guided and stabilized such that the gas pressure can be converted into rotational mechanical energy. Then, once again, this energy is transmitted, converted to electricity, conditioned, stored, and exported to the application of interest. Blending is an important functionality in this system as well, and is represented in the functional model in the same way.

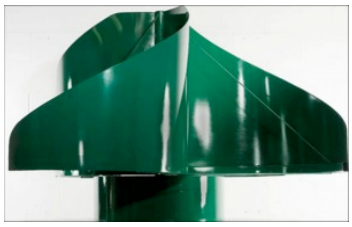

Figure 6.4 Enviro-Energies vertical-axis wind turbine (Enviro-Energies)

These three systems have different inputs (motion of a hand, forces between a foot and the ground, and relative motion of wind to a structure) but use similar function chains to interface with the environment, prepare the energy for harvesting, extract or

collect the energy, and transform the energy into a form most efficient for conversion to electricity. After using the systems' core technologies to make the conversion to electricity, the remaining functionality is close to identical among the three systems, consisting of conditioning the electricity into a state suitable for electronics, storing it until needed, and then supplying it for use in the application. Through the whole process, the visual interaction with the user remains a constant need, including overall visual appearance and visual or tactile status signals.

We propose that energy harvesters in general will embody the following string of overall driving functions:

1. Interface (attach, position, etc.) with environment
2. Direct (filter, concentrate) energy from the environment
3. Separate (extract, collect, capture) energy
4. Transform (amplify, change) energy into form ready for conversion
5. Convert energy to electrical energy
6. Condition (rectify, process, smooth, change) electrical energy for storage or use
7. Store electrical energy
8. Supply electrical energy to application
9. Interface (interaction with light, status signals, visual/tactile/audio feedback) with user

The actual common basis functions included in each step may vary, depending on, for example, whether the direction and transformation of incoming energy needs to be actively controlled by the user or occurs passively. These steps may be complicated or simple, but will occur in some form in any energy-harvesting process.

6.3.4 Applications in Design

The insights gained through functional modeling can have direct application to the design of new energy harvesters. Each of the functions described above presents an opportunity for innovation:

1. *Interface with environment*: Improve energy flow into the system through closer coupling with the environment.
2. *Direct energy from environment*: Instead of capturing only the portion of environmental energy directly available, redirect and concentrate previously unused energy into the system. For example, a horizontal-axis wind turbine captures energy from just one direction. A vertical-axis turbine can capture wind energy from any direction in the horizontal plane.
3. *Separate energy*: Increase efficiency of energy collection or extraction.
4. *Transform energy*: Amplify conjugates or otherwise alter energy into a form more conducive to conversion to electricity (e.g., increasing velocity, amplitude, or frequency).
5. *Convert energy*: This is the system's core technology and is more difficult to improve without basic research
6. *Condition electrical energy*: Use active control to improve efficiency beyond that of passive rectifying and smoothing techniques.
7. *Store electrical energy*: Consider different forms of electrical storage (batteries, capacitors, ultra-capacitors, etc.) and non-electrical storage (flywheels, springs, fluid capacitances, etc.) to increase efficiency and reduce losses in short-term and long-term storage.

8. *Supply electrical energy to application*: Increase efficiency and ease of use through sensing power needs and actively optimizing power delivery.
9. *Interface with user*: Enhance user control and status feedback, and assess ways to integrate better aesthetics, usability, and blending.

As designers become familiar with these driving functions, their roles in energy harvesting, and the opportunities available for innovation, concept generation can be focused on innovative solutions to these smaller design problems. Many of these driving functions are largely independent, meaning that existing solutions and analogies can be borrowed from systems in vastly different fields. These sub-solutions can then be combined into working architectures customized for the specific applications at hand.

In many autonomous harvesters, the main goal of the driving functions is simply to capture and convert the available energy as efficiently as possible. However, with energy harvesters that interact with humans or animals, a second main focus is to actually encourage the contribution of more energy. This is often done by giving positive visual feedback to the user. For example, the Seiko Kinetic Direct Drive watch is powered primarily through normal body motion. However, power can also be generated manually by winding the crown. A colorful gauge on the face acts like a tachometer as the crown is wound, inspiring the user to see how much power can be generated. The Sustainable Dance Floor (SDC, 2007) generates power from the pressure and vibration of dancing partygoers. It encourages participation through LED lights on the floor tiles and a large LED meter near the DJ. The Toyota Prius, while not strictly an energy harvester, employs a very similar method by giving real-time visual feedback of power flow between the gas engine, electric motor, batteries, and regenerative brakes, as well as displaying

instantaneous miles per gallon estimates and giving the option for “power,” “eco,” or “EV” (electric vehicle) settings.

6.3.5 Insights into Functional Modeling

This study allows further review of functional modeling, and more specifically the functional common basis, as a tool in design. In using functional modeling, one common complaint is the non-uniformity in language, resolution, and conventions. The functional common basis makes many improvements in providing a common vocabulary. Much of the remaining confusion concerning functional modeling seems to come from difficulty standardizing and explaining organizational conventions and terminology.

For example, mechanical energy and human energy are two energy flows identified in the functional common basis. These two energies are physically similar (solids exerting forces and velocities), but it is useful to separate them due to differing relationships to customer needs (ergonomics and user safety introduce additional needs and functionality into human-related systems). This separation, however, often requires a conversion at some point from human energy to mechanical energy. There is currently no standard convention to model when and how this occurs. Does the human energy become mechanical energy the instant it enters the system with the human? When it is transferred from the human into the structure of the product? When it is converted into “useful” motion such as shaft work? Small variations such as these are irrelevant when working with a single functional model, but make it difficult to effectively compare functional models of different systems and from different designers, just as non-standard function terminology has in the past.

Beneficial future research in this area would more carefully clarify function and flow definitions and give standardized examples of common sources of confusion. Some

of this information is available in previous literature, but much is merely implied or has been explained orally. A straightforward introduction and guide to functional modeling using the functional common basis would be an invaluable tool to designers not familiar with the process.

6.4 Conclusions From Functional Modeling

Functional modeling can be an excellent tool for understanding and creating new designs. By applying functional modeling to energy harvesting, the designer can identify key opportunities for innovation in the driving functions of the systems. Through the modeling and analysis of 39 example energy harvesters, a close functional relationship among such systems was observed and quantified. Systems in the same domain typically follow very similar function structures, differing only by the addition or subtraction of a few supplementary functions. Systems in different harvesting domains usually employ similar functions as well, differing by the material and energy flows that interact with the system. A generalized energy harvester can be described by the nine main functions identified in Section 6.3.3 and 6.3.4. With the exception of the core energy conversion function, which may require extensive basic research to bring substantial improvement, each of the functions present clear opportunities for innovation.

The identification of these functions can also assist in the design of new systems by facilitating design by analogy with other domains. For example, solar harvesters often make use of mirrors and lenses to direct energy (redirecting and concentrating it). How would this be accomplished in the vibration domain? In the thermal domain? Because these other domains make use of different materials and energies, it is beneficial to have foreknowledge of what functions may be necessary and how these might be practically employed in each domain. Familiarity with typical functional models of energy

harvesters across domains enables greater innovation through identification of driving functions of interest and how they relate to equivalent functions in other energy domains.

Chapter 7: Concept Generation for an Energy Harvester Portfolio

7.1 Specific Design Problem

The design problem pertaining to this dissertation is part of a NIST-sponsored joint venture involving the Mechanical Engineering, Civil, Architectural, & Environmental Engineering, and Electrical & Computer Engineering Departments of The University of Texas at Austin; National Instruments; and Wiss, Janney, Elstner Associates. As stated in its initial proposal, the purpose of this venture is the "development of low-power, wireless sensor networks for long-term monitoring of highway bridges" (Development, 2009). The same proposal details the focus of its energy-harvesting portion as identifying "the best combination of energy sources (in terms of energy density, quality of available energy, efficiency of conversion, robustness, and cost) to support long-term monitoring of highway bridges." The specific design problem addressed in this dissertation can thus be summarized:

Design Problem: *Develop an energy-harvesting system or suite of systems that can power a wireless sensor network on a variety of different highway bridges, with focus on powering National Instruments hardware on one or more example bridges in central Texas.*

Innovating a solution to this design problem would aid in the assessment of this dissertation's primary hypothesis, as discussed in Chapter 1:

Research Hypothesis: *Energy-harvesting systems can power wireless sensor nodes in a typical bridge environment with greater efficiency and longer life than currently exists in the state-of-the-art.*

Because of the wide variety among bridges of environmental energy sources, bridge geometry, monitoring needs, and other characteristics, the design process for this problem will pursue multiple solutions using different energy-harvesting domains. The end user can then choose one of a suite of interchangeable systems to power the wireless nodes, depending on the characteristics and needs of that location.

7.2 CUSTOMER NEEDS AND KEY FUNCTIONS

As with any design problem, an important part of the process is "understanding the opportunity" through the identification of customer needs and key functionality. These can then be translated into a set of engineering specifications. One procedure for producing such a specification list was developed by Franke (1975) and described by Otto and Wood (2001). Franke studied several existing specification processes then in use in the industry and developed specification categories that can be examined to aid in developing a complete set of specifications. This breakdown is listed in Table 7.1. Specifications should include both functional requirements (what the system must do) and constraints (conditions or boundaries that must not be violated).

Table 7.1 Categories for searching and decomposing specifications (Otto & Wood, 2001)

Specification Category	**Description**
Geometry	Dimensions, space requirements, etc.
Kinematics	Type and direction of motion, velocity, etc.
Forces	Direction and magnitude, frequency, load imposed by, energy type, efficiency, capacity, conversion, temperature
Material	Properties of final product, flow of materials, design for manufacturing (DFM)
Signals	Input and output, display
Safety	Protection issues
Ergonomics	Comfort issues, human interface issues
Production	Factory limitations, tolerances, wastage

Quality Control	Possibilities for testing
Assembly	Set by DFMA or special regulations or needs
Transport	Packaging needs
Operation	Environmental issues such as noise
Maintenance	Servicing intervals, repair
Costs	Manufacturing costs, material costs
Schedules	Time Constraints

To generate specifications for the current project, customer needs were first identified and assessed. This was primarily done through discussion with venture partners with relevant expertise (such as civil engineering professors, hardware engineers at National Instruments, and structural-health-monitoring project managers at WJE Associates), as well as outside sources such as staff at the Texas Department of Transportation and people of non-engineering background similar to those who would be installing the final system. These customer needs were formalized into a draft specification sheet, which was then discussed and modified at a meeting involving the mechanical engineering team, civil engineering team, and National Instruments representatives. The revised specification sheet is found in Appendix F.

The specified functional requirements primarily relate to the power requirements to support a wireless sensor network, including low-power end nodes, router nodes, and gateway nodes. The calculations of these requirements are detailed in Chapter 4. Major constraints for the system include geometric, ergonomic, and assembly requirements to enable easy installation on a variety of bridges, material, force, and safety requirements to ensure secure and safe operation, and thresholds for operation life, maintenance intervals, and cost.

7.3 INSIGHTS FROM FUNCTIONAL MODELING

In designing new energy-harvesting systems, substantial improvements over existing products may be possible through focusing on the key driving functions discussed in Chapter 6. Innovation may bring improvement in two main ways. First, existing subsystems and functionality can be refined with a better understanding of their overall functional purpose. For example, a vane on a wind turbine may be used to fulfill the function "direct energy from the environment." With this in mind, the designer may focus not only on developing a better vane, but a more innovative means to direct, filter, and concentrate wind energy into the harvester, perhaps from multiple directions and from a larger area.

A second way innovation focused on the nine driving functions may bring improvement is by introducing previously unharnessed functionality. For example, many inexpensive wind turbines use a direct drive to transmit energy from the turbine blades to the generator. Adding a gear train or similar subsystem introduces the new functionality of "transform energy into form ready for conversion" and will increase the efficiency and power output of the harvester.

As new concepts are developed, it is useful to periodically step back and assess how the proposed concepts address these key driving functions. By working to include and improve as many of the functions as feasible, the initial concepts can be improved and developed into fully functional, complete systems for energy harvesting.

7.4 CONCEPT GENERATION PROCESS

Several avenues of concept generation were followed in the design of a suite of energy-harvesting systems. The first ideation processes consisted of formal brainstorming sessions in groups, relying heavily on intuitive methods like mind mapping and 6-3-5 (as

discussed in Chapter 2). These brainstorming sessions were deliberately open-ended, allowing for many energy domains and scales, and welcoming unconventional and even impractical ideas. Later concept generation involved group and individual ideation focused on developing concepts in a specific domain and developing the most promising ideas into proof-of-concept prototypes.

7.4.1 ME 366-J Students

The first instance of formal concept generation was conducted in May, 2009, in a senior-level engineering design class at the University of Texas, ME 366-J. Approximately seventy students were divided into nineteen teams. The teams were given a brief introduction to the design problem, including the following explicit customer needs:

- Supply enough energy throughout the day to power a sensor (thermocouple, strain gage, etc.) and a wireless transmitter
- Sensor and wireless transmitter may be used intermittently or continuously
- Operation should not affect normal bridge operation and traffic
- System is resistant to vandalism and theft
- Service life of >10 years without maintenance
- System can be easily installed on new and existing bridges

The teams were also given an "Energy Morph Matrix," a table listing various forms of energy storage, transmission, and conversion to aid in formulating complete energy systems (Appendix G). The teams were given several minutes to brainstorm, using a mind map to record ideas and focusing on finding solutions with as many different energy sources as possible. They were then encouraged to compare their results to the Energy Morph Matrix, filling in any gaps in the matrix with additional ideas.

Finally, the teams did several rounds of 6-3-5, focusing specifically on the domains of solar, wind, and vibration.

Following this format, the nineteen teams came up with 119 unique solutions, with an average of 20 total solutions per team (6 unique solutions per team). The concepts illustrated solutions to six key functions, identified then as "import energy," "transform energy to electricity," "transmit energy," "direct energy," "store energy," and "secure harvester." Many solutions were found to each key function. Over fifty were given for "import energy," including examples of thermal, chemical, radiant, fluid mechanical, solid mechanical, electrical, biological, and seismological energy. Several examples of the teams' 6-3-5 sketches and resulting concepts and trends are shown in Appendix H.

7.3.2 USAFA Cadets

Concept generation for this design problem was also done in the fall of 2009 by engineering cadets at the US Air Force Academy as part of a study examining the effect of different concept generation techniques (Walker, Jensen, Crider, Weaver, Wood, & Maixner, 2010). The primary effect being investigated was the possibility of design fixation resulting from early prototyping experience. Two teams of cadets were formed, a control group and an experimental group. After completing some initial background research and customer needs analysis, the experimental group jumped directly to selecting a concept and producing a rapid prototype in the first two weeks of the design process (a piezoelectric based micro wind turbine, Fig. 7.1). Then, the experimental and control groups both completed a round of 6-3-5 brainstorming. Sample results from this process are shown in Appendix J.

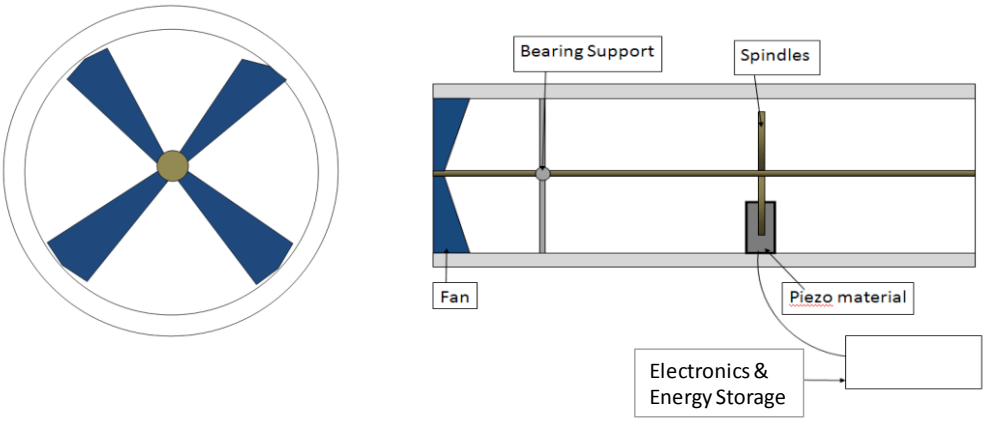

Figure 7.1 Piezoelectric micro wind turbine prototype (Walker, et al., 2010)

Following the completion of these activities, three experts (engineering faculty members) evaluated the results from each team for innovation, diversity, and feasibility. The findings of this evaluation are shown in Table 7.2. This analysis determined that incorporating early experience with prototyping in the design process resulted in concepts that were more feasible, but less diverse. After experimenting with physical prototypes, the designers were better equipped to generate solutions that would work in real life. However, they did exhibit a certain amount of design fixation, generating a less diverse group of solutions than the control group.

Table 7.2 Expert ratings of control and experimental design teams (Walker, et al., 2010)

	Average Ratings		
	Innovation	**Diversity**	**Feasibility**
Control	5.5	5.3	4.2
Experimental	5.4	4.9	6.3
Avg. Difference Between Raters' Scores = 1.39			
"Control" produced 30% more unique concepts then "experimental"			

7.3.3 Graduate Students

Following the two initial concept generation exercises, additional graduate students were brought on board the energy-harvesting team. In keeping with the intent to develop a suite of interchangeable energy-harvesting systems, each student was given responsibility to lead development of a different energy domain. The areas chosen for initial focus were wind harvesting, vibration harvesting using electromagnetic induction, and vibration harvesting using piezoelectric materials. These three areas were chosen because they had been shown to be feasible for the desired application, but had not thus far been widely implemented commercially. Because of the already widespread use of solar power and the relative maturity of the technology, this domain was deferred to later study, as will be described in the next section.

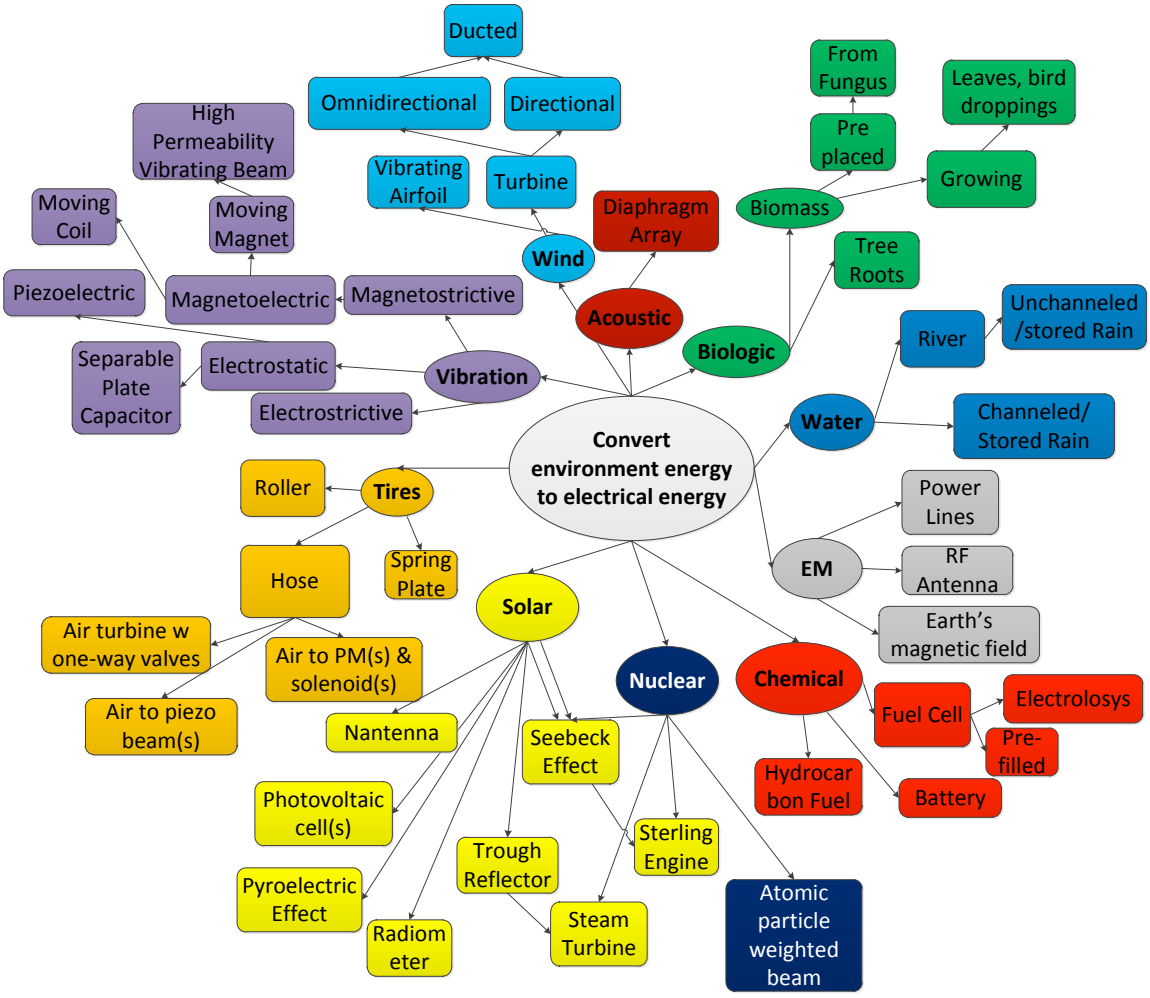

Figure 7.2 Mind map assembled by graduate students to summarize earlier efforts

Wind Harvesting

As has been discussed previously, wind harvesting in a bridge environment presents several unique challenges. Turbine location is limited to avoid interference with traffic. In many cases, this means that the turbine must be positioned up between the I-girders and cannot hang below the structure (Fig 7.3). Because wind speed drops considerably within the structure, there is only a narrow layer above the bottom where wind is available. This wind is often low velocity, turbulent, and highly variable in both

direction and speed. Attaching to the bridge is also a major issue, as no permanent changes to the bridge (such as welds or holes) are usually permitted.

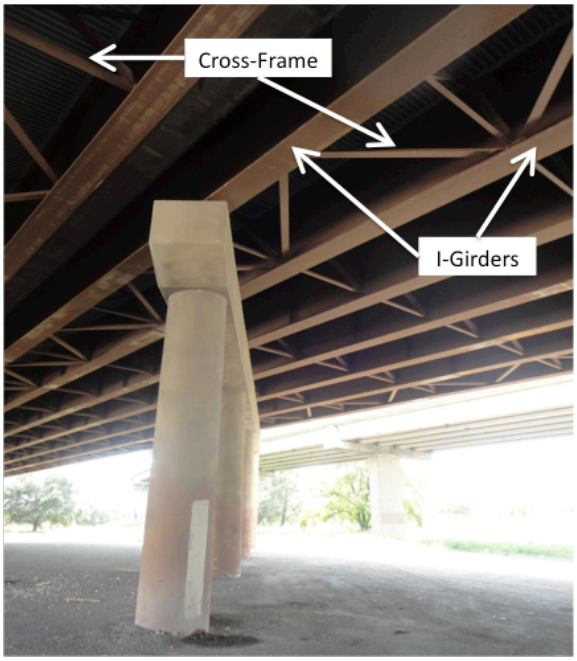

Figure 7.3 Substructure of I-35N Medina River Bridge in San Antonio, Texas

Concept generation of a novel wind harvester primarily focused on presenting solutions to these challenges. Vertical-axis wind turbines were considered most appropriate, as they are omnidirectional and can operate at lower speeds than horizontal-axis turbines. Several ideas were proposed to capture power at wind speeds lower than what is currently possible with electric generators, including counter-rotating stators and transitioning to a piezoelectric generator (like the USAFA cadets built) at low speeds. Concepts also included innovative methods to attach to the I-girders and cross frames, including both magnetic connections and more traditional clamping mechanisms. Several example concepts are shown in Fig. 7.4 (McEvoy, 2011).

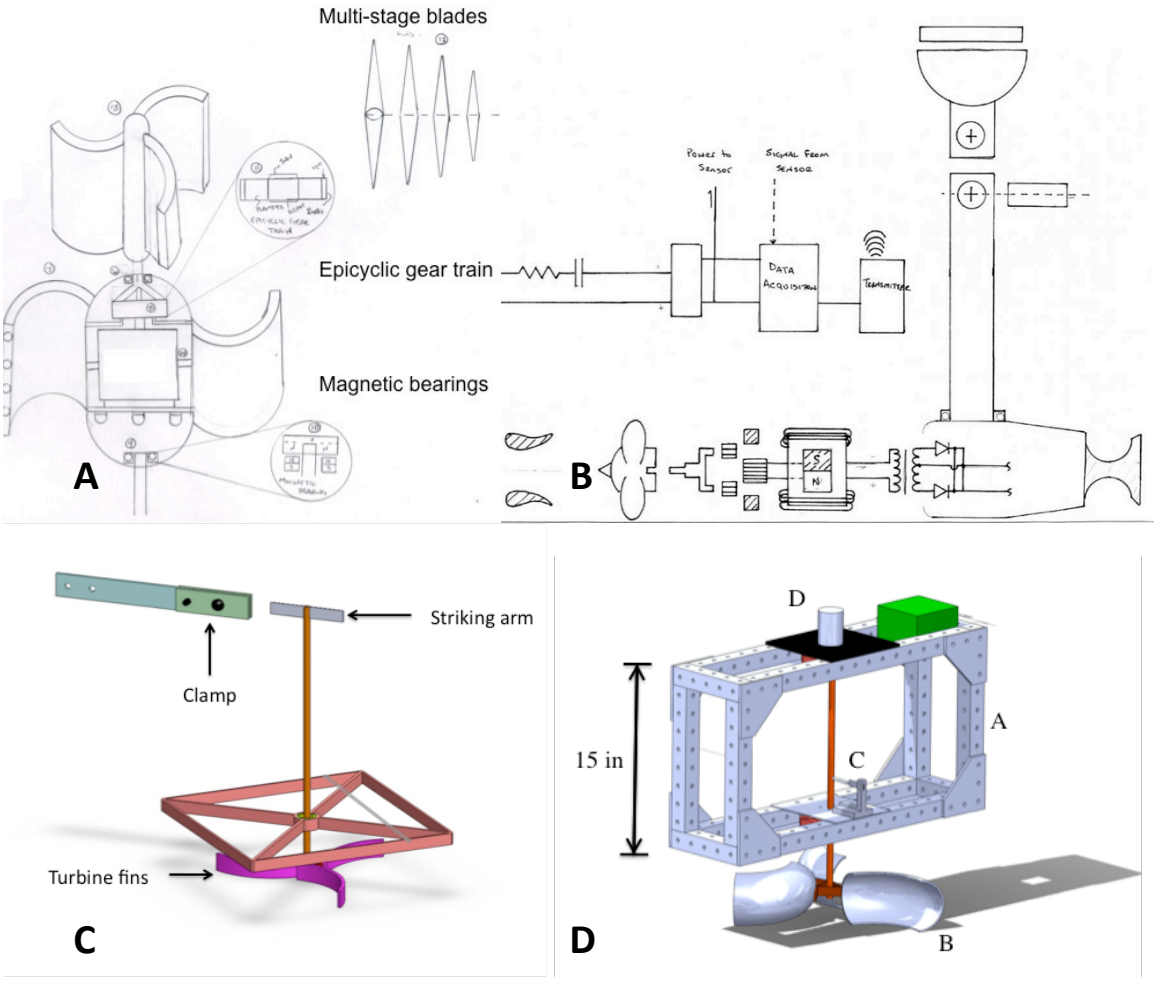

Figure 7.4 Concepts for wind harvesting on a highway bridge

Concept A shows a Savonius-type vertical-axis turbine, including a counter-rotating electric generator, maglev-type magnetic bearings, an epicyclic gear train, and possibly an array of different size turbine blades for different wind speeds. Concept B shows a horizontal-axis turbine with a vane to direct it into the wind, a nozzle-type structure in front to concentrate and amplify wind flow, an epicyclic gear train, and a magnetic coupling to attach the mounting shaft to the bridge. Concept C shows a Savonius turbine with a striking arm that repeatedly hits a piezoelectric ceramic to

generate electricity instead of an inductive generator, with turbine blade shape optimized for the narrow region of useful air flow at the bottom edge of the I-girders. Concept D shows a more developed version of this idea, with a single turbine powering both a traditional inductive generator and a low-speed piezoelectric generator.

Inductive Vibration Harvesting

Vibration harvesting on a bridge presents several challenges compared to existing vibration-harvesting applications. In order to maximize power output, vibration harvesters are typically designed to naturally resonate at the same frequency as the incoming vibration. Because of this, these harvesters are only usable over a narrow, fixed frequency bandwidth. For example, many inductive harvesters are designed to capture the vibration resulting from motors running on grid power at 50 or 60 Hz (or double the frequency at 100 or 120 Hz). This application works well because the vibration is constantly occurring and reliably within a narrow bandwidth. However, vibration on a bridge can be intermittent and vary significantly from bridge to bridge. It can even vary somewhat with time of day and season, due to changes in temperature.

Concept generation in this area addressed these challenges by investigating ways to capture additional frequencies by either widening the bandwidth or tuning to different resonant frequencies. In particular, designs used adjustable threads, magnets, or springs to alter the spring constant and therefore the natural frequency of the system, and magnets, nonlinear springs, and novel geometries were proposed to introduce nonlinearity and increase bandwidth. Several of these concepts are shown in Fig. 7.5 (Dierks, 2011).

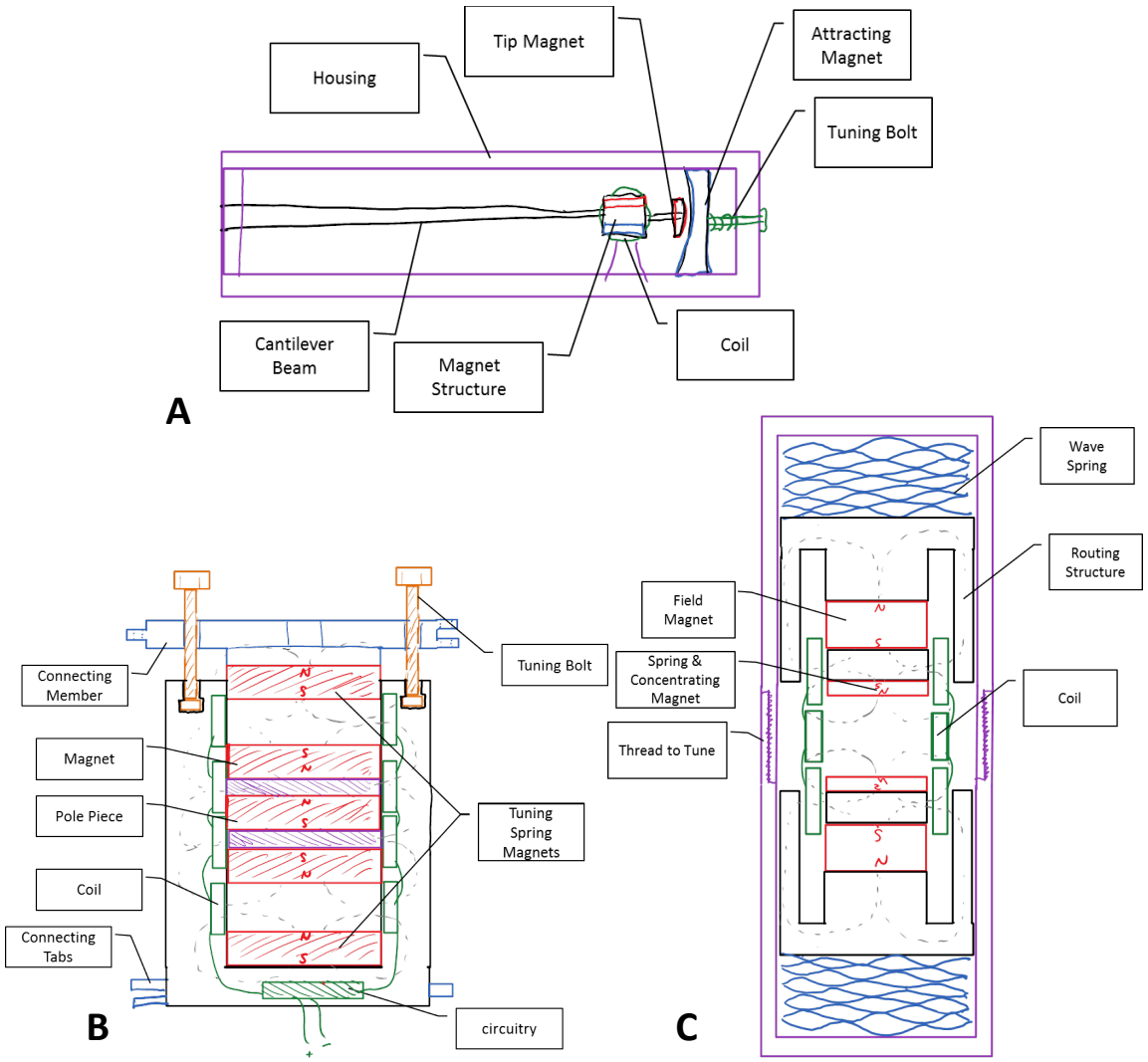

Figure 7.5 Concepts for inductive vibration harvesting on a highway bridge

Concept A shows a long cantilever beam with a mass at the tip, with the beam and mass sized to oscillate at a specific frequency. The tip mass is magnetic, and it moves past a coil as the beam moves, generating current. The natural frequency of the structure can be altered by moving a pair of magnets (one attached to the beam and one to the enclosure) closer together. Concept B shows a set of stacked magnets that moves vertically within a coil. Using the multiple magnets increases the gradient of the magnetic

field between around each magnet, increasing the output from the coils. The magnetic core is supported by a spring or pair of repelling magnets, which can be adjusted to tune the system's natural frequency. Concept C shows a similar idea, with wave springs returning the oscillating core to conserve space. Tuning in this system is accomplished by moving threads to lengthen or shorten the enclosure. In addition, the multiple magnets in the core are positioned so that they pass through the coil at different times, creating a multiple-phase signal (as opposed to a simple sine wave) that is more efficiently converted to a DC signal.

Piezoelectric Vibration Harvesting

There are two widely used configurations for piezoelectric-based energy harvesting. Piezoelectric materials exhibit polarization along one axis, as shown in Fig. 7.6. The ratio between strain and electric field (or alternately, between charge density and stress) is the piezoelectric strain coefficient, *d*.

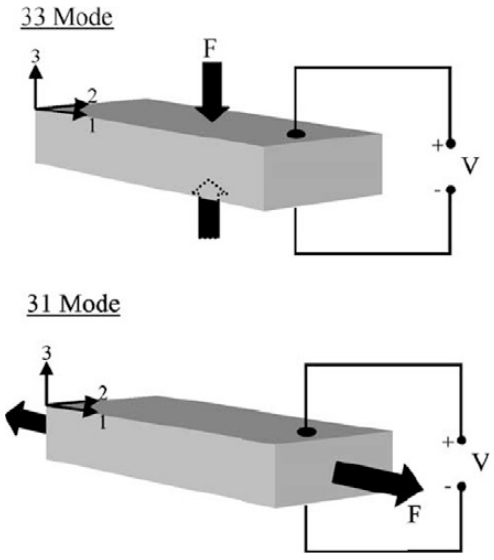

Figure 7.6 Polarization and notation of axes (Roundy, Wright, & Rabaey, 2003)

The highest piezoelectric strain constant is found by inducing strain in the material along the same axis, typically referred to as d_{33} because both strain and voltage are directed along the z (or 3) axis. Many piezoelectric systems use this mode, often using sudden impact loads to induce voltages (e.g., igniters for gas stoves and grills). However, operation in this mode is often limited by losses in the mechanical impact, brittleness of the piezoelectric ceramic, and the high cost of manufacturing solid ceramics of sufficient size (use of solid materials thicker than a few millimeters is rare because of the high voltage gradients needed to polarize through the thickness). In many cases, it is preferable to induce strain perpendicular to the voltage, using the strain constant d_{31}. This strain constant is roughly half of d_{33}, but overall efficiency often proves much higher. The typical configuration for this type of harvesting is to use a cantilever beam with piezoelectric ceramic or film affixed to the top and/or bottom of the beam. As the beam vibrates up and down, the piezoelectric material is alternately placed in tension and compression. Such a structure is called a bimorph if it includes two piezoelectric layers or a monomorph if it includes just one. An example bimorph harvester is shown in Fig. 7.7.

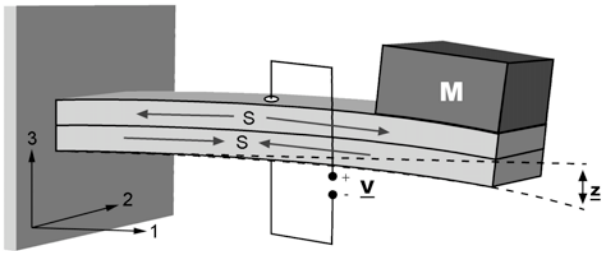

Figure 7.7 Example cantilever bimorph (Roundy & Wright, 2004)

As an example of harvesters using the d_{33} and d_{31} directions, Fig. 7.8 shows two prototypes that harvest compression in shoes. The first captures compression directly in the d_{33} direction (Kymissis, Kendall, Paradiso, & Gershenfeld, 1998). The second uses a

spring-like structure to convert compression into bending along the d_{31} axis, with improved results (Shenck & Paradiso, 2001).

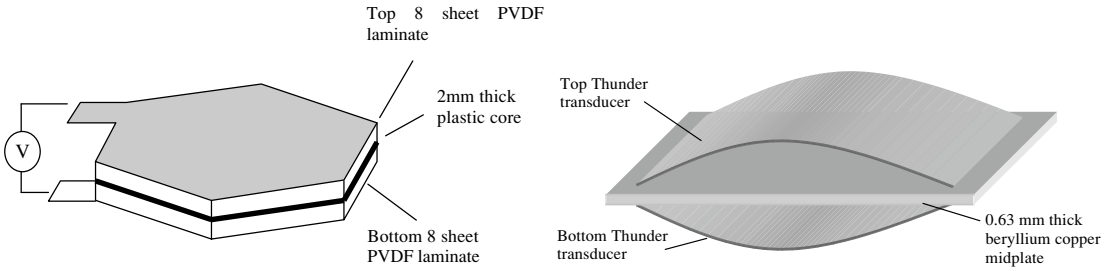

Figure 7.8 Two alternate prototypes for harvesting from shoe impacts (Kymissis, et al., 1998; Shenck & Paradiso, 2001).

There are several key differences between inductive and piezoelectric vibration harvesting that may or may not be advantageous. In general, inductive systems generate a relatively low voltage and high current; while a piezoelectric harvester rated at the same power will produce a higher voltage but lower current. The oscillating motion in inductive systems can be produced by a spring of virtually any material, since the magnet and coil themselves are not being stressed. Because the power in a piezoelectric system is due to strain within the ceramic itself, the performance envelope is more limited and material dependent; stresses must be consistently high enough to generate power, but not so high as to fracture the brittle ceramic element. In addition, these ceramics are fairly stiff, limiting the overall spring constant of the systems. Finally, piezoelectric film can be screen-printed and etched using processes typical for microchips and MEMS devices, but magnets and coils become difficult to incorporate at small scales.

Because of these differences, the primary use of piezoelectric harvesters today is in systems with high-frequency vibration (>100 Hz, often >1 kHz) or in MEMS devices too small to build coils and magnets with sufficient magnetic field strength (Beeby, Tudor, & White, 2006). However, there are currently many studies examining how

piezoelectric vibration harvesting can be beneficial beyond these narrow applications (Ferrari, et al., 2010; Jung & Yun, 2010; Wickenheiser & Garcia, 2010).

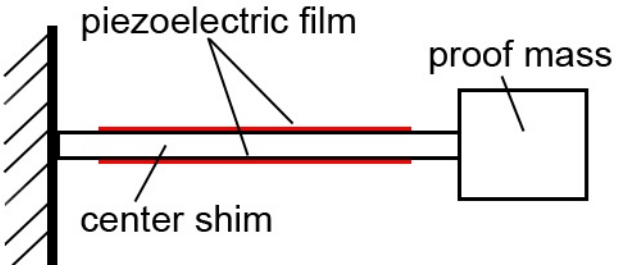

Figure 7.9 Basic piezo cantilever bimorph

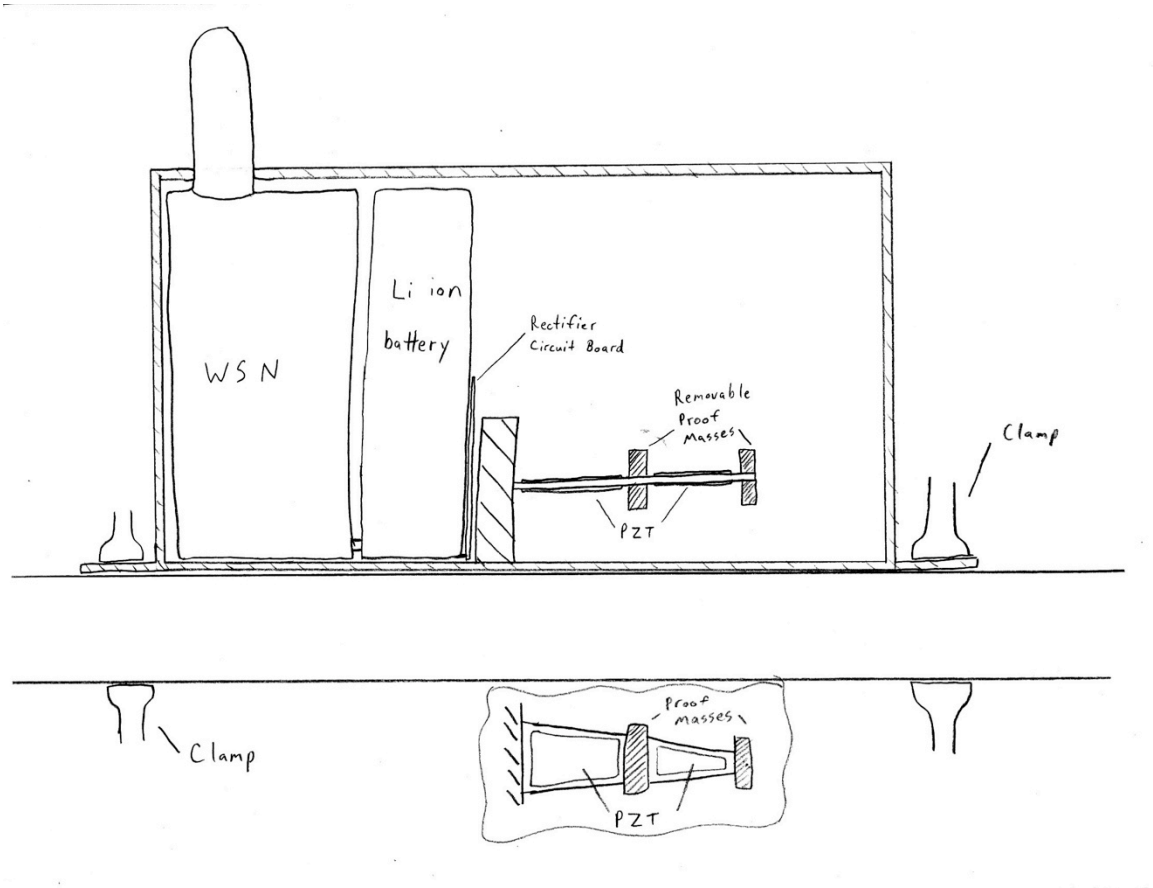

Figure 7.10 Concept A: two-mass bimorph harvester

The starting point for generating concepts for piezoelectric vibration harvesting is the standard cantilever bimorph, shown in Fig. 7.9. One of the first concepts sketched out is shown in Fig. 7.10. This concept illustrates a self-contained enclosure with a single bimorph charging a lithium ion battery to power the wireless node. Several key innovations that are included are drawn from previous literature:

- Multiple proof masses to amplify resonance at the first two harmonic frequencies
- Separate piezo elements on two regions of the beam to capture alternating strain due to the second harmonic
- Triangular beam geometry to create equal strain levels throughout the length of the beam, instead of concentrating it at the base (as with rectangular geometries)

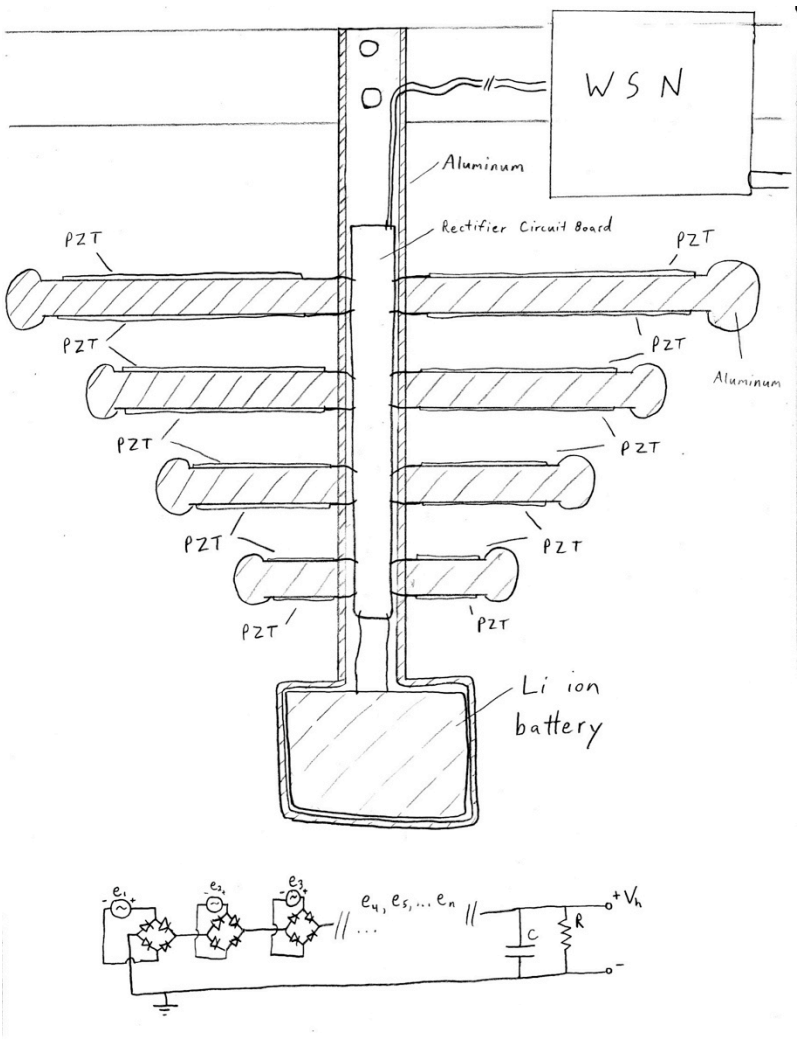

Figure 7.11 Concept B: “tree” bimorph array

Figure 7.11 shows a second concept. This system draws on an analogy of a tree, branches waving in the breeze. Here, the “branches” of the tree are an array of bimorphs of different sizes, tuned to vibrate at a range of frequencies resulting from traffic on the bridge. The central “trunk” is also outfitted with piezoelectric material, and is tuned to vibrate at the frequency of turbulent vortex shedding resulting from wind (turbulence in the wind causes alternating low-pressure points on either side of the structure, leading to a resonant behavior).

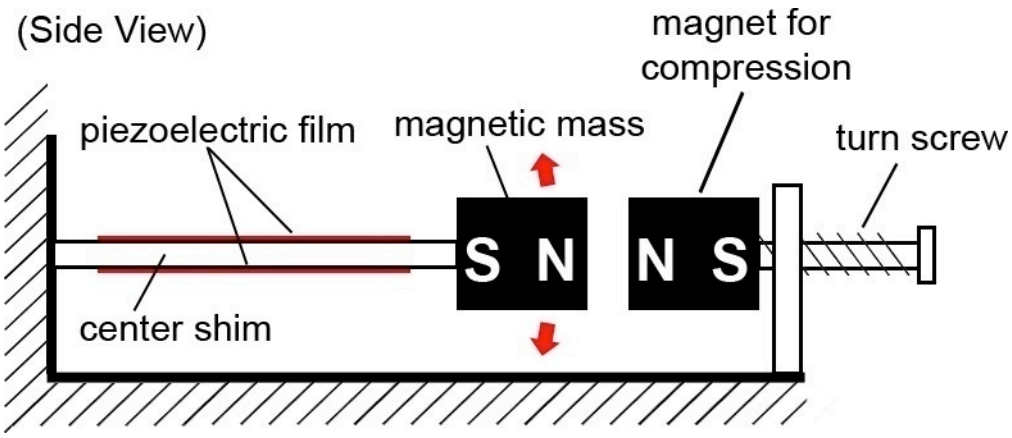

Figure 7.12 Concept C: magnet-based bistable structure

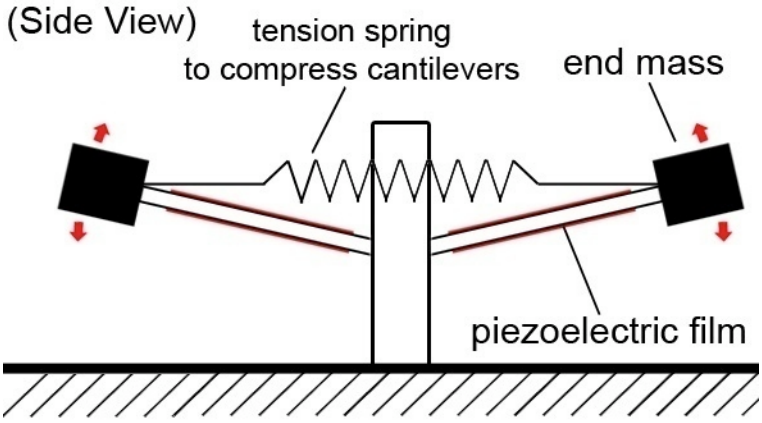

Figure 7.13 Concept D: spring-based bistable structure

Figures 7.12 and 7.13 show two additional concepts that incorporate nonlinearity and adjustable parameters to tune the harvesters to specific frequencies. In Fig. 7.12, a magnet fixed to the base is positioned to repel a magnet on the tip of the beam. As the two magnets are moved closer together, a bistable system is created. The beam can vibrate above or below the center point at one frequency, or assuming a high enough supplied mechanical energy, it can jump back and forth across the center point at a lower frequency (Ferrari, et al., 2010). The ability to move the fixed magnet closer and farther from the beam allows for tunability, as moving it closer will increase the magnitude of

the bistable behavior and lower the effective resonant frequency (see Jung & Yun, 2010). Figure 7.13 shows a similar concept that uses tension springs to pre-compress twin cantilever beams, leading to the same bistable behavior (see Clingman & Ruggeri, 2006).

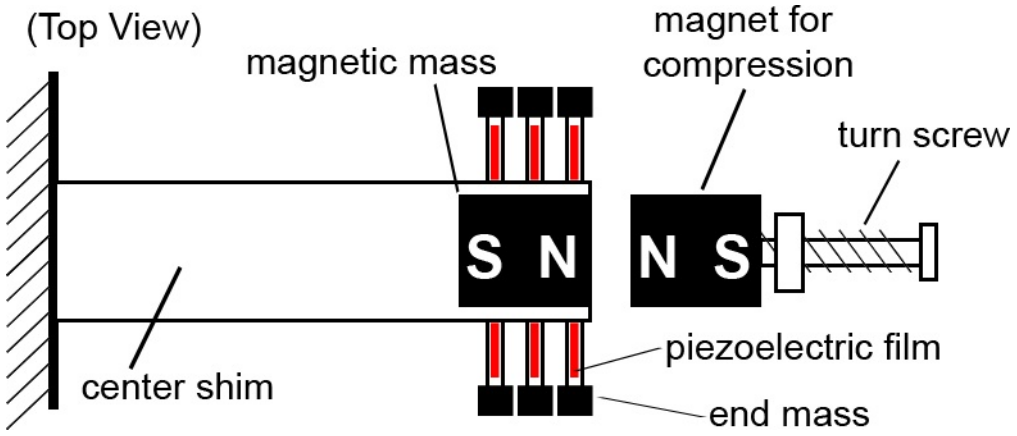

Figure 7.14 Concept E: Up-converting bimorph array

Initial calculations indicate that it may be difficult to size a bimorph that can resonate at low frequency (1-10 Hz) and remain within the ultimate strength of the piezoelectric ceramic. A low natural frequency requires a large mass and a low stiffness of spring constant. Both of these requirements increase the total displacement of the oscillating beam and the maximum stresses at the base. If placing piezoelectric material on the main beam is not feasible, it may be desirable to incorporate a method of converting a low incoming frequency into a higher frequency for harvesting (Jung & Yun, 2010). One such concept is shown in Fig. 7.14. Here, the opposing magnets create a bistable behavior with such force that there is a sudden snapping or popping action whenever the beam crosses the center point. This snap transmits an impulse load to several smaller bimorphs that are attached to the main beam, exciting them. These small bimorphs then resonate freely at their own higher natural frequencies.

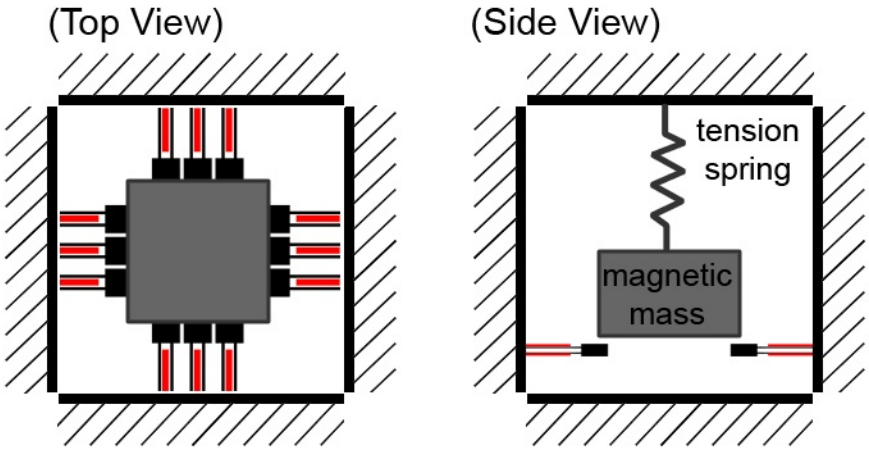

Figure 7.15 Concept F: bimorph array with "plucking" action

One final concept is shown in Fig. 7.15. Here, a large magnetic proof mass is tuned to oscillate at a low frequency. This mass moves past an array of small bimorphs, exciting them either by direct contact or through its magnetic field. These bimorphs then resonate at their higher frequency, damping out by the next time the mass passes them and re-excites them (see Rastegar, Pereira, & Nguyen, 2006).

7.3.4 ME 266-K Capstone Team #1

The domain of solar harvesting was given to a three-person senior design team enrolled in ME 266-K. They were asked specifically to focus on creating an innovative and versatile method for supporting a solar panel and mounting it to a bridge of variable geometry, as well as making the system resistant to external threats from the elements, wildlife, and vandalism (McFarland, Mullis, & Riley, 2010). The team chose to design their system to be able to power a 10 W CompactRIO and to be mounted on the I-35/US-290 Interchange, a box-girder bridge (McFarland, Mullis, & Riley, 2010).

The first concept they described (Fig. 7.16) is a three-degree-of-freedom mounting system that can rotate about two axes and also telescopes. Lock pins inserted

into holes are used to fix its position. This concept calls for installation by drilling anchors into the concrete near the edge of the deck, which may or may not be allowable.

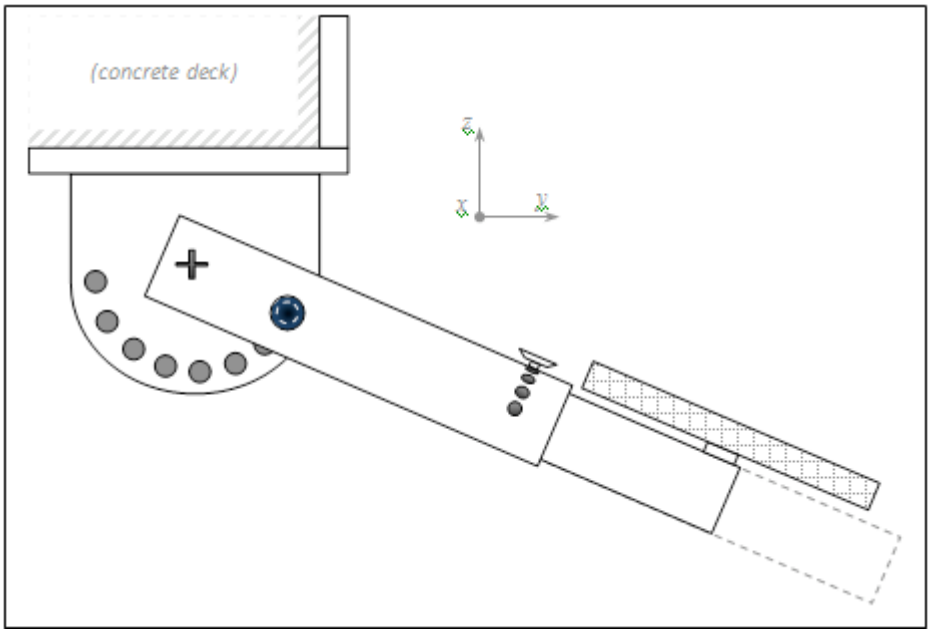

Figure 7.16 Concept A: Three-DOF "fly machine" concept with lock pins

A second concept described relies on three off-the-shelf components to facilitate easy installation and adjustable geometry. The panel is supported by a Unirac pole mount, which connects to a steel pipe (Fig. 7.17). This in turn is bracketed to a brace constructed of Unistrut angle iron (Fig. 7.18). The brace is attached to the bottom of the box girder by clamping on to two flanges with I-beam clamps (Fig. 7.19). This results in a modular system that can be mounted to adjustable height and offset from the bridge. The solar panel is connected to a charge controller that monitors the voltages of the panel and a lithium-ion battery and adjusts the load to ensure maximum efficiency.

Figure 7.17 Unirac pole mount for 40-W solar panel

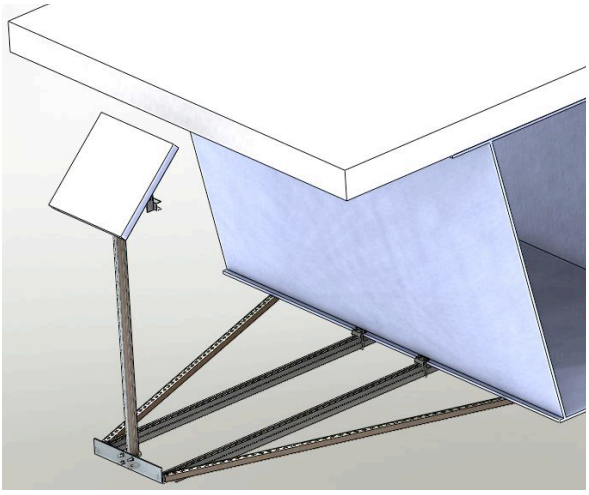

Figure 7.18 Concept B: Modular mount using Unirac pole mount and Unistrut angle iron

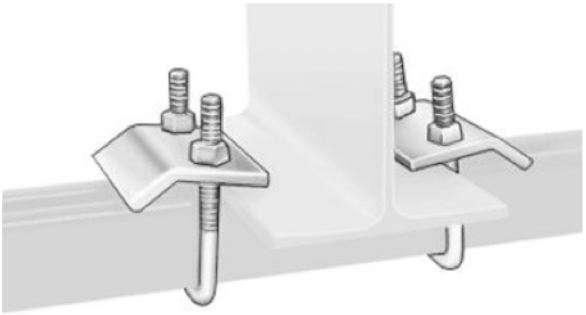

Figure 7.19 I-beam clamps

7.4 Concept Evaluation and Selection

The areas of solar, wind, inductive vibration and piezoelectric vibration each have different advantages and limitations. Since many of these characteristics are highly dependent on the local environment and geometry of each bridge, it is desirable to develop a portfolio of related energy-harvesting systems that can be interchanged according to circumstance. Because of this, it was decided to pursue at least one concept in each of the areas. Figures 7.20-7.23 show initial CAD models of the selected concept variants, based on the concepts described in the previous sections. In selecting the concepts to pursue through prototyping and testing, special attention was given to the ability of the concept to fulfill the specifications listed in Appendix F. In particular, primary importance was given to whether the concept could (A) provide power at least sufficient to power the low-power wireless node on the lowest setting and (B) be successfully manufactured as a proof-of-concept prototype within the scope of a dissertation, thesis, or capstone project, as appropriate.

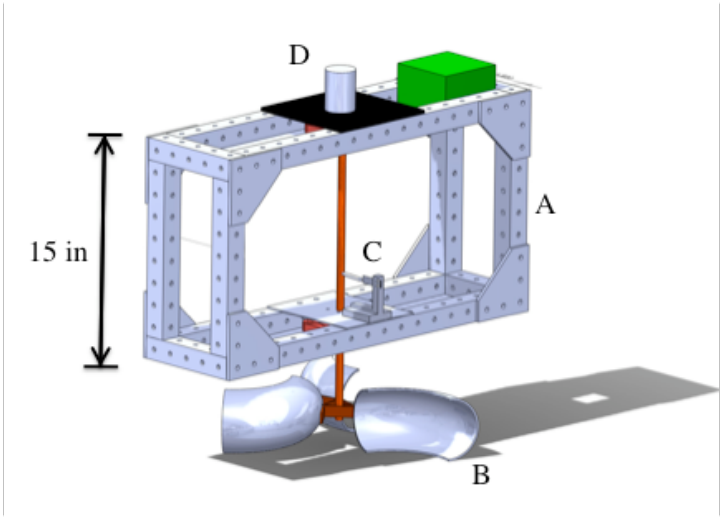

Figure 7.20 Selected concept variant for wind harvesting (Concept D)

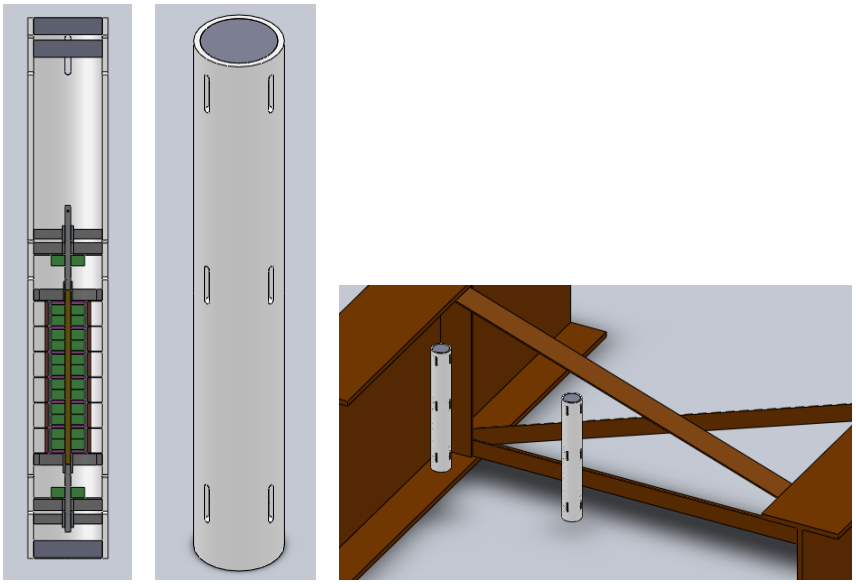

Figure 7.21 Selected concept variant for inductive vibration harvesting (Concept B)

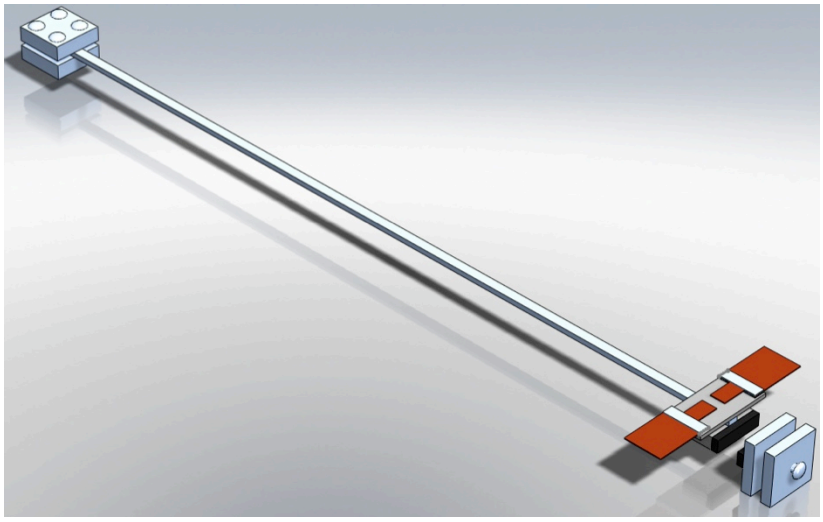

Figure 7.22 Selected concept variant for piezoelectric vibration harvesting (Concept E)

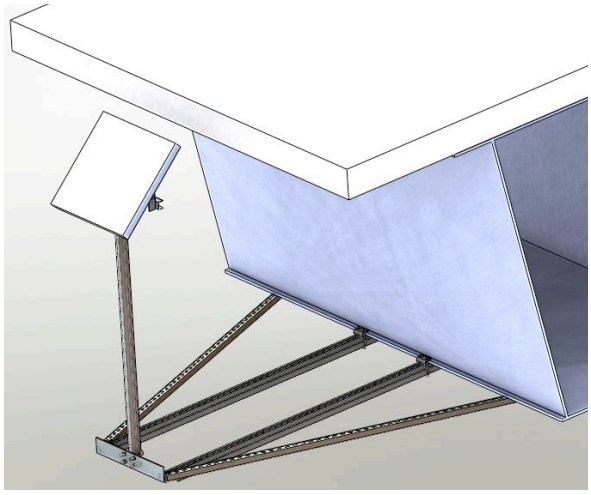

Figure 7.23 Selected concept variant for solar harvesting (Concept B)

Chapter 8: Development of an Exemplar Vibration Harvester

8.1 Selection of a Piezoelectric Concept Variant

Following the initial concept generation described in Chapter 7, concept variants in the areas of solar, wind, inductive vibration, and piezoelectric vibration were selected for further development. The development and testing of the solar, wind, and inductive vibration concepts are described in several concurrent theses and reports (McEvoy, 2011; Dierks, 2011; McFarland, Mullis, & Riley, 2010). This chapter details the development of a piezoelectric energy harvester concept through analytical modeling, physical prototyping, and laboratory testing.

In selecting a piezoelectric concept, several factors were considered. It was apparent that most existing piezoelectric harvesters were designed for higher frequencies and were generally not tunable. The concepts shown in the previous chapter address these issues by introducing innovations in several of the key functions mentioned in Chapter 6, namely, directing energy from the environment from multiple or changing frequencies and transforming energy from low to high impedance and frequency. Concepts A and B offer innovative geometries that capture vibration at multiple frequencies; however, they do not introduce advantages in low-frequency resonance beyond the original bimorph model. Concepts C and D offer means (via magnets and springs) to both lower the natural frequency of the system and allow for tuning about this new frequency. Existing systems utilizing these same techniques can be found in Fig. 8.1-8.4.

Piezoelectric systems operate most effectively under high-impedance loading, meaning a high force and low velocity. At low frequencies like the ones experienced on bridges, the simple cantilever bimorph may undergo greater displacement and velocity

relative to the loading force than at higher frequencies typical of most piezoelectric harvesters. In order to capture incoming vibration at a low frequency and preserve the high-impedance characteristics of the system, the incoming vibration can be transformed mechanically from continuous harmonic motion or free vibration into periodic impulses that excite bimorphs at more suitable frequencies. Concepts E and F introduce methods for "up-converting" the frequency similar to the existing systems shown in Fig. 8.5-8.6. These existing systems illustrate practical examples of using discontinuous impulses to transform low-impedance vibrational power into a higher-impedance form more suitable for the physics of the piezoelectric effect.

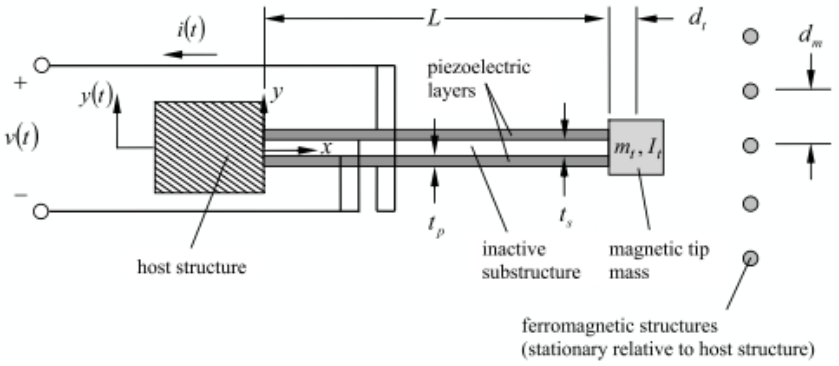

Figure 8.1 Magnetic attraction can increase frequency (Wickenheiser & Garcia, 2010)

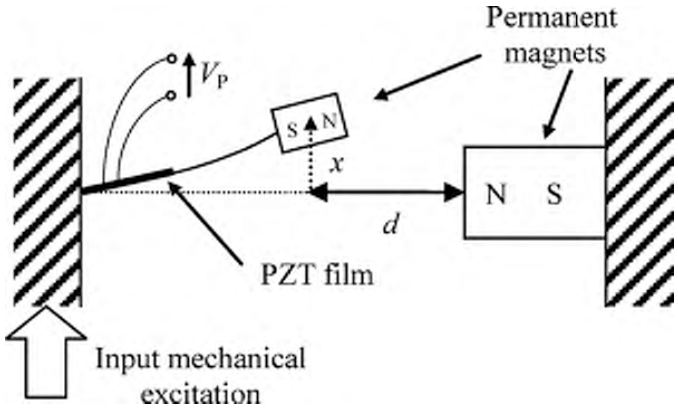

Figure 8.2 Magnetic repulsion can decrease frequency (Ferrari, et al., 2010)

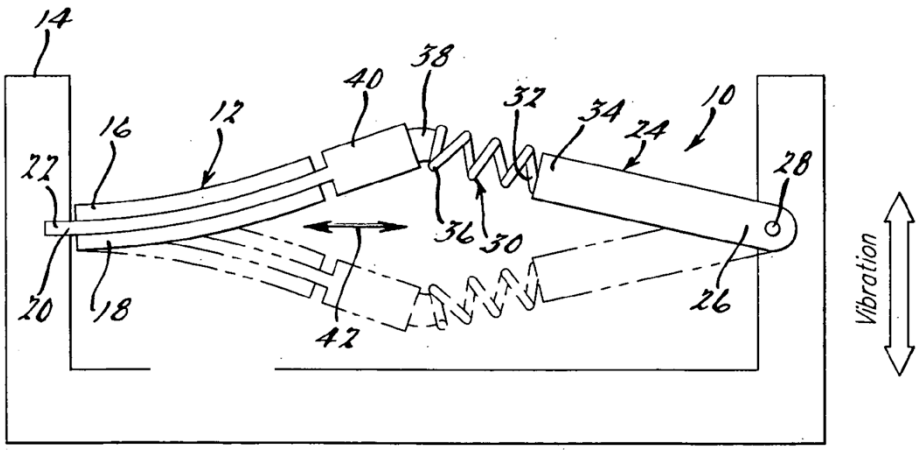

Figure 8.3 Spring-loaded bistable piezo harvester (Clingman & Ruggeri, 2006)

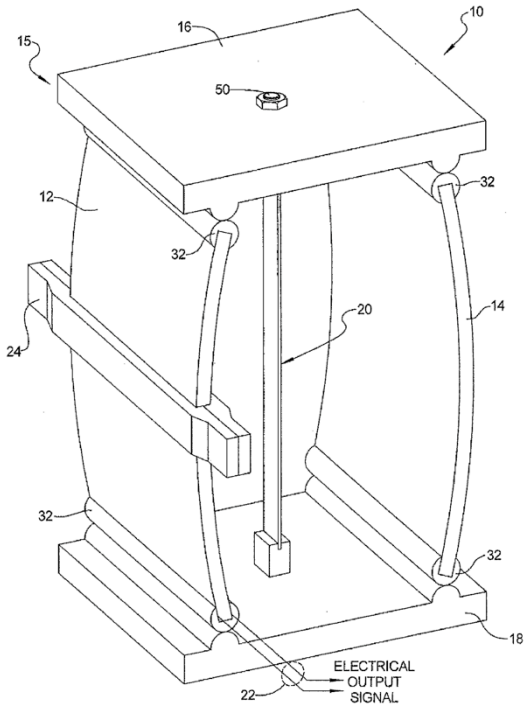

Figure 8.4 Improved bistable piezo harvester (Clingman & Ruggeri, 2009)

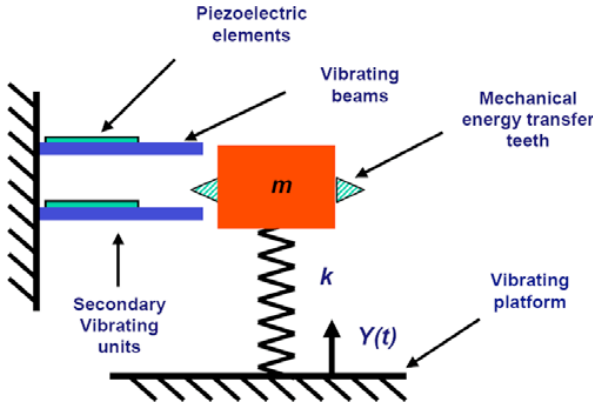

Figure 8.5 Up-converting "plucker" harvester (Rastegar, Pereira, & Nguyen, 2006)

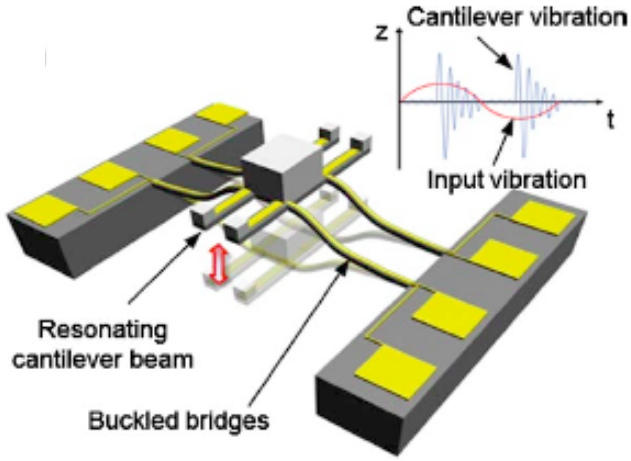

Figure 8.6 Up-converting bimorphs and bistable structure (Jung & Yun, 2010)

As the subsequent section will show, material and geometry choices that would allow a bimorph tuned to as low as two hertz to vibrate without fracturing are very limited. In addition, vibrating a piezoelectric bimorph at low frequency would result in a low-impedance input to a naturally high-impedance system. Because of this, the main focus of physical prototyping going forward is Concept E, shown again below in Fig. 8.7.

In the selected concept, low-frequency bridge vibration is transmitted to the main beam, a homogenous aluminum cantilever. As the vibration causes the main beam to

oscillate at its resonant frequency, the tip is subjected to sudden accelerations and decelerations due to interaction between the opposing magnetic fields of the two tuning magnets (later design uses mechanical impact of the tip with a fixed object to the same end). This acceleration causes an impulse loading in the small bimorph harvesters, which then undergo damped free vibration at their own, higher, resonant frequency. This results in the conversion of low frequency, low-impedance vibration to periodic high-impedance impulses exciting the harvesters at high frequency.

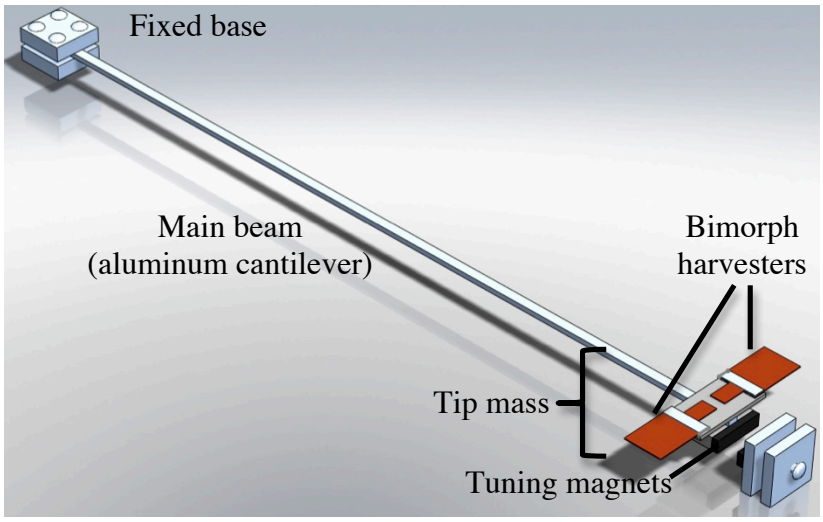

Figure 8.7 Selected concept variant for piezoelectric vibration harvesting (Concept E)

8.2 Analytical Modeling of the Harvesting System

In developing analytical models for the piezoelectric harvester concept, two main scenarios were considered. First, it was necessary to determine whether the conventional bimorph configuration (a single cantilever beam layered with piezoelectric material) was possible for the low-frequency vibration found on bridges. This model involved a static analysis and a rough estimate of dynamic effects (quasi-static analysis). Second, the up-converting structure was analyzed in a similar fashion to determine feasibility and

examine possible geometries for correct resonant frequency and suitable static factor of safety.

8.2.1 Static Analysis of a Simple Cantilever Bimorph

The first modeling completed was a static analysis of a simple cantilever bimorph consisting of a narrow center shim, piezoelectric layers on the top and bottom, and a mass on the tip (as shown in Fig. 7.9). This model considered the geometry required to resonate at a chosen frequency and then determined a static factor of safety for the beam at equilibrium, including gravity. In this analysis, several materials were considered for each component. Material properties used are listed in Table 8.1. Table 8.2 lists the relevant geometric parameters for the calculations, with some selected parameters illustrated in Fig. 8.8.

Table 8.1 Physical properties for selected materials

Material	**Density (ρ)**	**Modulus of Elasticity (E)**	**Yield Strength (S_y)**
Steel	7850 kg/m^3	2.00 x 10^{11} N/m^2	5.00 x 10^8 N/m^2
Brass	8500 kg/m^3	1.00 x 10^{11} N/m^2	3.00 x 10^8 N/m^2
Aluminum	2800 kg/m^3	7.17 x 10^{10} N/m^2	3.00 x 10^8 N/m^2
Graphite	1700 kg/m^3	2.00 x 10^{10} N/m^2	2.55 x 10^7 N/m^2
Polyamide	1430 kg/m^3	2.50 x 10^9 N/m^2	9.00 x 10^7 N/m^2
Polycarbonate	1300 kg/m^3	2.40 x 10^9 N/m^2	6.20 x 10^7 N/m^2
Nylon	1150 kg/m^3	1.30 x 10^9 N/m^2	5.52 x 10^7 N/m^2
PZT	7700 kg/m^3	5.00 x 10^{10} N/m^2	5.00 x 10^7 N/m^2
PVDF	1780 kg/m^3	3.00 x 10^9 N/m^2	5.20 x 10^7 N/m^2

Table 8.2 Variables used in static analysis

Symbol	Parameter	Units	Min (for Solver alg.)	Max (for Solver alg.)
ρ_p	piezo density	kg/m^3		
ρ_s	shim density	kg/m^3		
E_p	piezo modulus of elasticity	N/m^2		
E_s	shim modulus of elasticity	N/m^2		
S_{yp}	piezo yield strength	N/m^2		
S_{ys}	shim yield strength	N/m^2		
η_s	ratio of piezo modulus to shim modulus	-		
t_p	thickness of piezo layer	m	0.00001	0.01
t_s	thickness of shim	m	0	0.05
b	distance, center of shim to center of piezo	m		
W	width of beam	m	0.001	0.1
L	length of beam	m	0.001	0.5
I_{eff}	effective beam area moment of inertia	m^4		
m_t	mass of tip mass	kg	0	2
m_b	mass of beam (shim and piezo)	kg		
m_{eff}	effective point mass at tip	kg		
k_{eff}	effective spring constant	N/m		
ω_n	natural frequency of system	rad/s		
f_n	natural frequency of system	Hz		
M_{static}	max static moment (at base of bimorph)	Nm		
σ_{static}	max static stress (in piezo at base)	N/m^2		
SF_{stat}	safety factor under static loading	-		

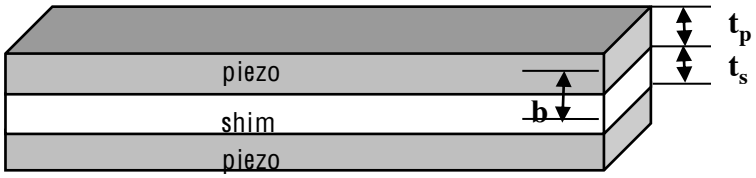

Figure 8.8 Bimorph layers and notation

The natural frequency of a massless cantilever with a point load from a mass at the tip can be defined as the square root of the spring constant over the tip mass. Because the bimorph system has both distributed mass in the beam and a non-homogeneous modulus of elasticity through the thickness, an effective mass and spring constant must be determined. The spring constant of a homogeneous cantilever is expressed as

$$k = 3EI/L^3 \qquad \text{Eq. 8.1}$$

Since *E* is not constant, the term *EI* can be replaced with the overall effective *EI* from all layers:

$$E_{\text{eff}}I_{\text{eff}} = \left(E_pI_p\right) + (E_sI_s) = 2\left(E_p\left[Wt_p{}^3/12 + Wt_pb^2\right]\right) + E_s(Wt_s{}^3/12)$$
$$= E_p\left(Wt_p{}^3/12 + Wt_pb^2 + \eta_s\, Wt_s{}^3/12\right) \qquad \text{Eq. 8.2}$$

Therefore, the modulus for the piezo can be taken as the effective modulus, and the expression inside the parentheses can be taken as the effective area moment of inertia.

To determine an effective point mass, the contribution of the distributed mass to the mode shapes must be considered. Humar (1990) gives the natural frequencies of a cantilever beam with distributed loading as

$$\omega_n = \alpha_n^2\sqrt{EI/mL^4} \text{ where } \alpha_n = 1.875, 4.694, 7.855 \ldots \qquad \text{Eq. 8.3}$$

By extracting the expression for *k* as given in Eq. 8.1, we can find the effective mass contributed from the distributed mass:

$$m_{\text{eff,b}} = (3L/\alpha_n^4)\, m_b = (0.243L)m_b \qquad \text{Eq. 8.4}$$

Thus the effective point mass at the tip for the complete system can be found:

$$m_{\text{eff}} = (0.243L)m_b + m_t \qquad \text{Eq. 8.5}$$

To determine a factor of safety for static loading, we first must determine the maximum moment, which occurs at the base of the cantilever. Through superposition, this is equal to the sum of the moments contributed by the tip mass and beam mass:

$$M_{\text{static}} = \tfrac{1}{2}(\rho_s t_s + 2\rho_p t_p) W g L^2 + m_t g L \qquad \text{Eq. 8.6}$$

The maximum stress for each material occurs at the outer surface of the material at the same location:

$$\sigma_{\text{static, s}} = M_{\text{static}}(0.5t_s)/I_s\,, \;\; \sigma_{\text{static, p}} = M_{\text{static}}(0.5t_s + t_p)/I_{\text{eff}} \qquad \text{Eq. 8.7}$$

Each of these can be compared to the yield strength of the respective materials to determine an overall factor of safety:

$$SF_{\text{static}} = \min\left({}^{S_{y,s}}/_{\sigma_{\text{static, s}}},\; {}^{S_{y,p}}/_{\sigma_{\text{static, p}}}\right), \text{ feasible if } SF_{\text{static}} \geq 1.0 \qquad \text{Eq. 8.8}$$

In essence, the goal is to maximize the factor of safety and minimize the resonant frequency (to a point). The equations for these two variables (assuming the piezo layer as the failure-critical element) are expanded below:

$$SF_{\text{static}} = S_{y,p} I_{\text{eff}}/(m_t + 0.5m_b)\big(0.5t_s + t_p\big) g L \qquad \text{(maximize)} \qquad \text{Eq. 8.9}$$

$$\omega_n = \sqrt{3E_p I_{\text{eff}}/m_{\text{eff}} L^3} \qquad \text{(minimize)} \qquad \text{Eq. 8.10}$$

From these two equations, we can see that S_y should be maximized, E_p and overall thickness should be minimized, and the area moment of inertia, length, and masses have nonlinear effects. In addition, Eq. 4.4 (from Chapter 4) indicates that, for multiple solutions that fulfill the criteria for resonant frequency and factor of safety, the largest mass possible should be chosen to maximize power output.

After choosing materials for the shim and piezoelectric layers and setting upper and lower bounds on the beam geometry, we can use Excel's Solver functionality (which incorporates a Generalized Reduced Gradient search algorithm) to find the geometries and materials that result in the correct resonant frequency and a generous factor of safety.

Running the Solver algorithm revealed that for most combinations, it is difficult to create a geometry that will reliably vibrate at two hertz (the frequency of the I-35/US-290 Bridge) without breaking the piezoelectric material. Some example geometries are

shown in Table 8.3 that do have a static safety factor of at least unity. The two piezoelectric materials considered are PZT 500 (lead zirconate titanate), which is the most common thin-film ceramic, and PVDF, a relatively new polymer-based material. PVDF is much more flexible than the brittle PZT ceramic, with a lower modulus of elasticity and a higher tensile strength. This would make it much more attractive for this low frequency, high-displacement motion. However, the power density of PVDF is far inferior to PZT, with a strain coefficient d_{31} just 6% of the coefficient for PZT and a dielectric constant of only 0.3% of PZT.

Table 8.3 Sample Geometries for Different Material Combinations

Materials	Natural Freq	Safety Factor	Length	Shim Width & Height	Piezo Thickness	Tip Mass
Steel/PVDF	2.0 Hz	2.8	0.50 m	3x1 mm	7 mm	500 g
Steel/PZT	2.0 Hz	1.0	0.50 m	6x2 mm	0.3 mm	66 g
Alum./PVDF	2.0 Hz	2.1	0.50 m	1x4 mm	8 mm	500 g
Alum./PZT	2.0 Hz	1.5	0.48 m	10x1 mm	0.01 mm	180 g
Graphite/PVDF	2.0 Hz	1.5	0.50 m	14x2 mm	2 mm	91 g
Graphite/PZT	2.8 Hz	1.5	0.50 m	19x1 mm	0.5 mm	37 g
Polycarb/PVDF	2.0 Hz	2.9	0.39 m	7x5 mm	2 mm	500 g
Polycarb/PZT	2.7 Hz	1.5	0.50 m	9x1 mm	0.2 mm	60 g
Nylon/PVDF	2.0 Hz	2.9	0.50 m	3x3 mm	6 mm	500 g
Nylon/PZT	2.7 Hz	1.5	0.50 m	12x1 mm	0.2 mm	8 g

As can be seen, geometries using PVDF are possible that reach 2 Hz with a safety factor of almost 3 and allow a reasonably large tip mass. However, this tip mass must be supported by a very narrow beam. Even though the beam will theoretically not yield under the load, it will experience excessive displacement and introduce balance issues that may lead to unstable behavior in other directions. In addition, the very small surface area of the beam places a very low limit on the amount of piezoelectric material and thus

the power output. Geometries using PZT require, in general, a very thin piezoelectric layer and a much smaller tip mass. Even with these allowances, they are barely able to approach 2 Hz and still support their own weight, let alone withstand resonant vibration.

8.2.2 Dynamic analysis of a Simple Cantilever Bimorph

To estimate maximum stresses under dynamic loading, the static analysis was used to make a rough estimate of dynamic loading at resonance. This continuous vibration at resonance was used as a worst-case scenario, with actual vibration patterns from bridge accelerations likely less pronounced. Actual dynamic analysis of a resonant system before actually building a prototype is significantly less precise than static analysis because of the large effect of damping, which is largely unknown until the system is built. However, rough estimates of damping can be made considering comparable systems, which can then be used to determine how the dynamic loading affects the system behavior.

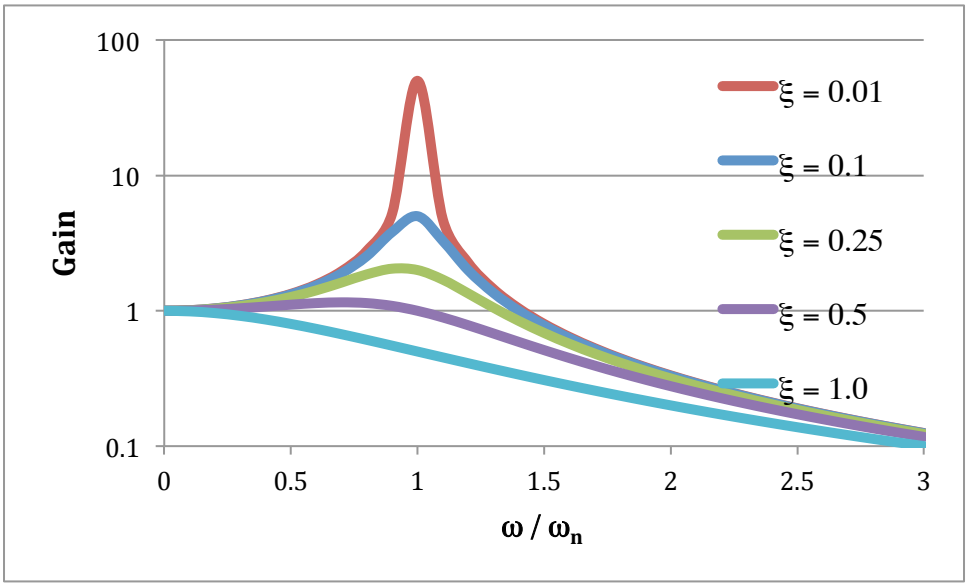

Figure 8.9 Bode plot of gain at resonance

For resonant vibration of the main beam, the maximum stress can be found by examining the maximum acceleration experienced by the tip mass. This would occur at the lowest point of displacement, when gravity and inertia are operating in the same direction. The effective acceleration at this moment would be the sum of the acceleration due to gravity and the acceleration of the tip. Figure 8.9 shows a Bode plot of the gain (or magnification factor) resulting from resonant vibration. In a viscous under-damped system with forced harmonic vibration, the particular solution to its differential equation can be expressed as

$$x_p = C'\sin(\omega t - \phi') \qquad \text{Eq. 8.11}$$

where the constants *C'* and *Φ'* are

$$C' = \frac{F_0/k}{\sqrt{\left(1+[\omega/\omega_n]^2\right)^2+(2[c/c_C][\omega/\omega_n])^2}} \qquad \text{Eq. 8.12}$$

$$\phi' = \tan^{-1}\left(\frac{2[c/c_C][\omega/\omega_n]}{1-[\omega/\omega_n]^2}\right) \qquad \text{Eq. 8.13}$$

The magnification factor is the ratio of the amplitude of deflection caused by the forced vibration to the deflection caused by input force amplitude F_0:

$$MF = \frac{1}{\sqrt{\left(1+[\omega/\omega_n]^2\right)^2+(2[c/c_C][\omega/\omega_n])^2}} \qquad \text{Eq. 8.14}$$

In this system, an effective tip mass of 0.56 kg (with actual tip mass of 0.5 kg) and a spring constant of 90.5 N/m are assumed, which is similar to the PVDF-based systems above. For many mechanical systems, a damping ratio (c/c_c) between 0.02 and 0.2 is typical. This means that a gain anywhere from 2 to about 20 may be possible. If a gain of 10 and an incoming vibration of 2 Hz and 0.1 g are assumed, the resulting acceleration of the tip would be 10 x 0.1 g = 1 g. Therefore, the maximum acceleration

the harvester would be exposed to would be 1 g (from gravity) plus 1 g (from tip acceleration) for a total of 2 g.

Equations 8.6 can be used to find the maximum moment, substituting in the total acceleration of 2 g for the static acceleration of g. This yields, through Eq. 8.7, dynamic stresses at the base of the cantilever twice the stress under static loading. This result carries through to Eq. 8.8, yielding a dynamic factor of safety half that of the static analysis. Thus, a static factor of safety of at least 2 would be necessary to operate the beam under this level of harmonic vibration. As can be seen, none of the PZT geometries are able to pass this threshold, and the few PVDF geometries that do leave little room for the still remaining uncertainties of damping and changing input characteristics.

8.2.3 Assessment of Simple Cantilever Bimorph

From the static and dynamic analyses presented above, the following conclusions can be drawn regarding the use of a simple cantilever bimorph at 2 Hz and 0.1 g:

- PZT is not a viable material for this configuration of harvester at 2 Hz, although it does become feasible for frequencies of about 10 Hz or higher.
- PVDF is a structurally feasible alternative material at this frequency. However, power output is likely to be extremely low and the factor of safety is barely acceptable for well-understood behavior. For vibration on a bridge, which is semi-random in both frequency spectrum and amplitude, this may not be sufficient for long-term reliability.

8.2.4 Static and Dynamic Analyses of an Up-Converting Harvester Structure

After the analysis of a conventional cantilever bimorph, a similar analysis was done to create a model of the chosen concept variant (Fig. 8.7), which consists of a

homogeneous cantilever beam without piezoelectric material, a large tip mass, and an array of small bimorphs horizontally on the tip mass that are excited by impulses resulting from sudden accelerations applied to the main beam's tip by the opposing magnets or mechanical impact. Using the same general formulas as before, static and dynamic analyses of the system were completed in two steps.

A static analysis of the main beam was studied first, considering homogenous beams of aluminum, steel, and brass and a variable tip mass. For simplicity, starting dimensions of 1 cm x 0.5 cm x 1 m were assumed with a tip mass of 0.5 kg. Using the Excel Solver algorithm, parameters for some example geometries were derived (Table 8.4). These results show that such a configuration is indeed feasible (including dynamic loading as described above), and allows a reasonable amount of freedom in the design of specific prototype geometry. To design the beam for extended field use, the effect of fatigue would need to be considered. However, as the initial prototypes were expected to be used only for short-term experimentation (on the order of 10^3-10^4 cycles), fatigue was deemed not to be an immediate concern. Design of later prototypes should evaluate the fatigue limit for extended or infinite life in the field.

Table 8.4 Sample Geometries for Different Homogenous Beams

Material	**Natural Freq**	**Safety Factor**	**Length**	**Width & Height**	**Tip Mass**
Steel	2.0 Hz	4.3	1.00 m	3x1 mm	500 g
Aluminum	2.0 Hz	4.8	0.76 m	6x2 mm	66 g
Brass	2.0 Hz	3.4	0.80 m	1x4 mm	500 g

To model the small bimorphs installed on the tip, a typical off-the-shelf bimorph is considered, the MIDE Volture V20W (Fig. 8.10). This harvester is 4.6 cm long and 3.8

cm wide, with each of the two piezoelectric layers and the shim layer approximately 0.3 mm.

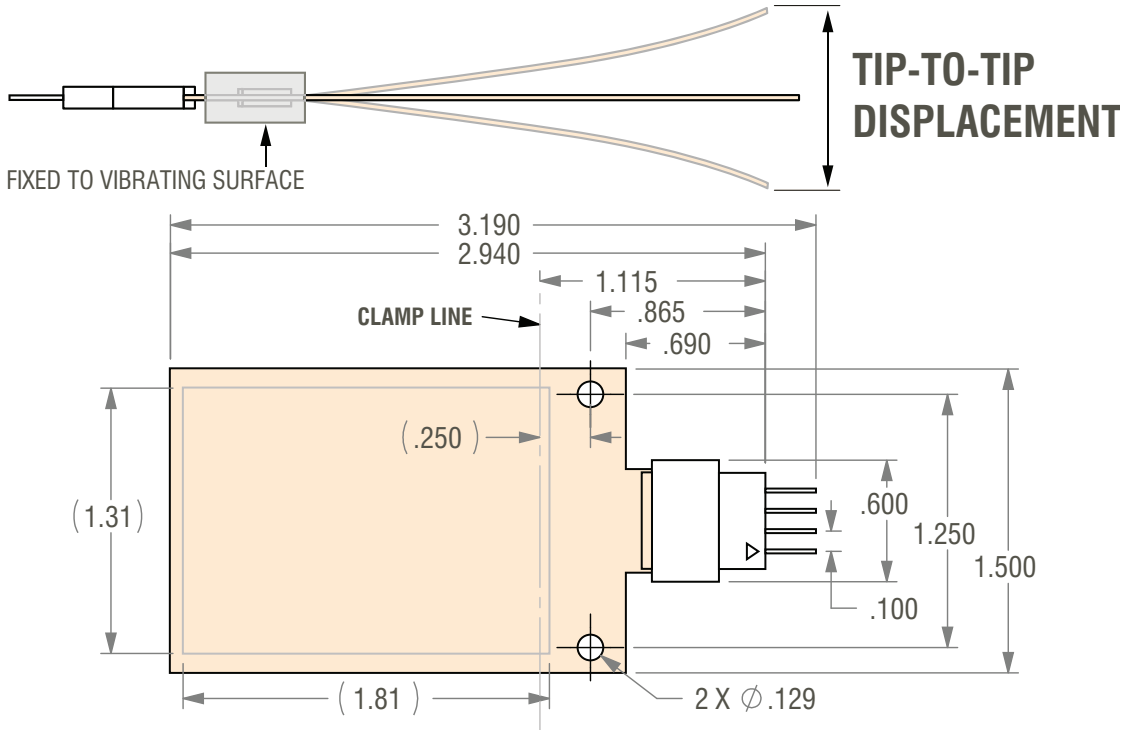

Figure 8.10 MIDE Volture V20W bimorph harvester (MIDE, 2010)

Specifications for this product indicate that it is rated up to a maximum displacement of 3 mm tip to tip, or a maximum strain of 800 micro-strain. It also lists the overall tensile strength to be 10^8 N/m^2. Using the geometry and material properties provided, the equations used earlier yield a natural frequency of 180 Hz and a static factor of safety of 25 with no tip mass. By adding the largest recommended tip mass available, 75 g, the calculated natural frequency drops to 25 Hz, with a static factor of safety of 10. In comparison, the listed natural frequencies available by adding tip masses range from 175 Hz down to 75 Hz.

To calculate the maximum dynamic loading the bimorph might experience, the maximum momentum transferred from the main beam must be determined. If the beam has an effective tip mass of 0.56 kg and an effective spring mass of 90.5 N/m^2, resonates at 2 Hz, has a damping ratio of 0.02, and experiences an input acceleration peaking at 0.1 g, the resulting peak acceleration of the main beam's tip mass at resonance would be 2 g (19.6 m/s^2) at 2 Hz (12.6 rad/s). The acceleration of the tip can thus be described as

$$A(t) = 19.6 \sin(12.6t) \text{ m/s}^2 \qquad \text{Eq. 8.15}$$

and the velocity and position can be found by integrating:

$$V(t) = -\left(\tfrac{19.6}{12.6}\right)\cos(12.6t) = -1.56 \cos(12.6t) \text{ m/s} \qquad \text{Eq. 8.16}$$

$$X(t) = -\left(\tfrac{19.6}{12.6^2}\right)\sin(12.6t) = -0.124 \sin(12.6t) \text{ m} \qquad \text{Eq. 8.17}$$

The maximum momentum occurs at dead center, where the momentum can be expressed as

$$L = mv = (0.56 \text{ kg})(1.56 \text{ m/s}) = 0.874 \text{ kg·m/s} \qquad \text{Eq. 8.18}$$

If the steel tip mass strikes a fixed surface with a coefficient of restitution of 0.55 (typical for steel), the tip velocity immediately after impact can be calculated:

$$v_{i,\text{ tip}} = -0.55(1.56 \text{ m/s}) = -0.86 \text{ m/s} \qquad \text{Eq. 8.19}$$

Thus immediately after impact, the tip of the main beam is traveling upward at 0.86 m/s, while the tip of each bimorph is still moving downward at 1.56 m/s. The relative velocity of the bimorph tip to its base (on the tip of the main beam) can be expressed as

$$V(t) = -(1.56 + 0.86) \cos(471t) = -(2.42) \cos(471t) \text{ m/s} \qquad \text{Eq. 8.20}$$

where the cosine term indicates the bimorph's resonant frequency of 75 Hz, or 471 rad/s. The acceleration resulting from this velocity can be expressed as

$$A(t) = (2.42\times471)\sin(471t) = 1140\sin(471t)\ \mathrm{m/s} \qquad \text{Eq. 8.21}$$

With a 7.8-g tip mass on the bimorph, the peak acceleration of 1,140 m/s^2 would cause maximum force on the tip of 8.9 N. This, in turn, would result in a maximum moment at the base of 0.34 Nm and a maximum stress in the piezoelectric material of 7.4x10^8 Pa, which is approximately seven times the material's yield strength. In other words, the worst-case shock scenario would be sufficient to fracture the bimorphs. Any force inputs to the beam, whether from shock impacts or from bistability, will need to be used with care to stay below the fracture limit of the bimorphs.

8.2.5 Power Output From Impulse Loading on Bimorph

The rated power specifications for the Volture V20W bimorph are shown in Fig. 8.11. The data presented do not extend to the acceleration levels relevant here (0.1 g). By extending the trend lines down, it appears likely that about 0.25 to 0.5 mW could be generated by a constant excitation at frequencies between 50 Hz and 80 Hz, depending on the tip mass included. To get an idea of the power generated from free vibration after an impulse load, an analytical model must be developed.

The bimorph experiences viscous damped free vibration after an impulse load. If the resulting sinusoid output is rectified and smoothed to DC, we can expect an attenuation of the form $P(t) = P_0 e^{-\zeta t}$, where P_0 is the power from a constant sinusoid input of the same amplitude. Roundy, et al. (2004) gives the following equation for power output from harmonic input at resonance:

$$P = \frac{RC^2(Edtb^*)^2{A_{\mathrm{in}}}^2}{\varepsilon\omega^2([4\zeta^2+k^4][RC\omega]^2+4\zeta k^2[RC\omega]+2\zeta^2)} \qquad \text{Eq. 8.22}$$

Assuming a power level at resonance of 0.5 mW and a mechanical damping ratio of 0.01, the average power over one second of free vibration (found by integrating and

dividing by the time) is approximately 0.2 mW. Thus, with multiple bimorphs and frequent enough excitation, a sufficient level of power may be available.

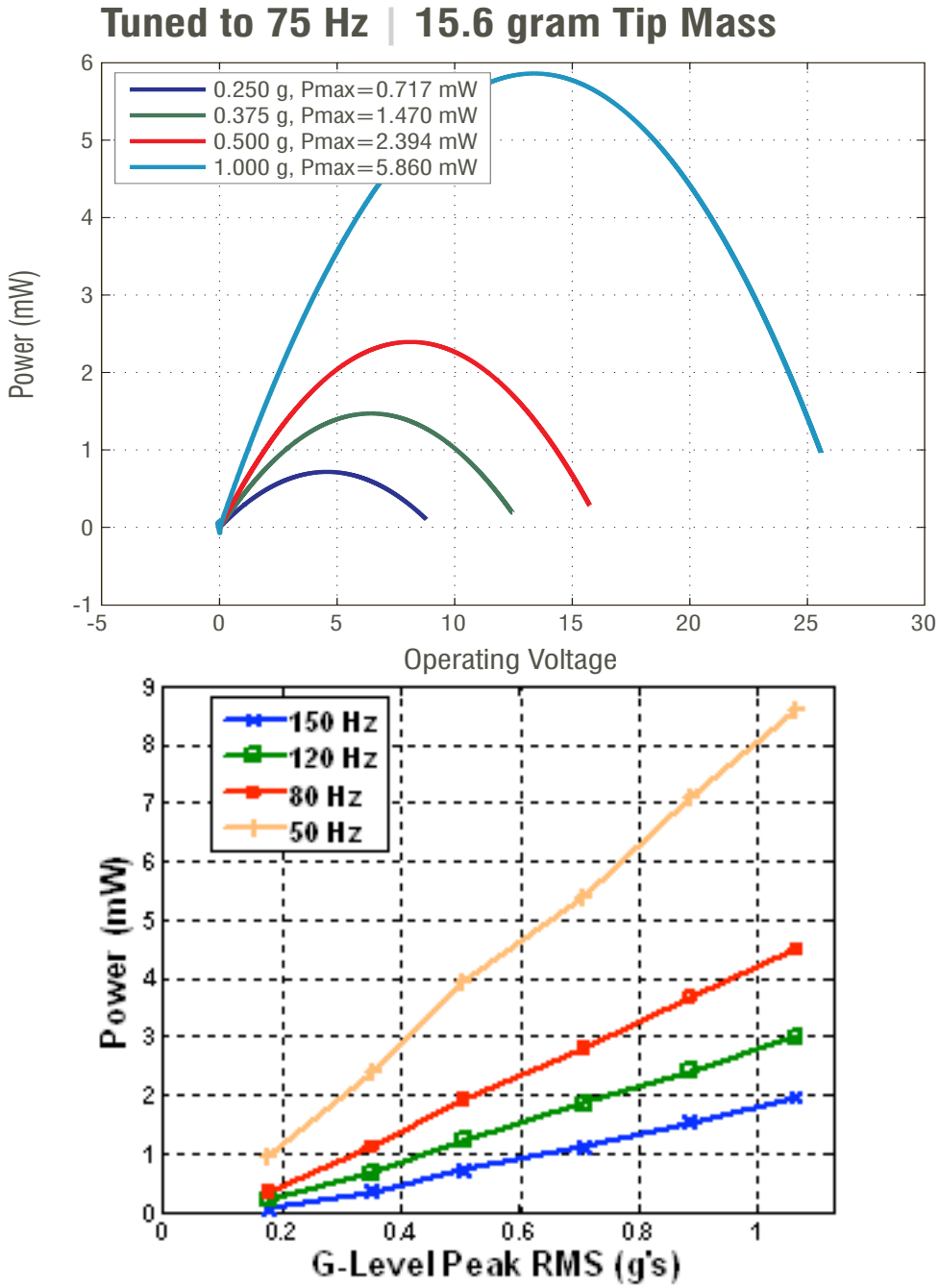

Figure 8.11 Power specifications for V20W bimorph (MIDE, 2010)

8.2.6 Assessment of Up-Converting Harvester Structure

From the above analysis, it seems very likely that an up-converting harvester would both have sufficient factors of safety for the main beam and bimorphs (derived from static analysis and resonant gain) and generate enough power to fulfill the required application under at least some conditions. The next section details the design, construction, and testing of proof-of-concept prototypes to validate these predictions.

8.3 PHYSICAL PROTOTYPING AND TESTING

A series of prototypes were designed to test their feasibility in powering wireless sensor nodes. An initial prototype was designed to match the vibration characteristics of the I-35/US-290 Bridge, and a second revised prototype was designed for use on the Medina River Bridge.

8.3.1 Parameterization of First Prototype for I-35/US-290 Bridge

The first prototype is based on the concept that has been previously studied (Fig. 8.7). In order to avoid excessive instability from rotational oscillation, the concept was changed to have two beams supporting the tip mass, as shown in Fig. 8.12.

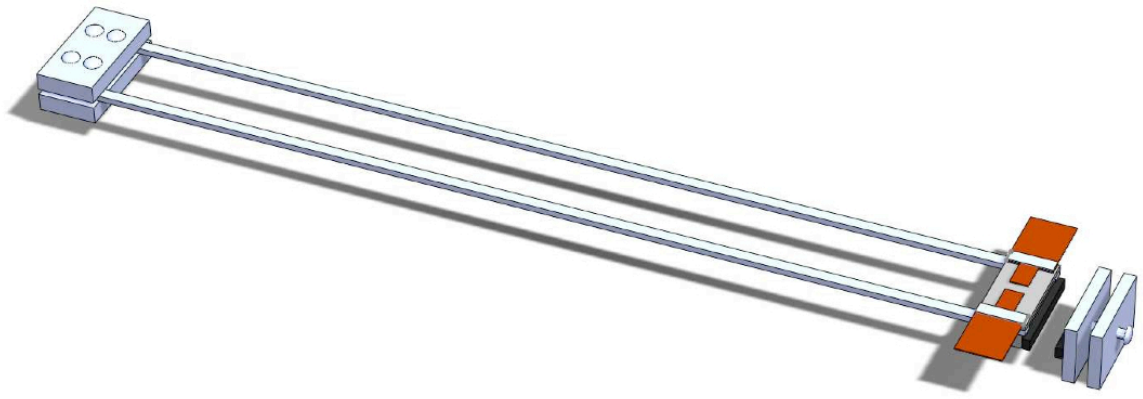

Figure 8.12 CAD model of first prototype

To resonate at the appropriate frequency, the following materials and dimensions were selected:

- 2 aluminum beams, 0.85 x 0.01 x 0.005 m
- 2 Volture V20W bimorphs
- Tip mass consisting of 1 steel block, 0.08 x 0.04 x 0.01 m, and 1 steel block, 0.08 x 0.02 x 0.01 m
- 1 N52 neodymium block magnet, 0.08 x 0.01 x 0.006 m
- A matching neodymium magnet to be attached to the base

A summary of the parameters necessary for analytical modeling of the system is contained in Table 8.5.

Table 8.5 Geometry and characteristics of initial prototype's two main beams

Material	Natural Freq	Beam Static Safety Factor	Free Length	Width & Height	Tip Mass
Aluminum	2.03 Hz	5.23	0.79 m	1x0.5 cm	505 g

8.3.2 Construction of First Prototype

Because of the uncertainty remaining after analytical modeling and the need to investigate different configurations, the prototype was built to be easy to put together, take apart, and adjust. The main beam was formed by bonding the aluminum beams and steel masses in place with JB-Weld steel-reinforced epoxy. This proved to be sufficient for testing purposes, although final construction would more likely use single-piece construction or permanent fasteners. To ease adjustment during testing, the main structure was fixed to a test fixture using a C-clamp and two steel plates. This allowed for easy removal and enabled the effective length of the beam to be changed to adjust the natural frequency. The bimorphs were attached to the steel tip mass by 1-cm disk

magnets, allowing for easy removal and adjustment as well. The completed prototype is shown below in Fig. 8.13.

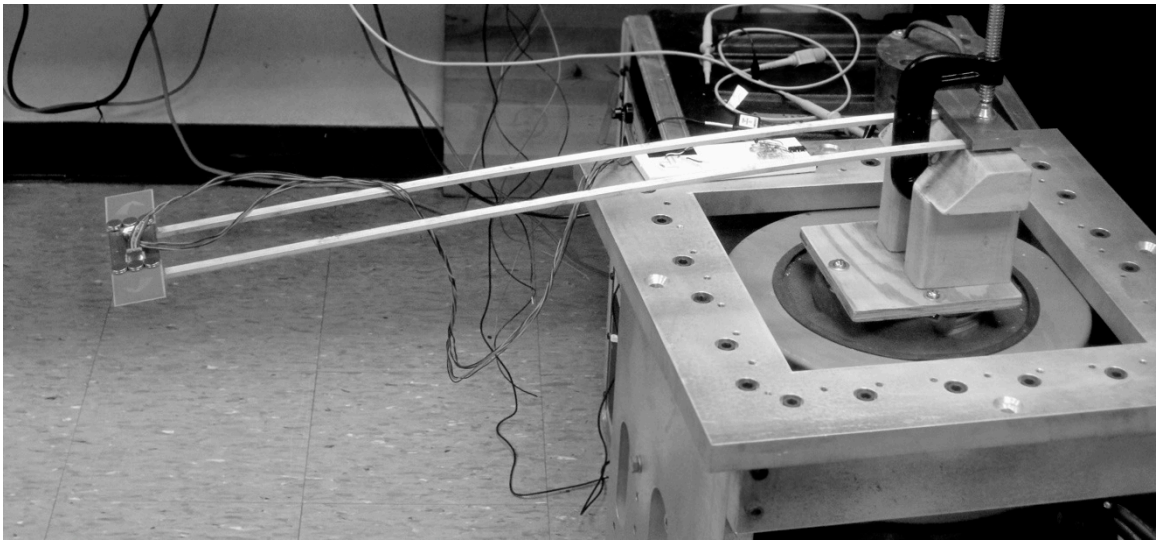

Figure 8.13 Completed prototype for use at 2.03 Hz

8.3.3 Experimental Method

As shown in Fig. 8.13, the completed prototype was fixed to a wood test structure attached to a shaker table. The complete laboratory setup for experimental testing is listed below and shown in Fig. 8.14:

- PC laptop running LabVIEW 2010
- CompactDAQ with NI-9269 4-Channel Voltage Output Module and NI-9205 32-Channel Voltage Input Module
- Labworks PA-123-500 Linear Power Amplifier
- Labworks ET-127 Electrodynamic Shaker

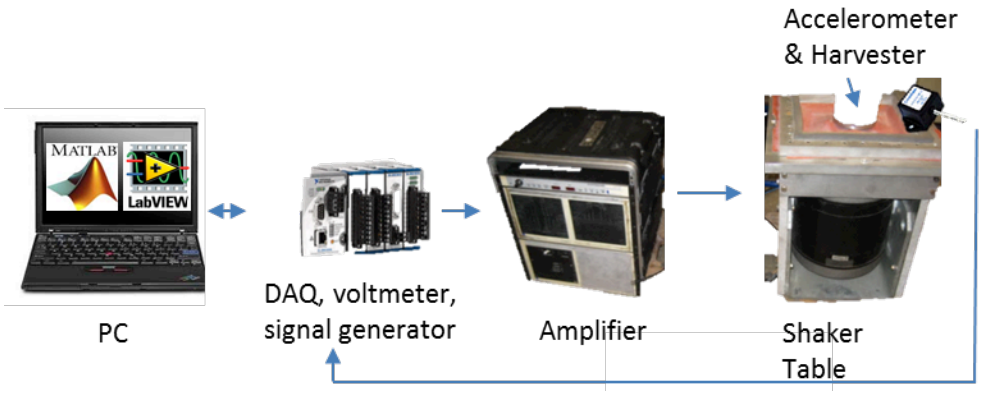

Figure 8.14 Experimental setup for laboratory testing

To aid in the testing of the prototype, several tests were drawn up in an experimental method. These tests examined the natural frequency, damping, impedance, and power output under several inputs (sine excitation at resonance, sine sweep, bridge accelerations from file):

Test 1 – Determine Resonant Frequency and Damping Visually

Before the setup with LabVIEW was completed, the resonant frequency and damping were analyzed using a video camera.

1. Securely fasten beam to work surface
2. Measure free length of beam
3. Place ruler behind tip mass positioned to measure displacement
4. Begin video-recording beam
5. Gently strike the beam
6. Allow the beam to ring until it stops vibrating
7. Strike the beam four more times, allowing it to ring freely
8. Stop video recording
9. Using the video, determine the time stamps of peak displacement
10. Calculate the observed resonant frequency

11. Using the video, determine the vertical displacement at peak displacement
12. Calculate the observed damping in the system
13. Compare observed frequency to modeled frequency
14. If significantly different, change free length and or tip mass to adjust frequency
15. Use observed damping and natural frequency to update analytical models

Test 2 – Determine Resonant Frequency Under Forced Vibration

Next, the resonant frequency was determined by adjusting an input sine wave excitation from LabVIEW.

1. Securely fasten beam and accelerometer to shaker table
2. Following the steps to run the shaker table, excite the harvester with a sine wave
3. Frequency = 2 Hz, Amplitude = 0.1 V, Gain (on main amp) = 1.0
4. Change the amplitude in LabVIEW until the accelerometer measures an easy-to establish acceleration, like 0.01 g, 0.05 g, etc.
5. Change the frequency until it appears that the harvester is resonating
6. Record the excitation frequency and amplitude and the measured acceleration at the resonant frequency
7. In a randomized order, excite the harvester by increments of 0.01 Hz to frequencies up to 0.5 Hz above and below the resonant frequency
8. For each excitation, use a ruler or measuring tape to visually measure and record the maximum displacement (in cm) at the tip of the harvester from the resting position
9. Record the frequency where maximum displacement is greatest as the resonant frequency

Test 3 – Determine Power Output at Resonance

1. Connect the V20W bimorph to the breadboard so that the following circuit is formed: harvester, small resistor (~1-10 Ω), and large resistor (> 1 kΩ)) are in series, cDAQ channel a3 measures the voltage across the large resistor, cDAQ channel a4 measures the voltage across the small resistor
2. In LabVIEW, set the resistance for the current to the small resistor
3. Starting at the frequency and acceleration settings determined in Test 1, excite the harvester
4. Record the resulting RMS voltage, current, and power
5. Change the excitation frequency in 0.1-Hz increments, to at least 0.5 Hz greater and less than the resonant frequency. Measure the voltage, current, and power at each point. If needed, refine with smaller increments (0.05 Hz)
6. Reset the frequency to the resonant frequency and gradually increase the amplitude, measuring the acceleration and the voltage/current/power at regular intervals
7. When maximum amplitude is reached without overloading the harvester or the shaker table, note the acceleration, voltage, current, and power, and use a ruler or measuring tape to visually measure the maximum displacement (in cm) at the base and tip of the harvester
8. Remove the large resistor, creating an open circuit. Record the voltage
9. Starting with the largest resistances, place each resistor in the circuit and measure the voltage across it, the current through the small resistor, and the calculated power
10. Determine what resistance yields the greatest power output

11. If time permits, multiple resistors can be combined to more closely determine the optimal load resistance
12. Connect a V25W bimorph to the breadboard circuit instead of the V20W bimorph. Compare the voltage/current/power output. Adjust the resistance to find the load with maximum power output

Test 4 – Determine Effect of Magnets on Natural Frequency

Next, a pair of opposing magnets was introduced (one on the tip, one stationary) and adjusted to change the natural frequency

1. Securely fasten beam with bimorphs to shaker table
2. Install magnets on tip mass and fixed base
3. Position fixed magnet 10 cm away horizontally from the magnet on the beam
4. Excite shaker table at predetermined resonant frequency
5. Adjust shaker table frequency to match maximum resonance
6. Measure voltage output from bimorph
7. Move magnet 5 mm closer
8. Allow system to stabilize to measure new profile
9. Adjust shaker table frequency to match maximum resonance
10. Repeat steps 6-9 until a distance of 0.5 cm is reached

Test 5 – Determine Resonant Frequency and Power Output with Striker

Next, a flat aluminum "striker" plate was introduced and the power generated by the tip mass striking the plate and exciting the bimorphs was examined

1. Excite the harvester at the resonant frequency and maximum amplitude
2. Use a ruler or measuring tape to visually measure the displacement at the tip

3. Stop the harvester and place the striker plate below the tip at 50% of the maximum displacement
4. Restart the excitation and gradually increase the gain back to the full amplitude, ensuring that the harvester is not overloaded
5. Change the frequency in small increments and observe if a higher displacement is achieved
6. Record the new resonant frequency, if changed
7. Install the V20W bimorph, with the load resistance from Test 3 in the circuit
8. Excite the harvester, with the striker plate at the same position as in Step 3
9. Measure the acceleration and RMS voltage/current/power
10. Move the striker plate up and down in small increments (0.5 cm or less) and determine the position that yields the greatest voltage and/or power

Test 6 – Frequency Sweep Testing

To support the results of the previous tests for resonant frequency, the harvester was also subjected to a conventional sine sweep

1. Choose a minimum frequency, maximum frequency, acceleration amplitude, and run time
2. Run LabVIEW VI that generates a sine sweep by smoothly moving from low frequency to high frequency and back while adjusting the voltage to ensure a constant acceleration level
3. Record the voltage from the bimorph and export to Excel
4. Convert time scale to frequency and plot

Test 7 – Determine Power Output from Bridge Vibration

1. Convert acceleration data gathered from bridge to velocity (voltage to the shaker table is proportional to velocity)
2. Run LabVIEW VI that reads velocity data from LVM (LabVIEW data) file and excites the shaker table appropriately
3. Adjust gain on main amp so that the resulting acceleration matches that found on the bridge
4. Determine voltage and power both over short term (during large acceleration) and long-term average over the test

8.3.4 Results for First Prototype

Test 1 – Determine Resonant Frequency and Damping Visually

The main beam (without magnets or bimorphs attached) was clamped to a work surface with a C-clamp and positioned in front of a wall. A measuring tape was placed behind it, fixed with the top of the harvester resting at the mark for 30 cm, as shown in Fig. 8.15. This setup was video-recorded while the tip was displaced upwards by 4 cm, then released.

The displacement measurements gathered from the video footage are shown in Fig. 8.16. These measurements can be fit to a general solution for viscous damped free vibration of the form

$$x = D\left(e^{-\zeta t}cos[\omega_d t]\right) \qquad \text{Eq. 8.23}$$

The damping ratio ζ for the system was measured at 0.022, on the lower end of the expected range of 0.02 to 0.2. The damped resonant frequency was 2.26 Hz. Because of low damping, the damped frequency was essentially equivalent to the natural frequency ($\omega_d = \omega_n\sqrt{1-\zeta^2}$). The predicted natural frequency of the system was 2.03 Hz, with the small difference likely caused by variation in the clamp position.

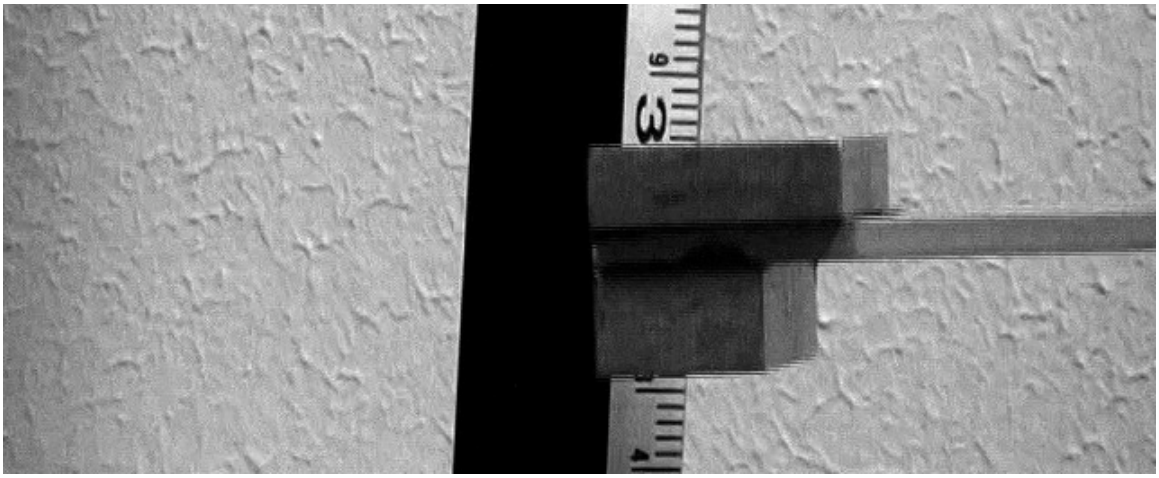

Figure 8.15 Experimental setup for laboratory testing

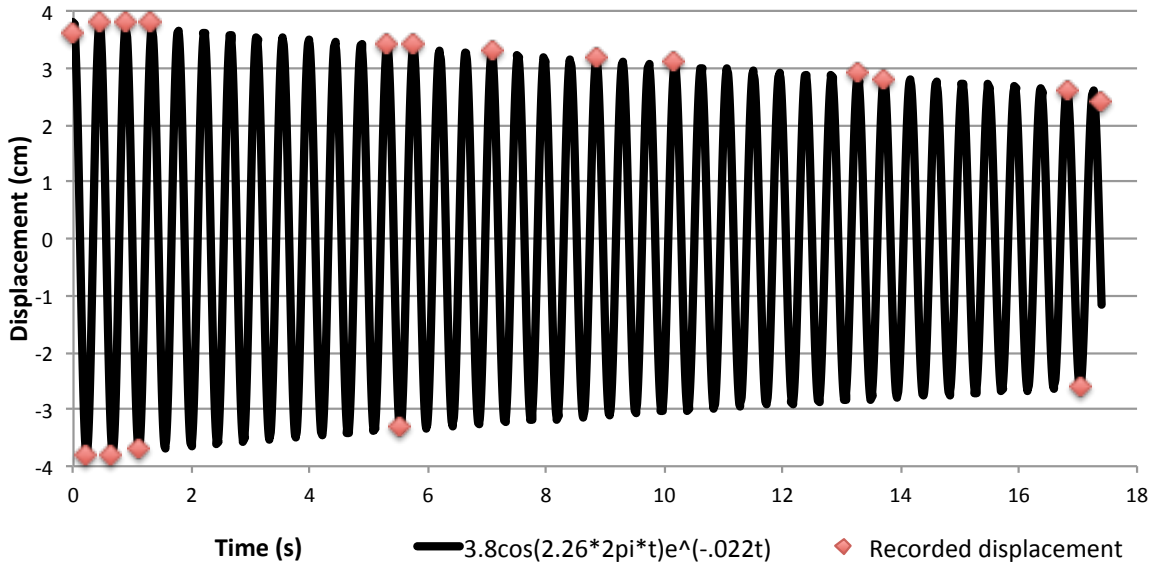

Figure 8.16 Unforced damped vibration of harvester beam

Test 2 – Determine Resonant Frequency Under Forced Vibration

The harvester was clamped to a test fixture on the shaker table. A LabVIEW VI was used to excite the shaker table at frequencies ranging from 1.7 to 2.6 Hz, in increments of 0.01 Hz or less. The order of frequencies selected was randomized, and the harvester was allowed to come to rest between tests. The resulting amplitude of

displacement as a function of frequency is shown in Fig. 8.17. These measurements show a resonant frequency of 2.15 Hz (the variation from the previous test due to differences in the clamping). The bandwidth, which is typically defined as the range of frequencies over which 50% or more power is available, is from 2.14 Hz to 2.17 Hz. This very narrow bandwidth of 0.03 Hz is due to the low damping of the system. The quality factor Q based on these measurements is 71.7, where

$$Q = \frac{\omega_n}{\Delta\omega} \text{ and } \Delta\omega \text{ is the bandwidth} \qquad \text{Eq. 8.24}$$

The quality factor can also be used to calculate the damping ratio:

$$\zeta = \frac{1}{2Q} \qquad \text{Eq. 8.25}$$

The resultant damping ratio is 0.007, which is about a third of the damping ratio observed in Test 1, but still within an order of magnitude. The difference is likely again due to mounting, as a firmer clamp was used. If the system were to be designed with more damping, the quality factor would be lower, leading to a lower peak value, but the wider bandwidth.

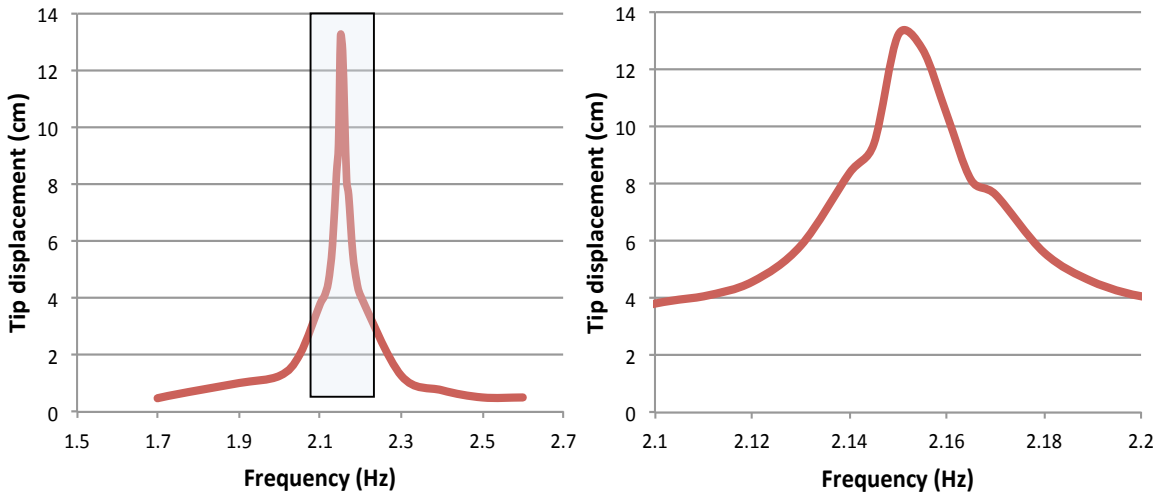

Figure 8.17 Bandwidth of main beam by displacement

Test 3 – Determine Power Output at Resonance

For this test, the two bimorphs were attached to the tip mass using small disk magnets. One bimorph harvester was placed in a circuit as shown in Fig. 8.18, in series with a two resistors. Current generated by the harvester was calculated from the voltage measured across the first resistor (10 Ω). Voltage across a resistive load was measured across the second, larger resistor, which ranged from 470 Ω to 20 MΩ. Voltage across open and short circuits were measured as well.

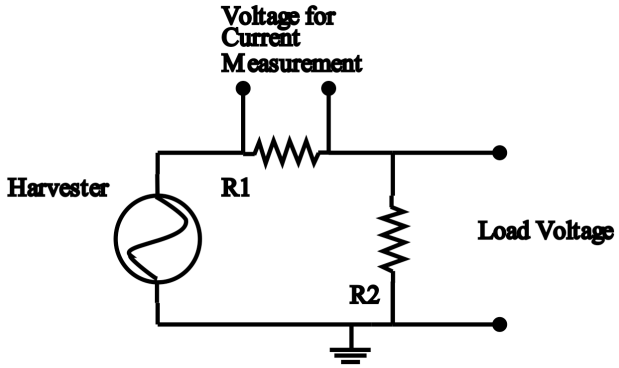

Figure 8.18 Circuit for measuring resistive load voltage and current

After the resonant frequency was verified, the shaker was excited at the resonant frequency at acceleration amplitude of 0.1 g. The resistance was changed, in a randomized order, and the load voltage, current, and calculated power were recorded. These results are shown in Fig. 8.19-8.21. The power characteristics show a maximum power at a resistive load of 2 MΩ. The maximum power was very low, less than a microwatt, but this was to be expected since the vibration is not occurring at the bimorph's resonant frequency. Instead, the power is created through the strain induced in the piezoelectric material through the inertia of the bimorphs moving at the lower frequency.

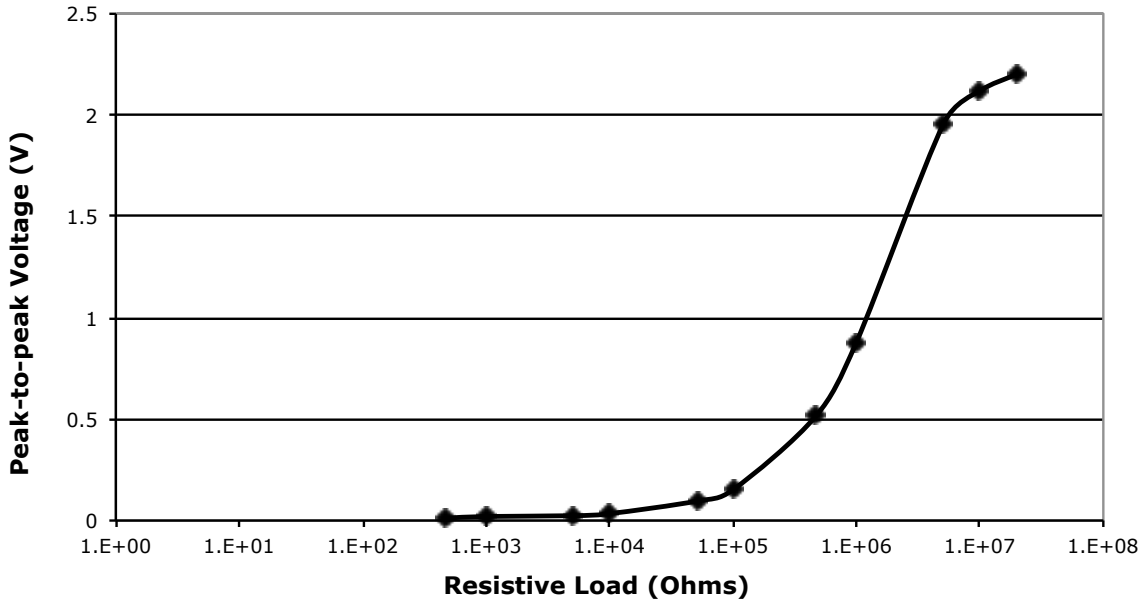

Figure 8.19 Voltage produced in one bimorph versus resistive load

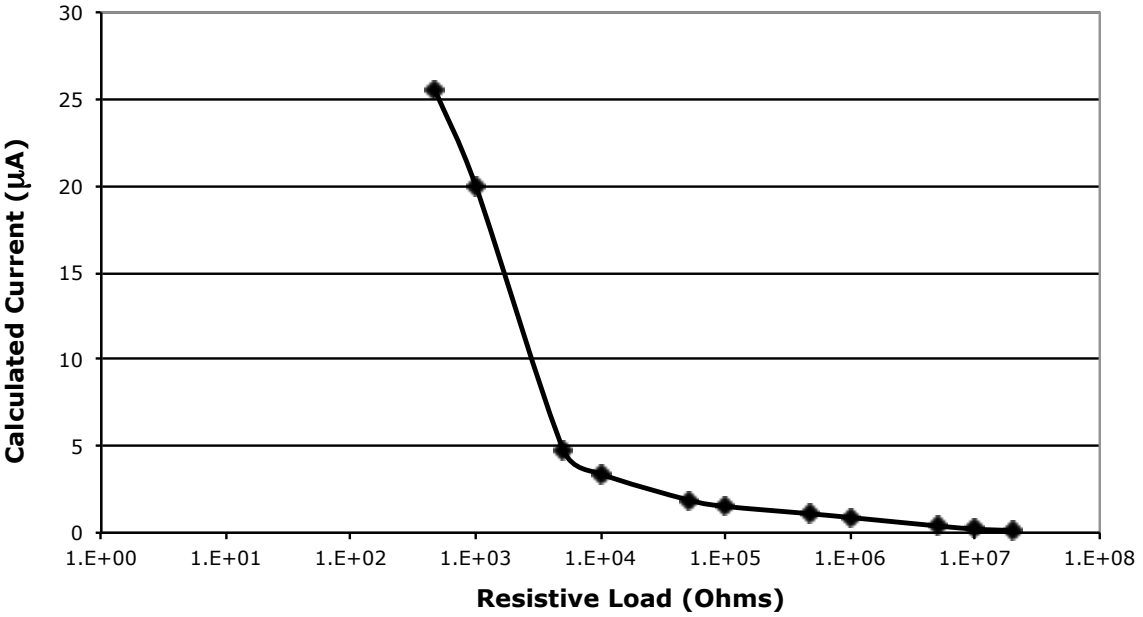

Figure 8.20 Calculated current versus resistive load

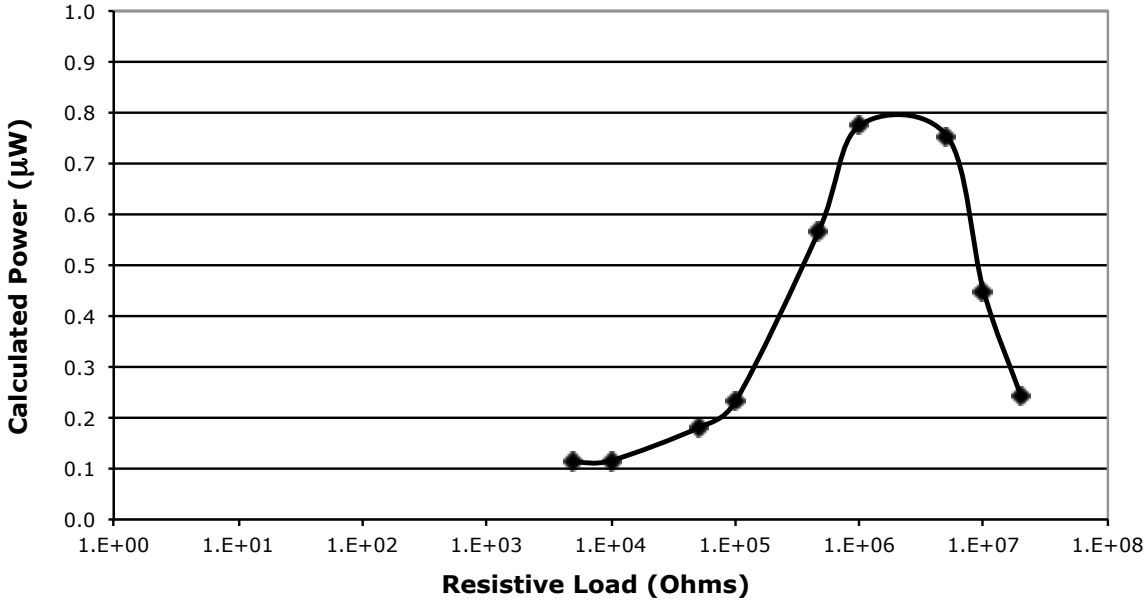

Figure 8.21 Calculated power versus resistive load

Test 4 – Determine Effect of Magnets on Natural Frequency

Next, neodymium magnets were placed in opposing directions, with one on the tip mass and the other fixed nearby. The experimental method for this test involved moving the magnets incrementally closer together and measuring how the behavior of the harvester changed. The magnets have two purposes. First, as the magnets are moved closer or farther apart, the resonant frequency of the beam is decreased or increased, allowing for tuning capability. Second, the bistable "popping" action resulting from the opposing magnets is intended to excite the bimorphs with an impulse load.

The harvester was initially excited at a resonant frequency of 2.02 Hz and a base acceleration of 0.1 g. By moving the opposing magnet close to the magnet on the tip mass, the resonant frequency was lowered to below 1 Hz, and moving the attractive side of the magnet close increased the resonant frequency to above 3 Hz. However, it was

observed that interaction with the magnet (either attractive or repulsive) greatly reduced the amplitude of the harvester. When the magnets were attracting, the tip mass was pulled towards the center, limiting its amplitude. When opposing magnets were used at close range, the magnet did slow down as expected at the center, but only slightly accelerated after passing through the center point. At greater distances, the change in velocity from the magnetic fields remained smooth and insufficient to cause any substantial load on the bimorphs. At smaller distances, the stronger magnetic field prevented the tip from moving past the center point at all. Over the entire tested range of distances and frequencies, the maximum voltage measured from the bimorph was only 0.8 V peak to peak.

If the harvester were exposed to greater accelerations, it may build enough momentum to pass through a stronger magnetic field, which could be more successful in delivering an impulse load. With the low acceleration levels typically found on bridges, it seems unlikely that the bistable magnet concept will be capable of exciting the bimorphs as proposed. However, the use of magnets in small degrees is feasible for fine-tuning the main beam's resonant frequency.

Test 5 – Determine Resonant Frequency and Power Output with Striker

Because of the ineffectiveness of the bistable magnet concept, the prototype was modified to excite the bimorphs by allowing the steel tip mass to strike a stationary "striker plate" with each oscillation, as shown in Fig. 8.22. To test the effectiveness of this new concept, Test 5 was conducted, which measured the power output and changes in resonant frequency with different striker plate characteristics. After observing the behavior of the harvester with the striker plate at 50% of the initial displacement, three positions were chosen for testing: 5.5 cm below the tip's resting position, 6.0 cm, and 6.5

cm. The results for this test, using a 2.17-Hz signal with base acceleration of 0.1 g, are shown in Fig. 8.23.

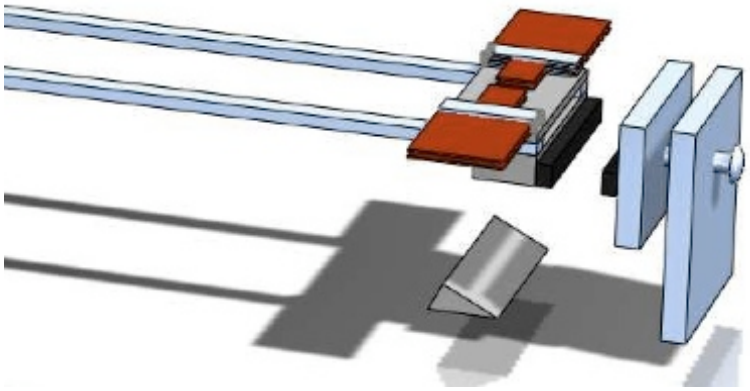

Figure 8.22 Modified prototype with striker plate

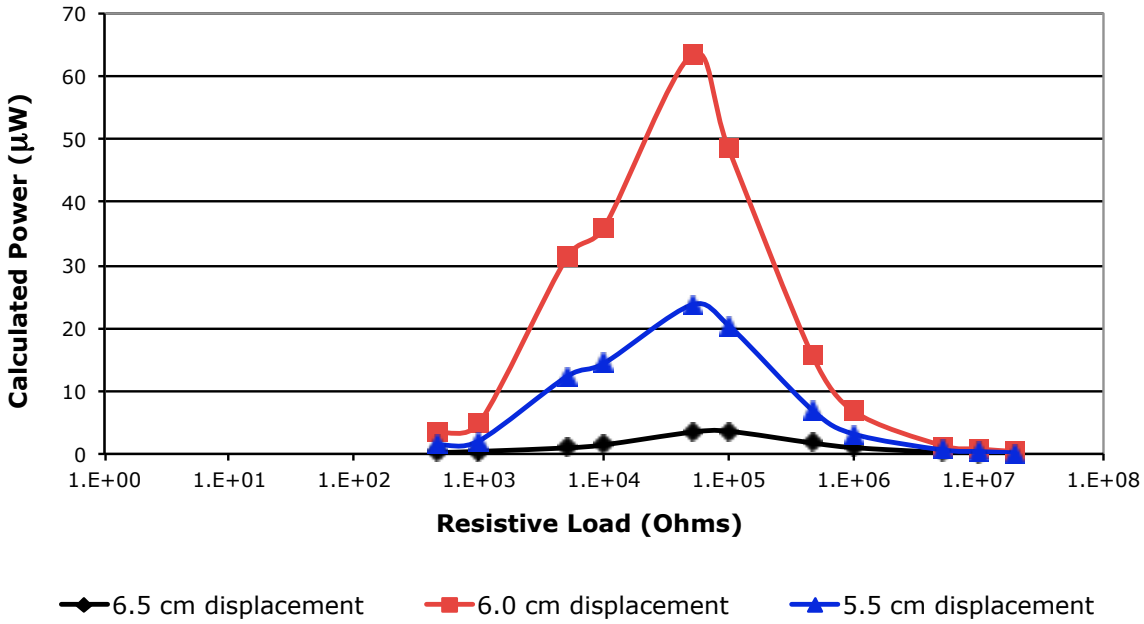

Figure 8.23 Calculated power versus load and striker position

With a maximum power output of 64 μW per bimorph, the harvester was finally approaching feasibility for the wireless sensor application, which requires a minimum of 300 μW. The original resonant frequency did not appear to diminish with the use of the

striker plate. Instead, because the striker limits the motion of the tip mass, the bandwidth appeared to widen slightly. In addition, the optimal load resistance changed from the previous test, indicating that the overall mechanical damping of the system had changed.

Test 6 – Frequency Sweep Testing

To confirm the bandwidth results from Tests 1 and 2, the harvester was also subjected to a sine sweep. The first instance involved a sweep from 1 Hz to 3 Hz and back to 1 Hz, with a constant base acceleration of 0.03 g and a run time of 100 seconds. The voltage excitation to the shaker table, acceleration measured on the table, and voltage output from one bimorph harvester are shown in Fig. 8.24.

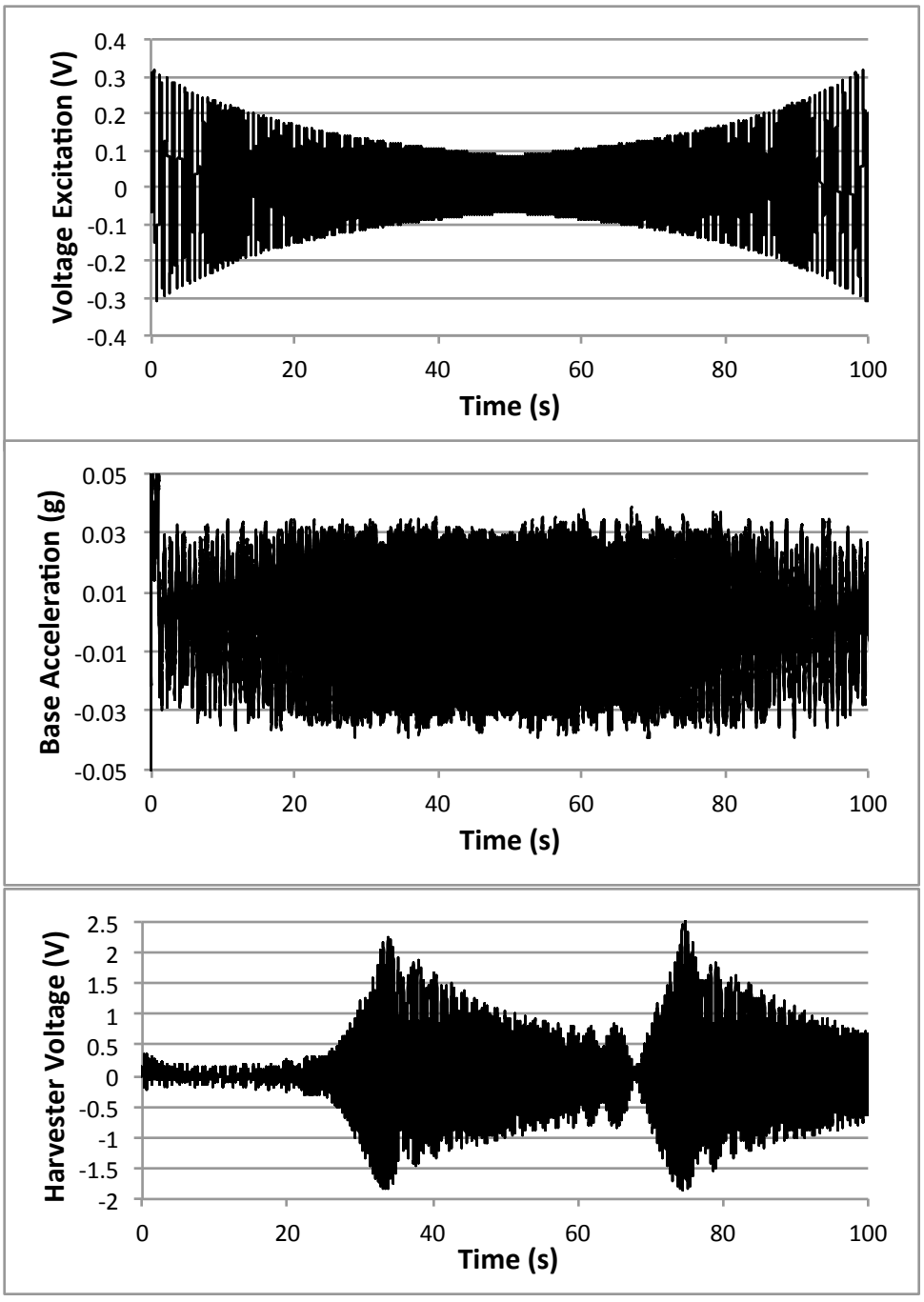

Figure 8.24 1-3 Hz, 100 s excitation, base acceleration, and harvester voltage

The voltage measurements from the harvester reveal a strong resonant peak, with the system continuing to phase in and out of resonance as the test continued. Because the low damping of the system allowed the beam to continue vibrating through the remainder of the test, a second test was run with greater focus: a frequency range of 1.7 Hz to 2.4 Hz, an acceleration level of 0.03 g, and a run time of 500 second, shown in Fig. 8.25.

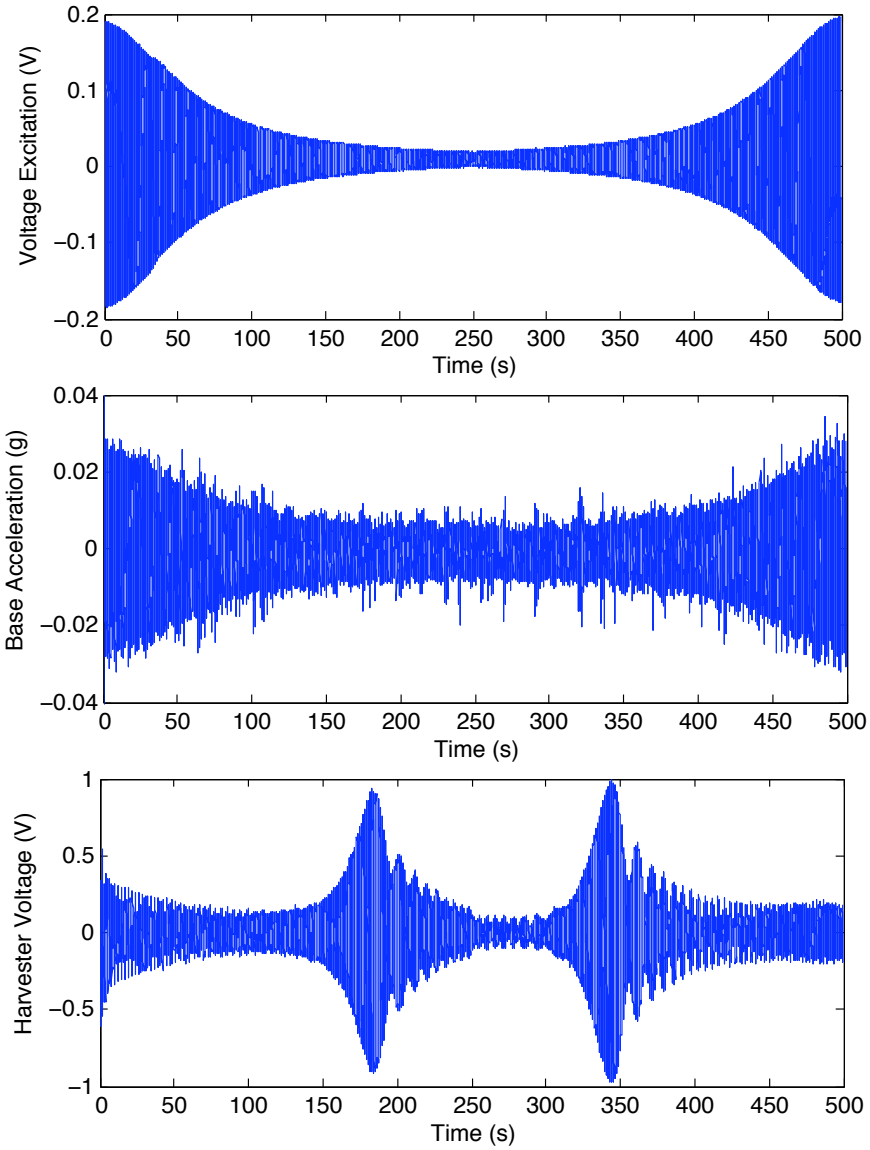

Figure 8.25 1.7-2.4 Hz, 500 s excitation, base acceleration, and harvester voltage

These results show that this test performed similarly to the first test, but with cleaner results. To find the resonant frequency of the system, the harvester voltage measurements can be converted to the frequency domain through a fast Fourier transform (FFT). This spectral analysis is shown in Fig. 8.26.

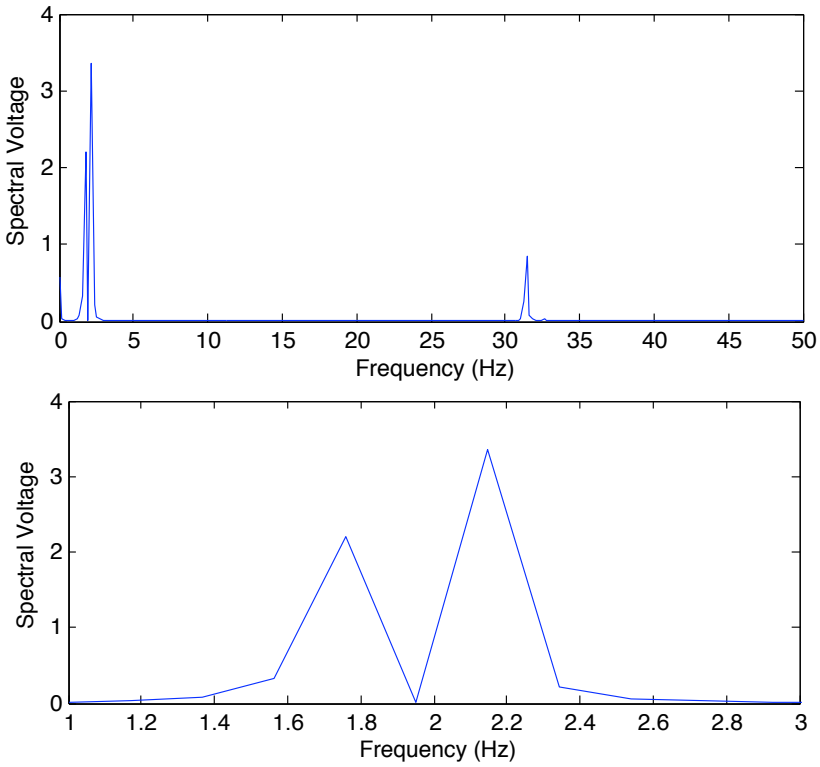

Figure 8.26 Above – full FFT of harvester voltage; below – zoom of low frequencies

The expected resonant frequency appears here at 2.18 Hz, but another spike unexpectedly appears at a lower frequency of 1.75 Hz. Further analysis revealed that this secondary resonance moved around through the sine sweep, while the actual resonant frequency remained steady throughout the test. This is illustrated in the spectrogram in Fig. 8.27, where the resonant frequency (vertical red band) remains steady with time (vertical axis), while the secondary frequency (>-shaped red band) appears to be a function of the forced input frequency.

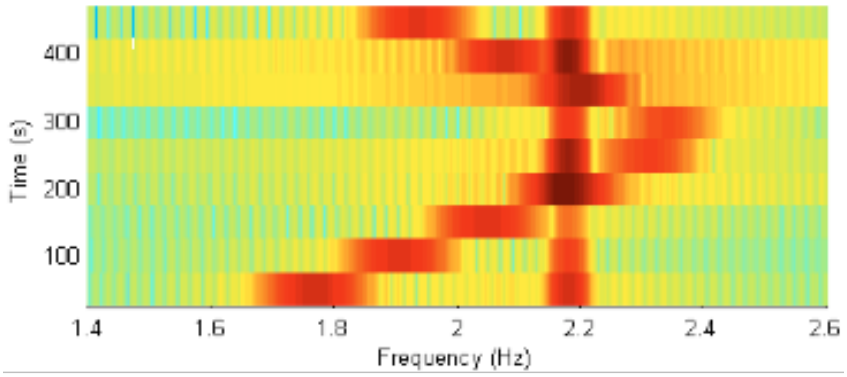

Figure 8.27 Spectrogram revealing resonant frequency and shifting secondary frequency

This test proved useful in demonstrating how the harvester behaves when outside its resonant frequency, showing how it continues to resonate in and out of phase after being excited. However, because of this time-dependent interaction between the harvester and the input vibration, as well as time delays between the LabVIEW VI and the shaker table, analysis of specific resonant frequencies and the power output is more easily accomplished by the "one-at-a-time" tests described previously.

Test 7 – Determine Power Output from Bridge Vibration

After measuring the capabilities of the harvester prototype under ideal conditions (constant sinusoid excitation at resonance), it was time to observe its performance in more realistic conditions. Acceleration measurements were taken previously on the I-35/US-290 Interchange (see Chapter 4). Data taken from five accelerometers is shown in Fig. 8.28. The voltage excitation to the shaker table is proportionate to the table's velocity, so the acceleration data first needed to be integrated to yield velocity. The resulting velocity waveforms are shown in Fig. 8.29. By feeding this signal to the shaker table, the resulting motion could be matched to the original acceleration signature.

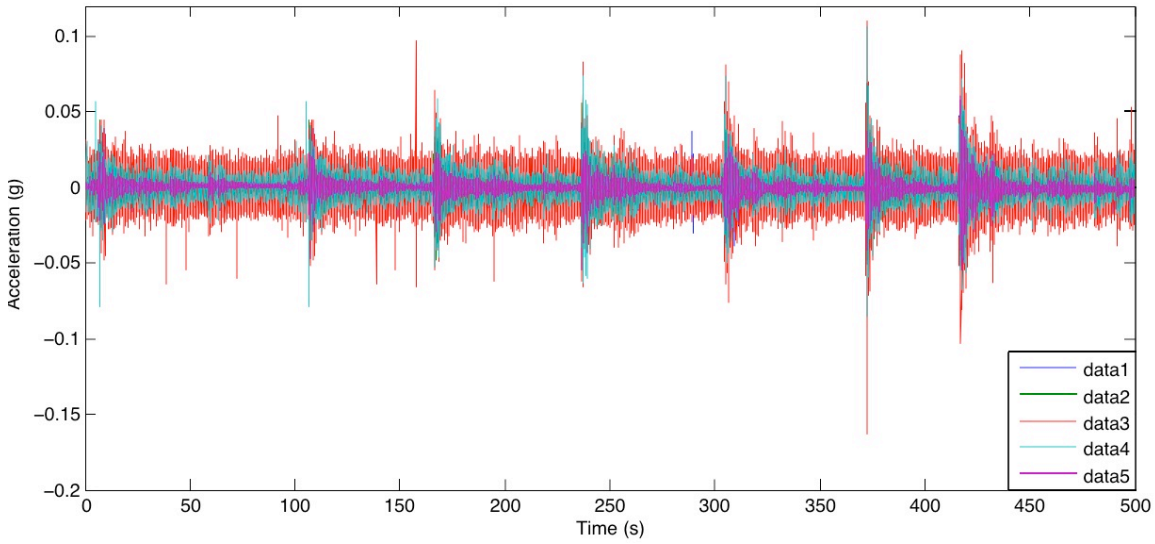

Figure 8.28 Accelerations on I-35/Hwy 290

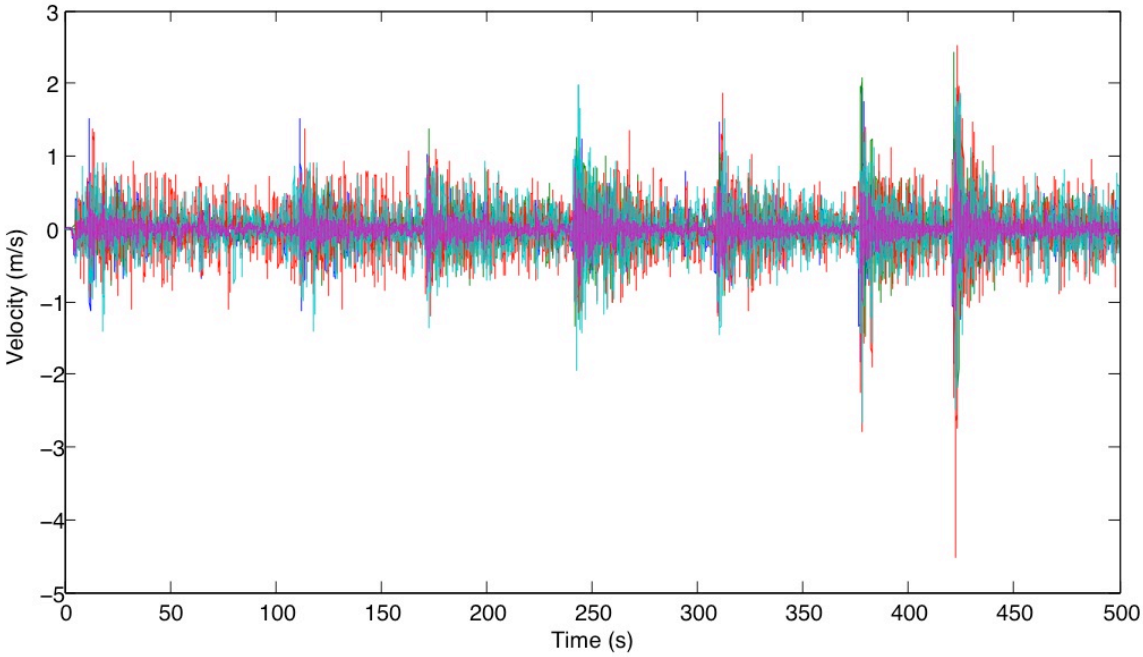

Figure 8.29 Velocities on I-35/Hwy 290

Unfortunately, the bridge vibration did not sufficiently excite the harvester prototype. Though the harvester resonated very efficiently under prolonged sinusoid input, the bridge signal, consisting of strong initial loading with vibration dropping off

exponentially, did not amplify the tip displacement enough to hit the striker. The striker was moved closer to the tip mass resting position to enable contact at the smaller displacement, but the resulting impact was of too low a velocity to transfer any useful power to the bimorphs. Because of this result, a second prototype was proposed that would instead be tuned to the Medina River Bridge in San Antonio, Texas. This bridge exhibits acceleration levels at greater amplitude, slightly higher frequencies, and across a wider bandwidth, each of which would be beneficial to the vibration harvester output.

8.3.5 Design of Second Prototype for Medina River Bridge

A second prototype was constructed, based on lessons learned from the successes and shortcomings of the first prototype. To increase power output, six Volture V20W bimorphs were stacked on the tip mass. The harvester was attached to an enclosure that also included an aluminum cylinder for a striker. This geometry was chosen so that the tip mass could impact perpendicular to the striker surface regardless of its position.

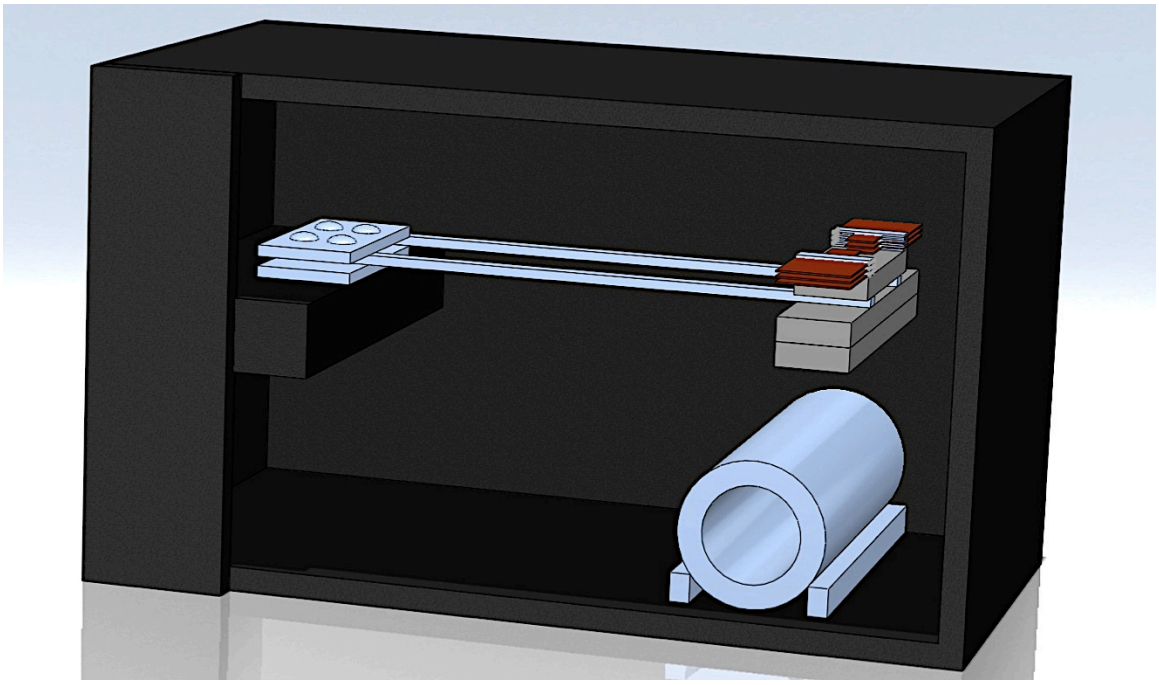

Figure 8.30 CAD model of second prototype

Because of the low excitation levels from the acceleration on the I-35/US-290 Bridge, this prototype was designed with the I-35N Medina River Bridge in mind. This bridge vibrates with greater amplitude, a wider bandwidth, and at higher frequency, with several power spikes between 5 and 10 Hz. The resulting main beam is shorter (which means a more compact system) and has a larger tip mass (which should result in greater power output). A CAD model of this second prototype is shown in Fig. 8.30.

To resonate at the appropriate frequency, the following materials and dimensions were selected:

- 2 aluminum beams, 0.31 x 0.01 x 0.005 m
- 6 Volture V20W bimorphs
- Tip mass consisting of 3 steel blocks, 0.1 x 0.04 x 0.01 m each

- 8 N42 neodymium block magnets for attaching the bimorphs to the tip mass, 0.0254 x 0.0064 x 0.0048 m
- An enclosure of Delrin acetal copolymer measuring 0.46 x 0.30 x 0.22 m

A summary of the parameters necessary for analytical modeling of the system is contained in Table 8.6.

Table 8.6 Geometry and characteristics of second prototype's two main beams

Material	**Natural Freq**	**Beam Static Safety Factor**	**Free Length**	**Width & Height**	**Tip Mass**
Aluminum	7.50 Hz	7.85	0.25 m	1x0.5 cm	1.25 kg

Initial testing of the prototype revealed that using a cylindrical striker plate resulted in a low coefficient of restitution (how strongly the beam bounced back after impact). Better results were observed by using a point contact. A triangular striker was used thereafter. The constructed prototype is shown in Fig. 8.31.

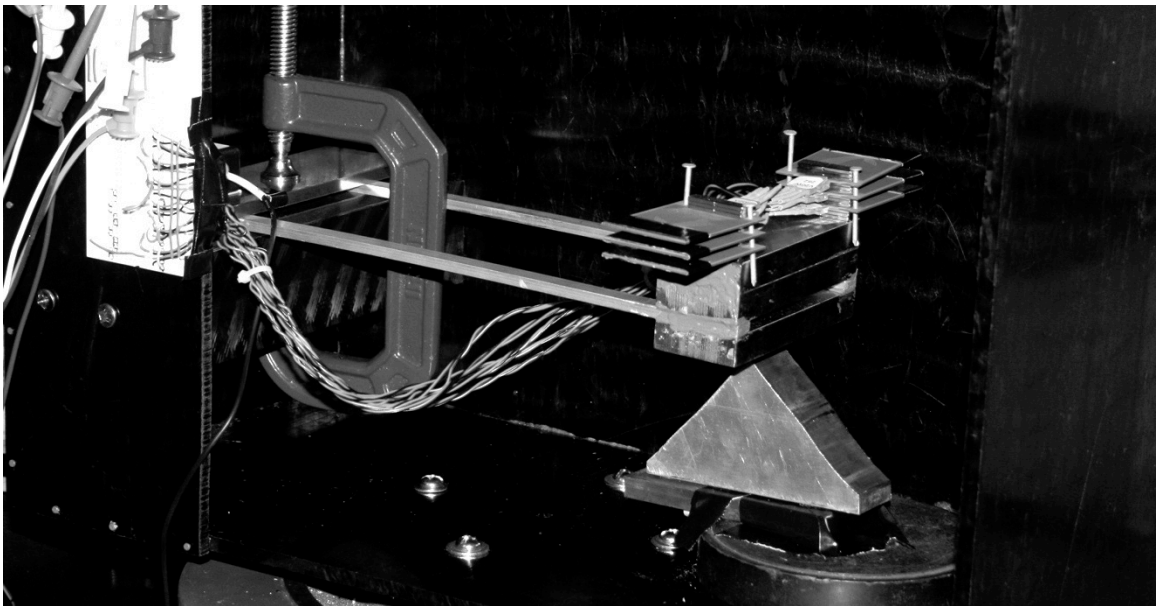

Figure 8.31 Completed prototype for use at 7.5 Hz

8.3.6 Results for Second Prototype

This second prototype was subjected to similar tests to the first prototype, including finding the natural frequency, power output without a striker plate, power with the striker output at different locations, and power output from bridge vibration data. The results of these tests are discussed below.

Test 1 – Determine Natural Frequency Under Forced Vibration

The harvester was subjected to forced vibration of frequencies ranging from 1 Hz to 15 Hz, randomly selected and with resolution of 0.05 Hz in the region around the expected resonant frequency and 0.1 H elsewhere. The voltage excitation created a 0.1-g acceleration at a frequency of 6.5 Hz. The resulting voltage (peak-to-peak) generated by all six V20W bimorphs wired in series is shown in Fig. 8.32.

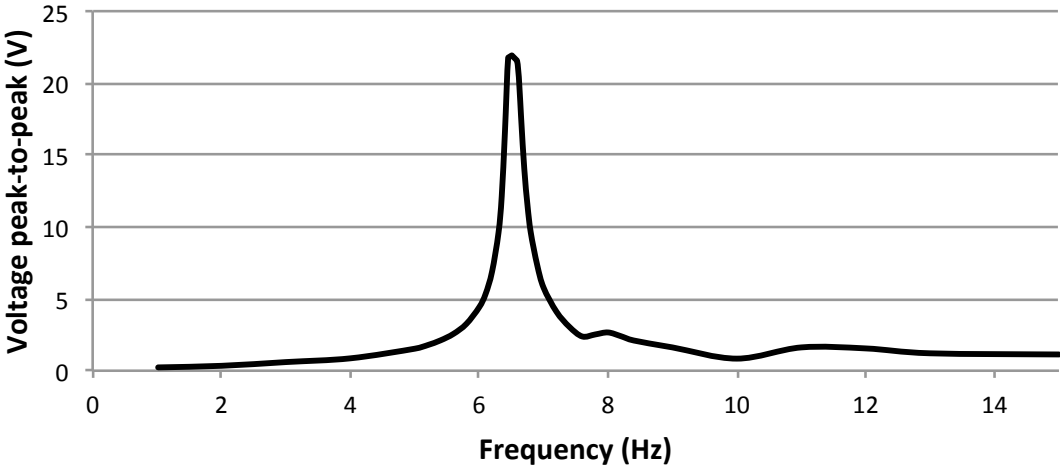

Figure 8.32 Voltage output from second prototype

Because the excitation voltage is proportionate to velocity, the acceleration changes linearly with changes in frequency, as shown in Fig. 8.33. The harvester output can be corrected for this factor, as shown in Fig. 8.34. The maximum peak-to-peak voltage generated at resonance was 21.94 V at 6.45 Hz.

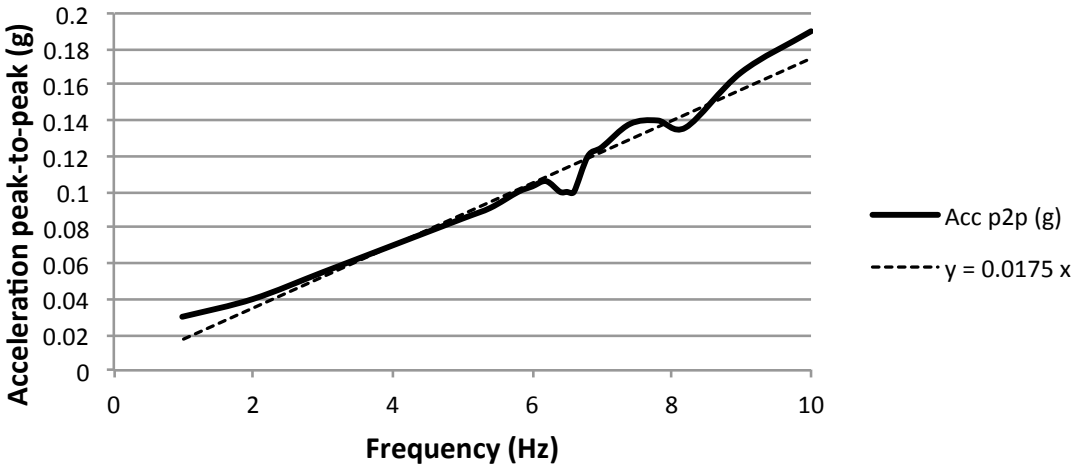

Figure 8.33 Acceleration as a function of driving frequency

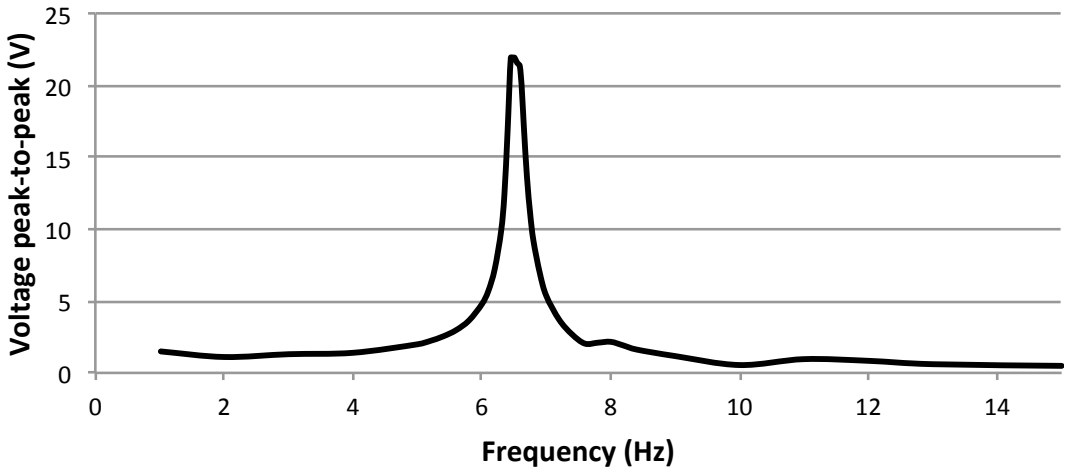

Figure 8.34 Voltage output corrected for acceleration

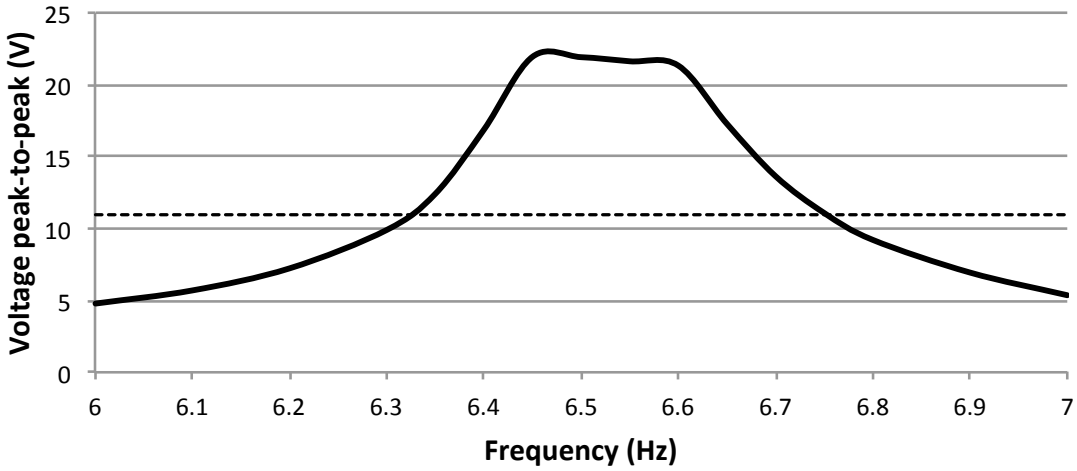

Figure 8.35 Bandwidth of second prototype

Figure 8.35 zooms in on the resonant frequency of 6.45 Hz and shows that the bandwidth of 50% or greater voltage ranges from 6.3 Hz to 6.75 Hz. This bandwidth of 0.45 Hz is still relatively narrow for practical purposes, but is more than ten times the bandwidth of the first prototype. The quality factor Q was calculated to be 14.3. The resultant damping ratio is 0.035, slightly higher than the first prototype, as expected.

Test 2 – Determine Power Output at Resonance

Next, the prototype was excited at resonant frequency without the striker in place, and the power output of the bimorphs was measured. To measure the power in the first prototype, only a load resistor was included in the circuit, and power and current were calculated directly from the voltage and resistance. For this second test, the current and voltage were both measured by placing the harvester in a circuit with two resistors (Fig. 8.36). A 10-Ω resistor was included for calculating current from its voltage drop. The second was a high-resistance load, from which the load voltage was measured.

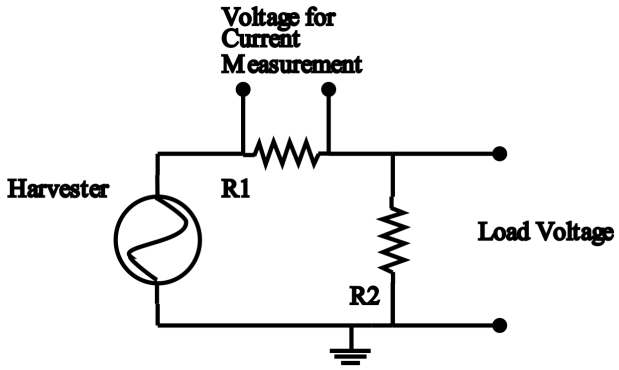

Figure 8.36 Circuit for measuring resistive load voltage and current

However, it quickly became apparent that the current calculated from the 10-Ω resistor and the current calculated directly from the load resistance did not usually match. Table 8.7 shows the voltages produced under different resistive loads, (using 6.5-Hz, 0.1-g input and no striker), the measured current, and the power calculated from each of the two resistors in the circuit.

Table 8.7 Voltage as a function of load resistance

Load Resistance	Load Voltage (RMS)	Voltage Drop Across 10 Ω	Measured Current	Power (VI)	Power (V^2/R)
open-circuit	14.1 V	-	-	-	-
40 MΩ	14.2 V	67 mV	6.7 mA	95 mW	5 μW
20 MΩ	14.1 V	63 mV	6.3 mA	89 mW	10 μW
10 MΩ	14.2 V	73 mV	7.3 mA	103 mW	20 μW
2 MΩ	7.8 V	3 mV	0.3 mA	2 mW	30 μW
1 MΩ	4.4 V	3 mV	0.3 mA	1 mW	21 μW
200 kΩ	1.0 V	3 mV	0.3 mA	0.3 mW	5 μW

Both of the methods of measuring power yielded results higher than that of the first prototype, but with a difference of 5 orders of magnitude. It was hypothesized that the original method of calculating power directly from the load resistance and voltage was the correct one, yielding power without the striker in the range of tens of microwatts.

The variation in the other method possibly could be due to the difficulty of the compactDAQ accurately measuring the low voltages across the 10-Ω resistor above noise and drift. Testing continued monitoring both calculation methods until one could be conclusively identified as correct.

Test 3 – Determine Power Output with Striker

Because six bimorphs were used, each of which included a top and bottom piezoelectric layer, there were twelve layers that could be placed in series or in parallel in the circuit. Placing two layers in series would double the voltage, as compared to a single layer, while placing two layers in parallel would preserve the lower voltage and allow up to double the maximum current. Because power is the product of voltage and current, the overall power output should remain identical among the different combinations.

Table 8.8 shows the open-circuit voltages attained by the bimorphs in different configurations under a sine input of 6.5 Hz and 0.1 g (using the striker). To achieve the six volts needed to power the WSN-3202 wireless node, it would be necessary to operate all twelve layers in series, which would limit the available current. However, using two parallel banks may also be possible, as the node can operate on slightly less than 6 volts.

Table 8.8 Open-circuit voltages of series and parallel bimorph banks

Configuration	Peak-to-peak Voltage	RMS Voltage
1 layer	2.9 V	1.3 V
2 layers in series (1 bimorph)	5.0 V	2.5 V
3 parallel banks of 4 layers in series	8.0 V	3.5 V
2 parallel banks of 6 layers in series	12.2 V	5.3 V
12 layers in series	20.5	10.4 V

Power was measured in the same way as in the previous test, with the striker now installed. As before, measuring the current from the small resistor yielded abnormally

high power levels (~25 mW). Power levels measured from the load for varying resistances are shown in Table 8.9.

Table 8.9 Calculated power from harvester with striker

Load Resistance	12 Layers in Series	2 Parallel Banks of 6 Layers in Series
40 MΩ	6 μW	12 μW
20 MΩ	10 μW	16 μW
10 MΩ	20 μW	26 μW
5 MΩ	32 μW	40 μW
2 MΩ	44 μW	31 μW
1 MΩ	52 μW	28 μW
200 kΩ	48 μW	18 μW

Now that harvester behavior under a resistive load had been measured, the next step was to observe behavior under a capacitive load. A 0.1 mF capacitor rated at 50 V was placed in series with the resistive load, as shown in Fig. 8.37. The voltage from the harvester was also rectified before it reached the capacitor, allowing the capacitor to smooth the input into a steady DC voltage. The harvester was operated with a range of resistive loads, as before, and the voltage across the capacitor was measured as a function of time.

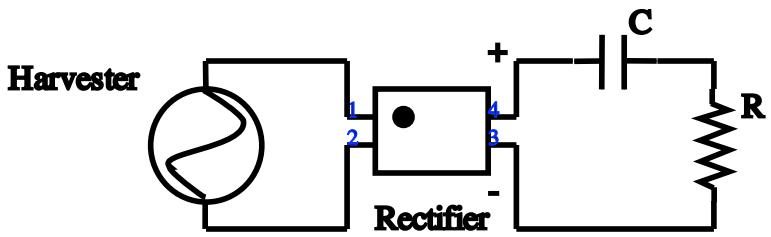

Figure 8.37 Circuit for measuring capacitive load voltage and power

Figure 8.38 shows the behavior of the RC circuit with eight different resistances. At low resistances, a very smooth voltage was created, but it leveled off at only three to

four volts. At mid-range resistances, the voltage continued to climb to almost 10 V by 200 seconds and appeared to continue upward. At the highest resistances, the resistance overcame the capacitance and the resulting voltage remained a full-wave rectified voltage.

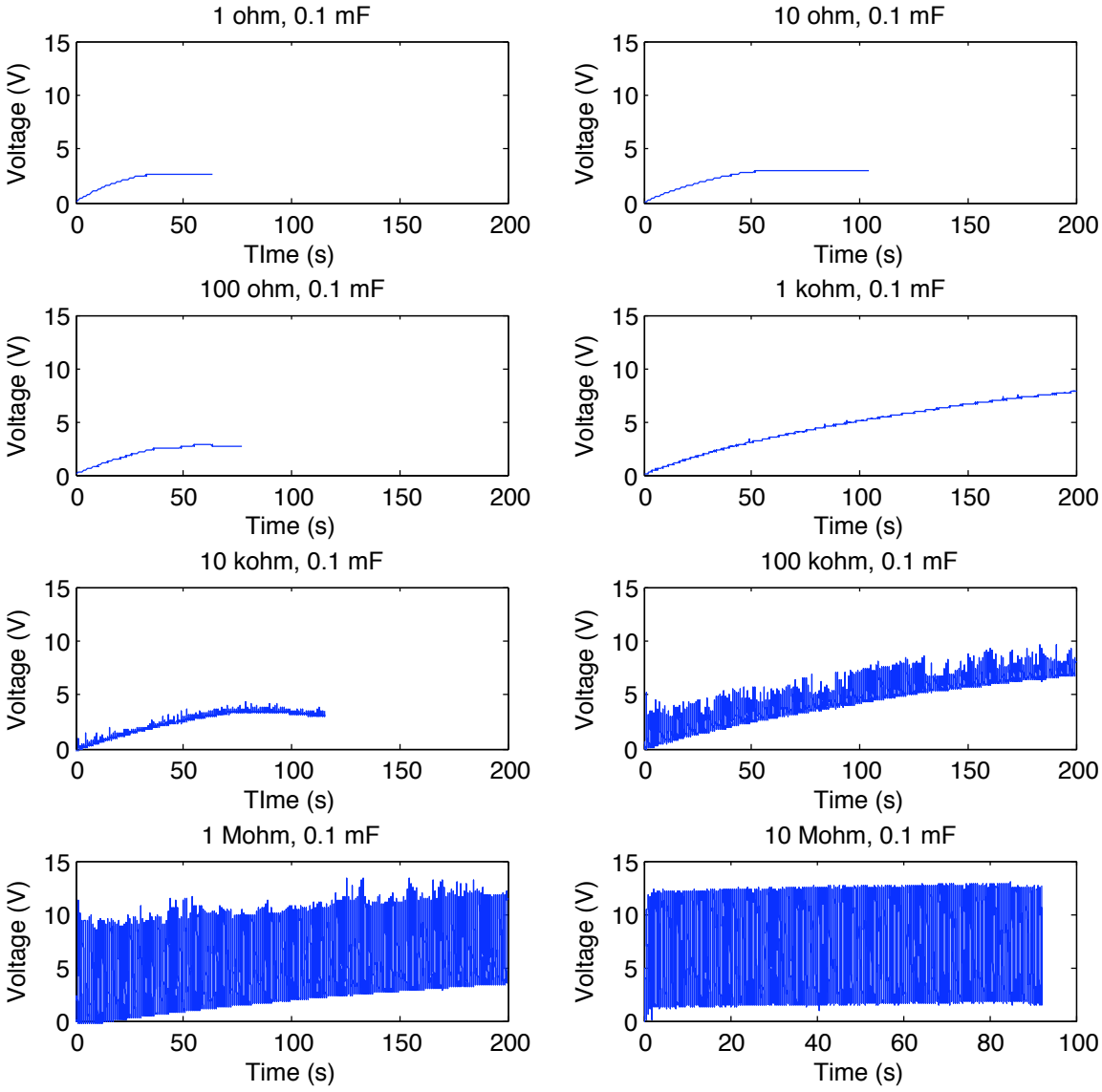

Figure 8.38 Load voltage with RC circuit

The energy stored in the capacitor can be divided by the relevant time frame to yield the average power from the harvester. Table 8.10 shows the work done in establishing the electric field (or the energy stored in the capacitor) for each resistance after 50 seconds, according to the relationship $E_{\text{stored}} = \frac{1}{2}CV^2$. The power is then calculated by dividing by the time.

Table 8.10 Calculated power with a capacitive load

Resistance	Capacitance	Work over 50 s	Average Power
1 Ω	0.1 mF	0.36 mJ	7 μW
10 Ω	0.1 mF	0.41 mJ	8 μW
100 Ω	0.1 mF	0.34 mJ	7 μW
1 kΩ	0.1 mF	0.47 mJ	10 μW
10 kΩ	0.1 mF	0.33 mJ	7 μW
100 kΩ	0.1 mF	0.42 mJ	9 μW
1 MΩ	0.1 mF	0.23 mJ	5 μW
10 MΩ	0.1 mF	0.49 mJ	9 μW

This test confirmed that in the earlier tests, the lower power calculations (directly from the load resistances) were more correct. Thus the power output of the second prototype even under sinusoid input at resonance was not sufficient to power the wireless node. This was confirmed by connecting the node to the circuit in parallel with the capacitor. If the capacitor was allowed several minutes, it was observed to charge up to at least 16 V. Whenever the wireless node was attached, however, the voltage would immediately drop to 1.6 V and remain steady.

Test 7 – Determine Power Output from Bridge Vibration

After these controlled tests with sinusoid input, harvester behavior during acceleration from a bridge was assessed. As discussed, this second prototype was designed to vibrate at a resonant frequency present in the I-35N Medina River Bridge in

San Antonio, Texas. The first step in preparing the acceleration data for use (Fig. 8.39) was to integrate it to yield the velocity. The acceleration data for this bridge contained significantly more drift than the I-35/US-290 Bridge did. To counteract this drift, a band-pass filter was applied to block frequencies below 0.5 Hz or above 80 Hz. The original velocity waveform and the filtered velocity for one sensor are shown in Fig. 8.40. The filtered velocity for this sensor is also shown (zoomed) in Fig. 8.41. The velocity waveforms for all the recorded sensors, scaled correctly to meters per second, are shown in Fig. 8.42.

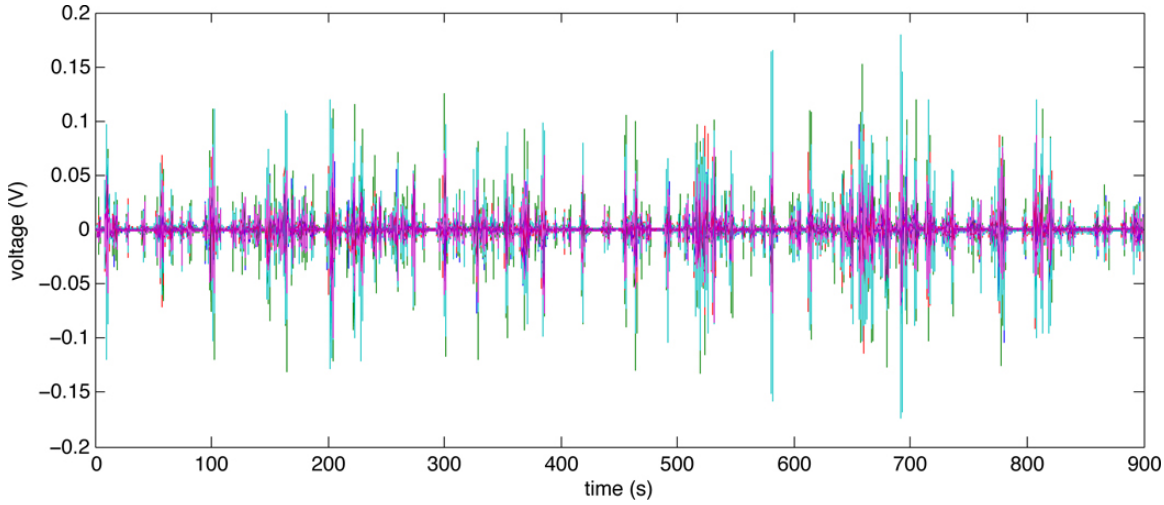

Figure 8.39 Voltage from acceleration on Medina River Bridge

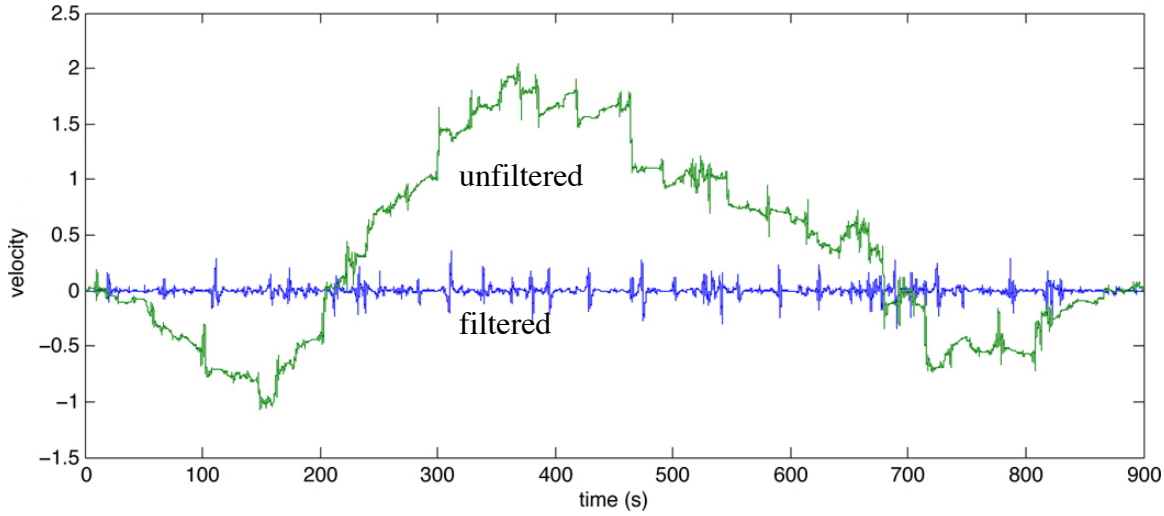

Figure 8.40 Channel 5 velocity filtered and unfiltered

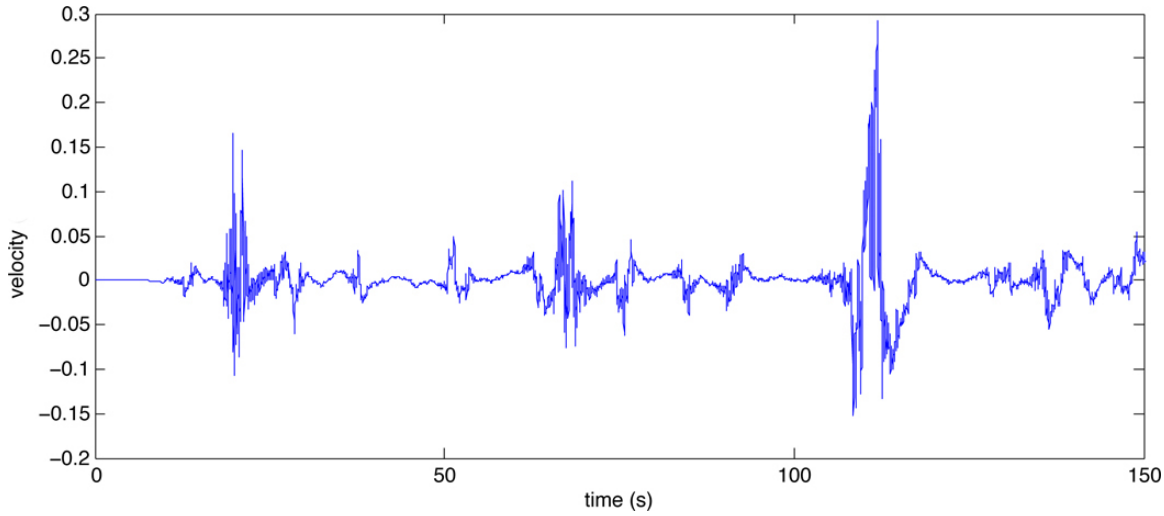

Figure 8.41 Channel 5 velocity, zoomed

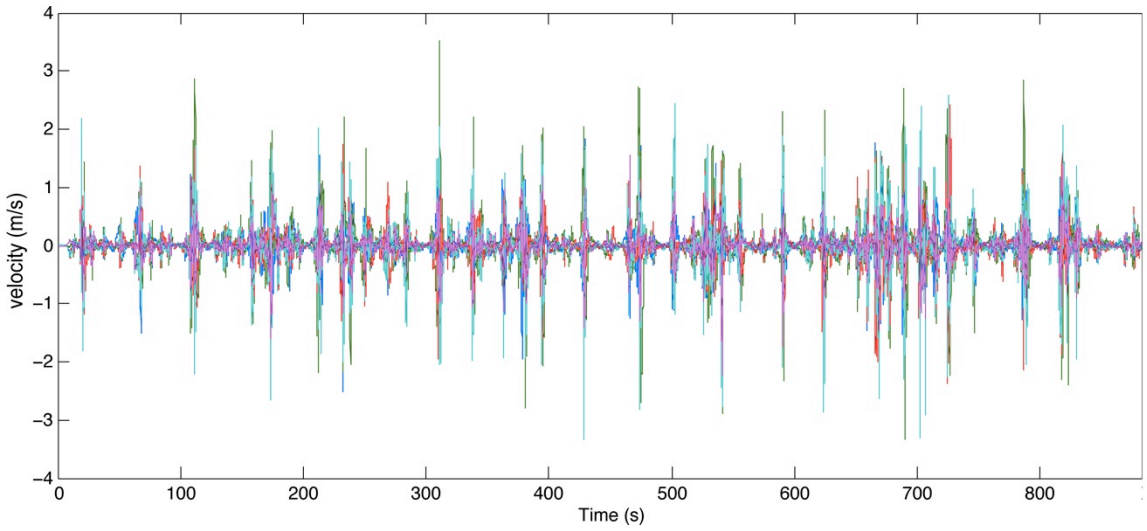

Figure 8.42 Velocity on Medina River Bridge Rescaled to Meters Per Second

When the harvester was excited by the acceleration data from the Medina River Bridge, it did not quite reach the striker as previously positioned. However, by moving the striker to within about 0.5 cm of the tip, the harvester was able to successfully excite the bimorphs from the impacts and produce viable power. The voltage and power generated by the harvester from 50 seconds of bridge vibration are shown in Fig. 8.43 and 8.44.

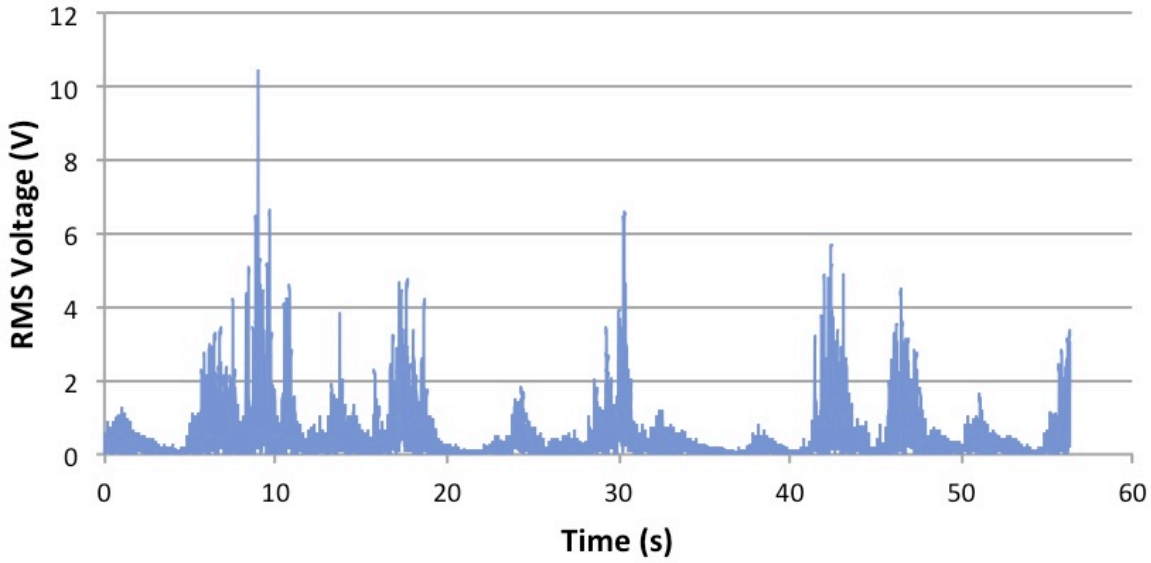

Figure 8.43 Voltage generated by second prototype from Medina River Bridge vibration

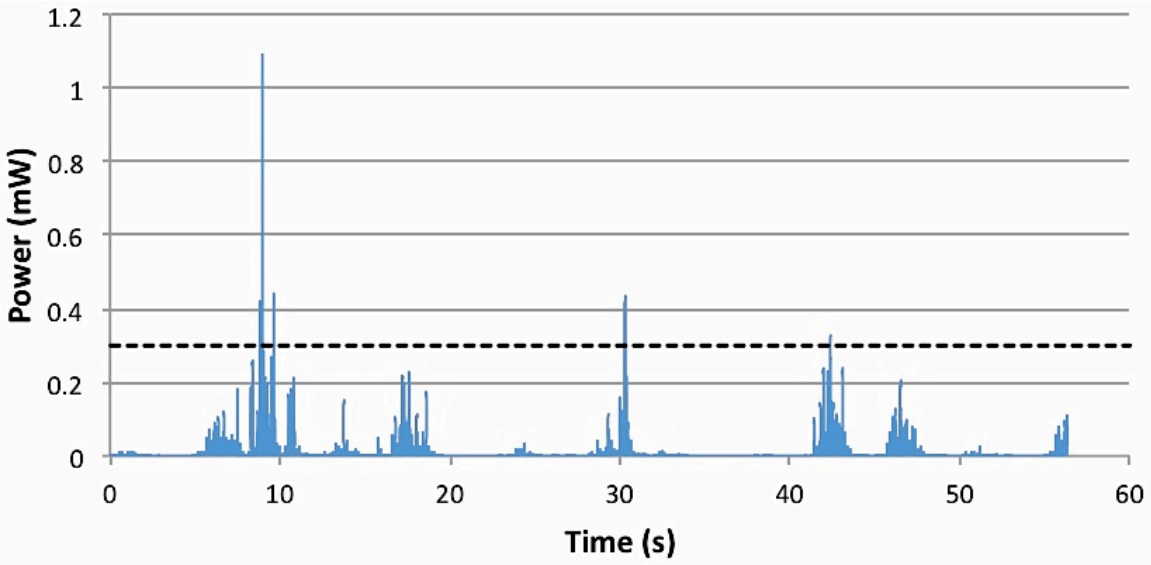

Figure 8.44 Power generated by second prototype from Medina River Bridge vibration

The threshold for being able to power the WSN-3202 wireless node is shown in Fig. 8.44 at 0.3 mW. The prototype was not able to successfully generate this level of power, but it did contribute a significant amount that may be useful as a supplementary power source or for other low-power applications. A spectrogram of the voltage output

from the harvester during the bridge vibration is shown in Fig. 8.45. The bright stripes show moments when power was successfully generated. When power was generated, it predominately came at 6.5 Hz, showing that the primary source of strain in the bimorphs in this instance was the motion of the main beam, not higher-frequency free vibration after the impact loading (No visible stripe was observed in the 60-120-Hz range).

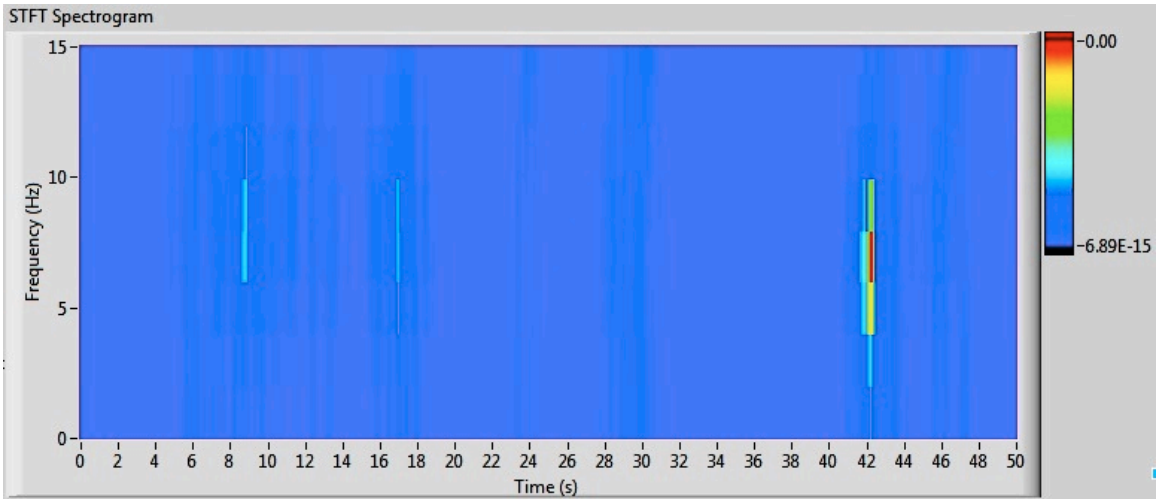

Figure 8.45 Spectrogram of voltage generated from Medina River Bridge acceleration

8.4 Evaluation of Final Embodiments

Following the construction and testing of the two prototypes of the chosen piezoelectric vibration harvester concept, the following conclusions can be drawn:

- The two prototypes were capable of producing power in the neighborhood of 40-70 μW from constant sine excitation of 0.1 g at resonance.
- Neither prototype was capable of providing the required power level of 0.3 mW.
- The first prototype generated a negligible amount of energy from the vibration of the main beam, but generated a large portion of its power by exciting the bimorphs through an impact with the striker.

- The second prototype, because of the higher frequency and larger tip mass, was able to transfer a much larger amount of energy directly to the bimorphs from the main beam. Because the higher frequency translated to lower peak velocities, however, the additional power generated through the impact with a striker was less significant, leading to less overall power being generated than in the first prototype.
- The various components of the system like the striker plate and the main beam/tip bimorphs show great promise as supplementary power sources in other harvesting systems, such as inductive vibration harvesting or wind harvesting.
- Overall, the range of frequencies and amplitudes typical of this application can be harvested more effectively using inductive vibration harvesting than with the proposed piezoelectric prototype. Inductive harvesters can more easily be designed to oscillate at low frequencies. For example, an initial prototype developed concurrently with the piezoelectric prototype successfully generated up to 26 mW from a sinusoid input at 2.2 Hz and 0.08 g (McEvoy, et al., 2011; Dierks, 2011).
- Other configurations of piezoelectric harvesters, discussed in the next chapter, may also be possible for use on bridges, particularly in locations in and around the supports, where the vibration energy is already high impedance (high force and low velocity).

Chapter 9: Recommendations and Conclusions

9.1 Recommended Energy Harvesting Systems for Application

The environment and energy sources surrounding a highway bridge can vary significantly among bridges and even from location to location on a single bridge. Because of this reality, there is no "best" solution to powering wireless sensor nodes on a bridge. Grid power, primary batteries, solar, wind, and vibration each have a place in powering such systems. From the research completed in this dissertation regarding existing harvester technology, power and cost feasibility, functional analysis, concept generation, and the modeling and prototyping of example harvesters, the following recommendations may be made:

- **Grid power** has the lowest ongoing costs, but can have extremely excessive installation costs for materials and labor. In most cases, completely wiring a bridge for structural health monitoring would not be recommended. However, this may be an attractive option if an electrical system is already in place (e.g., for lighting) or for new construction.
- **Primary batteries** can be an attractive option for end nodes operating at duty cycles of one hour or longer. In these situations, the batteries would likely need to be replaced approximately every three to five years to ensure reliable operation. If biennial inspections coincide with these replacements, the additional cost may be fairly reasonable. However, primary batteries are not currently feasible for long-term operation of end nodes running real-time measurements (30 Hz), nodes configured as routers, or central gateway nodes, all of which are necessary for the proposed wireless sensor network.

- **Solar power** is the next most viable option. Photovoltaic panels are the most cost-effective and energy-dense form of energy harvesting, provided that direct sunlight is available for a significant and predictable percent of the time. Solar panels can easily be scaled to match anticipated solar insolation and system power requirements, and such a system is capable of powering all the required types of nodes in the network, from low-power end nodes through 10-watt (or higher) gateway nodes. Issues such as attachment to the bridge and protection from the environment (hail, debris, vandalism, birds, etc.) must be considered, but solutions to these problems are readily accessible. The primary concern is the availability of direct sunlight; efficiency and power density drop off considerably in the shade. If sunlight reaches the vicinity of a wireless sensor for at least a few hours each day, solar harvesting can be a good fit. If, however, the proximate feasible area of installation is perpetually in the shade and extensive wiring would be required to reach sunlight, a different solution may be needed.
- **Wind power** is the next option that should be considered. Wind turbines are similar in price to equivalent solar panels, though their power density is generally lower. Wind turbines require consideration of many of the same issues as solar panels: protection from the environment and vandalism, predictability of wind patterns, etc. Wind turbines are an attractive solution where sensors and associated power systems must be located in shaded areas, or where inclement weather frequently blocks sunlight but creates strong winds. The need to not interfere with traffic under the bridge may often limit how far out from the structure wind turbines can extend, which further limits the available wind. In addition, the exposed moving parts may require more frequent maintenance,

particularly due to the particulates, grime, and pollution incident to roadways. Micro-wind turbines on the bridge should be able to power the wireless nodes in both end-node and router configurations, and larger turbines positioned away from the structure could power the higher-power central gateway.

- **Vibration power** is another viable option for powering wireless sensor nodes. Because of the higher cost, lower power density, and possibly additional labor to tune the systems to the bridges' natural frequencies, it is suggested that solar and wind harvesting be considered first. Vibration harvesting is particularly attractive where solar and wind harvesting is completely infeasible (such as inside box girders), on old fracture-critical bridges where vibration is particularly excessive, in locations where extensive wiring is required to reach available wind or sunlight, or where a completely maintenance-free service life is required. Vibration harvesting is currently only able to power the wireless nodes on the lowest-power duty cycle, but continued development of inductive harvesters and compressive-style piezoelectric harvesters should make support of real-time rainflow analysis and router operation feasible as well. It is unlikely that vibration harvesting would be capable of powering the 10-watt central gateway.
- **Hybrid systems** present a great opportunity for combining the strengths of several different energy domains. One combination that works particularly well is a hybrid solar/wind system. Solar-and-wind-powered street lamps are becoming popular, capable of delivering all-night lighting and even wireless Internet connectivity from the combination of sun and wind. Piezoelectric systems can be used to supplement other types of energy harvesters during off-peak conditions. For example, the wind concept described in Chapter 7 and developed by McEvoy

(2011) makes use of piezoelectric bimorphs to capture small amounts of energy at wind speeds too low to engage the main generator. Similarly, a vibration harvester may include both inductive and piezoelectric elements. The main inductive element can harvest the majority of energy at low frequencies, while the piezoelectric material harvests ambient vibration at higher frequencies, such as above 20 Hz. Solar panels could also be placed on the top of vibration harvesters, giving a power boost even in partial shade. Finally, hybrid solar/thermal panels currently in development use multiple layers to capture both visible light through photovoltaics and infrared radiation through the thermoelectric effect.

9.2 USE OF PORTFOLIO

Because multiple concept variants in solar, wind, and vibration harvesting have been developed in parallel, the project is now in a good position to develop a portfolio or suite of interchangeable energy-harvesting systems that can easily be connected to the selected wireless sensor nodes. Common functions such as attachment mechanisms, energy storage, and power conditioning can be shared among the different systems, creating a family of product architectures with greater ease of installation, interchangeability of harvester modules after installation, and lower overall cost. A suggested portfolio of energy harvesters that would completely power a bridge-mounted wireless sensor network may include the following:

- A 50 to 80-watt solar panel or hybrid solar/wind system to power a central gateway node installed in an area with accessibility to prolonged direct sunlight.
- Small solar, wind, or hybrid harvesters to power router nodes positioned periodically along the length of the bridge. The position of these nodes is still fairly flexible, making it still easy to find access to wind and/or sunlight.

- Solar, wind, vibration, or hybrid systems to power end nodes. These nodes must be placed within a short distance of the locations being monitored, so it essential that a wide variety of options is available for delivering power to the nodes. Plug-and-play connections and shared battery and power-conditioning hardware would ease the installation and interchanging of different harvesting systems.

9.3 INSIGHTS INTO ENERGY HARVESTING DESIGN

Energy harvesting is a field in which innovation is vital to success. The essence of energy harvesting is providing power for a specific application from sources that were previously untapped and even thought unusable. Because environmental energy in its natural state is often diffuse, unrefined, and unpredictable, a major consideration of the energy-harvesting process is how to capture, concentrate, and prepare the energy efficiently and innovatively. As discussed in Chapter 6, there are nine key functionalities that are central to the energy-harvesting process:

1. Interface (attach, position, etc.) with environment
2. Direct (filter, concentrate) energy from the environment
3. Separate (extract, collect, capture) energy
4. Transform (amplify, change) energy into form ready for conversion
5. Convert energy to electrical energy
6. Condition (rectify, process, smooth, change) electrical energy for storage or use
7. Store electrical energy
8. Supply electrical energy to application
9. Interface (interact with light, signals, visual/tactile/audio feedback) with user

In the design of any new energy-harvesting system, the designer should carefully consider each of these key functionalities and note areas where current solutions fall

behind or could easily be improved. For example, the piezoelectric concept developed in Chapter 8 attempts to *transform* vibrational energy from low frequency to high frequency in order to more efficiently *separate* or collect it. The inductive vibration harvester mentioned in Chapter 7 examined means to capture a wider bandwidth of vibration by more effectively *directing* the energy through tuning or nonlinear behavior. The wind turbine also mentioned in Chapter 7 included a conventional inductive generator and a small piezoelectric generator to *direct* additional energy from previously unharnessed low-speed wind energy. The solar panel system developed focused on effectively *conditioning*, *storing*, and *supplying* the energy and innovative attachment mechanisms to *interface* with the bridge environment without interfering with normal operation.

As design and development of new energy harvesting technology proceeds, a thorough examination is needed of how analytical modeling, numerical analysis, laboratory experimentation, and field-testing will most effectively lead the designer to a successful solution. Analysis of system behaviors well studied and easy to model, such as the motion of simple cantilever beams or the long-term power output from solar panels under known conditions, can yield very accurate predictions of actual real-world response. However, harder to model interactions like energy transfer between impacting bodies and energy conversion efficiency in randomized, non-ideal situations may be impossible to accurately study without a physical working prototype.

The distribution between physical prototyping and analytical modeling of energy harvesters, like many other fields of design, is best correlated to the experience of the designers in comparable systems. Issues such as damping and other mechanical losses, electrical efficiencies, human user interaction, and manufacturing time and cost are areas that designers exploring new territory can only fully consider after physical prototyping.

Only after this initial level of experience can the designer characterize these issues in ways that can usefully contribute to accurate modeling of future systems.

As energy harvester design moves forward, the trend is towards further miniaturization and ubiquity of harvesters and wireless sensors seamlessly woven into everyday applications. To a great extent, successful design in this cutting-edge landscape requires considerable investment in optimizing the entire system for the specific application. To truly seize the most opportunity in this field, the question should not merely be "how much power can I deliver to a given wireless sensor node?" but "given the total amount of energy available in this environment, what is the most I can do with it?" This involves a tight integration between sensors, wireless hardware, energy storage, and energy harvesting sub-systems. As the energy-harvesting effectiveness increases through specialization and active optimization to the environment, the wireless sensor technology must also be actively optimized and specialized for the individual application. General-purpose wireless nodes that are designed to approximately meet the needs for many different applications will, through their overhead in power, cost, and size, not effectively be able to compete against more specialized products. Thus, synergy and cooperation of interdisciplinary teams is essential to creating a complete package that fulfills the often-daunting goals involved in energy harvesting.

9.4 FUTURE WORK

With the completion of the initial research in this project, including product benchmarking, power and cost analysis, concept generation, and proof-of-concept prototyping, work will continue as the chosen concepts in solar, wind, and vibration are developed to market readiness. The first phase of future research is the design of alpha prototypes that will be field tested on actual bridges. Improved prototypes for wind and

solar harvesting are currently being developed, with subsequent focus on a vibration harvester prototype as well. From the modeling and prototyping results described in this dissertation, it is recommended that induction vibration harvesting be the primary focus of continued concept development, followed by new concepts in piezoelectrics that more effectively take into account the high-impedance nature of piezoelectric materials. The insights gathered from the current line of research in piezoelectric vibration harvesting should be also be evaluated for possible inclusion as supplemental power sources for hybrid vibration or wind systems.

After the completion of alpha prototyping, the resulting systems should be reevaluated according to the key functionalities described in Chapter 6 and the design specification sheet found in Appendix F. At this point, system-level design should involve increased interaction between the various design teams on the project (ME, CAEE, ECE, NI, WJE). Full support and involvement of each design team in the energy harvesting area of product design will allow the sharing of knowledge and experience regarding how energy harvesting will be expected to interact with the other components of the system and will encourage better communication of how these other components may be further designed and optimized to better capture the strengths of energy harvesting.

Continued system development is expected to lead to at least one beta-level prototype in each of the three energy domains, suitable for real-life operation with the complete wireless sensor network system. The completed system, including the energy harvesting subsystems, would then be brought to market for widespread use on highway bridges and possible application on other structures like skyscrapers, convention centers, and factories. Variations of this system could also be applied to a vast scope of other

applications, with actions like health monitoring, lighting, data-logging, emergency communication, and device control being embedded in automobiles, aircraft, handheld electronics, appliances, and even clothing.

In addition to the concepts currently selected for further development, several other design avenues exist that have not yet been explored in detail. As shown in Chapter 8, the configuration chosen for the constructed piezoelectric prototypes did not perform well under the conditions tested. Piezoelectric materials are high-impedance; they function most effectively under conditions of high effort and low flow (high force and low velocity). The traditional cantilever bimorph configuration (Fig. 7.7 and 7.9) achieves these conditions at high frequencies. However, as the designed resonant frequency drops, the system becomes relatively low impedance, with low force and high velocity. The proposed concepts transformed this low-impedance input back into a high-force, low-velocity excitation through the shock impact with the striker mechanism. However, this also resulted in delivering a short burst of power just once each oscillation.

Piezoelectric materials could more effectively be used in low-frequency vibration harvesting by pursuing alternative configurations that more naturally lend themselves to high impedance. Instead of focusing on areas of highway bridges where large-amplitude vibration could introduce bending moments to cantilevers, piezoelectric material could be placed within supports, bearings, and expansion joints in bridges where high forces would directly compress the material (Fig. 9.1). This approach would be limited to sensors near these high-force areas, and would sometimes require greater installation cost to properly position the material within the bridge structure itself. In situations where this approach would be feasible, the movement of the bridge would compress and expand the material with much lower displacement and higher force than the bimorph configuration,

with power generated continuously instead in discontinuous bursts. Such a harvesting system would be similar to existing systems that harvest energy from dance floors (SDC, 2007) and train stations (East Japan Railway Company, 2008).

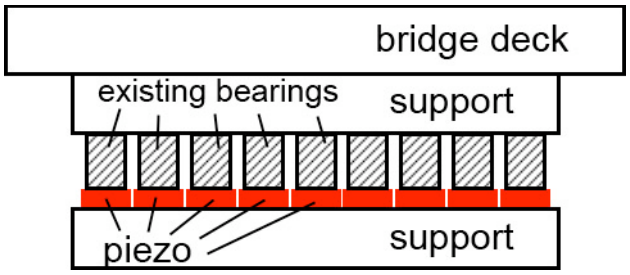

Figure 9.1 Concept for harvester in bridge bearings (not to scale)

A variation of the direct pressure configuration could also be employed at other locations along the bridge as shown in Fig. 9.2. In this concept, piezoelectric material is placed within the mounting mechanism of a cantilever beam with proof mass at the tip. This configuration would transfer the energy of the beam's motion to high-force, low-velocity compression of the piezoelectric material. This would allow the use of the more power-dense d_{33} polarization of the material (see Fig. 7.6) and operate only in compression, avoiding the piezoelectric material's lower tensile strength. This concept would not yield the power output possible from the bridge supports themselves, but would be another possible option to provide location-independent vibration harvesting. Again, instead of providing a brief spike of power once each oscillation (as with the prototype in Chapter 8), this concept would generate power under high impedance through the oscillation's entire cycle.

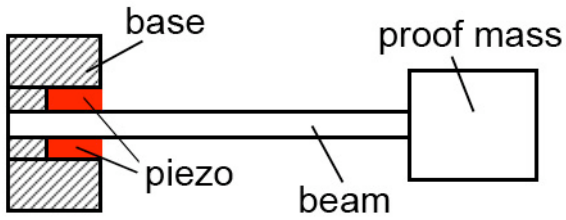

Figure 9.2 Concept for compressive piezoelectric cantilever system

The development of these two concepts would require careful planning of modeling and experimentation. For the concept in Fig. 9.2, a finite element analysis of the system would be the most beneficial means of modeling, as the interactions at the base would only be roughly approximated by closed-form analytical modeling. Such a model would be able to predict not only the stresses in the piezoelectric material, but the power generation as well through the piezoelectric coupled equations that relate strain and electric charge density displacement to stress and electric field strength (Roundy, Wright, & Rabaey, Energy scavenging for wireless sensor networks: With special focus on vibrations, 2004). The model would also be able to predict the impedance of the system, and thus, the required impedance of the load to maximize power output. Because the compression of the piezoelectric material is continuous and directly related to the motion of the beam (instead of depending on discontinuous impacts as in Chapter 8's prototype), a more accurate prediction of dynamic behavior should be possible. Parameterization of this model would lead to the construction of a prototype with well-understood physical behavior and power generation.

Testing in Chapter 8 showed that driving the harvester at resonance severely overestimated behavior while driven at bridge vibration, but excitation from bridge vibration does not lend itself to easy and repeatable characterization. An appropriate intermediate step in testing would be to use a simulated damped free vibration, of the

form $x = D\left(e^{-\zeta t}cos[\omega_d t]\right)$. This excitation would operate at the resonant frequency of the harvester, ω_d, and attenuate from the exponential term. Using this input and later, actual bridge input, power output should be calculated by measuring the time to charge the capacitor of the predicted optimal RC load. This test should be repeated with changed values for the load resistance and capacitance, the input frequency, time constant of attenuation, and maximum acceleration. Variation of these parameters will lead to a sensitivity analysis that indicates how power output changes with each variable. Following experimental testing, the power output and physical parameters of the harvester (resonant frequency, damping, impedance, etc.) can be compared to the predicted values from the numerical model. Adjustments can be made to account for discrepancies (e.g., adding an efficiency or loss term to account for power differences) and a new prototype may be constructed using the revised parameters.

Development of the concept in Fig. 9.1 would require both an accurate numerical model and, most likely, a scale model prototype. Installing the piezoelectric harvesters with the bearings in the bridge support would likely require jacking or otherwise supporting the bridge structure (bearings are replaced in bridges periodically in this manner, and the harvesters could be installed then). Thus, an accurate idea of harvester behavior and power density would be essential before such large-scale implementation. Involvement of civil engineers is highly recommended in the development of an accurate model of the bridge and its support system. Care must be taken that forces are transmitted through the bearings and piezoelectric layers in a manner that sufficiently strains the piezoelectric material without fracturing it, as it would essentially become part of the support system. Scale prototyping and testing would also require careful planning. Dimensional analysis would help identify how various parameters such as bridge mass,

piezo size, and vibration signal can be properly scaled to yield results convertible to predictions of real-world behavior. Analysis of this scale prototype would necessitate higher accuracy of measurement than was available for testing the current prototype, due to the need to correctly scale the results. If there is a general agreement between testing of the scale prototype and the numerical model, then a second scale or full-size prototype may be pursued.

A similar approach may be used in developing hybrid wind/piezoelectric harvesters. As described previously, the prototypes built so far by graduate students and cadets have relied on the same action of striking a bimorph and allowing it to vibrate freely at its own resonant frequency. Alternative configurations may also be possible that transmit energy to the piezoelectric material continuously and in a high-impedance (high-force, low-velocity) manner. One possible concept is shown in Fig. 9.3. This concept includes a horizontal-axis wind turbine that is positioned facing the wind. At high wind speed, the turbine turns a shaft connected to an inductive generator. At wind speeds too low to turn the turbine, the blades and the plate supporting the shaft are still buffeted by the wind, compressing the thin piezoelectric supports connected to a fixed base. The resulting loading on the piezoelectric material would be low velocity and high force, due to the thin geometry of the piezoelectric supports and the large surface area buffeted by the wind. This and other similar concepts would offer alternative methods for capturing energy at low wind speed.

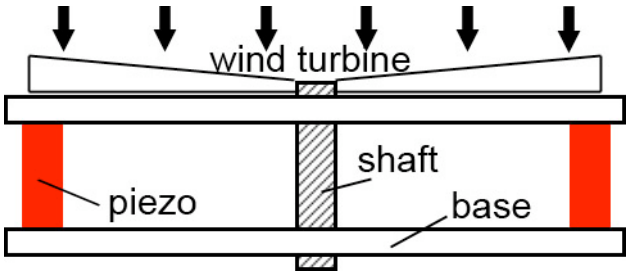

Figure 9.3 Concept for piezo-assisted wind harvester (top view)

In the development of these and other piezoelectric harvesting concepts, improved predictive modeling would help assess feasibility and limitations before experimentation begins. In all but the simplest cases, closed-formed solutions may prove inadequate to accurately predict system behavior and power generation. However, as the systems are usually composed of discrete parts of homogenous material (steel, aluminum, PZT, etc.), simple finite element analysis would accurately model both the mechanical behavior under various loading conditions and the resulting power output and electrical properties. These analyses would allow more thorough understanding of the systems' performance characteristics before physical prototyping begins. However, some prototyping would still be necessary to identify parameters and mechanical interactions that may have escaped the model. In particular, mechanical damping is particularly difficult to model without some initial physical prototyping.

9.5 Conclusions

Energy harvesting is a field that shows great promise in replacing or supplementing grid power and disposable batteries for many applications. With the urgent need to maintain and monitor the aging highway infrastructure, the development of energy-harvesting-powered wireless sensor networks for automated structural health monitoring would have widespread marketability and would make maintenance of

highway bridges much more cost effective, flexible, and safe. The technology from this venture would also have varied applications in many other fields.

Careful analysis of the power requirements and available power densities relevant to this application has shown that powering wireless sensors on a bridge is indeed feasible using solar radiation, wind, or vibration from the surroundings. Cost analysis revealed that disposable batteries are still perhaps the most attractive option for end nodes with expected operation between replacement of under five years, but that they are not suited for prolonged operation of a complete system with routers and central gateways, nor do they meet the desired lifespan of ten years. Here, energy harvesting can make a significant contribution to the advancement of long-term structural health monitoring.

The design of energy harvesting technology is almost always deeply rooted in its specific application and environment. Because of this, a thorough characterization of the energy available and the design constraints is necessary; a "one-size-fits-all" approach will not typically suffice. System-level design of the energy harvesting and wireless sensing components together will yield greatly improved design, where each is optimized to meet only the needs of the specific application and the other sub-systems.

Finally, it must be emphasized that a suite-based approach to energy harvesting is the most likely to yield widespread success. Even within the single application of structural health monitoring on bridges, environmental conditions change drastically from location to location. The availability of multiple interchangeable or even hybrid energy harvesters will ensure that a viable option is available to the consumer for every situation.

Appendix A: Functional Common Basis

Primary Flow Class: Energy	**Power Conjugate Complements**	
Secondary *Tertiary*	*Effort Analogy*	*Flow Analogy*
Human	Force	Velocity
Acoustic	Pressure	Particle velocity
Biological	Pressure	Volumetric flow
Chemical	Affinity	Reaction rate
Electrical	Electromotive force	Current
Electromagnetic Optical, Solar	Intensity	Velocity
Hydraulic	Pressure	Volumetric flow
Magnetic	Magnetomotive force	Magnetic flux rate
Mechanical		
Rotational	Torque	Angular velocity
Translational	Force	Linear velocity
Vibrational	Amplitude	Frequency
Pneumatic	Pressure	Mass flow
Radioactive	Intensity	Decay rate
Thermal	Temperature	Heat flow
Primary Flow Class: Material		
Secondary	*Tertiary*	*Correspondents*
Human		Hand, foot, head
Gas		Homogeneous
Liquid		Incompressible, compressible, homogeneous
Solid	Object, particulate, composite	Rigid-body, elastic-body, widget
Plasma		
Mixture	Gas-gas, liquid-liquid, solid-solid, solid-liquid, solid-gas, liquid-gas, solid-liquid-gas, colloidal	Aggregate, aerosol
Primary Flow Class: Signal		
Secondary	*Tertiary*	*Correspondents*
Status	Auditory	Tone, Verbal
	Olfactory	
	Tactile	Temperature, pressure, roughness
	Taste	
	Visual	Position, displacement
Control	Analog	Oscillatory
	Digital	Binary

Class (Primary)	Secondary	Tertiary	Correspondents
Branch	Separate		Isolate, sever, disjoin
		Divide	Detach, isolate, release, sort, split, disconnect, subtract
		Extract	Refine, filter, purify, percolate, strain, clear
		Remove	Cut, drill, lathe, polish, sand
	Distribute		Diffuse, dispel, disperse, dissipate, diverge, scatter
Channel	Import		Form entrance, allow, input, capture
	Export		Dispose, eject, emit, empty, remove, destroy, eliminate
	Transfer		Carry, deliver
		Transport	Advance, lift, move
		Transmit	Conduct, convey
	Guide		Direct, shift, steer, straighten, switch
		Translate	Move, relocate
		Rotate	Spin, turn
		Allow DOF	Constrain, unfasten, unlock
Connect	Couple		Associate, connect
		Join	Assemble, fasten
		Link	Attach
	Mix		Add, blend, coalesce, combine, pack
Control magnitude	Actuate		Enable, initiate, start, turn-on
	Regulate		Control, equalize, limit, maintain
		Increase	Allow, open
		Decrease	Close, delay, interrupt
	Change		Adjust, modulate, clear, demodulate, invert, normalize, rectify, reset, scale, vary, modify
		Increment	Amplify, enhance, magnify, multiply
		Decrement	Attenuate, dampen, reduce
		Shape	Compact, compress, crush, pierce, deform, form
		Condition	Prepare, adapt, treat
	Stop		End, halt, pause, interrupt, restrain
		Prevent	Disable, turn-off
		Inhibit	Shield, insulate, protect, resist
Convert	Convert		Condense, create, decode, differentiate, digitize, encode, evaporate, generate, integrate, liquefy, solidify, transform
Provision	Store		Accumulate
		Contain	Capture, enclose
		Collect	Absorb, consume, fill, reserve
	Supply		Provide, replenish, retrieve
Signal	Sense		Feel, determine
		Detect	Discern, perceive, recognize
		Measure	Identify, locate
	Indicate		Announce, show, denote, record, register
		Track	Mark, time
		Display	Emit, expose, select
	Process		Compare, calculate, check
Support	Stabilize		Steady
	Secure		Constrain, hold, place, fix
	Position		Align, locate, orient

Appendix B: Estimated Power Consumption of NI WSN-3202 Wireless Sensor Node

Average Power (mW)			
Duty Cycle	*Always on*	*Deep sleep*	*Shut down*
Router mode	207	207	207
100 Hz sampling, hourly transmission	73.4	73.4	73.4
30 Hz sampling, hourly transmission	60.7	60.7	60.7
1 sample/second	10.9	10.7	10.7
1 sample /minute	0.5	0.2	0.2
1 sample /hour	0.3	0.007	0.003
1 sample /day	0.3	0.009	0.0001
1 sample /month	0.3	0.009	0.000004

Yearly Energy Usage (J / year)			
Duty Cycle	*Always on*	*Deep sleep*	*Shut down*
Router mode	6,527,952	6,527,952	6,527,952
100 Hz for 10 weeks, daily for 42 weeks	451,570	444,229	444,000
100 Hz for 2 weeks, daily for 50 weeks	97,883	89,149	88,876
30 Hz for 10 weeks, daily for 42 weeks	374,760	367,419	367,190
30 Hz for 2 weeks, daily for 50 weeks	82,521	73,787	73,514
1 sample/second	343,742	337,435	337,435
1 sample /minute	15,768	6,307	6,307
1 sample /hour	9,460	221	95
1 sample /day	9,460	284	3
1 sample /month	9,460	284	0.1

Appendix C: Product-Product Matrix

Appendix D: Function-Function Matrix

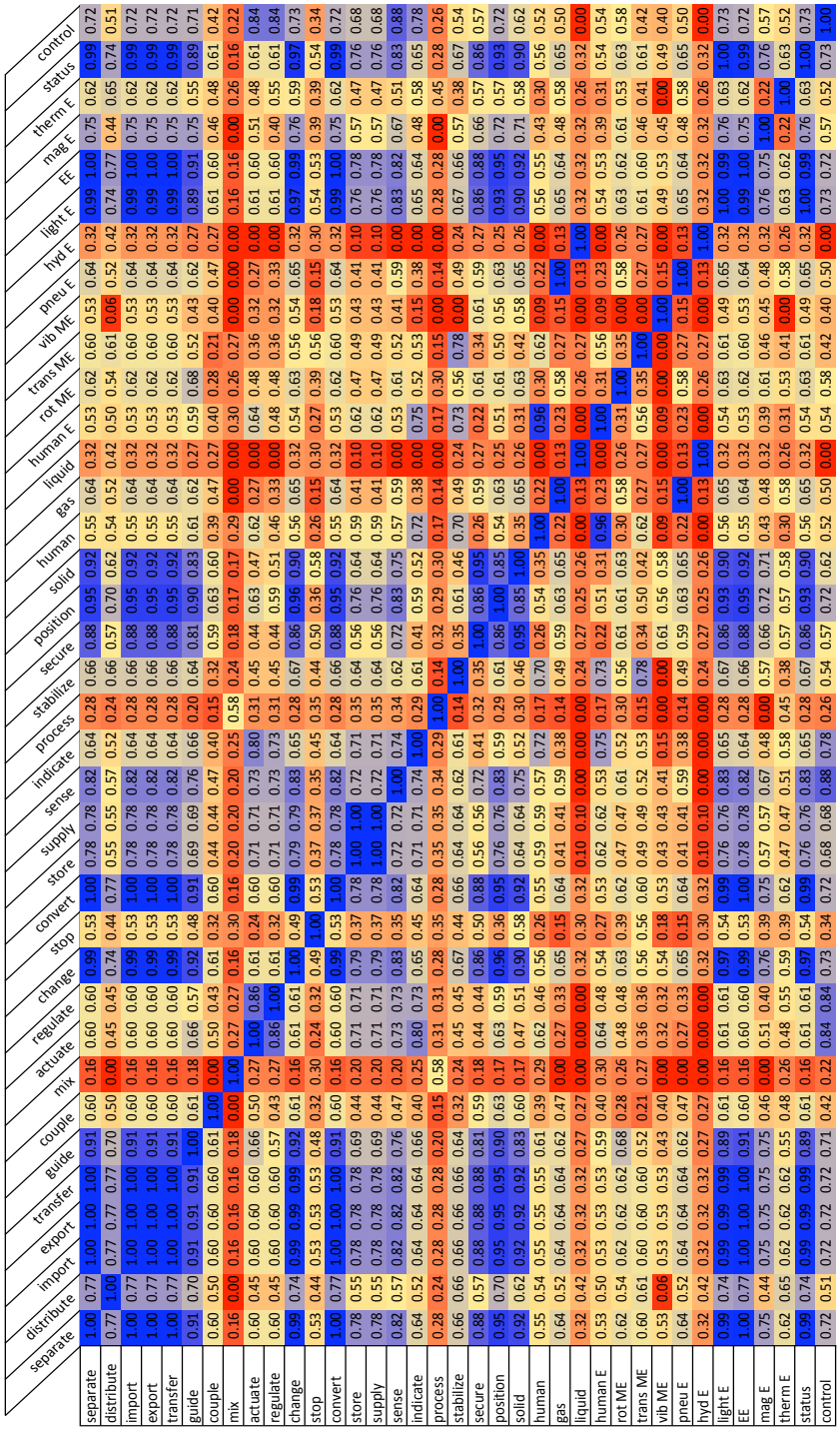

Appendix E: Functional Models

Enviro-Energies Wind Turbine

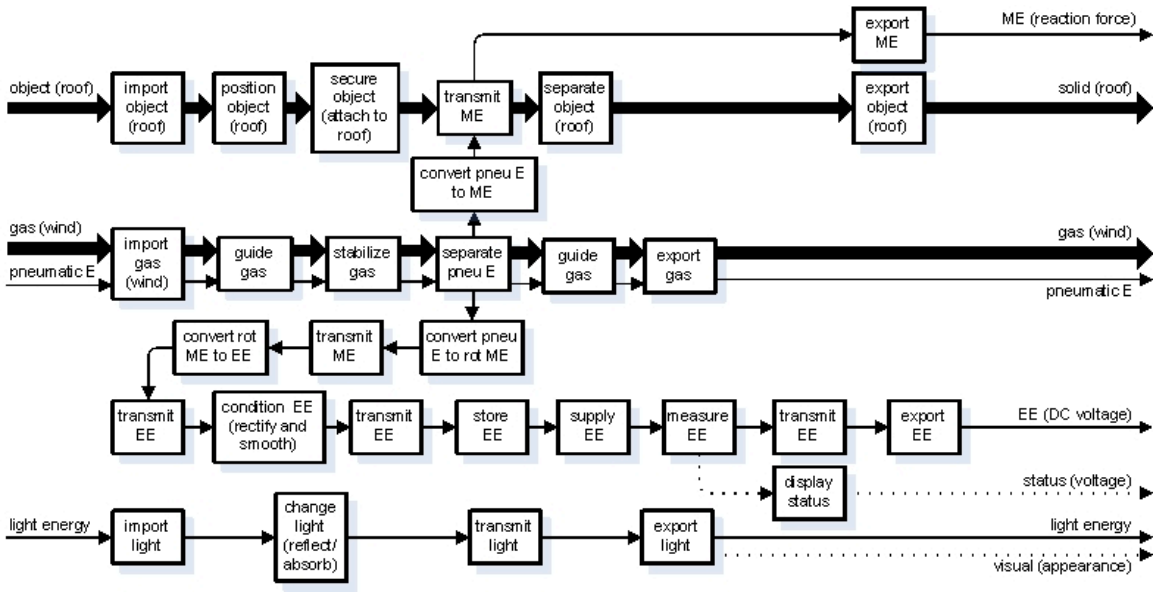

Piezoelectric Shoe-Heel-Impact Harvester

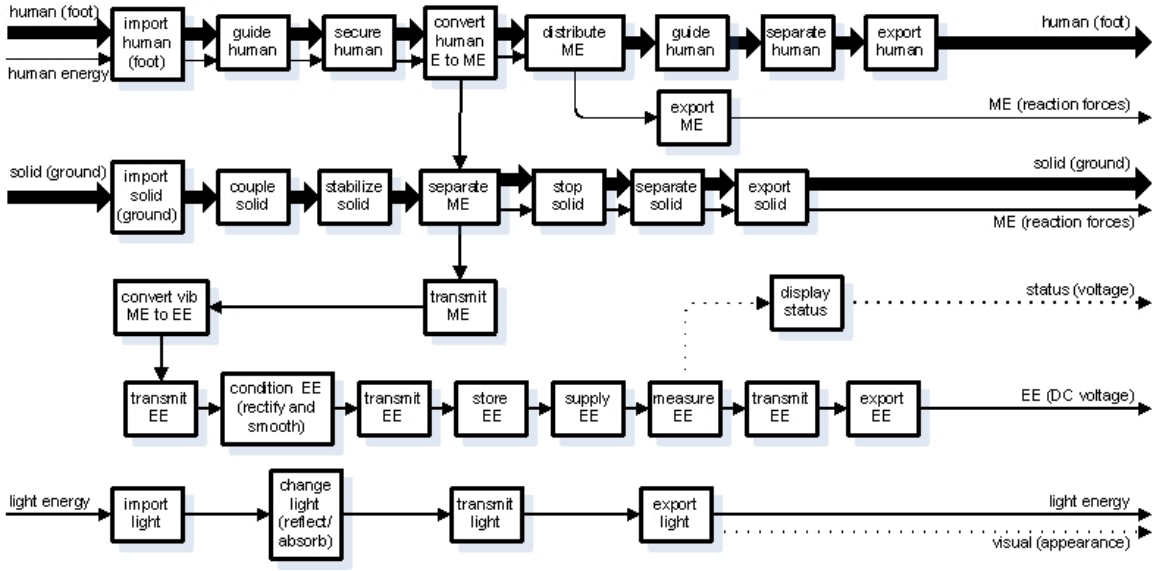

Seiko Kinetic Watch

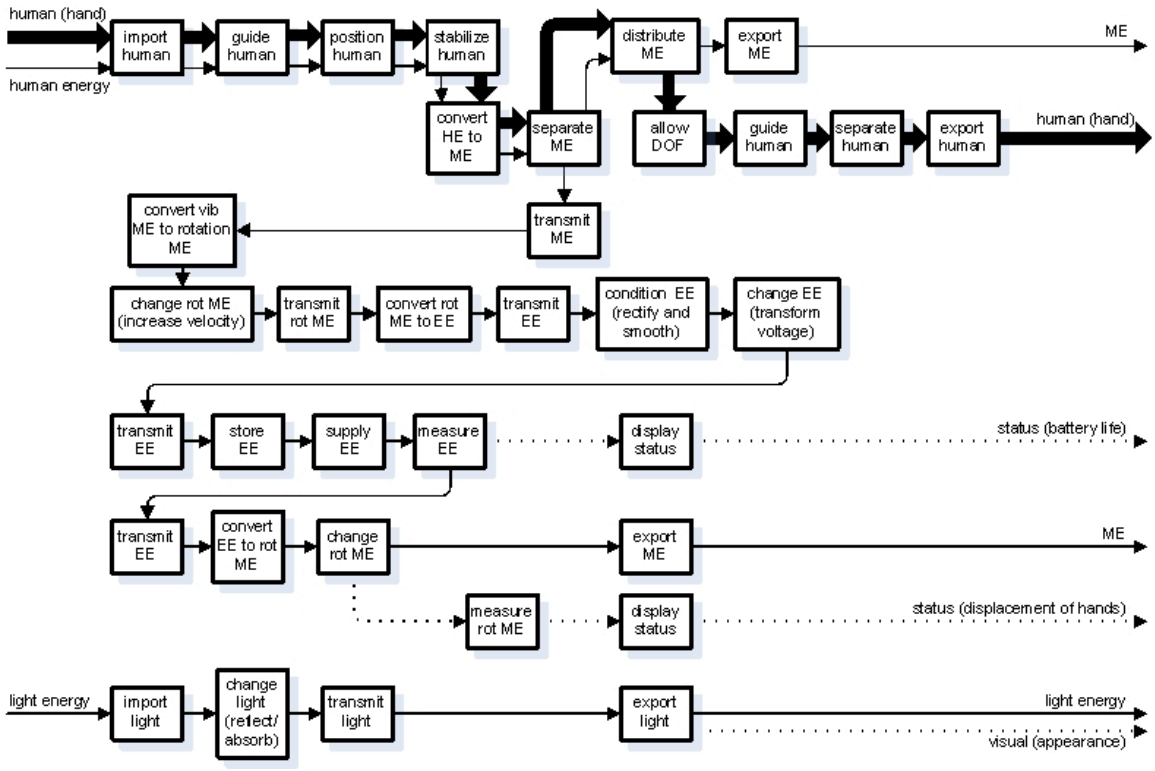

Appendix F: Design Specification Sheet

Demand or Wish	Specification	
Functional Requirements		
D	Generate long-term energy level of	> 104 Wh/year (375 kJ/year)
D	Provide power level continuously for 2 weeks of	> 61 mW
W	Provide continuous power for router of	> 207 mW (1.8 kWh/year, 6.5 MJ/year)
W	Provide continuous power to gateway like CompactRio	> 10 W (88 kWh/year, 315 MJ/year)
D	Store enough energy to go two weeks with no harvesting input	> 20 Wh (75 kJ)
D	Provide DC voltage	6 V DC, constant
D	Provide DC current	200 mA, max pulse
W	Communicate to central node	*lack of power, *malfunction
Constraints		
Geometry		
D	Dimensions: Volume	< 1 ft3
D	Dimensions: Area of largest surface	< 4 ft2
W	Width of any module sitting on bottom flange of I-beam	< 5 inches
D	Clearance of bottom of system above bottom of bridge structure	> 0 inches
D	Maximum length of wiring connecting system modules	< 10 ft / node
Forces		
D	Force needed to detach from bridge	> 100 lb
D	Torque needed to detach from bridge	> 200 ft-lb
D	Protected from forces, impact, and chewing by	ice, hail, gravel, debris, rats/mice and squirrels, birds and bats, bird nests, bird and bat excrement
Material		
D	Resistant to humidity and moisture for	> 10 years
D	Resistant to damage from temperatures	-20° F - 120° F
D	Resistant to corrosion from moisture and acidic substances (bird excrement, pollution) for	> 10 years
D	Resistant to deterioration from UV rays for	> 10 years
Signals		
W	EM interference with WSN and other systems from energy harvester	none
Safety		
D	Will not detach from bridge	(see "Forces")
D	Does not interfere with clearance of traffic	(see "Geometry")
W	Number of parts on driving surface of road	0
W	Vandalism/Theft-resistant: tools to access or remove from bridge	ladder or man-lift
Ergonomics		
D	Weight of complete system	< 20 lb
W	Time to install system	< 1.5 hours
D	Skill level to install	general technician or less
Assembly		
W	Number of permanent changes to bridge such as welds and drilled holes (drilling into concrete is acceptable if needed)	0
D	Number of drilled holes to steel structure	0
D	Locations system can be installed on bridge	*space between steel I-beam girders, *interior and/or exterior of hollow steel box girders
W	Location system can be installed	Any steel surface, above or below deck, on exterior or interior (e.g. trusses)
Operation		
D	Service life	> 10 - 15 years
Maintenance		
W	Maintenance interval	> 10 years
D	Maintenance interval	> 5 years
Costs		
W	Manufacture cost	< $200
D	Manufacture cost	< $600

Appendix G: Energy Morph Matrix (Putnam, 2008)

Energy Morph Matrix

STORAGE MEDIA	TRANSMISSION CHANNELS	CONVERTERS from	to
Rotational Kinetic	Electromagnetic Radiation	Photovoltaic Panel	
Translational Kinetic	-Light	Rectenna Array	
Spring Potential	-Microwaves	Photosynthetic Organism	
Rotational Kinetic	Mechanical Coupling	Piezoelectric Generator	
Translational Kinetic	Solid Momentum/Force	Electric Motor Generator	
Compressed Fluid Potential	Fluid Momentum/Force	Turbine	
Battery	Conduction	Air Engine	
Ultracapacitor	Induction	LASER	
Liquid Phase	Moving Chemicals	Microwave Emitter	
-Fossil Fuel	Convection	Resistor	
-Alcohol	Conduction	Electric Motor	
Gas Phase	Radiation	Electrolysis	
-Propane		Piezoelectric Actuator	
-Hydrogen		Fuel Cell	
Solid Phase		Piston Engine	
-Hydrogen Metal Hydride		Jet Engine	
-Other Powder Fuel		Chemical Muscle	
Hot, Insulated Mass		Various Living Bacteria	
		Exothermic Reaction (general)	
		Endothermic Reaction (general)	
		Thermoelectric Generator	
		Shape-Memory Alloy	
		Stirling Engine	

THERMAL | FLUID MECH | SOLID MECH

CHEMICAL | ELECTRICAL | RADIANT

Appendix H: Concept Generation Results From ME 366-J

- Expansion joints have pistons with hydraulic fluid that is squeezed into small tube for higher velocity, activates turbine generator
- Passing cars attract magnets positioned on sides of lanes or on road surface, the magnets move through a coil as they travel.
- A bar magnet hanging freely from two wires sways back and forth through a coil from vibration (or wind)
- Use Peltier effect – the mass of the bridge will stay at constant temperature, while the surroundings (air) will vary, or use gradient between sun and shade
- Harness excess energy from cars as they go downhill at either end of the bridge
- Large plates hung at side of lanes are pushed outward against a spring from wind as car goes by
- Two buckets on a pulley are alternately filled with rain water, which turns the pulley as the relative weight changes
- Wind turbine with a magnet/coil inside that shifts back and forth from gravity as the turbine rotates
- Brushes contact passing cars to generate static electricity
- Use high voltage signs or shock warnings to prevent graffiti/vandalism
- Store rain water in tall vertical column to maximize hydrostatic head going into turbine under the bridge
- Use mirrors to reflect direct sunlight to solar panels under the bridge
- Use steam generator with solar heating
- Paint lane lines using photovoltaic paint
- Helical wind turbines aligned horizontally along sides of lanes
- Toll booth where cars “pay” in energy
- Alternate black and white paint on surface for Peltier effect

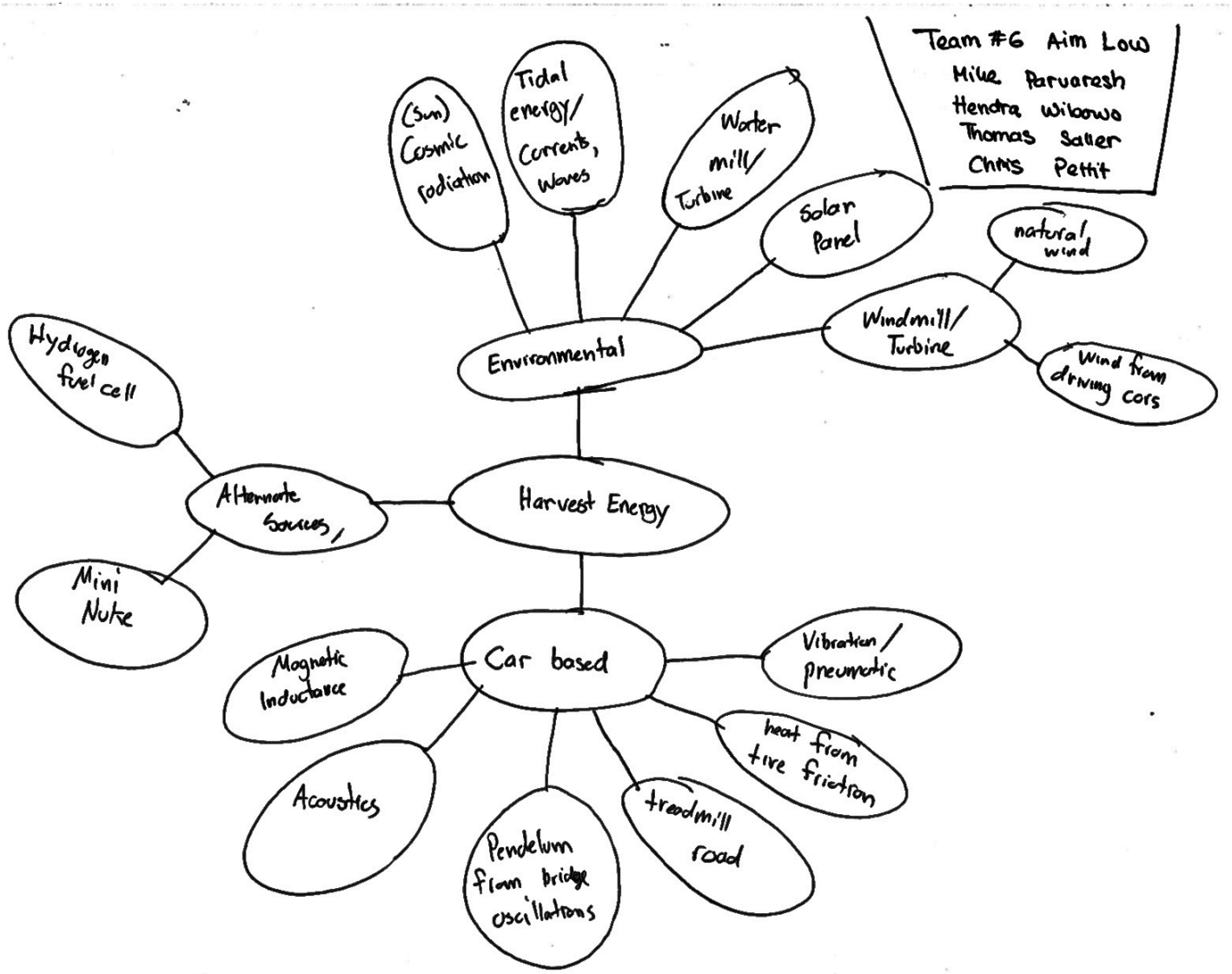
Team #6 Aim Low
Mike Paruaresh
Hendra Wibowo
Thomas Sailer
Chris Pettit
(Sun) Cosmic radiation
Tidal energy/ Currents, Waves
Water mill/ Turbine
Solar Panel
natural wind
Windmill/ Turbine
Wind from driving cars
Environmental
Hydrogen fuel cell
Alternate Sources,
Mini Nuke
Harvest Energy
Magnetic Inductance
Car based
Vibration/ Pneumatic
heat from tire friction
Acoustics
Pendelum from bridge oscillations
treadmill road

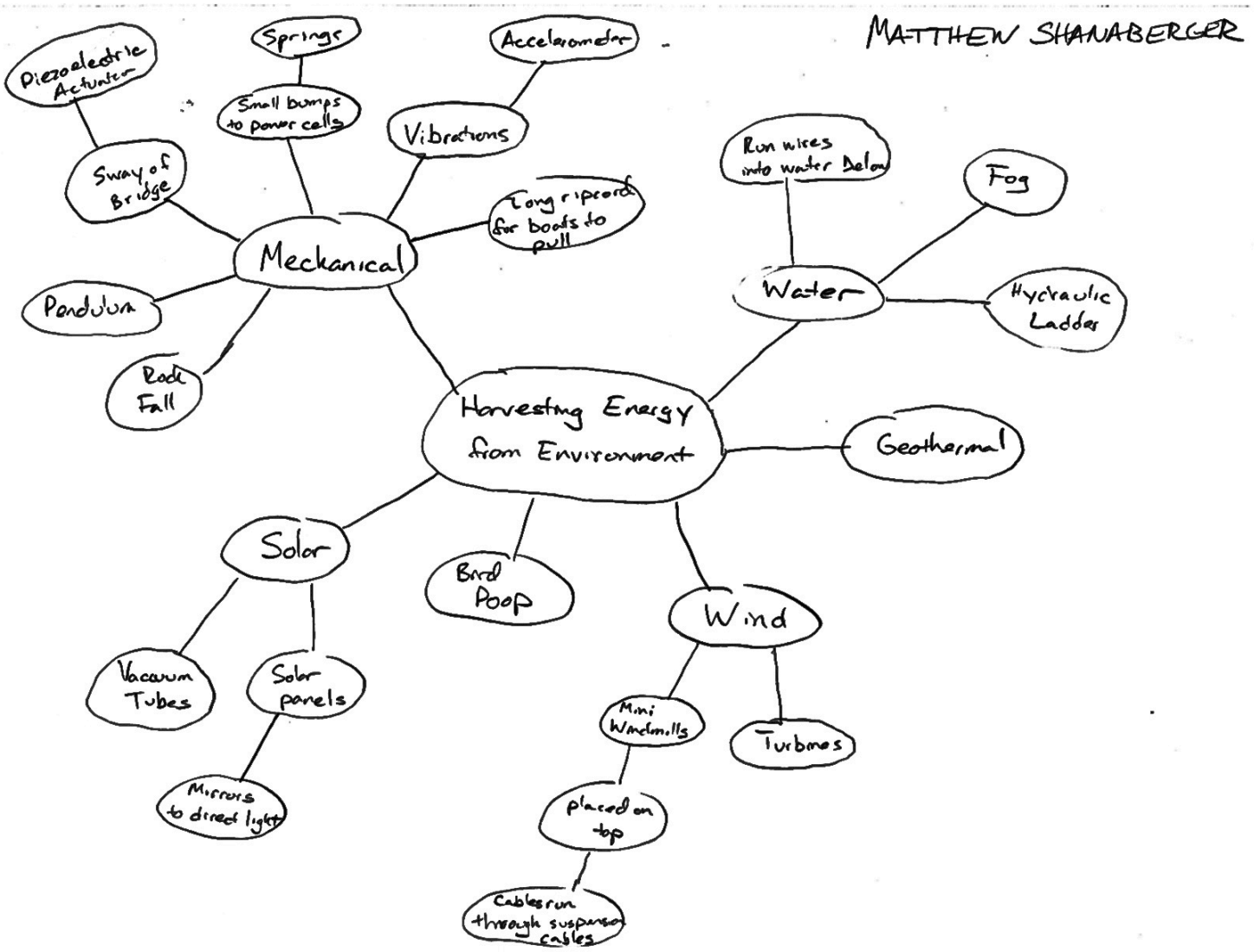
MATTHEW SHANABERGER
Harvesting Energy from Environment
Mechanical
Piezoelectric Actuator
Sway of Bridge
Springs
Small bumps to power cells
Accelerometer
Vibrations
Long riprod for boats to pull
Pendulum
Rock Fall
Water
Run wires into water below
Fog
Hydraulic Ladder
Geothermal
Solar
Vacuum Tubes
Solar panels
Mirrors to direct light
Bird Poop
Wind
Mini Windmills
placed on top
Cables run through suspension cables
Turbines

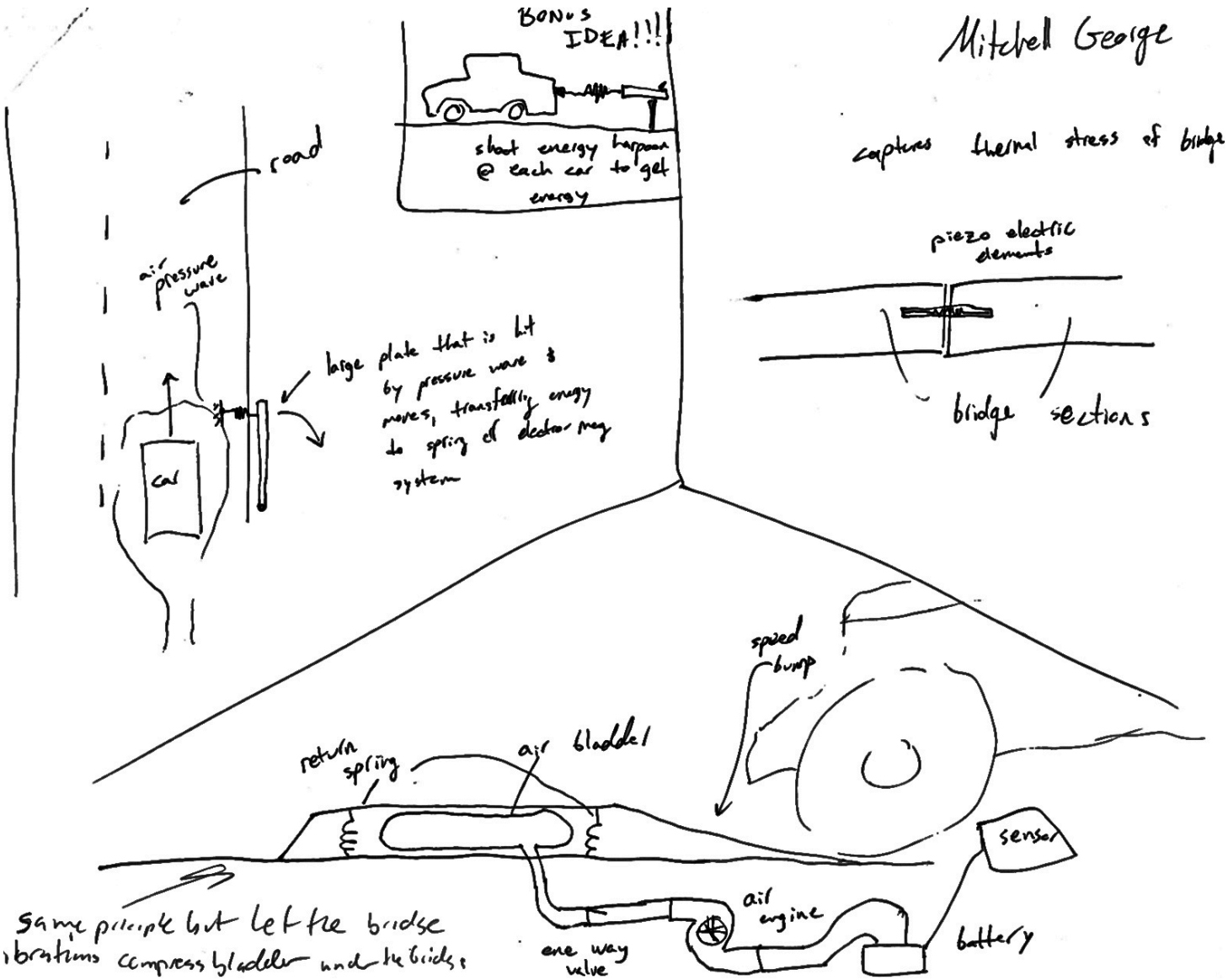
BONUS IDEA!!!
shoot energy harpoon @ each car to get energy
road
air pressure wave
large plate that is hit by pressure wave & moves, transfering energy to spring of electric regen system
car
Mitchell George
captures thermal stress of bridge
piezo electric elements
bridge sections
speed bump
return spring
air bladder
sensor
air engine
battery
one way valve
same principle but let the bridge vibrations compress bladder under the bridge

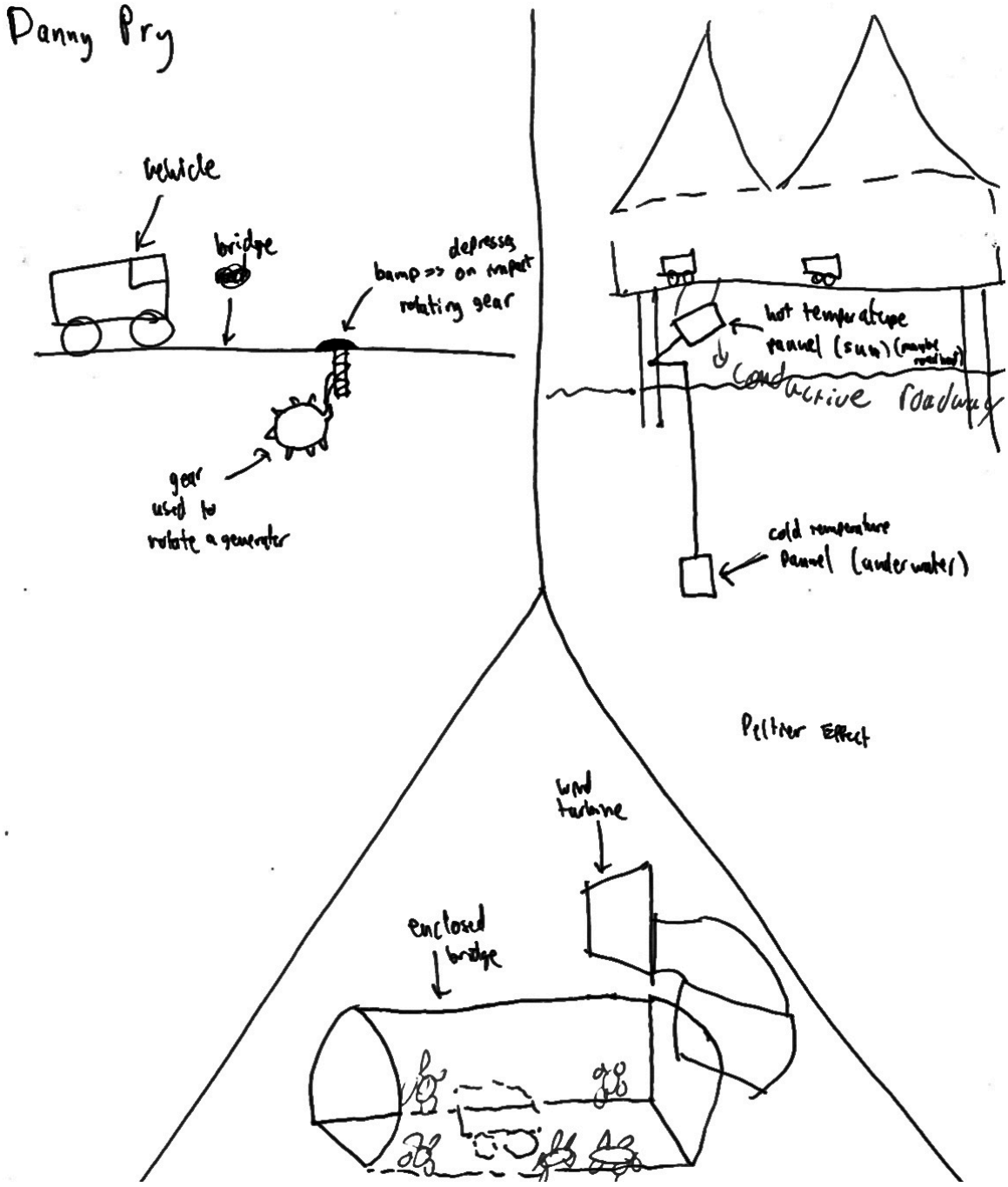
Danny Pry
vehicle
bridge
depress bump => on rotating gear
gear used to rotate a generator
hot temperature panel (sun)
conductive roadway
cold temperature Panel (underwater)
Peltier Effect
wind turbine
enclosed bridge

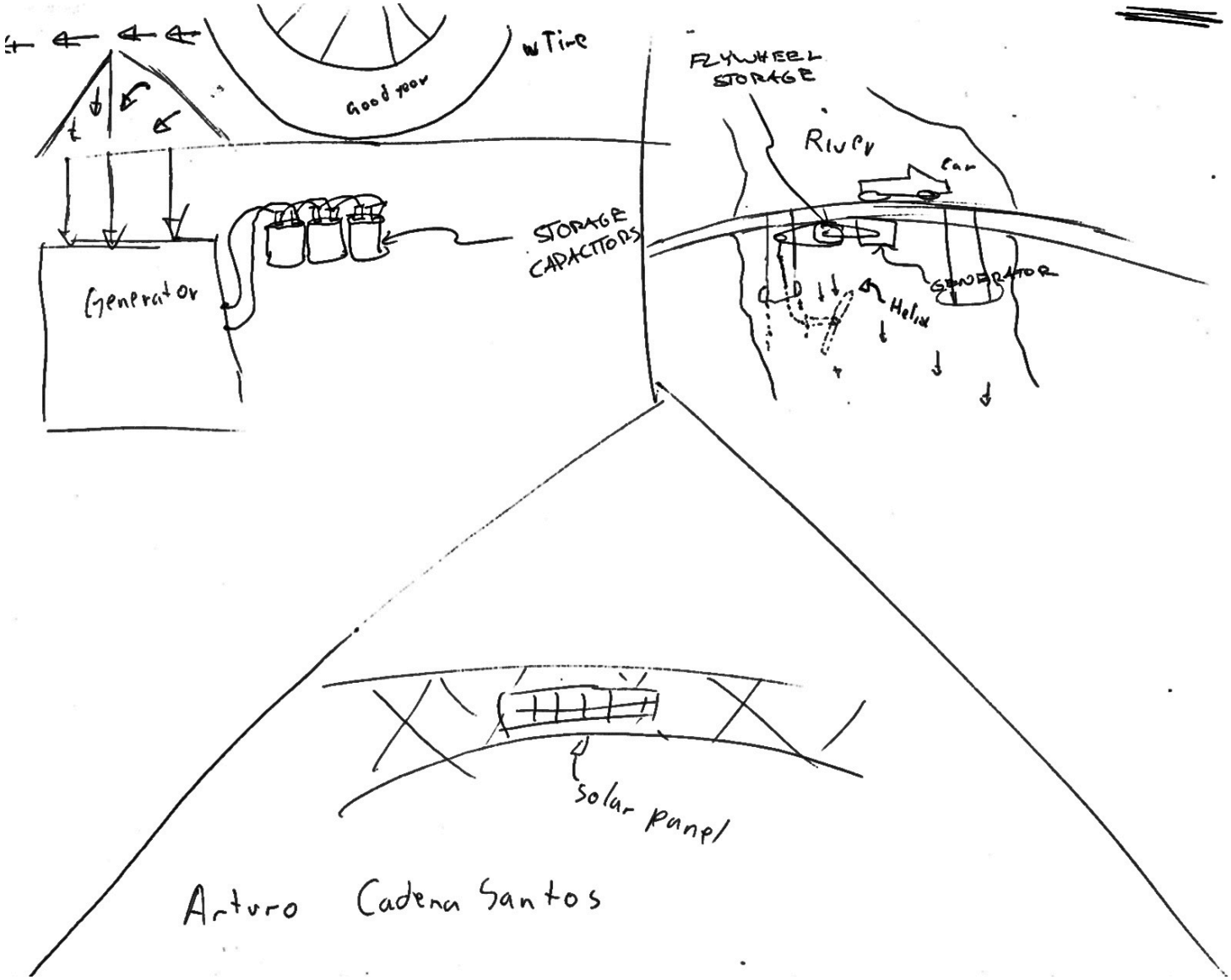
wTire
Good year
FLYWHEEL STORAGE
River
Car
STORAGE CAPACITORS
Generator
Helix
Solar panel
Arturo Cadena Santos

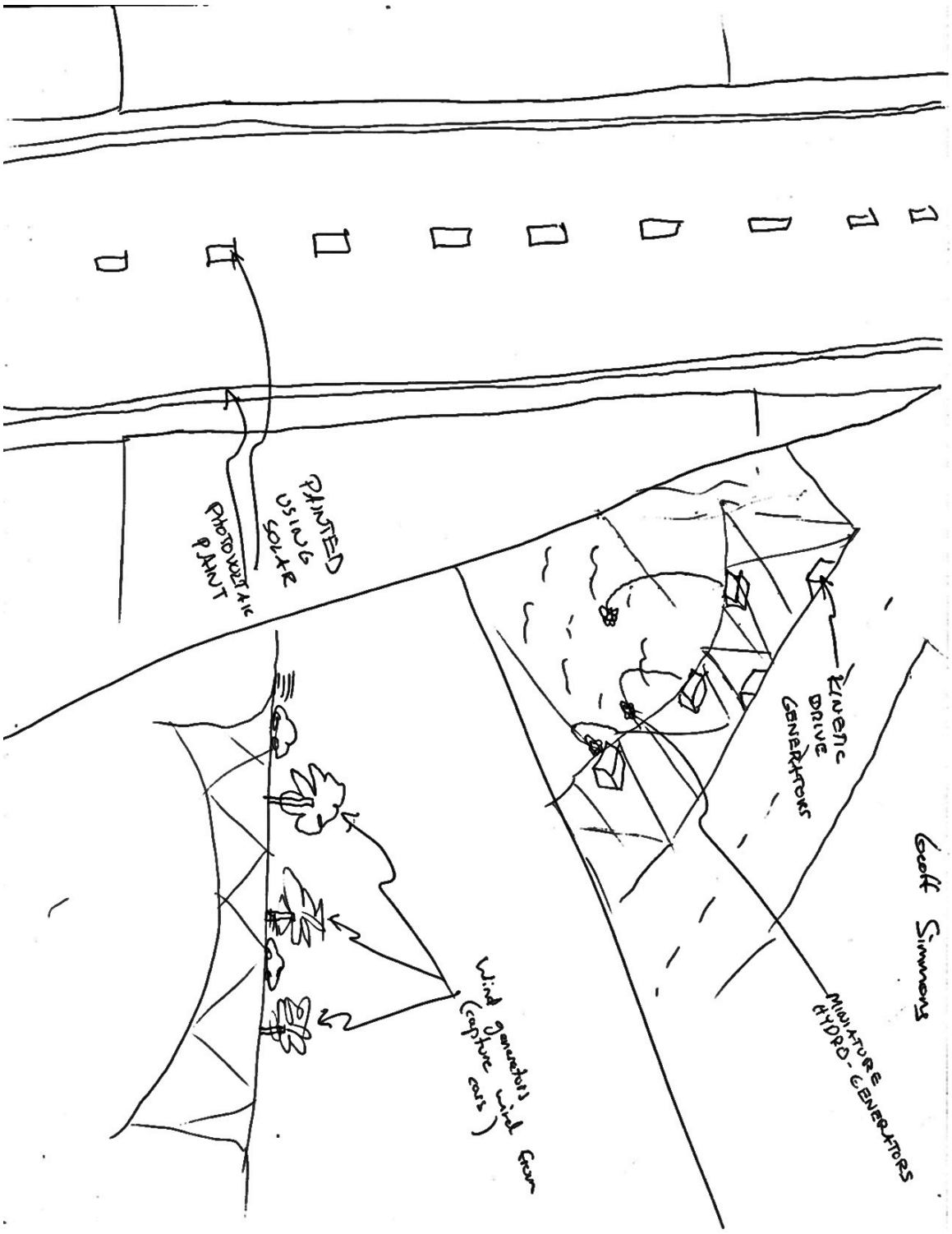
PAINTED USING SOLAR PHOTOVOLTAIC PAINT
KINETIC DRIVE GENERATORS
MINIATURE HYDRO-GENERATORS
Wind generators (capture cars)
Geoff Simmons

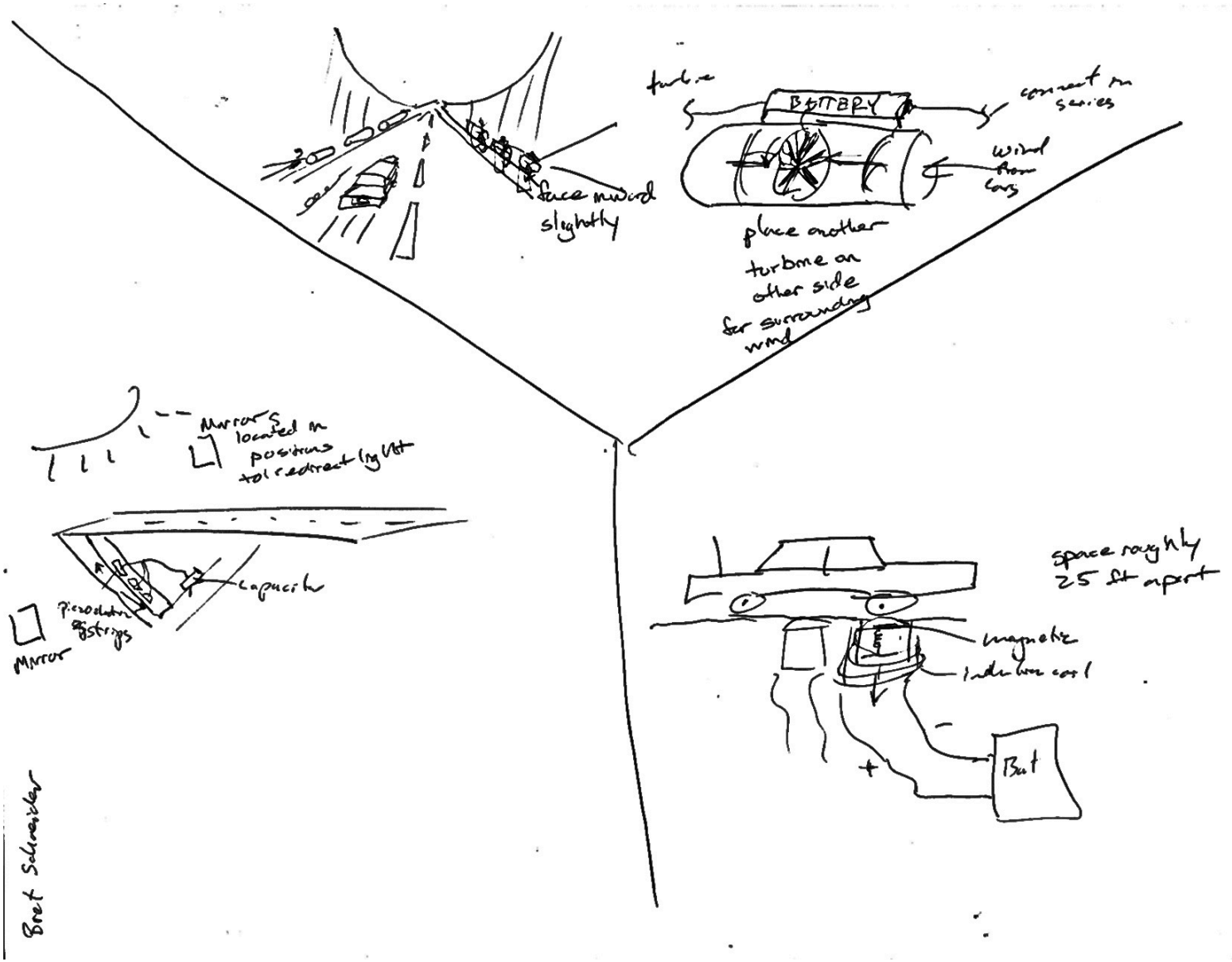
turbine
BATTERY
connect in series
Wind flow
Space inward slightly
place another turbine on other side for surrounding wind
Mirrors located in positions to redirect light
Capacitor
Piezoelectric strips
Mirror
space roughly 25 ft apart
magnetic
induction coil
Batt
Brent Schwenker

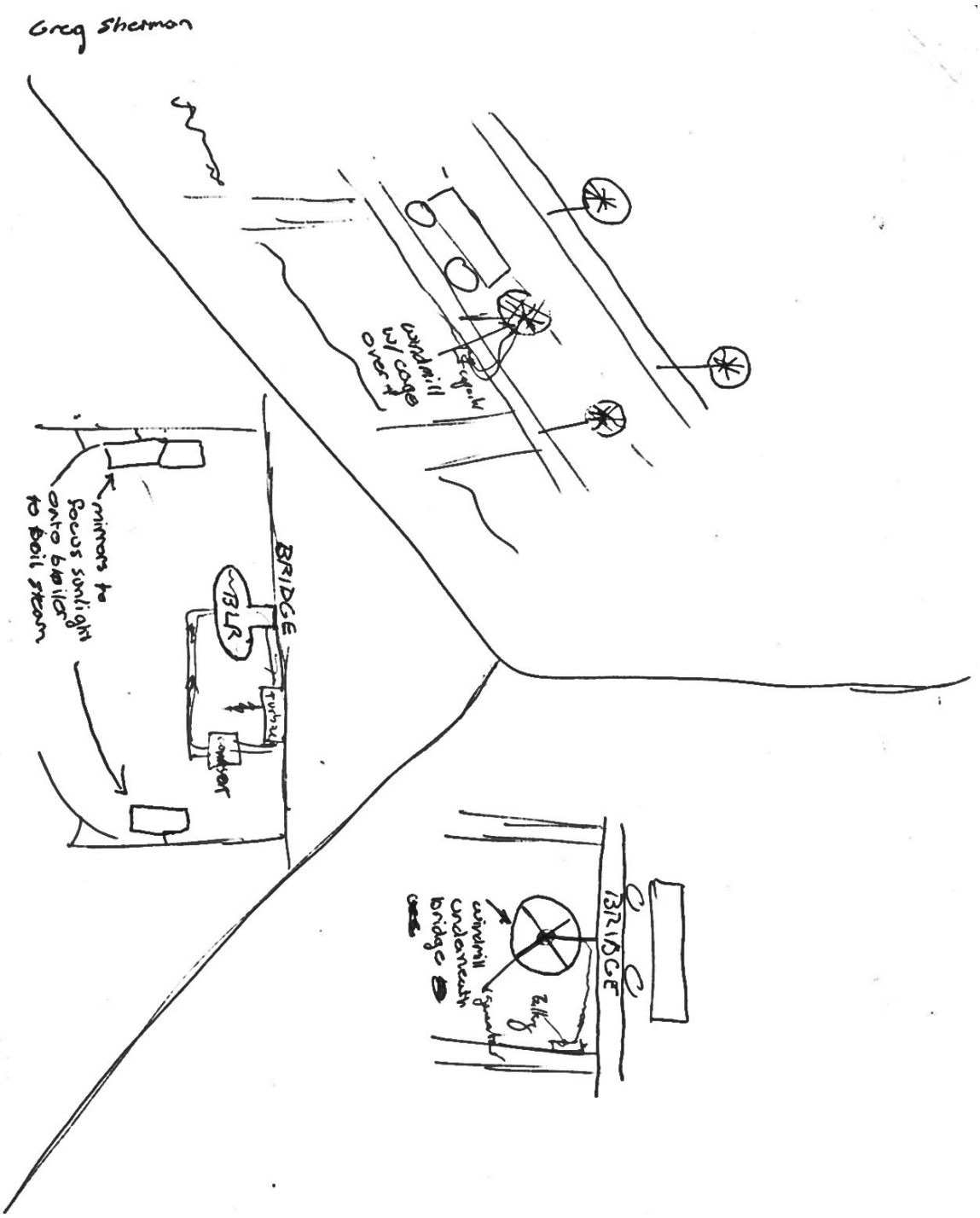
Greg Sherman
windmill w/ cage over it
mirrors to focus sunlight onto boiler to boil steam
BRIDGE
MBLR
BRIDGE
windmill underneath bridge

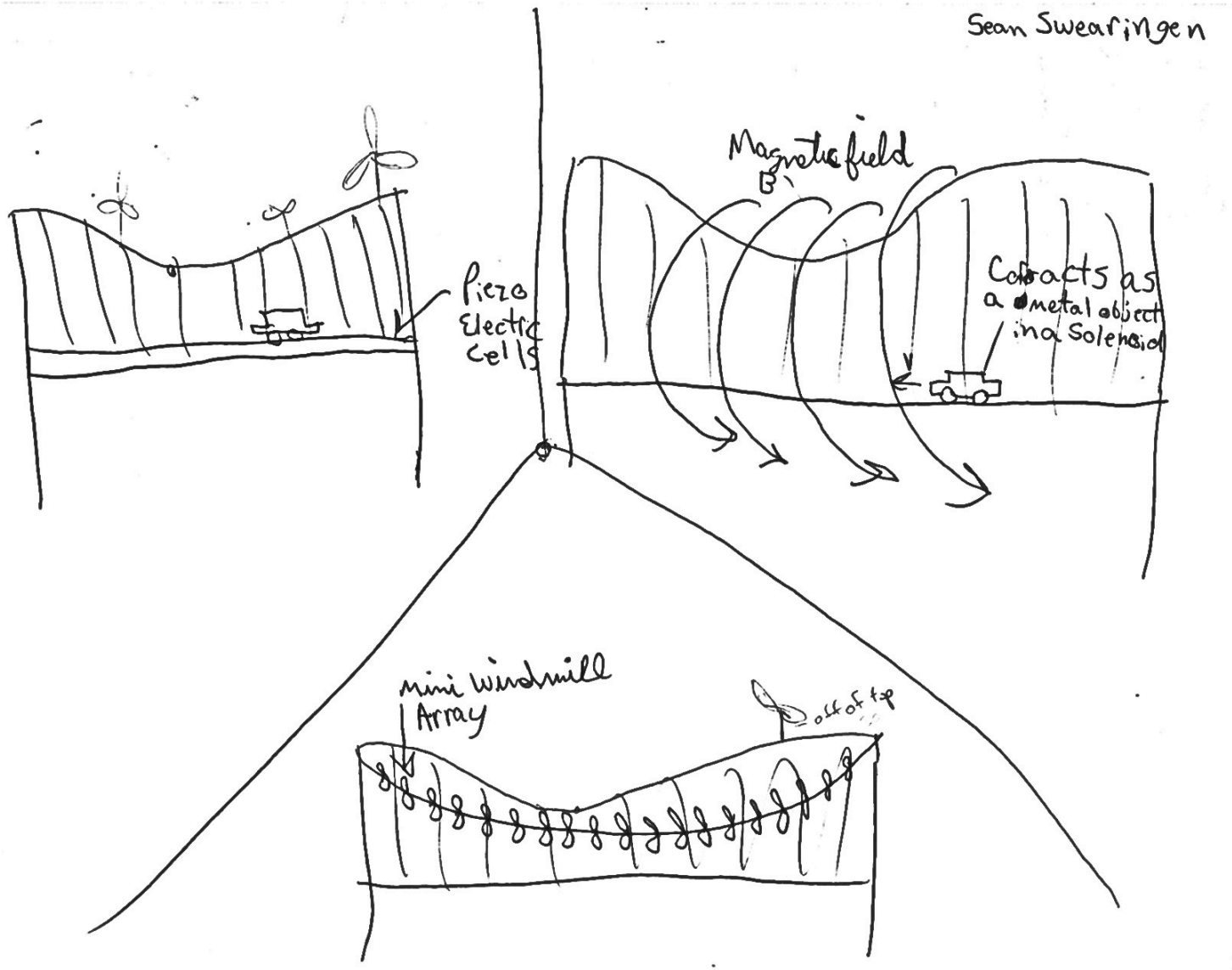
Sean Swearingen
Piezo Electric Cells
Magnetic field
B
Coil acts as a metal object in a Solenoid
mini windmill Array
off of top

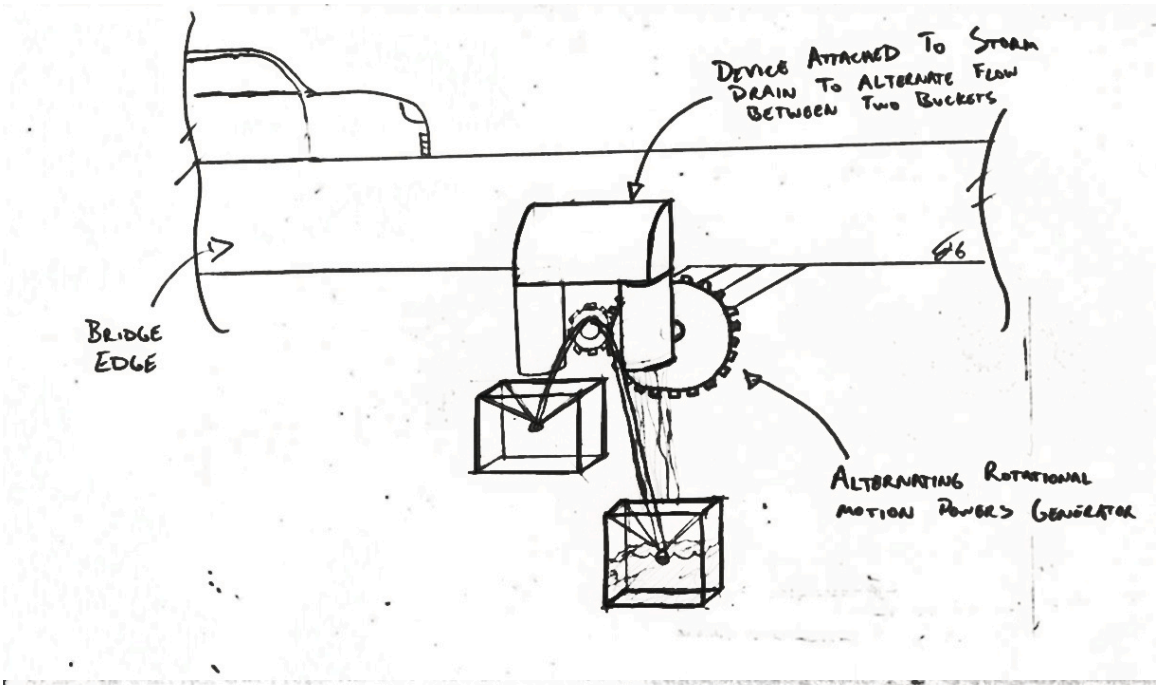
DEVICE ATTACHED TO STORM DRAIN TO ALTERNATE FLOW BETWEEN TWO BUCKETS
BRIDGE EDGE
ALTERNATING ROTATIONAL MOTION POWERS GENERATOR

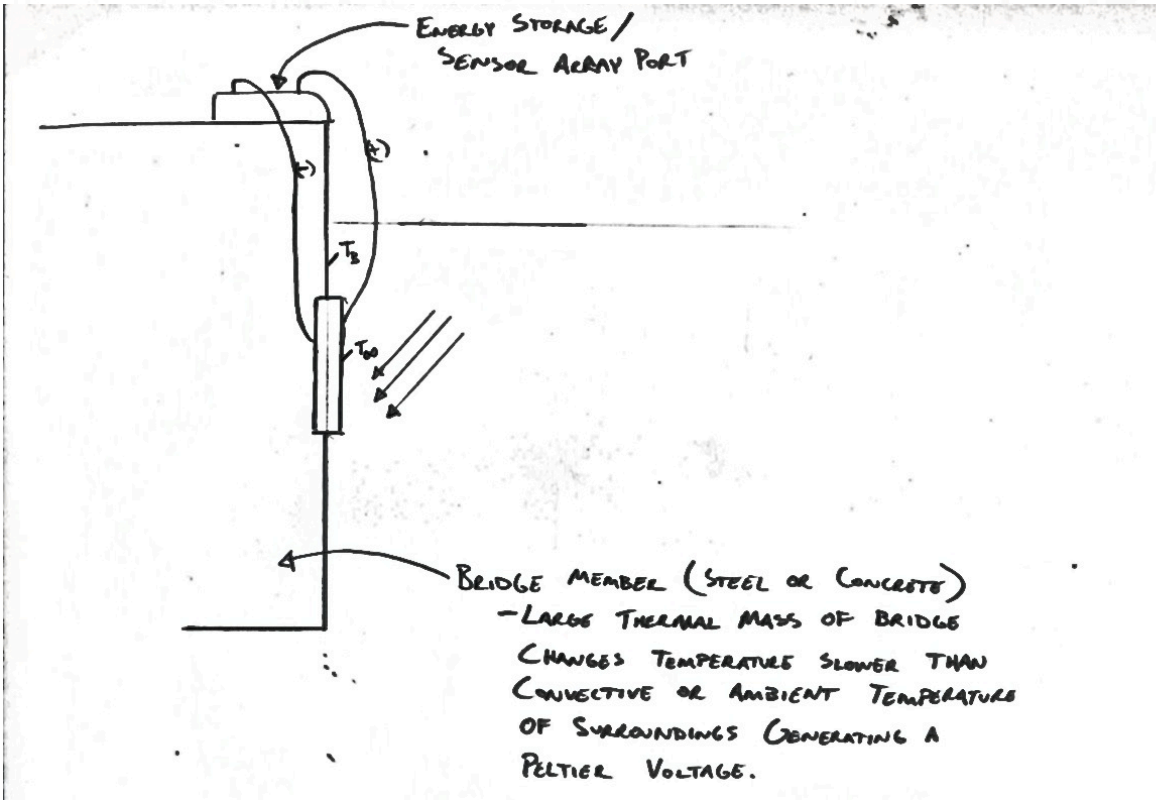
ENERGY STORAGE / SENSOR ARRAY PORT
T_s
T_∞
BRIDGE MEMBER (STEEL OR CONCRETE)
-LARGE THERMAL MASS OF BRIDGE CHANGES TEMPERATURE SLOWER THAN CONVECTIVE OR AMBIENT TEMPERATURE OF SURROUNDINGS GENERATING A PELTIER VOLTAGE.

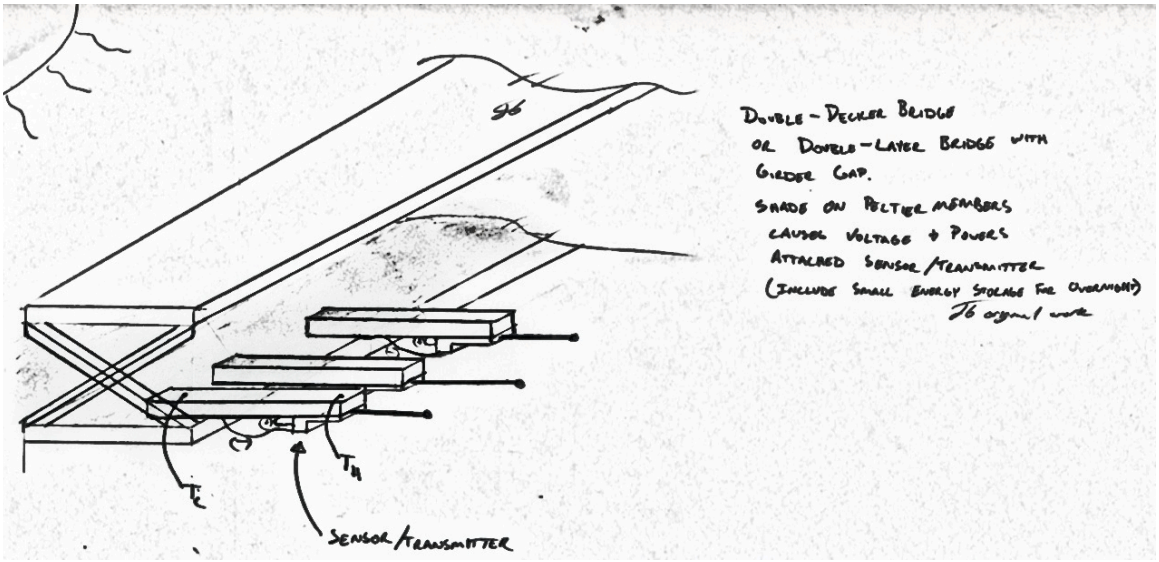

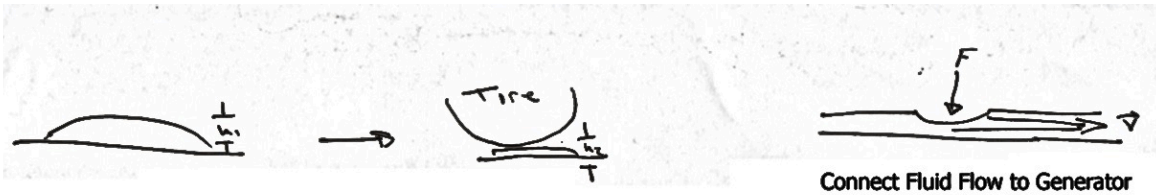

Connect Fluid Flow to Generator

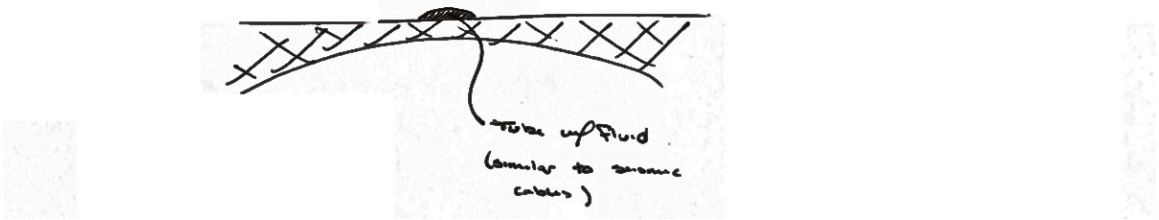

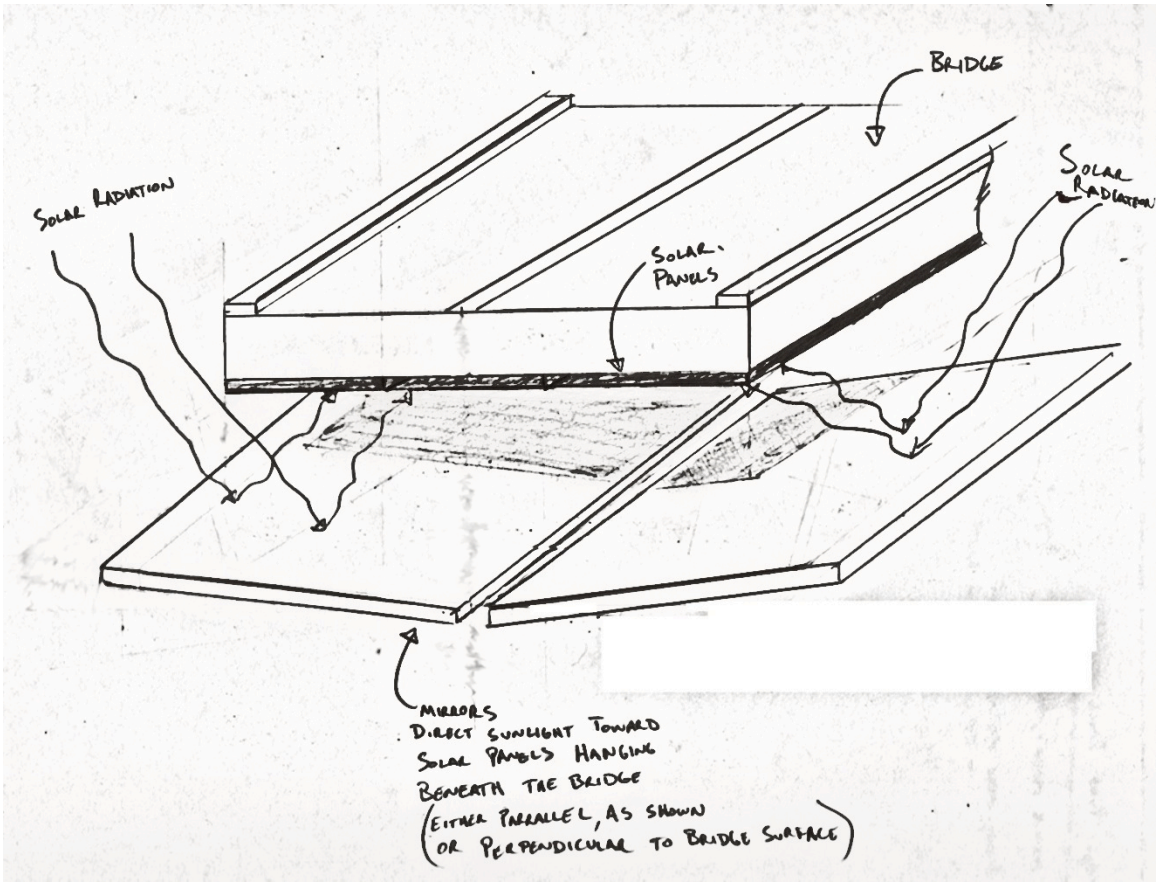
BRIDGE
SOLAR RADIATION
SOLAR PANELS
SOLAR RADIATION
MIRRORS
DIRECT SUNLIGHT TOWARD
SOLAR PANELS HANGING
BENEATH THE BRIDGE
(EITHER PARALLEL, AS SHOWN
OR PERPENDICULAR TO BRIDGE SURFACE)

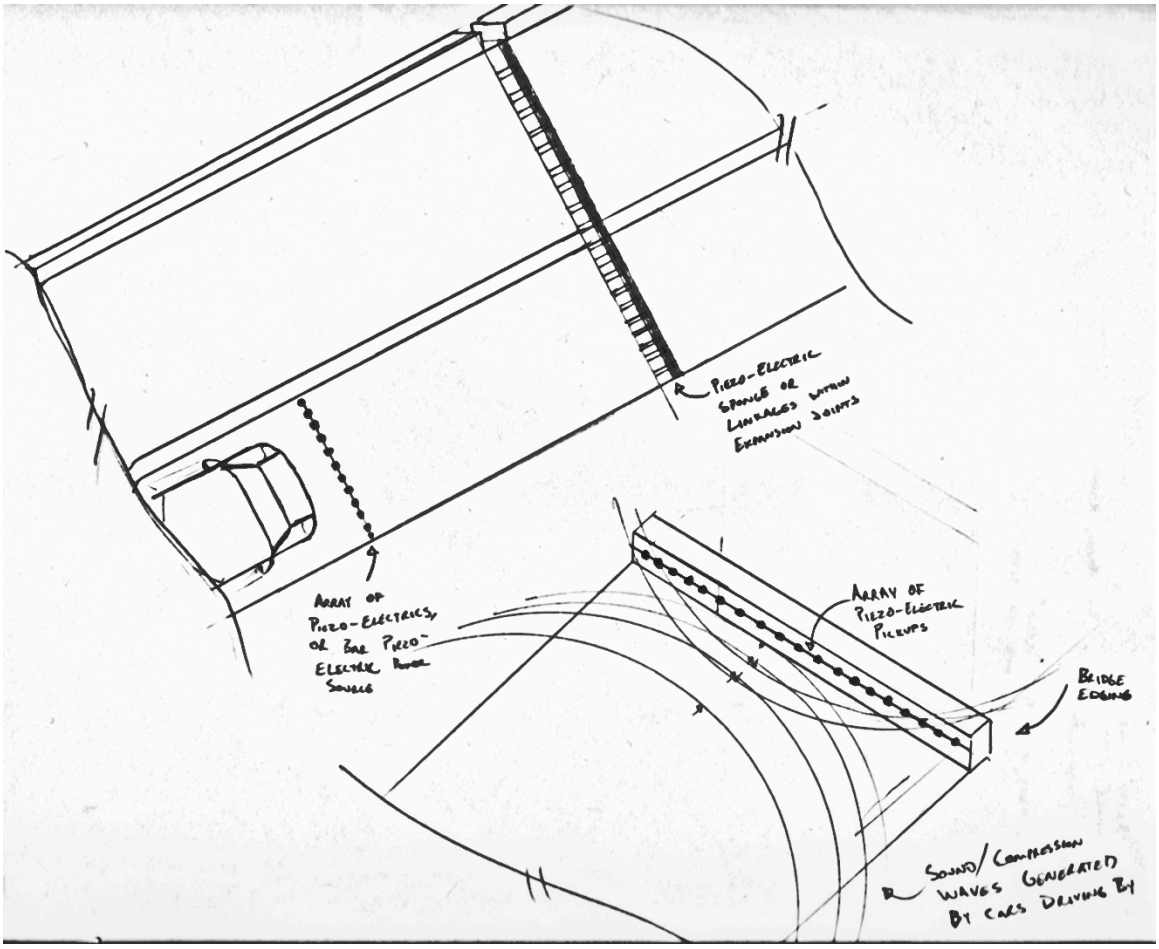
PIEZO-ELECTRIC SPONGE OR LINKAGES WITHIN EXPANSION JOINTS
ARRAY OF PIEZO-ELECTRICS, OR BAR PIEZO-ELECTRIC POWER SOURCE
ARRAY OF PIEZO-ELECTRIC PICKUPS
BRIDGE EDGING
SOUND/COMPRESSION WAVES GENERATED BY CARS DRIVING BY

Conclusions	
Avg # of solutions per function:	**20**
Function groups:	**6**
Function subgroups:	**28**
Total unique solutions:	**119**
Total sol'n with doubles:	**388**
Avg unique team count:	6.2
Avg doubles team count:	**20.4**

team	doubles	unique
	19	17
	18	26
	17	17
	16	21
	15	25
	14	15
	13	20
	12	14
	11	32
	10	18
	9	25
	8	35
	7	18
	6	19
	5	25
	4	23
	3	17
	2	17
	1	4
Avg Count	20.4210526	

Import _____ energy	**team**
using:	
Thermal	
peltier effect (top/bottom, submerged/exposed)	13,11,9,8,7,3
car friction on surface (tires)	19,14,5,2
geothermal sink	18
geo powered steam cycle	15,10
piezo in tension cable (expansion/contraction)	8
capture vehilcle heat	15,6,5,3
capture road heat	9
capture vehicle exhaust	10
Chemical	
local exothermal processes	14,8
Radiant	
solar panel	19, 18, 17,16,15,13,12,11,10,9,8,7,6,5,4,3,2
vacuum tube	16
p-v paint (under research)	15
thin film panel	18,7,5
solar heating	5
Fluid Mechanical	
Axial wind vanes (ambient, car, convection)	19,18,17,16,14,13,12,11,10,9,8,6,5,4,3,2,1
wind concentrators and vanes	15
Helical wind vanes	19,14,11
wave capture plates	19,9,8,4
bladder and pump under spring plate	18,11,8,7,2
tidal current turbine	15,11,10,8,3,2
rain collector	18,15,14,11,6,5
water turbines	15,10,7,6
hydrolic bouy/bilge pump	13,11,9,8,4
solar heated boiler	16
wind pendulum	10
capture ambient mist	15,8,1
Solid Mechanical	
mass-spring-plate	19, 17, 16,15,14,13,12,11,8,6,5,4,3
piezo cells under cars	18,17,12,11,5,4
vibration passing cars	19,10,9,8,2
vibration of bridge	10,8,6,5,4,3
piezo in tension cable (vibration)	18
cars on spring board and ratchet	18
piezo in expansion gaps	18,15,14,11,10,6
crank in expansion joint	9,6
piezo in bridge members	17, 16,13,11,7
cars on rack and pinion plate	10, 9
tires turn a wheel/treads	10,9,8,5,3,2
shape memory alloy (struck by wave, vibration)	8
spring in vacuum	5
acoustic/transducers	2
Electrical	
solenoid in bridge (magnets/induction from cars)	19,18,17,15,13,9,7,5,2
magnet solenoid pair - car actuated	8,4
lightning rod	18,13,11,7,4,3
piezo-electric	13,11
LVDT (in expansion joint)	7
static electricity collection	6,3
Biological	
algae	17,12,9,4
bacteria	14
photobioreactor	12,8
combust local materials	11,9
human	18,8,3
lemon trees/ potatoes grown on bridge	19
Other	
earthquake	8

Transform ____ energy to electrical energy	team	Transmit ____ energy	team
Thermal		**Thermal**	
conducting strip (peltier effect)	13,11,9,8,7,3	conducting strip	19
cars generate friction (peltier effect)	19	heat pump	4
recombust car exhaust	10,5,3	**Chemical**	
Chemical		**Radiant**	
burn trash from passing cars	11,9	**Fluid Mechanical**	
burn captured emissions	10	**Solid Mechanical**	
Radiant		crank	19,18,17,16,9,5
PV- panels	19, 18, 17,16,15,13,12,11,10,9,8,7,6,5,4,3,2	**Electrical**	
thin film coating	18		
vacuum tubes	16		
Fluid Mechanical			
water turbine	18,14,11,8,6,4		
wind turbine	16,15,8,6,5,1		
passive fluid-pump/bouy and piezo on rope	13,11,9,8,4		
micro hydroplant	18,15,11		
hydroelectric turbine	9		
water wheel	18,4,2		
ambient mist/steam turbine	15,8,1		
string of bucket turbine modules 'sea dragon'	2		
piston-airflow-turbine	14,13,6		
Solid Mechanical			
piezo-electric	18,17,16,15,14,13,12,11,10,7,6,4,2		
generator	19,18,17,16,15,14,13,12,5,4,2		
fluid bladder w/ turbine	18,11,8,7		
crank and generator	19,17, 16		
thermal expansion	18,15		
rack and pinion?	4,3		
ratchet and generator	18		
passing boats pull cord	19		
rocking solenoid/magnet	19		
Electrical			
solenoid in bridge	19,18,17,15,13		
magnet solenoid pair - bridge actuated	5		
magnet solenoid pair - car actuated	8,4		
Biological			
algae	17,12,9		
compost organic materials	11,9		
photo-bioreactor	12,8		
Other			
teleporter	12		
flying cars only	12		

Direct ____ Energy	team	Store _____ energy	team	Secure Harvester	team	Deploy harvester
Thermal		**Thermal**		**Solid Mechanical**		
Chemical		thermal mass (bridge, other materials)	7,6	friction	19	
Radiant		earth	16	bolting	all applicable	
mirrors	16,5,3	**Chemical**				
Fluid Mechanical		energy storing chemicals	17,9			
tube (implied)	all applicable	temp change of liquid	13,10			
Solid Mechanical		state change of liquid	6			
wire (implied)	all applicable	temp change of gas				
Electrical		fuel cell	11,2			
		liquid salt	5			
		temp change of substance(salt, wax)	8			
		Radiant				
		laser system	11			
		Fluid Mechanical				
		retention pond/dam	18,13,8			
		compressed oxygen	12			
		water tower	16,7			
		water tank	15,11,5,4			
		rain buckets				
		bladder	11			
		Solid Mechanical				
		flywheel	17, 16,15,14,11,9			
		spring	16,8,7,4			
		magnets	11			
		pendulum	16,15,14,9,8,2			
		ponential energy mass	5			
		shape memory alloy	8			
		Electrical				
		batteries (lithium, other)	18,17,16,15,13,12,11,10,9,8,7,6,5,4,2			
		capacitor	16,15,11,8,7,6,5,4			

Appendix J: Concept Generation Results From USAFA

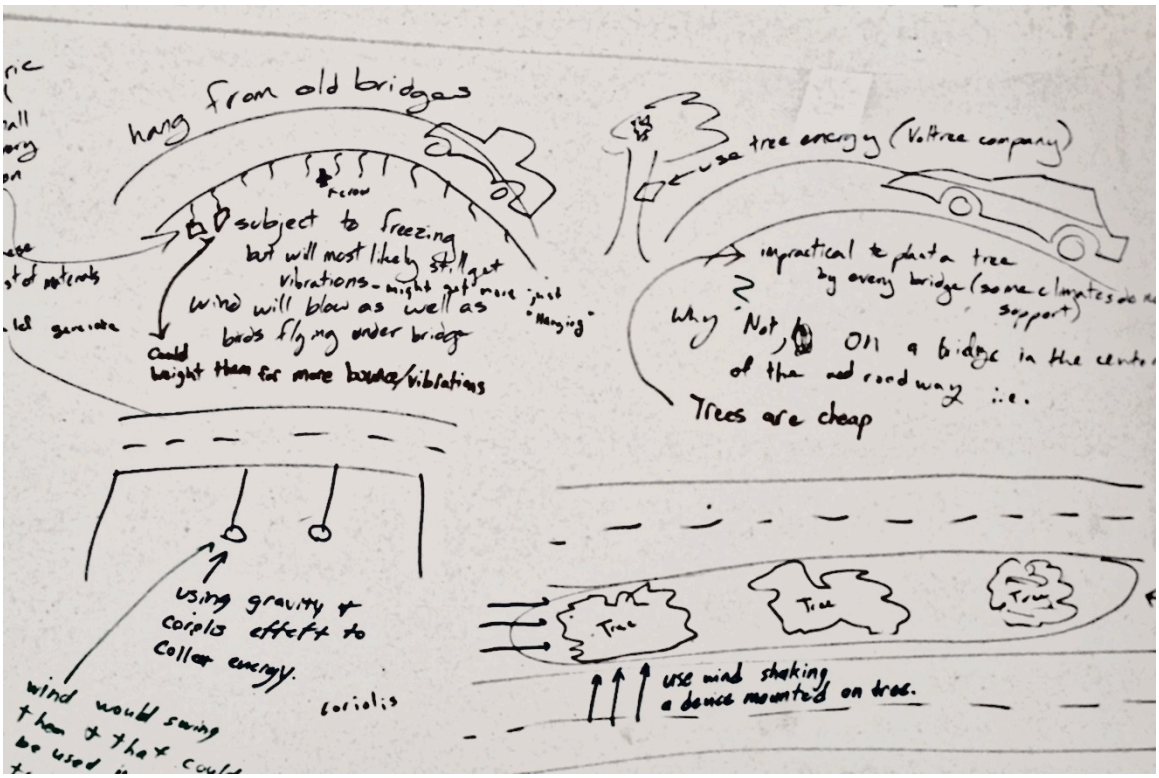

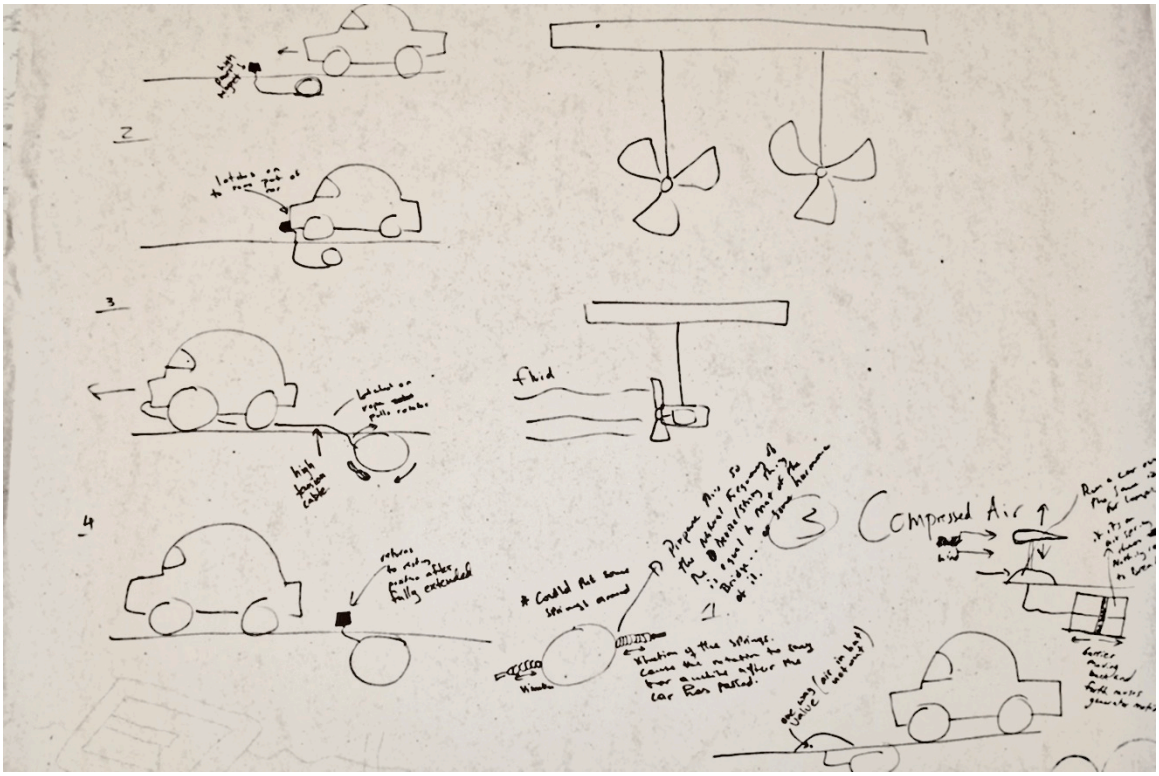
2
3
fluid
4
Compressed Air
Maybe pass out
Maybe make this a train car
so people can continue to load the
box cars.

Bibliography

A genuine 1870 solar-powered steam engine. (1975, Nov/Dec). *Mother Earth News*.

A123 Systems: About us. (n.d.). Retrieved Mar 28, 2011, from A123 Systems: www.a123systems.com/about-us.htm

Abbasi, A. A., & Younis, M. (2007). A survey on clustering algorithms for wireless sensor networks. *Computer Communications, 30* (14-15), 2826-2841.

Abdel-Ghaffar, A. M., & Scanlan, R. H. (1985). Ambient vibration studies of Golden Gate Bridge. *J. Engineering Mechanics, 111* (4), 463-483.

Advanced Energy Group. (2005). *Solar power insolation for U.S. major cities*. Retrieved Oct 26, 2009, from Solar 4 Power: http://www.solar4power.com/solar-power-insolation-window.html

AIT. (1997). *Shake flashlights*. Retrieved May 20, 2011, from Applied Innotech: http://www.appliedinnotech.com/products/shake-flashlights/shake-flashlights.php

Akiyama, K. (1991). *Function analysis: Systematic improvement of quality performance*. New York, NY: Productivity Press.

Akkaya, K., & Younis, M. (2005). A survey on routing protocols for wireless sensor networks. *Ad Hoc Networks, 3* (3), 325-349.

Allied Tube and Conduit. (n.d.). *Tyco Electrical and Metal Products*. Retrieved Oct 26, 2009, from Allied Tube and Conduit: http://www.alliedtube.com

Altshuller, G. S. (1984). *Creativity as an exact science*. Luxembourg: Gordon and Breach.

Ambiosystems. (2010). *Demonstrations and application examples*. Retrieved Jan 20, 2010, from Ambiosystems, LLC: http://www.ambiosystems.com/index.php/Demonstrations-and-Application-examples

Antaki, J., Bertocci, G. E., Green, E. C., Nadeem, A., Rintoul, T., Kormos, R. L., et al. (1995). A gait-powered autologous battery charging system for artificial organs. *ASAIO Journal, 41* (3), M588-595.

Anton, S. R., & Sodano, H. A. (2007). A review of power harvesting using piezoelectric materials (2003-2006). *Smart Materials and Structures, 16*, R1-R21.

Appa, K. (2000). *Patent No. 6127739*. United States.

Arms, S. W., Townsend, C. P., Churchill, D. L., Hamel, M. J., Augustin, M., Yeary, D., et al. (2009). Energy harvesting wireless sensors. In S. Priya, & D. J. Inman (Eds.), *Energy Harvesting Technologies* (pp. 195-208). New York, NY: Springer Science+Business Media.

Bahaj, A. S., Myers, L., & James, P. A. (2007). Urban energy generation: Influence of micro-wind turbine output on electricity consumption in buildings. *Energy and Buildings, 39* (2), 154-165.

Beeby, S. P., Tudor, M. J., & White, N. M. (2006). Energy harvestin vibration sources for microsystems applications. *Measurement Science and Technology, 17* (12), R175-195.

Begg, R. D., Mackenzie, A. C., Dodds, C. J., & Loland, O. (1976). Structural integriaty monitoring using digital processing of vibration signals. *Proc. 8th Annual Offshore Technology Conference*, (pp. 305-311). Houston, TX.

Bouchard, T. J. (1969). Personality, problem-solving procedure, and performance in small groups. *J. of Applied Psychology Monograph, 53* (1), 1-29.

Brownjohn, J. W., Dumanoglu, A. A., Severn, R. T., & Taylor, C. A. (1987). Ambient vibration measurements of the Humber Suspension Bridge and comparison with calculated characteristics. *Proc. Instn Civ. Engrs, Part 2, 83*, 561-600.

Brune, C. S., Spee, R., & Wallace, A. K. (1994). Experimental evaluation of a variable-speed, doubly-fed wind-power generation system. *IEEE Trans. on Industry Applications, 30* (3), 648-655.

Bryant, C. R., Stone, R. B., McAdams, D. A., Kurtoglu, T., & Campbell, M. I. (2005). Concept generation from the functional basis of design. *Proc. of the International Conference of Engineering Design*. Melbourne, Australia.

Buchmann, I. (2006). *Is lithium-ion the ideal battery?* Retrieved Oct 26, 2009, from Battery University, Part One: http://www.batteryuniversity.com/partone-5.htm

Cagan, J., & Vogel, C. M. (2002). *Creating breakthrough products: Innovation from product planning to program approval*. Upper Saddle River, NJ: Prentice Hall.

Caldwell, B. W., & Mocko, G. M. (2010). Functional similarity at varying levels of abstraction. *Proc. of the International Design Engineering Technical Conferences*. Montreal, Quebec, Canada.

Campbell, J. P. (2008). *ROW Utility Manual*. Austin, TX: Texas Department of Transportation.

Carbon Trust. (2008, Aug 7). *Carbon Trust study clarifies the potential of small-scale wind energy*. Retrieved May 23, 2011, from Carbon Trust Press Releases: http://www.carbontrust.co.uk/news/hews/press-centre/2008/Pages/Small-Scale-Wind-Energy.aspx

Cardei, M., & Du, D.-Z. (2005). Improving wireless sensor network lifetime through power aware organization. *Wireless Networks, 11* (3).

Carden, E. P., & Fanning, P. (2004). Vibration based condition monitoring: A review. *Structural Health Monitoring, 3* (4), 355-377.

Cascio, J. (2005, May 15). *Ultra-long-life battery*. Retrieved Mar 28, 2011, from World Changing: Change Your Thinking: www.worldchanging.com/archives/002725.html

Castellucci, J. (1988, Jan. 23). Crack in bridge shuts down Rte. 95. *Providence J.-Bulletin*.

Catbas, F. N., Susoy, M., & Frangopol, D. M. (2008). Structural health monitoring and reliability estimation: Long span truss bridge application with environmental monitoring data. *Engineering Structures, 30* (9), 2347-2359.

Cawley, P., & Adams, R. D. (1979). A vibration technique for non-destructive testing of fibre composite structures. *J. of Composite Materials, 13*, 161-175.

Challa, V. R., Prasad, M. G., Shi, Y., & Fisher, F. T. (2008). A vibration energy harvesting device with bidirectional resonance frequency tunability. *Smart Materials and Structures, 17*.

Chang, C.-H., & Meroney, R. N. (2003). Concentration and flow distributions in urban street canyons: Wind tunnel and computational data. *J. of Wind Engineering and Industrial Aerodynamics, 91*, 1141-1154.

Chatterjee, P. K., Datta, T. K., & Surana, C. S. (1994). Vibration of continuous bridges under moving vehicles. *J. of Sound and Vibration, 10* (5), 619-632.

Christensen, C. M., Anthony, S. D., & Roth, E. A. (2004). *Seeing what's next: Using the theories of innovation to predict industry change*. Boston, MA: Harvard Business School Publishing Corporation.

Churchill, D. L., Hamel, M. J., Townsend, C. P., & Arms, S. W. (2003). *Strain energy harvesting for wireless sensor networks*. Retrieved 4 4, 2011, from MicroStrain White Papers: http://www.microstrain.com/white/pdf/strainenergyharvesting.pdf

Civil Engineer. (2011, Mar 11). *History of solar energy*. Retrieved May 21, 2011, from Civil Engineer Link: http://civilengineerlink.com/history-solar-energy

Clingman, D. J., & Ruggeri, R. T. (2009). *Patent No. 7,521,841*. United States.

Clingman, D. J., & Ruggeri, R. T. (2006). *Patent No. US2006.0175937A1*. United States.

(2008). *Collapse of I-35W Highway Bridge, Minneapolis, Minnesota, August 1, 2007*. Washington D.C.: National Transportation Safety Board.

Collins, J., Hagan, B., & Bratt, H. (1976). The failure-experience matrix - A useful design tool. *Trans. of the ASME, Series B, J. of Eng. in Industry, 98*, 1074-1079.

Coppolino, R. N., & Rubin, S. (1980). Detectability of structural failures in offshore platforms by ambient vibration monitoring. *Proc. 12th Annual Offshore Tech. Conference*, *4*, pp. 101-110.

Corbus, D., Newcomb, C., Baring-Gould, E. I., & Friedly, S. (2002). Battery voltage stability effects on small wind turbine energy capture. *AWEA Windpower Conference*. Portland, OR.

Corke, P., Valencia, P., Sikka, P., Wark, T., & Overs, L. (2007). Long-duration solar-powered wireless sensor networks. *Fourth Workshop on Embedded Networked Sensors*. Cork, Ireland.

Cornwell, P. J., Goethal, J., Kowko, J., & Damianakis, M. (2005). Enhancing power harvesting sing a tuned auxiliary structure. *J. Intelligent Material Systems and Structures, 16* (10), 825-834.

Costco. (2011). *Sunforce 60 watt solar panel back up power kit with 1.8 watt solar battery maintainer*. Retrieved Jun 6, 2011, from Costco: http://www.costco.com/Browse/Product.aspx?Prodid=11298029&Ne=5000000%2040000000&eCat=BC|3960|21248&N=4043955%205000014&Mo=0&No=0&Nr=P_CatalogName:BC&Ns=P_Price|1||P_SignDesc1&lang=en-US

Daim, T. U., Rueda, G., Martin, H., & Gerdsri, P. (2006). Forecasting emerging technologies: Use of bibliometrics and patent analysis. *Technological Forecasting and Social Change, 73* (8), 981-1012.

Davis, C., & Lesieutre, G. (2000). An actively tuned solid-state vibration absorber using capacitive shunting of pieoelectric stiffness. *J. Sound and Vibration, 232* (3), 601-617.

Decotignie, J.-D., Enz, C., Peiris, V., & Hubner, M. (2010). WiseNET: An ultra low-power concept for wireless sensor networks. *Technisches Messen, 77* (2), 107-112.

Deline, C. (2009). Partially shaded operation of a grid-tied pv system. *IEEE Photovoltaic Specialists Conference*. Philadelphia, PA: IEEE.

Deraemaeker, A., Reynders, E., De Roeck, G., & Kullaa, J. (2008). Vibration-based structural health monitoring using output-only measurements under changing environmnet. *Mechanical Systems and Signal Processing, 22* (1), 34-56.

(2009). *Development of rapid, reliable, and economical methods for inspection and monitoring of highway bridges*. The University of Texas at Austin, National Instruments, & Wiss, Janney, Elstner Associates, Inc., Austin, TX.

Dierks, E. C. (2011). *Electromagnetic energy harvester development for powering wireless structural health monitoring of bridges through vibration*. Austin, TX: The University of Texas at Austin.

Doebling, S. W., Farrar, C. R., Prime, M. B., & Shevitz, D. W. (1996). *Damage identification and health monitoring of structural and mechanical systems from changes in their vibration characteristics: A literature review (Report LA-13070-MS)*. Los Alamos, NM: Los Alamos National Laboratory.

Dong, S., Zhai, J., Li, J. F., Viehland, D., & Priya, S. (2008). Multimodal system for harvesting magnetic and mechanical energy. *Applied Physics Letters, 93*.

Dudney, N. J. (2009). Thin film batteries for energy harvesting. In S. Priya, & D. J. Inman (Eds.), *Energy Harvesting Technologies* (pp. 355-362). New York, NY: Springer Science+Business Media.

Duggan, D. M., Wallace, E. R., & Caldwell, S. R. (1980). Measured and predicted vibrational behavior of Gulf of Mexico platforms. *Proc. 12th Annual Offshore Tech. Conf.*, (pp. 92-100).

East Japan Railway Company. (2008, Jan 11). *Demonstration experiment of the "power-generating floor" at Tokyo Station*. Retrieved Sep 14, 2010, from East Japan Railway Company Press Releases: http://www.jreast.co.jp/e/development/press/20080111.pdf

Edwards, L. (2010, Apr 9). *New Hitachi Li-ion batteries to last ten years*. Retrieved Jun 6, 2011, from PhysOrg.com: http://www.physorg.com/news190018064.html

El-Khattam, W., & Salama, M. M. (2004). Distributed generation technologies, definitions and benefits. *Electric Power Systems Research, 71* (2), 119-128.

Elvin, N. G., Lajnef, N., & Elvin, A. A. (2006). Feasibility of structural monitoring with vibration powered sensors. *Smart Materials and Structures, 15* (4).

Energizer. (2009). *Lithium iron disulfide handbook and application manual*. Retrieved Oct 26, 2009, from Energizer Battery Manufacturing, Inc.: http://data.energizer.com/PDFs/lithium191192_appman.pdf

Energizer. (2008). *Product Datasheet, Energizer E91*. Retrieved Oct 26, 2009, from Energizer Battery Manufacturing, Inc.: http://data.energizer.com/PDFs/E91.pdf

Energy Information Administration. (n.d.). *Average Retail Price of Electricity to Ultimate Customers by End-Use Sector, by State*. Retrieved Oct 26, 2009, from US Department of Energy: http://www.eia.doe.gov/cneaf/electricity/epm/table5_6_a.html

Enger, C. C., & Kennedy, J. H. (1964). An improved bioelectric generator. *Trans. ASAIO, 10* (1), 373-377.

EnOcean. (2011). *Energy harvesting wireless sensor solutions and networks*. Retrieved Jun 8, 2011, from EnOcean: http://www.enocean.com/en

Enviro-Energies. (n.d.). *Maglev vertical axis wind turbine*. Retrieved Feb 12, 2011 from Enviro-Energies: http://www.enviro-energies.com

Ertuk, A., & Inman, D. J. (2008). A distributed parameter electromechanical model for cantilevered piezoelectric energy harvesters. *ASME J. of Vibration and Acoustics, 130* (4).

Ertuk, A., & Inman, D. J. (2009). An experimentally validated bimorph cantilever model for piezoelectric energy harvesting from base excitations. *Smart Materials and Structures, 18* (2).

Farrar, C. R., & Cone, K. M. (1995). Vibration testing of the I-40 bridge before and after the introduction of damage. *Proc. 13th International Modal Analysis Conference*, 203-209.

Farrar, C. R., & Lieven, N. A. (2007). Damage prognosis: The future of structural health monitoring. *Phi. Trans. R. Soc. A, 365* (1851), 623-632.

Farrar, C. R., & Worden, K. (2007). An introduction to structural health monitoring. *Phil. Trans. R. Soc. A, 365*, 303-315.

Farrar, C. R., Baker, W. E., Bell, T. M., Cone, K. M., Darling, T. W., Duffey, T. A., et al. (1994). *Dynamic characterization and damage detetion in the I-40 bridge over the Rio Grande (Report LA-12767-MS)*. Los Alamos, NM: Los Alamos National Laboratory.

Ferrari, M., Ferrari, V., Guizzetti, M., Ando, B., Baglio, S., & Trigona, C. (2010). Improved energy harvesting from wideband vibrations by nonlinear piezoelectric converters. *Sensors and Actuators A: Physical, 162* (2), 425-431.

Franke, H.-J. (1975). Methodische Schritte beim Klaren konstruktiver Aufgabenstellungen. *Konstruktion, 27*, 395-402.

Friswell, M. I., & Adhikari, S. (2010). Structural health monitoring using shaped sensors. *Mechanical Systems and Signal Processing, 24* (3), 623-635.

Gadomski, J. (n.d.). *Tadiran PulsesPlus batteries ideal for lang-term, maintenance-free GPS tracking*. Retrieved Mar 28, 2011, from Tadiran Batteries: http://www.tadiranbat.com/index.php/tadiran-batteries-ideal-for-long-term-gps-tracking

Galbreath, J. H., Townsend, C. P., Mundell, S. W., & Arms, S. W. (2003). Civil structure strain monitroing with power-efficient high-speed wireless sensor networks. *International Workshop for Structural Health Monitoring*. Stanford, CA.

Gipe, P. (1995). *Wind energy comes of age*. Hoboken, NJ: John Wiley and Sons.

Global Energy Concepts. (2002). *New Mexico wind resource assessment - Lee Ranch*. Albuquerque, NM: Sandia National Laboratories.

Gordon, J. (2001). *Solar energy*. London: James & James.

Green Column. (2009). Retrieved Jun 1, 2011, from Bright Green Energy: http://www.wirefreedirect.com/green_column.asp

Green, M. A., Emery, K., Hishikawa, Y., & Warta, W. (2010). Solar cell efficiency tables (version 36). *Progress in Photovoltaics: Research and Applications, 18*, 346-352.

Gungor, V. C., & Hancke, G. P. (2009). Industrial wireles sensor networks: Challenges, design principles, and technical approaches. *Industrial Electronics, IEEE, 56* (10), 4258-4265.

Guyomar, D., Badel, A., Lefeuvre, E., & Richard, C. (2005). Toward energy harvesting using active materials and conversion improvement by nonlinear processing. *Ultrasonics, Ferroelectrics and Frequency Control, 52* (4), 584-595.

Hande, A., Polk, T., Walker, W., & Bhatia, D. (2007). Indoor solar energy harvesting for sensor network router nodes. *Microporocessors and Microsystems*, *31* (6), 420-432.

Harb, A. (2010). Energy harvesting: State-of-the-art. *Renewable Energy*, 1-14.

Hasler, E., Stein, L., & Harbauer, G. (1984). Implantable physiological power supply with PVDF film. *Ferroelectrics*, *60* (1), 277-282.

Hill, D. R. (1991, May). Mechanical engineering in the medieval near east. *Scientific American*, pp. 64-69.

Hirtz, J., Stone, R. B., McAdams, D. A., Szykman, S., & Wood, K. L. (2002). A functional basis for engineering design: Reconciling and evolving previous efforts. *J. of Research in Engineering Design*, *13* (2).

Hoppin, J. (2007, Aug 21). *Recovery ends, rebuilding begins*. Retrieved Aug 25, 2007, from Pioneer Press: http://www.twincities.com/collapse/ci_6684072

Hubka, V. (1996). *Design science*. London: Springer-Verlag.

Humar, J. L. (1990). *Dynamics of structures*. Upper Saddle River, NJ: Prentice-Hall.

Hundal, M. (1990). A systematic method for developing function structures. *Mech. Mach. Theory*, *25* (3), 243-256.

HYmini. (2011). *HYmini micro wind turbine*. Retrieved Jun 1, 2011, from HYmini: http://www.hymini.com

Javier, A., & Foos, E. E. (2009). Nanocrystal photovoltaic paint sprayed with a handheld airbrush. *IEEE Trans. on Nanotechnology*, *8* (5), 569-573.

Jo, B. W., Park, J. C., & Kim, C. H. (2005). Wind characteristics of existing long span bridge based on measured data. *KSCE Journal of Civila Engineering*, *9* (3), 219-224.

Johnson, R. C. (2007). *New York Bridge to Get WIreless Monitor*. Retrieved Oct 26, 2009, from EE Times: http://www.eetimes.com/showArticle.jhtml?articleID=201500113

Jowder, F. A. (2006). Weibull and Rayleigh distribution functions of wind speeds in Kingdom of Bahrain. *Wind Engineering*, *30* (5), 439-445.

Jung, S.-M., & Yun, K.-S. (2010). Energy-harvesting device with mechanical frequency-up conversion mechanism for increased power efficiency and wideband operation. *Applied Physics Letters*, *96*, 1-3.

KidWind. (2011). *Wind energy science*. Retrieved May 30, 2011, from KidWind Project: http://learn.kidwind.org

Kim, S., Pakzad, S., Culler, D., Demmel, J., Fenves, G., Glaser, S., et al. (2007). Health monitoring of civil infrastructures using wireless sensor networks. *IPSN '07*. Cambridge, MA.

Kinney, P. (2003). ZigBee technology: Wireless control that simply works. *Communications Design Conference*. San Jose, CA.

Kirshman, C., & Fadel, G. (1998). Classifying functions for mechanical design. *J. of Mechanical Design, Trans. of the ASME*, *120* (3), 475-482.

Ko, J. M., & Ni, Y. Q. (2005). Technology developments in structural health monitoring of large-scale bridges. *Engineering Structures*, *27*, 1715-1725.

Ko, W. H. (1969). *Patent No. 3,456,134*. United States.

Koch, P., Peplinski, J., Allen, J., & Mistree, F. (1994). A method for design using available assets: Identifying a feasible system configuration. *Behavioral Science*, *30*, 229-250.

Kongtragool, B., & Wongwises, S. (2003). A review of solar-powered Stirling engines and low temperature differential Stirling engines. *Renewable and Sustainable Energy Reviews*, *7* (2), 131-154.

Kotter, D. K., Novack, S. D., Slafer, W. D., & Pinhero, P. (2008). Solar nantenna electromagnetic collectors. *Proc. of Energy Sustainability*. Jacksonville, FL.

Kozinsky, I. (2009). Study of passive self-tuning resonator for broadband power harvesting. *PowerMEMS2009*. Washington, D.C.

Kraemer, D., Hu, L., Muto, A., Chen, X., Chen, G., & Chiesa, M. (2008). Photovoltaic-thermoelectric hybrid systems: A general optimization methodology. *Applied Physics Letters*, *92* (24).

Kulah, H., & Najafi, K. (2008). Energy scavenging from low-frequency vibrations by using frequency up-conversion for wireless sensor applications. *IEEE Sensors Journal*, *8* (3), 261-268.

Kymissis, J., Kendall, C., Paradiso, J., & Gershenfeld, N. (1998). Parasitic power harvesting in shoes. *Digest of Papers, 2nd International Symposium on Wearable Computers*, 132-139.

Landt, J. (2005). The history of RFID. *Potentials, IEEE*, *24* (4), 8-11.

Leake, J. (2006, Apr 16). Home wind turbines dealt killer blow. *The Times*.

Leonov, V., & Vullers, R. M. (2009). Wearable thermoelectric generators for body-powered devices. *J. of Electronic Materials*, *38* (7), 1491-1498.

Lewin, G., Myers, G. H., Parsonnet, V., & Raman, K. V. (1968). An improved biological power source for cardiac pacemakers. *Trans. ASAIO*, *14* (1), 215-219.

Li, Y., Yu, H., Su, B., & Shang, Y. (2008). Hybrid micropower source for wireless sensor network. *IEEE Sensors Journal*, *8* (6), 678-681.

Little, A., Wood, K., & McAdams, D. (1997). Functional analysis: A fundamental empirical study for reverse engineering, benchmarking and redesign. *Proc. of the ASME Design Theory and Methodology Conference*. Sacramento, CA.

Loland, O., & Dodds, J. C. (1976). Experience in developing and operating integrity monitoring system in North Sea. *Proc. of the 8th Annual Offshore Technology Conference*, 313-319.

Lu, F., Lee, H. P., & Lim, S. P. (2004). Modeling and analysis of micro-piezoelectric power generators for micro-electromechanical-systems applications. *Smart Materials and Structures*, *13* (1), 57-63.

Lynch, J. P., & Loh, K. J. (2006). A summary review of wireless sensors and sensor networks for structural health monitoring. *The Shock and Vibration Digest*, *38* (2), 91-128.

Lynch, J. P., Sundararajan, A., Law, K. H., Kiremidjian, A. S., & Carryer, E. (2003). Power-efficient data management for a wireless structural monitoring system. *Proc. 4th International Workshop on Structural Health Monitoring*, *1*. Stanford, CA.

Magee, S. (2010). *Solar irradiance and insolation for power systems*. Charleston, SC: CreateSpace.

Mariyappan, J. (2001). *Solar thermal thematic review*. Washington, D.C.: The Global Environment Facility.

Markman, A. B., & Wood, K. L. (2009). *Tools for innovation*. New York, NY: Oxford University Press.

Martino, J. P. (2003). A review of selected recent advances in technological forecasting. *Technological Forecasting and Social Change*, *70* (8), 719-733.

Maxwell, J. C. (1865). A dynamical theory of the electromagnetic field. *Phil. Trans. of the Royal Society of London*, *155*, 459-512.

Mazurek, D. F., & DeWolf, J. T. (1990). Experimental study of bridge monitoring technique. *J. Structural Engineering*, *116* (9).

McAdams, D. A., Stone, R. B., & Wood, K. L. (1999). Functional interdependence and product similarity based on customer needs. *Researchin Engineering Design*, *11* (1), 1-19.

McEvoy, T. K. (2011). *Wind energy harvesting for bridge health monitoring*. Austin, TX: The University of Texas at Austin.

McEvoy, T., Dierks, E., Weaver, J., Inamdar, S., Zimowski, K., Wood, K. L., et al. (2011). Developing innovative energy harvesting approaches for infrastructure health monitoring systems. *Proc. of the International Design Engineering Technical Conferences*. Washington, DC.

McFarland, D., Mullis, M., & Riley, B. (2010). *Energy harvesting for bridge monitoring applications*. Austin, TX: The University of Texas Department of Mechanical Engineering.

Meguerdichian, S., & Potkonjak, M. (2003). *Low power 0/1 coverage and scheduling techniques in sensor networks (Technical Report 030001)*. UCLA, Los Angeles, CA.

Memmott, J. (2007). *Bureau of Transportation Statistics Special Report: Highway Bridges in the United States (Special Report SR-003)*. U.S. Department of Transportation, Research and Innovative Technology Administration, Washington D.C.

Meninger, S., Mur-Miranda, J. O., Amirtharajah, R., Chandrakasan, A. P., & Lang, J. H. (2001). Vibration-to-electric energy conversion. *IEEE Trans. on Very Large Scale Integration (VLSI) Systems*, *9* (1), 64-76.

Merabet, B., Cirio, L., Takhedmit, H., Costa, F., Vollaire, C., Allard, B., et al. (2009). Low-cost converter for harvesting of microwave electromagnetic energy. *Energy Conversion Congress and Exposition*, (pp. 2592-2599). San Jose, CA.

Met Office. (2008). *Small-scale wind energy technical report*. Devon: The Carbon Trust.

MicroStrain. (2007). *MicroStrain, Inc. solar powered wireless sensor networks monitor bridge spans*. Retrieved Nov 1, 2010, from MicroStrain News: www.microstrain.com/news/MicroStrain Solar Powered Bridge Press Release_rev d.pdf

MIDE. (2010). *Volture Datasheet*. Retrieved Jun 1, 2011, from MIDE Volture Piezoelectric Energy Harvesters: http://www.mide.com/pdfs/Volture_Datasheet_001.pdf

MIDE. (2011). *Volture vibration energy harvesting products*. Retrieved Jun 8, 2011, from MIDE - Engineering Smart Technologies: http://www.mide.com/products/volture/volture_catalog.php

Mitcheson, P. D., Green, T. C., Yeatman, E. M., & Holmes, A. S. (2004). Architectures for vibration-driven micropower generators. *J. of Microelectromechanical Systems*, *13* (3), 429-440.

Miyazaki, T., Akisawa, A., & Kashiwagi, T. (2005). Energy savings of office buildings by the use of semi-transparent solar cells for windows. *Renewable Energy*, *30* (3), 281-304.

Motjolopane, B. P., & van Zyl, R. (2009). A review of rectenna models for electromagnetic energy harvesting. *J. of Engineering, Design and Technology*, *7* (3), 282-292.

Muruganathan, S. D., Ma, D. C., Bhasin, R. I., & Fapojuwo, A. O. (2005). A centralized energy-efficient routing protocol for wireless sensor networks. *Communication Magazine, IEEE*, *43* (3), S8-13.

National Instruments. (2009). *WSN 1.0 Power Consumption*. Austin, TX: National Instruments.

National Transportation Safety Board. (2008). *Collapse of I-35W highway bridge, Minneapolis, Minnesota, August 1, 2007*. Washington, DC: Highway Accident Report NTSB/HAR-08/03.

Nedevschi, S., Popa, L., Iannaccone, G., Ratnasamy, S., & Wetherall, D. (2008). Reducing network energy consumption via sleeping and rate-adaptation. *Proc. 5th USENIX Symposium on Networked Systems Design and Implementation* (pp. 323-336). San Fransisco, CA: USENIX Association.

Nerf Missilestorm. (n.d.). Retrieved Jun 1, 2011, from Nerf Guns - Pics and Reviews of All Toy Nerf Guns: http://nerfguns.org/nerf-missilestorm

Nishimura, F., Tabors, R. D., Ilic, M. D., & Lacalle-Melero, J. R. (1993). Benefit optimization of centralized and decentralized power systems in a multi-utility environment. *IEEE Trans. on Power Systems*, *8* (3), 1180-1186.

Ntotsios, E., Papadimitriou, C., Panetsos, P., Karaiskos, G., Perros, K., & Perdikaris, P. C. (2009). Bridge health monitoring system based on vibration measurement. *Bulletin of Earthquake Engineering*, *7* (2), 469-483.

Okamoto, H., Onuki, T., Nagasawa, S., & Kuwano, H. (2009). Efficient energy harvesting from irregular mechanical vibrations by active motion control. *J. Microelectromechanical Systems*, *18* (6), 1420-1431.

Olson, L. (2002). *The art of speaker design*. Retrieved May 31, 2011, from Nutshell Hifi: http://www.nutshellhifi.com/library/speaker-design1.html

Olson, W. (2010, Feb 16). *An urban experiment in renewable energy*. Retrieved May 23, 2011, from Open Salon: http://open.salon.com/blog/william_olson/2010/02/16/

an_urban_experiment_in_renewable_energy

Only Batteries. (2011). *Lithium ion (li-ion) batteries*. Retrieved Jun 6, 2011, from OnlyBatteries.com: http://www.onlybatteries.com/cat_featured_items.asp?

cat1=27&cat=2&id=163&uid=1107

Ottman, G. K., Hofmann, H. F., & Lesieutre, G. A. (2003). Optimized piezoelectric energy harvesting circuit using step-down converter in discontinuous conduction mode. *Power Electronics*, *18* (2), 696-703.

Ottman, G. K., Hofmann, H. F., Bhatt, A. C., & Lesieutre, G. A. (2002). Adaptive piezoelectric energy harvesting circuit of wireless remote power supply. *IEEE Transactions on Power Electronics*, *17* (5), 669-676.

Otto, K. N., & Wood, K. L. (2001). *Product design: Techniques in reverse engineering and new product development*. Upper Saddle River, NJ: Prentice Hall.

Ou, J., & Li, H. (2010). Structural health monitoring in mainland China: Review and future trends. *Structural Health Monitoring*, *9* (3), 219-231.

Pahl, G., & Beitz, W. (1996). *Engineering design - A systematic approach* (2nd Ed. ed.). New York, NY: Springer.

Pandey, V., Kaur, A., & Chand, N. (2010). A review on data aggregation techniques in wireless sensor network. *J. of Electronic and Electrical Engineering*, *1* (2), 1-8.

Paradiso, J., & Starner, T. (2005). Energy scavenging for mobile and wireless electronics. *Pervasive Computing*, *4* (1), 18-27.

Parallax. (2011). *Solar Panel 6V at 1W, 125x63 mm*. Retrieved Jun 6, 2011, from Parallax Inc.: http://www.parallax.com/Store/Components/Optoelectronics/tabid/152/List/0/ProductID/619/Default.aspx?SortField=ProductName%2cProductName

Park, G., Rosing, T., Todd, M. D., Farrar, C. R., & Hodgkiss, W. (2008). Energy harvesting for structural health monitoring sensor networks. *J. Infrastruct. Syst.*, *14* (64).

Perpetuum. (2011). *Perpetuum - Applications*. Retrieved May 30, 2011, from Perpetuum: http://www.perpetuum.com.apps.asp

Perpetuum. (2009). *Perpetuum PMG27-17 (preliminary) helicopter vibration energy harvester module*. Retrieved Oct 26, 2009, from Perpetuum: http://perpetuum.isonlinehere.com/resource/PMG27_pspec.pdf

Perpetuum. (2011). *Products*. Retrieved Jun 8, 2011, from Perpetuum: The global leader in electromagnetic vibration energy harvesting: http://www.perpetuum.com/products.asp

Phani, G., Tulloch, G., Vittorio, D., & Skryabin, I. (2001). Titania solar cells: New photovoltaic technology. *Renewable Energy*, *22* (1-3), 303-309.

PicoTurbine. (2011). *PicoTurbine Savonius windmill kit V2*. Retrieved Jun 7, 2011, from PicoTurbine International: http://www.picoturbine.com/products/PicoTurbine-Savonius-Windmill-Kit-V2.html

Piezo Institute. (2011). *Piezo history*. Retrieved May 30, 2011, from Piezo Institute: http://www.piezoinstitue.com/about/piezohistory/index.php

Polastre, J., Hill, J., & Culler, D. (2004). Versatile low power media access for wireless sensor networks. *SenSys '04*, (pp. 95-107). Baltimore, MD.

Porter, A. L., Roper, A. T., Mason, T. W., Rossini, F. A., & Banks, J. (1991). *Forecasting and management of technology*. Hoboken, NJ: John Wiley & Sons.

Price, T. J. (2005). James Blyth - Britain's first modern wind power engineer. *Wind Engineering*, *29* (3), 191-200.

Priya, S. (2007). Advances in energy harvesting using low profile piezoelectric transducers. *J. Electroceramics*, *19*, 167-184.

Putnam, N. (2008). *Energy Systems in MAVs - Theoretical and Applied Perspectives*. Austin, TX: The University of Texas at Austin.

Quallion. (2009). *Secondary Battery Manufacturer - Quallion*. Retrieved Oct 26, 2009, from Quallion, LLC: http://www.quallion.com/sub-tc-secondary.asp

R. I. shores cracked viaduct. (1988, Feb.). *Engrg. News-Record*, 20-21.

Rage Battery. (2009). *6 volt sealed lead acid batteries*. Retrieved Oct 26, 2009, from Rage Battery: http://www.ragebattery.com/power-sonic/ps6v.html

Raghavendrachar, M., & Aktan, A. E. (1992). Flexibility by multireference impact testing for bridge diagnostics. *ASCE J. of Structural Engineering*, *118*, 2186-2203.

Raghunathan, V., Kansal, A., Hsu, J., Friedman, J., & Srivastava, M. (2005). Design considerations for solar energy harvesting wireless embedded systems. *Proc. of the International Conference on Information Processing on Sensor Network*.

Rastegar, J., Pereira, C., & Nguyen, H.-L. (2006). Piezoelectric-based power sources for harvesting energy from platrofms with low frequency vibration. *Proc. PSIE Int. Soc. Opt. Eng., 6171*. San Diego, CA.

Reichenbach, M. (2011). *Untitled thesis*. Austin, TX: The University of Texas at Austin.

Road transportation batteries. (n.d.). Retrieved Mar 28, 2011, from Quallion: www.quallion.com/sub-mo-road.asp

Rocha, J., Goncalves, L., Rocha, P., Silva, M., & Lanceros-Mendez, S. (2010). Energy harvesting from piezoelectric materials fully integrated in footwear. *IEEE Trans. Industrial Electronics*, *57* (3), 813-819.

Roundy, S. (2005). On the effectiveness of vibration-based energy harvesting. *J. of Intelligent Material Systems and Structures*, *16* (10), 809-823.

Roundy, S., & Wright, P. (2004). A piezoelectric vibration based generator for wireless electronics. *Smart Materials and Structures*, *13*, 1131-1142.

Roundy, S., Leland, E. S., Baker, J., Carleton, E., Reilly, E., Lai, E., et al. (2005). Improving power output for vibration-based energy scavengers. *IEEE Pervasive Computing*, *4* (1), 28-36.

Roundy, S., Steingart, D., Frechette, L., Wright, P., & Rabaey, J. (2004). Power sources for wireless sensor networks. *Wireless Sensor Networks: Lecture Notes in Computer Science*, *2920*, 1-17.

Roundy, S., Wright, P., & Rabaey, J. (2003). A study of low level vibrations as a power source for wireless sensor nodes. *Computer Communications*, *26* (11), 1131-1144.

Roundy, S., Wright, P., & Rabaey, J. (2004). *Energy scavenging for wireless sensor networks: With special focus on vibrations*. Boston, MA: Kluwer Academic.

Rowe, D. M. (2006). *Thermoelectrics handbook: Macro to nano*. Oxford: Taylor & Francis.

Salane, H. J., Baldwin, J. W., & Duffield, R. C. (1981). Dynamics approach for monitoring bridge deterioration. *Transportation Research Record*, *832*, 21-28.

Salawu, O. S. (1997). Detection of structural damage through changes in frequency: A review. *Engineering Structures*, *19* (9), 718-723.

Sazonov, E. (2007). *Energy harvesting as enabling factor for bridge monitoring*. Retrieved Oct 23, 2009, from Ambiosystems LLC: http://www.ambiosystems.com/index.php/Demonstrations-and-Application-examples/Bridge-10-2007.html

Sazonov, E. (2004). *Energy harvesting: Self-powered pressure sensor*. Retrieved Jan 20, 2010, from Personal site of Edward Sazonov: http://www.intelligent-systems.info/energy_harvesting/piezo_harvesting/pressure_sensor.htm

Sazonov, E., Janoyan, K., & Jha, R. (2004). Wireless intelligent sensor network for autonomous structural health monitoring. *Proc. SPIE*, *5384*, 305-314.

Sazonov, E., Jha, R., Janoyan, K., Krishnamurthy, V., Fuchs, M., & Cross, K. (2006). Wireless intelligent sensor and actuator network (WISAN): A scalable ultra-low-power platform. *Proc. SPIE*, *6177*, 234-244.

Sazonov, E., Li, H., Curry, D., & Pillay, P. (2009). Self-powered sensors for monitoring of highway bridges. *IEEE Sensors Journal*, *9* (11), 1422-1429.

SDC. (2007). *Sustainable dance floor*. Retrieved Feb 12, 2011 from SDC - Sustainable Dance Club - People Planet Party: http://www.sustainabledanceclub.com

SECO. (2007). *Small wind systems*. Retrieved Jun 1, 2011, from State Energy Conservation Office of Texas: http://seco.cpa.state.tx.us/re_wind_smallwind.htm

Seiko. (2007). *Kinetic*. Retrieved May 31, 2011, from Seiko Watch Corporation: http://seikowatches.com/technology/kinetic/index.html

Shah, A., Torres, P., Tscharner, R., Wyrsch, N., & Keppner, H. (1999). Photovoltaic technology: The case for thin-film solar cells. *Science*, *285* (5428), 692-698.

Shah, J. J. (1998). Experimental investigation of progressive idea generation techniques in engineering design. *Proc. of the ASME Design Theory and Methodology Conference*. Atlanta, GA.

Shah, J. J., Kulkarni, S. V., & Vargas-Hernandez, N. (2000). Evaluation of idea generation methods for conceptual design: Effectiveness metrics and design of experiments. *Trans. of the ASME J. of Mechanical Design*, *122*, 377-384.

Shah, J. J., Vargas-Hernandez, N., & Smith, S. M. (2003). Metrics for measuring ideation effectiveness. *Design Studies*, *24*, 111-134.

Shenck, N., & Paradiso, J. (2001). Energy scavenging with shoe-mounted piezoelectrics. *IEEE Micro*, *21* (3), 30-42.

Silicon Solar. (2010). *6V Charge Controller*. Retrieved Jun 6, 2011, from Silicon Solar: http://www.siliconsolar.com/6v-charge-controller-p-17850.html

Smith, C. (1995, Jul). Revisiting solar power's past. *Technology Review*, 38-47.

Sodano, H. A., Inman, D. J., & Park, G. (2004). A review of power harvesting from vibration using piezoelectric materials. *The Shock and Vibration Digest*, *36*, 197-205.

Sodano, H. A., Inman, D. J., & Park, G. (2005). Comparison of piezoelectric energy harvesting devices for recharging batteries. *J. Intelligent Material Systems and Structures*, *16*, 799-807.

Sodano, H. A., Magliula, E. A., Park, G., & Inman, D. J. (2002). Electric power generation using piezoelectric materials. *13th Int. Conf. on Adaptive Structures and Technologies*. Potsdam, Germany.

Sodano, H. A., Park, G., & Inman, D. J. (2004). Estimation of electric charge output for piezoelectric energy harvesting. *Strain*, *40* (2), 49-58.

Sohn, H. (2007). Effects of environmental and operational variability on structural health monitoring. *Phil. Trans. R. Soc. A*, *365* (1851), 539-560.

Sohn, H., Farrar, C. R., Hemez, F. M., Czarnecki, J. J., Shunk, D. D., Stinemates, D. W., et al. (2003). *A review of structural health monitoring literature: 1996-2001 (Report LA-13976-MS)*. Los Alamos, NM: Los Alamos National Laboratory.

Sohrabi, K., Gao, J., Ailawadhi, V., & Pottie, G. J. (2000). Protocols for self-organization of a wireless sensor network. *Personal Communications, IEEE*, *7* (5), 16-27.

Solar Panels Plus. (2007). *Solar insolation levels in North America*. Retrieved Jun 1, 2011, from Solar Panels Plus: http://www.solarpanelsplus.com/solar-insolation-levels

Spyrakos, C., Chen, H. L., Stephens, J., & Govidaraj, V. (1990). Evaluating structural deterioration using dynamic response characterization. *Proc. Intelligent Structures*, 137-154.

Starner, T. (1996). Human-powered wearable computing. *IBM Systems Journal*, *35* (3-4), 618-630.

Steingart, D. (2009). Power sources for wireless sensor networks. In S. Priya, & D. J. Inman (Eds.), *Energy Harvesting Technologies* (pp. 267-284). New York, NY: Springer Science+Business Media.

Stone, R. B., Wood, K. L., & Crawford, R. H. (1999). Product architecture development with quantitative functional models. *Proc. of the ASME Design Engineering Technical Conferences*. Las Vegas, NV.

Stone, R., & Wood, K. (2000). Development of a functional basis for design. *J. of Mechanical Design*, *122* (4), 359-370.

Sun, S., Fan, Z., Wang, Y., & Haliburton, J. (2004). Organic solar cell optimizations. *J. of Materials Science*, *40* (6), 1429-1443.

Sushkov, V., Mars, N., & Wognum, P. (1995). Introduction to TIPS: Theory for creative design. *J. of AI Engineering*.

Szykman, S., Racz, J. W., & Sriram, R. D. (1999). The representation of function in computer-based design. *Proc. of the 1999 ASME Design Engineering Technical Conferences*. Las Vegas, NV.

Tan, Y. K., & Panda, S. K. (2007). A novel piezoelectric based wind energy harvester for low-power autonomous wind speed sensor. *Industrial Electronics Society IECON*, (pp. 2175-2180). Taipei.

Tang, J. P., & Leu, K.-M. (1991). Vibration tests and damage detection of p/c bridges. *J. of the Chinese Institute of Engineers*, *14*, 531-536.

The White House. (n.d.). *A strategy for American innovation: Securing our economic growth and prosperity*. Retrieved Feb 4, 2011 from White House website: http://www.whitehouse.gov/innovation/strategy

Thermocouples. (2008). Retrieved May 23, 2011, from Temperatures.com: http://www.temperatures.com/tcs.html

Thermoelectric Generators. (2010). Retrieved May 23, 2011, from Tech-FAQ: http://www.tech-faq.com/thermoelectric-generators.html

Thomas, J. (2008, Feb 3). *New record: World's largest wind turbine (7+ megawatts)*. Retrieved May 23, 2011, from Metaefficient: The Guide to Highly Efficient Things: http://www.metaefficient.com/news/new-record-worlds-largest-wind-turbine-7-megawatts.html

Turner, J. D., & Pretlove, A. J. (1988). A study of the spectrum of traffic-induced bridge vibration. *J. of Sound and Vibration*, *122*, 31-42.

Ullman, D. G. (2002). *The mechanical design process* (3rd Ed. ed.). Boston, MA: McGraw-Hill.

Ulrich, K., & Eppinger, S. (2004). *Product design and development* (3rd Ed. ed.). New York, NY: McGraw-Hill.

USA Wind Generators. (2011). *Affordable wind power*. Retrieved Jun 6, 2011, from USA Wind Generators: http://www.usawindgen.com/30.html

Vandiver, J. K. (1977, Mar.). Detection of structural failure on fixed platforms by measurement of dynamic response. *J. of Petroleum Technology*, 305-310.

Varshney, P. (1996). *Distributed detection and data fusion*. New York, NY: Springer-Verlag.

Visser, H. J., Theeuwes, J., Van Beurden, M., & Doodeman, G. (2007, Aug 01). *High-efficiency RF-rectenna design*. Retrieved May 23, 2011, from EDN Europe: http://www.edn-europe.com/highefficiencyrfrectennadesign+article+1666+Europe.html

Walker, V., Jensen, D., Crider, K., Weaver, J., Wood, K., & Maixner, M. (2010). Effects of an early prototyping experience: Can design fixation be avoided. *ASEE Annual Conference*. Louisville, KY.

Wal-mart. (2009). *Walmart.com*. Retrieved Oct 26, 2009, from Wal-mart Stores, Inc.: http://www.walmart.com

Wan, C.-Y., Campbell, A. T., & Krishnamurthy, L. (2002). A reliable transport protocol for wireless sensor networks. *Proc. 1st ACM International Workshop on WIreless Sensor Networks and Applications*, (pp. 1-11). Atlanta, GA.

Wang, L., & Yuan, F. G. (2008). Vibration energy harvesting by magnetostrictive material. *Smart Materials and Structures*, *17*, 1-14.

Wang, T.-L., Huang, D., & Shahawy, M. (1999). Dynamic response of multigirder bridges. *J. of Structural Engineering*, *118* (8), 2222-2238.

Wang, X., Xing, G., Zhang, Y., Lu, C., Pless, R., & Gill, C. (2003). Integrated coverage and connectivity configuration in wireless sensor networks. *SenSys '03*. Los Angeles, CA.

Wang, Y., Lynch, J., & Law, K. (2007). A wireless structual health monitoring system with multithreaded sensing devices: Design and validation. *Structure & Infrastructure Engineering: Maintenance, Management, Life-Cycle*, *3* (2), 103-120.

Watts, R. J., & Porter, A. L. (1997). Innovation forecasting. *Technological Forecasting and Social Change*, *56* (1), 25-47.

Weather Underground. (2009, 11 17). *History for Conroe, TX*. Retrieved 1 20, 2010, from Weather Underground: http://www.wunderground.com/history/airport/KCXO/2009/11/17/DailyHistory.html?req_city=Conroe&req_state=TX&req_statename=Texas

Weaver, J. M., Wood, K. L., & Jensen, D. (2008). Transformation facilitators: A quantitative analysis of reconfigurable products and their characteristics. *Proc. of the International Design Engineering Technical Conferences*. Brooklyn, NY.

Weaver, J., Wood, K., Crawford, R., & Jensen, D. (2010). Design of energy harvesting technology: Feasibility for low-power wireless sensor networks. *Proc. of the International Design Engineering Technical Conferences*. Montreal, Quebec.

Weingroff, R. F. (1996, Summer). Federal-Aid Highway Act of 1956: Creating the Interstate System. *Public Roads*, *60* (1).

White, L. J. (1962). *Medieval technology and social change*. Oxford: Oxford Press.

Wickenheiser, A. M., & Garcia, E. (2010). Broadband vibration-based energy harvesting improvement through frequency up-conversion by magnetic excitation. *Smart Materials and Structures*, *19*.

Williams, C. B., & Yates, R. B. (1996). Analysis of a micro-electric generator for microsystems. *Sensors and Actuators A: Physical*, *52* (1-3), 8-11.

Williams, C. B., Pavic, A., Crouch, R. S., & Woods, R. C. (1999). Feasibility study of vibration-electric generator for bridge vibration sensors. *Shock and VIbration Digest*, *31* (6).

Wilson, R. C., & Mordvinov, A. V. (2003). Secular total solar irradiance trend during solar cycles 21-23. *Geophys. Res. Lett.*, *30* (5).

Wind Speed. (2008). Retrieved Jun 1, 2011, from Energy Bible: http://www.energybible.com/wind_energy/wind_speed.html

Wireless Sensor Network Programmable Analog Input Measurement Nodes: NI WSN-3202, NI WSN-3212, NI WSN-3226. (2011, May 6). Retrieved May 19, 2011, from National Instruments: http://sine.ni.com/ds/app/doc/p/id/ds-294/lang/en

Wolfram Alpha. (2011). *Wind speed in Austin Texas*. Retrieved Jun 1, 2011, from Wolfram|Alpha Knowledgebase: http://www.wolframalpha.com

Woo, A., Tong, T., & Culler, D. (2003). Taming the underlying challenges of reliable multihop routing in sensor networks. *Proc. 1st ACM Conference on Embedded Networked Sensor Systems*. Los Angeles, CA.

Worden, K., Farrar, C. R., Manson, G., & Park, G. (2007). The fundamental axioms of structural health monitoring. *Proc. R. Soc. A*, *463* (2082), 1639-2082.

Woyte, A., Nijs, J., & Belmans, R. (2003). Partial shadowing of photovoltaic arrays with different system configurations: Literature review and field test results. *Solar Energy*, *74* (3), 217-233.

Wu, L.-Y., Chen, L.-W., & Liu, C.-M. (2009). Acoustic energy harvesting using resonant cavity of a sonic crystal. *Applied Physics Letters*, *95* (1).

Xu, F. J., Yuan, F. G., Hu, J. Z., & Qiu, Y. P. (2010). Design of a miniature wind turbine for powering wireless sensors. *Proc. SPIE*. San Diego, CA.

Xu, N., Rangwala, S., Chintalapudi, K. K., Ganesan, D., Broad, A., Govindan, R., et al. (2004). A wireless sensor network for structural monitoring. *SenSys '04*. Baltimore, MD.

Yang, H., Lu, L., & Zhou, W. (2007). A novel optimization sizing model for hybrid solar-wind power generation system. *Solar Energy*, *81* (1), 76-84.

Yen, B. C., & Lang, J. H. (2006). A variable-capacitance vibration-to-electric energy harvester. *IEEE Trans. on Circuits and Systems*, *53* (2), 288-295.

Yick, J., Mukherjee, B., & Ghosal, D. (2008). Wireless sensor network survey. *Computer Networks*, *52* (12), 2292-2330.

Yin, X., Fang, Z., Cai, C. S., & Dang, L. (2010). Non-stationary random vibration of bridges under vehicles with variable speed. *Engineering Structures*, *32* (8), 2166-2174.

Zhang, C. L., Yang, J. S., & Chen, W. Q. (2010). Low-frequency magnetic energy harvest using multiferroic composite plates. *Physics Letters A*, *374*, 2406-2409.

Zhu, D., Tudor, M. J., & Beeby, S. P. (2010). Strategies for increasing the operating frequency range of vibration energy harvesters: A review. *Meas. Sci. Technol.*, *21*.

Vita

Jason Weaver was born in Salt Lake City, Utah, and spent much of his life in the Dallas/Fort Worth area of Texas. After serving a mission for The Church of Jesus Christ of Latter-day Saints in Bangalore India, he completed his undergraduate work in Mechanical Engineering at Brigham Young University. Jason received his Masters Degree in Mechanical Engineering from The University of Texas at Austin in 2008.

Permanent address: 333 Liberty Street, Hutto Texas 78634

This dissertation typed by Jason Michael Weaver.